



**Advanced Technology for Predicting the Fluid Flow Attributes of
Naturally Fractured Reservoirs from Quantitative Geologic Data and
Modeling**

Final Report for the Period

September 29, 2000 to January 15, 2004

Authors: Jon E. Olson, Larry W. Lake and Steve E. Laubach

Issued: November 2004

**Work Performed under Contract No. DE-FC26-00BC15308
Prepared for the U.S. Department of Energy**

Daniel J. Ferguson, Project Manager

**U. S. Department of Energy
National Energy Technology Laboratory
One West Third Street
Tulsa, Oklahoma 74103**

Prepared by

**The Center for Petroleum and Geosystems Engineering
The University of Texas at Austin
1 University Station Box C0300
Austin, TX 78712**

Disclaimer: This report was prepared as an account of work sponsored by an agency of the United States Government. Neither the United States Government nor any agency thereof, nor any of their employees, makes any warranty, express or implied, or assumes any legal liability or responsibility for the accuracy, completeness, or usefulness of any information, apparatus, product, or process disclosed, or represents that its use would not infringe privately owned rights. Reference herein to any specific commercial product, process, or service by trade name, trademark, manufacturer, or otherwise does not necessarily constitute or imply its endorsement, recommendation, or favoring by the United States Government or any agency thereof. The views and opinions of authors expressed herein do not necessarily state or reflect those of the United States Government or any agency thereof.

Abstract:

This report summarizes the work carried out during the period of September 29, 2000 to January 15, 2004 under DOE Research Contract No. DE-FC26-00BC15308. High temperatures and reactive fluids in sedimentary basins dictate that interplay and feedback between mechanical and geochemical processes significantly influence evolving rock and fracture properties. Not only does diagenetic mineralization fill in once open fractures either partially or completely, it modifies the rock mechanics properties that can control the mechanical aperture of natural fractures. In this study, we have evolved an integrated methodology of fractured reservoir characterization and we have demonstrated how it can be incorporated into fluid flow simulation. The research encompassed a wide range of work from geological characterization methods to rock mechanics analysis to reservoir simulation. With regard to the characterization of mineral infilling of natural fractures, the strong interplay between diagenetic and mechanical processes is documented and shown to be of vital importance to the behavior of many types of fractured reservoirs. Although most recent literature emphasizes Earth stress orientation, cementation in fractures is likely a critically important control on porosity, fluid flow attributes, and even sensitivity to effective stress changes. The diagenetic processes of dissolution and partial cementation are key controls on the creation and distribution of open natural fractures within hydrocarbon reservoirs.

The continuity of fracture-porosity is fundamental to how fractures conduct fluids. In this study, we have made a number of important discoveries regarding fundamental properties of fractures, in particular related to the prevalence of kinematically significant structures (crack-seal texture) within otherwise porous, opening-mode fractures, and the presence of an aperture size threshold below which fractures are completely filled and above which porosity is preserved. These observations can be linked to models of quartz cementation. Significant progress has been made as well in theoretical fracture mechanics and geomechanical modeling, allowing prediction of spatial distributions of fractures that mimic patterns observed in nature. Geomechanical modeling shows the spatial arrangement of opening mode fractures (joints and veins) is controlled by the subcritical fracture index of the material. In particular, we have been able to identify mechanisms that control the clustering of fractures in slightly deformed rocks. Fracture mechanics testing of a wide range of clastic rocks shows that the subcritical index is sensitive to diagenetic factors. We show geomechanical simulations of fracture aperture development can be linked to diagenetic models, modifying fracture porosity as fractures grow, and affect the dynamics of fracture propagation. Fluid flow simulation of representative fracture pattern realizations shows how integrated modeling can give new insight into permeability assessment in the subsurface. Using realistic, geomechanically generated fracture patterns, we propose a methodology for permeability estimation in non-percolating networks.

Table of Contents

Abstract.....	iii
Table of Contents.....	iv
List of Figures and Tables.....	v
1. Introduction.....	1
1.1. Task 1 - Observational Verification of Emergent Threshold.....	1
1.2. Task 2 - Geochemical Controls.....	2
1.3. Task 3 - Fracture Mechanics and Geomechanical Modeling.....	2
1.4. Task 4 - Fluid Flow Analysis.....	2
1.5. Technology Transfer.....	2
2. Executive Summary.....	6
3. Experimental.....	7
3.1. New Parameter Determination Procedure.....	8
3.2. Sample Preparation Procedures.....	10
4. Results and Discussion.....	12
4.1. Evidence for Simultaneous Fracturing and Diagenesis.....	12
4.2. The Importance of Subcritical Crack Growth.....	18
4.3. Experimental Quantification of Subcritical Index.....	19
4.4. Modeling Diagenesis and Fracturing.....	31
5. Conclusions.....	38
6. References.....	40
7. Appendix – Publications.....	43
8. Appendix - FRAC Technology Transfer Meeting.....	44

List of Figures

- Figure 3.1: Test configuration for Dual Torsion Beam tests.
- Figure 3.2: Representative load decay curve (a) and computed log-log plot of crack velocity vs. load (b), using conventional multiple polynomial approach to fit data. Open symbols are measured values. Data in each of three regions of the load decay are fit to different 6th order polynomials (see text). Velocity-load variations at large times (low loads) in (b) give appreciably different magnitude for the power-law exponent.
- Figure 3.2. (a) Load decay curve and (b) computed crack velocity vs. load for the same data set as Figure 3.1 using direct fit to integrated power-law behavior.
- Figure 4.1. Correspondence between measured and calculated quartz cement abundances for unfractured matrix of Travis Peak Formation sandstones, demonstrating effectiveness of quartz cementation modeling (Lander & Walderhaug 1999).
- Figure 4.2. Multiple parallel fracture events in the same quartz grain observed with SEM-based cathode-luminescence.
- Figure 4.3. Quartz bridge across a fracture with crack-seal texture and preserved fracture porosity.
- Figure 4.4. Kinematic reconstruction of fracture opening and filling with cement for a quartz bridge.
- Figure 4.5. Scanline of fracture opening event magnitudes from a crack-seal texture such as that shown in Fig. 4.4.
- Figure 4.6. Simulated dependency in fracture zone porosity on the ratio of net rate of fracture opening to quartz precipitation rate.
- Figure 4.7. Cretaceous Travis Peak Formation core sample near tip of a vertical fracture (core photograph). Quartz cement is more abundant toward tip of fracture (bottom part of image) than where aperture widens (top part of image). Sample depth is ~9,800 ft. See (Laubach 1988) for background information.
- Figure 4.8: Thin-section images of 3 test specimens. A) Evidence of growth both through the grains (transgranular) as well as along the grain boundaries (intergranular). B) En echelon character of the crack. C) Changes in fracture aperture.
- Figure 4.9. Histogram of subcritical index values determined from measurements for 92 siliciclastic rocks.
- Figure 4.10: Thin-section images of a sandstone, A), and carbonate, B). The experimental crack runs from left to right through both samples in the middle of the image.
- Figure 4.11: Grain size vs. Subcritical index. The inverse relationship of grain size with subcritical index as predicted by Gesing and Bradt (1983) holds for sedimentary rocks. Both siliciclastics as well as carbonate samples are included in this plot, where quartz grains are measured in the siliciclastics and “carbonate” grains are measured in the carbonates.
- Figure 4.12: Multivariable linear regression analysis for all sandstone samples as shown in Tables 2. Separate analyses were carried out for each of the pore fluids used during the investigation. All variables were normalized to range from 0 to 1.

- Figure 4.13: Multivariable linear regression analysis for samples with total carbonate content of less than 10%. Separate analyses were carried out for specimens with each of the four different pore fluids.
- Figure 4.14: Multivariable linear regression analysis for samples with total carbonate and clay content less than 10%. Results were analyzed for three of the pore fluids used: A) Ambient air, B) Fresh water, and C) Oil. The correlations show that porosity is the dominant factor for these samples, where an increase in porosity decreases the subcritical index.
- Figure 4.15: Plots of subcritical index value vs. relative fracture toughness for: A) Siliclastics in ambient air, B) Siliclastics in fresh water, C) Siliclastics in oil, D) Siliclastics in brine (40000 ppm NaCl), and E) Carbonates in ambient air.
- Figure 4.16: Map traces of fracture patterns for subcritical indices of $n = 5$, $n = 20$, and $n = 40$ generated by fracture-mechanics-based modeling. Top view of 3-D model volume where x and y axes refer to distance in meters. Extension magnitude in models is identical. Very short fractures in fracture patterns are seed flaws that never grew.
- Figure 4.17: Fracture length distributions for numerical simulation of Fig. 4.16 showing the impact of varying the subcritical index on results. Total strain applied perpendicular to fracture trend was 5.6×10^{-5} .
- Figure 4.18: Permeability multiplier for the equivalent permeability of a fractured media versus unfractured matrix as a function of cumulative fracture length in a 50m by 50m area for fracture populations with different average segment length.
- Figure 4.19: The effect of synkinematic cement on equivalent permeability for a simulated fracture pattern.
- Figure 4.20: Bedding plane exposure of natural fracture pattern with good trace pattern connectivity (6 inch scale in middle of photo).
- Figure 4.21: Fracture network generated by uniaxial strain in the y-direction (zero strain in x) and starting with an isotropic in situ stress. The body is 50x50 m in map view and the mechanical layer thickness is 8m. The subcritical index used was $n=20$. a) Fracture tracemap with no aperture information. b) Kinematic aperture map where apertures are exaggerated but appropriately scaled (maximum aperture is 3×10^{-3} m).
- Table 4.1. Summary of survey measurements of subcritical crack indices for sedimentary rock.
- Table 4.2: Summary of petrographic characteristics for the sub-set of specimens for which thin sections were prepared.

1. Introduction

The goal of this research was to develop new technology for the reliable prediction of fracture pattern attributes related to subsurface fluid flow. We focused on predicting natural fracture connectivity, clustering and aperture, attributes that are exceedingly difficult to measure but can be the controlling factors for fluid movement in an oil reservoir. The project involved a multi-disciplinary team, integrating geological observational techniques and modeling to the fluid flow quantification of fractured reservoir blocks.

According to recent estimates, the U.S. domestic potential for fractured oil reservoirs is on the order of tens of billion of barrels (the Rangely Field in Colorado, a fractured sandstone reservoir, is by itself a billion barrels). With domestic oil production depending more and more on mature fields, a technological breakthrough is the only way to significantly increase reserves. Particularly in fractured, deep, or nonconventional plays in siliciclastic and carbonate rocks, better technology for predicting and characterizing fractures that provide effective flow pathways is a key to producing hydrocarbons economically. Apart from the exploration potential of fractured reservoir plays, fractures are increasingly viewed as having a significant role in successful secondary recovery of resources, even in reservoirs that do not fit the production profile of a classic “fractured reservoir.” Yet the production responses and permeability of these non-conventional fractured reservoirs is challenging to model using conventional techniques and concepts owing in large part to the effects on flow of non-interconnected fracture systems, as we demonstrate in this report. Clearly, natural fracture characterization and modeling is of increasing concern as U.S. production shifts to more mature fields where secondary recovery is required, and as U.S. exploration ventures into more complex, deeper, fractured and unconventional reservoirs.

In most cases, fractures are difficult or impossible to characterize using currently available technology. Why has effective fracture network characterization been so elusive? The answer to this question falls into three main areas of challenge:

- we lack adequate sampling of flow-scale natural fractures, particularly in quantifying the flow aperture and the stress sensitivity of reservoir fractures,
- upscaling core and/or wellbore observations to reservoir scale fracture network geometry remains difficult, and
- it is difficult to efficiently model the combination of discrete fracture flow with matrix fluid transport.

This project addressed aspects of all these challenges. The project tasks are summarized below.

1.1. Task 1 - Observational Verification of Emergent Threshold

There has been a great deal of research on how fractures open. How do they close? Our research shows that diagenesis (natural cement precipitation) is the most important cause of fracture closure (sealing) in the rocks of interest to the petroleum industry, and that the role of in situ stress in many instances is less important than has previously thought

((Laubach et al. 2004a)). There are two ways that diagenetic cements close fractures. Empirical evidence from many formations shows that in the diagenetic environment, fractures with millimeter- to micron-scale kinematic apertures (distance between previously adjacent points on the fracture wall, regardless of mineral fill) systematically fill more readily with authigenic cement than centimeter-scale and larger fractures. Thus mm-scale and smaller microfractures are typically completely sealed, probably soon after they formed. Yet, contemporaneous large fractures in the same rock often still have remnant porosity. This structural/diagenetic phenomenon of *scale-dependent* porosity preservation in fractures above a certain threshold aperture size is termed the “emergent threshold” (Laubach 2003).

Not all large fractures escape complete mineral filling, however. The cement phase that precipitates simultaneously with the fracturing event typically leaves these partially open fractures whose kinematic fracture is above the emergent threshold. However, there is a second way that diagenesis can close fractures, and that is for later cements to fill in the remaining porosity. Although we observe this in reservoir rocks under various conditions, it was not the focus of this research.

1.2. Task 2 - Geochemical Controls

With geologic observations as the backdrop, this task involved geochemical modeling of mineral precipitation on fracture surfaces. The flow and diffusion of carbonate and quartz cements was considered, with an attempt to model realistic fracture geometry, thermodynamic properties and flow rates (Noh 2003, Noh & Lake 2002).

1.3. Task 3 - Fracture Mechanics and Geomechanical Modeling

The fracture mechanics task of this project had several goals. First was to make fracture mechanics measurements on suites of samples of various lithology and diagenetic state to understand the controlling rock parameters for subcritical crack growth (Rijken et al. 2002). Second was to use these fracture mechanics measurements as input to our fracture propagation model to characterize fracture network variability as a function of lithology and structural position. As described in this report, the result of the latter effort is a more realistic and accurate representation of fracture patterns.

1.4. Task 4 - Fluid Flow Analysis

The work of this task was to perform fracture permeability upscaling work of realistic natural fracture patterns. We used our geomechanical fracture code to generate fracture patterns for flow simulation, and imported those fracture patterns into a finite-difference flow simulator with a low permeability matrix. The effective permeability of the fractured media was anticipated to be a function of the boundary conditions imposed on the flow volume as well as the attributes of the fracture pattern itself.

1.5. Technology Transfer

Technology-transfer activities were distributed throughout the 3-year span of the project. In addition to DOE contract reports, we discussed progress each year with a select group of industry representatives who make up our industry sponsor group of the Fracture Research and Application Consortium (currently 12 oil and gas companies). We also published many conference papers, a dissertation and several archival journal papers incorporating results from this DOE-sponsored work. Below is a list of conference papers

and archival journal publications attributed at least in part to this project over its entire project period.

Refereed Archival Publications:

- Laubach, S. E. 2003. Practical Approaches to Identifying Sealed and Open Fractures. *AAPG Bulletin* **87**(4), 561-579.
- Laubach, S. E., Olson, J. E. & Gale, J. 2004a. Are open fractures necessarily aligned with maximum horizontal stress? *Earth and Planetary Science Letters* **222**(1), 191-195.
- Laubach, S., Olson, J., Reed, R., Lander, R., & Bonnell, L., 2004. Opening histories of fractures in sandstone. In: The initiation, propagation, and arrest of joints and other fractures: A field workshop dedicated to the memory of Paul Hancock (edited by Engelder, T. & Cosgrove, J.). Geological Society of London.
- Laubach, S. E., Reed, R. M., Olson, J. E., Lander, R. H. & Bonnell, L. M. 2004. Coevolution of crack-seal texture and fracture porosity in sedimentary rocks: cathodoluminescence observations of regional fractures. *Journal of Structural Geology* **26**, 967-982.
- Olson, J. E. 2003. Sublinear Scaling of Fracture Aperture Versus Length: an exception or the rule? *Journal of Geophysical Research* **108**(B9), 2413.
- Olson, J. E. 2004. Predicting fracture swarms -- the influence of subcritical crack growth and the crack-tip process zone on joint spacing in rock. In: The initiation, propagation, and arrest of joints and other fractures: A field workshop dedicated to the memory of Paul Hancock (edited by Engelder, T. & Cosgrove, J.). Geological Society of London.

Technical meeting papers and presentations:

- Albertoni, Alejandro, and Lake, Larry W. 2002. Inferring Interwell Connectivity from Well-rate Fluctuations in Waterfloods. 2002 SPE/DOE Thirteenth Symposium on Improved Oil Recovery. Tulsa, Oklahoma. April 13-17.
- Laubach, S. E., Reed, R. M., Olson, J., Ortega, Orlando, and Stowell, J. F. W. 2001. Fracture-surrogate analysis methods applied to Spraberry, Bone Spring, and Canyon cores: preliminary results, in The Permian Basin: microns to satellites, looking for oil and gas at all scales. West Texas Geological Society Fall Symposium. West Texas Geological Society Publication 01-110. p. 75-79.
- Noh, Myeong, and Lake, Larry W. 2002. Geochemical Modeling of Fracture Filling. 2002 SPE/DOE Thirteenth Symposium on Improved Oil Recovery. Tulsa, Oklahoma. April 13-17.
- Olson, J. E., Holder, J., and Rijken, P. 2002. Quantifying the Fracture Mechanics Properties of Rock for Fractured Reservoir Characterization. Arlington, TX. October 20-23.
- Olson, J. E., Laubach, S. E. & Lander, R. H. 2004. Improving fracture permeability prediction by combining geomechanics and diagenesis. In: Gulf Rocks - 6th North America Rock Mechanics Symposium, Houston, TX.
- Olson, J. E., Qiu, Y., Holder, J. & Rijken, P. 2001. Constraining the Spatial

Distribution of Fracture Networks in Naturally Fractured Reservoirs Using Fracture Mechanics and Core Measurements. In: 2001 SPE Annual Technical Conference and Exhibition, New Orleans, LA.

Park, N., Holder, J., and Olson, J.E. 2004. Discrete Element Modeling of Fracture Toughness Tests in Weakly Cemented Sandstone. Gulf Rocks - 6th North America Rock Mechanics Symposium, Houston, TX.

Philip, Z., Jennings, J. W., Jr., Olson, J. E. & Holder, J. 2002. Modeling Coupled Fracture-Matrix Fluid Flow in Fracture Patterns Generated using a Geo-Mechanical Crack Growth Simulator. In: 2002 SPE Annual Technical Conference and Exhibition, San Antonio, TX.

Philip, Z., J. W. Jennings, Jr., J. E. Olson, and J. Holder. 2002. Modeling coupled fracture-matrix fluid flow in fracture patterns generated using a geo-mechanical crack growth simulator. Naturally Fractured Reservoir Conference, University of Oklahoma and Oklahoma Geological Survey, Norman, OK, June 3-4.

Rijken, Peggy, Holder, Jon, Olson, Jon E. and Laubach, Stephen E. 2002. Natural Fracture Characterization within the Travis Peak Formation, East Texas. Gulf Coast Association of Geologists Society. Austin, TX. October 30-November 1.

Theses and Dissertations

Albertoni, Alejandro. 2002. Inferring Interwell Connectivity from Well-rate Fluctuations in Waterfloods. The University of Texas at Austin, M.S. Thesis, 187 pages.

Qiu, Yuan. 2002, "Natural Fracture Modeling and Characterization," The University of Texas at Austin, Ph.D. dissertation, 169 pages.

Noh, M. H. 2003. Reactive Transport Modeling in Fractures and Two-phase Flow. The University of Texas at Austin, Ph.D. thesis.

Philip, Zeno. 2003. Incorporating subcritical crack growth mechanics into natural fracture characterization for improved reservoir simulation. The University of Texas at Austin, Ph.D. thesis, 198 pages.

Presentations:

Stowell, J., Marrett, R., Laubach, S. and Olson, J., 2001, "Understanding fractured carbonate reservoirs," 2001 AAPG Annual Meeting and Technical Conference, Denver, CO, June 3-6.

Olson, J.E., 2001, "Predicting fracture length distributions and fracture clustering based on subcritical crack growth," Mechanisms of Jointing in the Crust: A Paul Hancock Memorial Meeting, Weston-super-Mare, England, August 1-4.

Laubach, S.E., and Olson, J.E., 2001, "Fractures and Diagenesis," Mechanisms of Jointing in the Crust: A Paul Hancock Memorial Meeting, Weston-super-Mare, England, August 1-4.

Short courses presented:

Olson, Jon E., Marrett, R., and Laubach, S., Nov. 2000, Fractured Reservoir Characterization (5 day short course), American Association of Petroleum

Geologists.

Olson, Jon E., 2001, "Fractured reservoir characterization," 3-day workshop for Japan National Oil Company (a FRAC consortium sponsor), Tokyo, Japan, July 2-4.

Olson, Jon E., Marrett, R., and Laubach, S., Nov. 2003, Fractured Reservoir Characterization (5 day short course), American Association of Petroleum Geologists.

Industrial Consortium Meetings Presented:

Winter Research Meeting, Fracture Research and Application Consortium. Austin, Tx. February 5-6, 2001.

Summer Research Meeting, Fracture Research and Application Consortium. Jackson, Wy. June 21-22, 2001.

Winter Research Meeting, Fracture Research and Application Consortium. Monterrey, Mexico. February 25-26, 2002.

Summer Applications Meeting, Fracture Research and Application Consortium. Jackson, Wy. June 2002.

Summer Research Meeting, Fracture Research and Application Consortium. Jackson, Wy. July 2003.

2. Executive Summary

High temperatures and reactive fluids in sedimentary basins dictate that interplay and feedback between mechanical and geochemical processes significantly influence evolving rock and fracture properties. Not only does diagenetic mineralization fill in once open fractures either partially or completely, it modifies the rock mechanics properties that can control the mechanical aperture of natural fractures. In this study, we have evolved an integrated methodology of fractured reservoir characterization and we have demonstrated how it can be incorporated into fluid flow simulation. The research encompassed a wide range of work from geological characterization methods to rock mechanics analysis to reservoir simulation. With regard to the characterization of mineral infilling of natural fractures, the strong interplay between diagenetic and mechanical processes is documented and shown to be of vital importance to the behavior of many types of fractured reservoirs. Although most recent literature emphasizes Earth stress orientation, cementation in fractures is likely a critically important control on porosity, fluid flow attributes, and even sensitivity to effective stress changes. The diagenetic processes of dissolution and partial cementation are key controls on the creation and distribution of open natural fractures within hydrocarbon reservoirs.

The continuity of fracture-porosity is fundamental to how fractures conduct fluids. In this study, we have made a number of important discoveries regarding fundamental properties of fractures, in particular related to the prevalence of kinematically significant structures (crack-seal texture) within otherwise porous, opening-mode fractures, and the presence of an aperture size threshold below which fractures are completely filled and above which porosity is preserved. These observations can be linked to models of quartz cementation. Significant progress has been made as well in theoretical fracture mechanics and geomechanical modeling, allowing prediction of spatial distributions of fractures that mimic patterns observed in nature. Geomechanical modeling shows the spatial arrangement of opening mode fractures (joints and veins) is controlled by the subcritical fracture index of the material. In particular, we have been able to identify mechanisms that control the clustering of fractures in slightly deformed rocks. Fracture mechanics testing of a wide range of clastic rocks shows that the subcritical index is sensitive to diagenetic factors. We show geomechanical simulations of fracture aperture development can be linked to diagenetic models, modifying fracture porosity as fractures grow, and affect the dynamics of fracture propagation. Fluid flow simulation of representative fracture pattern realizations shows how integrated modeling can give new insight into permeability assessment in the subsurface. Using realistic, geomechanically generated fracture patterns, we propose a methodology for permeability estimation in non-percolating networks.

3. Experimental

As a part of Task 3, subcritical crack growth measurements were carried out with a constant-displacement, double-torsion beam (DTB) tests (Evans 1972, Williams & Evans 1973). In this configuration, stress intensity is independent of fracture length, and a complete propagation velocity vs. stress intensity factor curve can be obtained from a single load decay measurement on opaque samples. The DTB test configuration is illustrated in Figure 3.1.

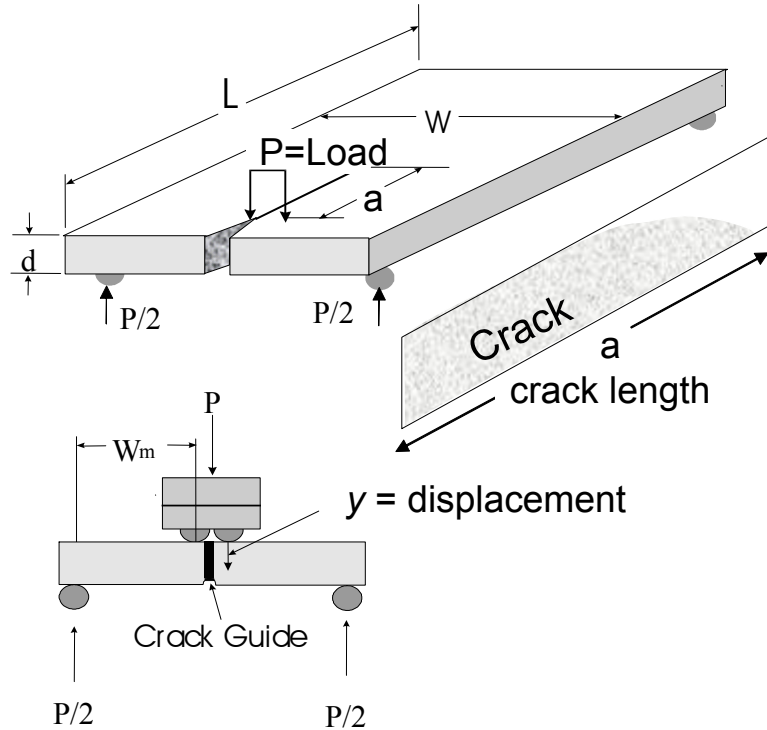


Figure 3.1: Test configuration for Dual Torsion Beam tests.

Constant displacement (load decay) DTB tests are based on the empirical evidence that the effective specimen compliance, S , is a linear function of crack length, a , (Evans 1972):

$$S \equiv y / P = S_0 + B \cdot a, \quad (3.1)$$

where y is the displacement in the y -direction, P is the load, S_0 is the intact specimen compliance and B is a constant. For a constant displacement, the crack propagation velocity, V , can be determined by the rate of change of the load, P (Williams & Evans 1973) as

$$V = -\frac{C}{P^2} \left(\frac{\partial P}{\partial t} \right), \quad (3.2)$$

where C is given by

$$C = y_0 \cdot P_t = \frac{S_0 + B \cdot a_t}{B} \cdot P_t, \quad (3.3)$$

and y_0 is a constant. The subscripts on a and P indicate values determined for a specific time, which is generally the end of a test. The crack velocity curve can then be determined from Equation 3.2 by numerical differentiation of load vs. time data. Direct numerical computation of load-time slopes from individual data points is generally not suitable because of measurement scatter, so raw data are usually smoothed by fitting load-time behavior to a curve.

Representative data from a typical load decay test are shown in Figure 3.2(a). In a conventional determination of subcritical crack velocity, a polynomial is fit to the load decay curve. Typically, a 6th order polynomial is necessary, and two to three separate polynomials are required to fit the entire load decay. Then a single smoothed curve is created by overlapping the regions fit to the different polynomials. A composite load vs. time curve is determined from the smoothed curve, and velocity-load variations are determined by applying Equation 3.2 to the smoothed curve. This process is tedious and time-intensive. By forcing a fit of load-time to a polynomial, the computed velocity-load variations often deviate from a well-defined power-law. This is evident in Figure 3.2(b) for the low load (long time) behavior derived from a three-polynomial fit shown in Figure 3.2(a). The best-fit power-law exponent increases from a value of 50 for the initial (high velocity) portion of the velocity-load plot to a value as high as 400 at very long times (low velocities).

3.1. New Parameter Determination Procedure

An alternative approach, in which no artificial curve fits are imposed on the load-time behavior, is to fit the measured data to the time dependent expression obtained by integration of Equation 3.2. For convenience, Equation 3.1 can be rearranged as

$$P = \frac{P_i}{(1+b \cdot a)}, \quad (3.4)$$

where b is a constant and P_i is the initial value of applied load. Differentiating Equation 3.4 with respect to time, t , and presuming the power-law relationship between subcritical propagation velocity and stress intensity factor,

$$v = A \left(\frac{K_I}{K_{Ic}} \right)^n, \quad (3.5)$$

results in

$$\frac{\partial P}{\partial t} = - \frac{C \cdot b}{P_i} \cdot P^{(n+2)}, \quad (3.6)$$

from which the constants C and b can be related to initial values of the load, P_i , and its time derivative, P_i' , as

$$C \cdot b = - \frac{P_i'}{P_i^{(n+1)}}. \quad (3.7)$$

Finally, integrating Equation (3.6) gives:

$$P = \frac{P_i}{[1 - (n + 1) \cdot (P_i' / P_i) \cdot t]^{1/(n+1)}} \quad (3.8)$$

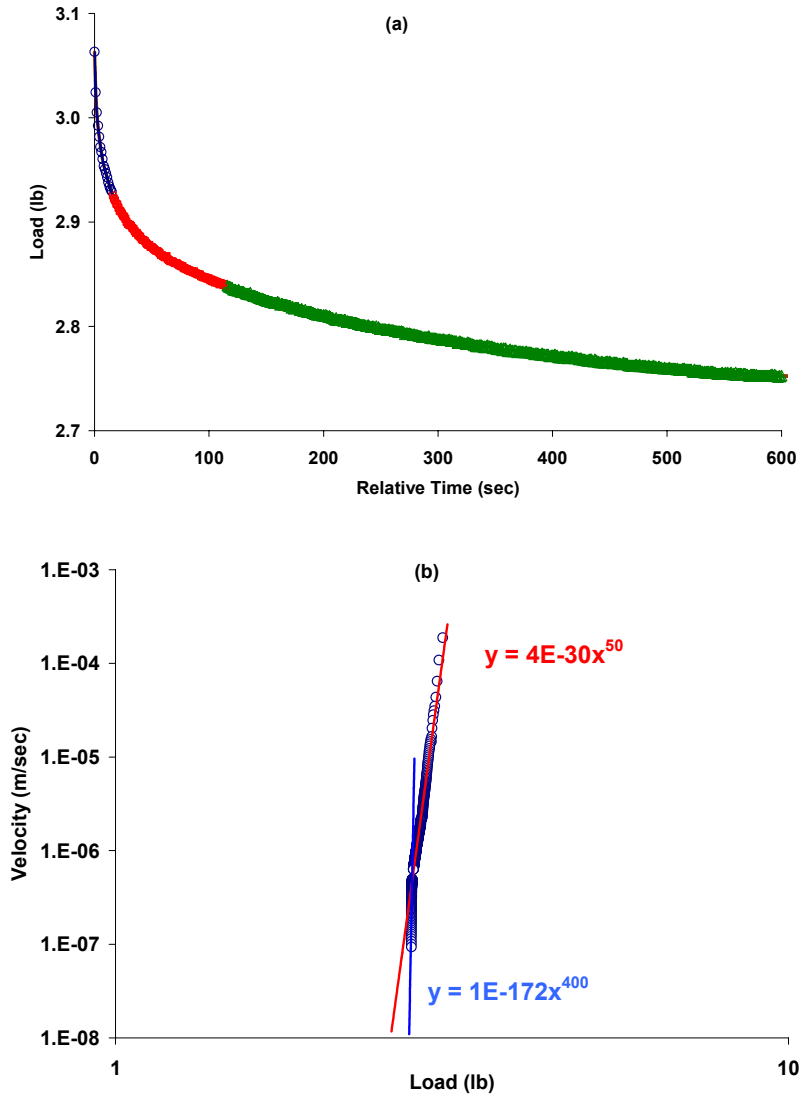


Figure 3.2: Representative load decay curve (a) and computed log-log plot of crack velocity vs. load (b), using conventional multiple polynomial approach to fit data. Open symbols are measured values. Data in each of three regions of the load decay are fit to different 6th order polynomials (see text). Velocity-load variations at large times (low loads) in (b) give appreciably different magnitude for the power-law exponent.

In principal, P_i and P_i' could be determined from measurements of the initial load-time behavior. However, experimental scatter is too high to directly determine these parameters, especially during the initial portion of the load decay. Instead, we perform a least squares best fit procedure to determine all three parameters in Equation 3.8 simultaneously. Crack velocity is then determined from Equation 3.2. This process can easily be set up in a spreadsheet, and the entire curve fit can be carried out within a few

seconds. The advantage of the revised procedure is illustrated by results shown in Figure 3.3, which uses the same load decay data as that in Figure 3.2. The solid line in Figure 3.3(a) shows the curve fit (it coincides with and is thus covered up by the data points), and Figure 3.2(b) show the improvement in the power-law fit.

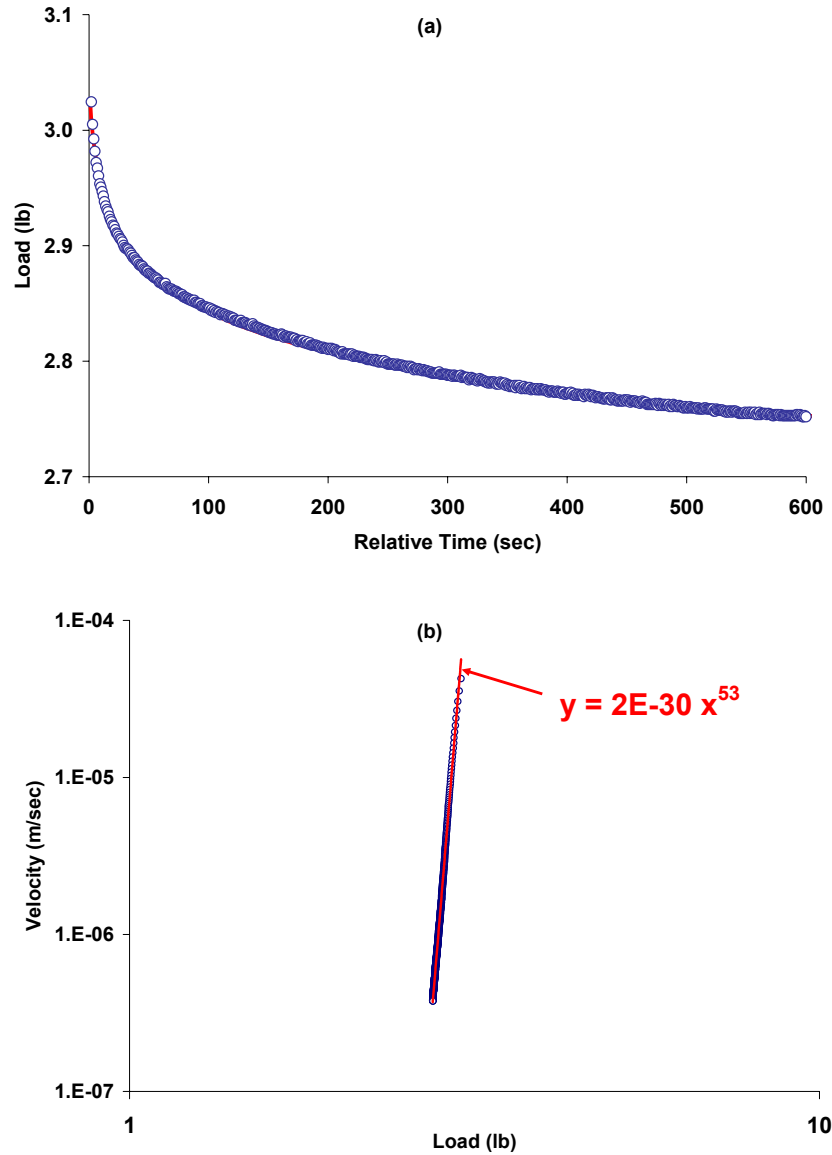


Figure 3.2. (a) Load decay curve and (b) computed crack velocity vs. load for the same data set as Figure 3.1 using direct fit to integrated power-law behavior.

3.2. Sample Preparation Procedures

For each of the rocks tested in this study, four to twelve 2.5cm x 7.5cm x 1.7mm test specimens were prepared. The specimens were polished on one side, and a central groove of at least 0.5mm was cut along the long specimen axis on the opposite side. The specimens were placed in toluene for several hours to remove excess oil and other

chemicals used during specimen preparation. The specimens were then heated in a nominal 100°C oven for several hours to remove the toluene. A small sub-set of tests was performed to ensure that results were not affected by the toluene. Specimens for these tests were heated in the oven for approximately 2 days to eliminate the oil and other chemicals. Results from these tests were found to be virtually identical to the tests performed using toluene as a cleaning agent.

Prior to testing of samples in different pore fluids, the specimens were placed in a vacuum vessel containing the pore fluid, and specimens were immersed. The vessel was evacuated and the specimen remained in the vessel, with vacuum applied, for a minimum of 2 days. The saturated specimens were placed in the measurement apparatus, and the specimen was submerged during the load decay measurements.

Most sedimentary rocks are relatively weak mechanically, and the transient decay of the un-cracked specimen can be difficult to separate from the load decay from crack propagation (Holder et al. 2001). In order to minimize this complication, test specimens were pre-loaded prior to the fracture propagation measurements in a series of nominal 30-second steps, during which the applied load was manually held constant. Transient behavior was largely completed over this interval, and subsequent decay was due solely to crack propagation. The time required for a typical load decay curve, from maximum velocities of a few centimeters per second down to measurement noise, was approximately 10 minutes. Total crack propagation during a single load decay was often much less than the length of the specimen, and multiple tests were often carried out on the same test specimen.

4. Results and Discussion

The research performed under this contract involved observational work on fractured rock, diagenetic and geochemical modeling of fracture rock systems, experimental fracture mechanics property measurements, geomechanical modeling of natural fracture pattern development, and the quantification of fracture permeability in a manner that fully utilized the richness of information that can be found in geologic fracture characterizations. The underlying theme that sets this work apart from previous attempts at fracture characterization and permeability estimation is the integration of mechanical and diagenetic processes in the characterization and modeling effort.

4.1. Evidence for Simultaneous Fracturing and Diagenesis

The key conceptual breakthrough we have made is the realization that rock diagenesis and rock deformation cannot be treated as separate, uncoupled processes. Quartz is the most abundant and widespread cement in sandstones exposed to temperatures in excess of ~ 90 °C for geologically significant periods (Bjørklykke & Egeberg 1993, McBride 1989). It is therefore not surprising that virtually all transgranular fractures in such sandstones show at least some degree of porosity loss due to quartz cementation. However, not all fractures are occluded by quartz cement. In a wide range of sandstones, there is a threshold kinematic fracture opening (separation between two previously adjacent points across the fracture regardless of later mineral filling) above which fracture porosity is preserved and below which fractures are completely filled. This fracture aperture size is the *emergent threshold* (Laubach 2003).

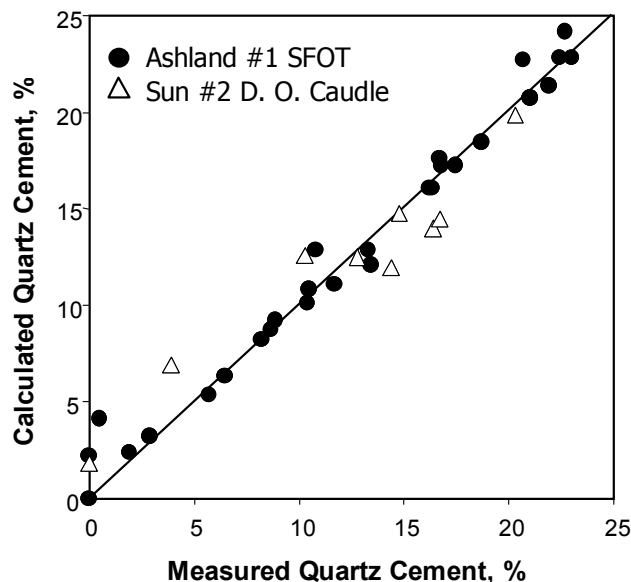


Figure 4.1. Correspondence between measured and calculated quartz cement abundances for unfractured matrix of Travis Peak Formation sandstones, demonstrating effectiveness of quartz cementation modeling (Lander & Walderhaug 1999).

Quartz cement in sandstones generally occurs as *overgrowths* that nucleate on detrital quartz grains. The concept that the kinetics of quartz crystal precipitation is the rate limiting process for the overall growth rate in many types of sandstone (Oelkers et al. 1996, Oelkers et al. 2000, Walderhaug 1994, 1996, 2000) represents an important

milestone in understanding the controls on quartz cement abundances. Using this concept, quartz cementation rates are a function of temperature and nucleation surface area. Computer simulators incorporating this concept accurately reproduce measured quartz cement abundances in sandstones from diverse geologic settings (Fig. 4.1) Lander & Walderhaug (1999) and have been used to (1) reconstruct the diagenetic evolution of sandstones and to predict reservoir quality when coupled with compaction models (e.g., Lander & Walderhaug (1999)), (2) constrain thermal histories, and (3) evaluate how the magnitudes and rates of pore volume loss associated with quartz diagenesis influence fluid overpressure development (Bjørkum et al. 1998, Wangen 1998).



Figure 4.2. Multiple parallel fracture events in the same quartz grain observed with SEM-based cathode-luminescence.

High-resolution cathodoluminescence imaging of fracture zones in sandstones reveals that fracture kinematic apertures represent the cumulative expression of hundreds or thousands of micron scale fracturing events (Fig. 4.2), commonly referred to as crack-seal texture (Laubach et al. 2004b). In some cases quartz cement may bridge across the fracture zone between micro-fracturing events (Fig. 4.3). To better understand this process and to get an idea of the magnitude of opening for each fracturing event, we performed a reconstruction of fracture opening through time (Figure 4.4). Figure 4.5 represents a scanline perpendicular to the fracture trend from Figure 4.4, showing variations in opening magnitudes for each fracture event from less than 5 to almost 30 microns. Thus the nucleation surface area for quartz cement within fracture zones may vary significantly through time as cementation reduces surface area by partial or complete sealing of fractures and micro-fracturing events increase surface area by crystal breakage.

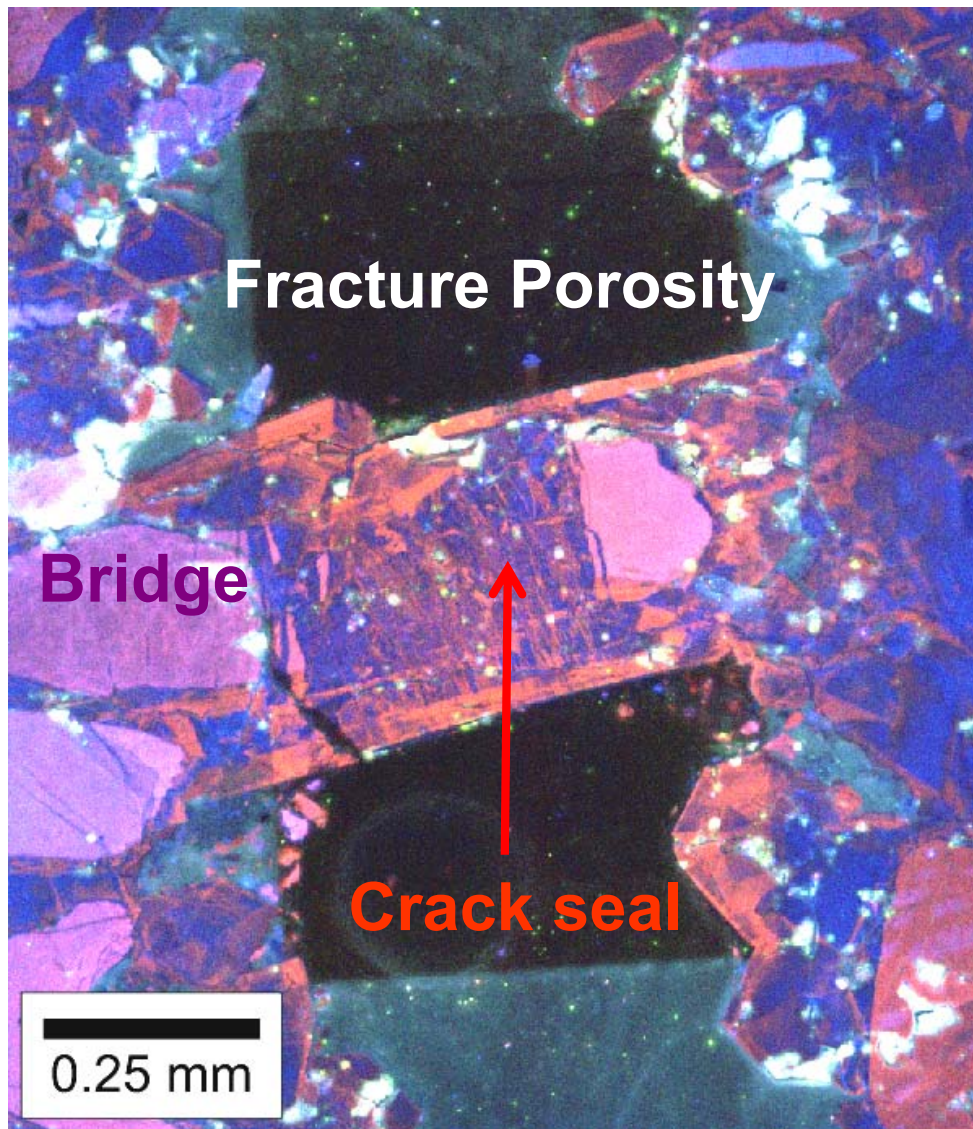


Figure 4.3. Quartz bridge across a fracture with crack-seal texture and preserved fracture porosity.

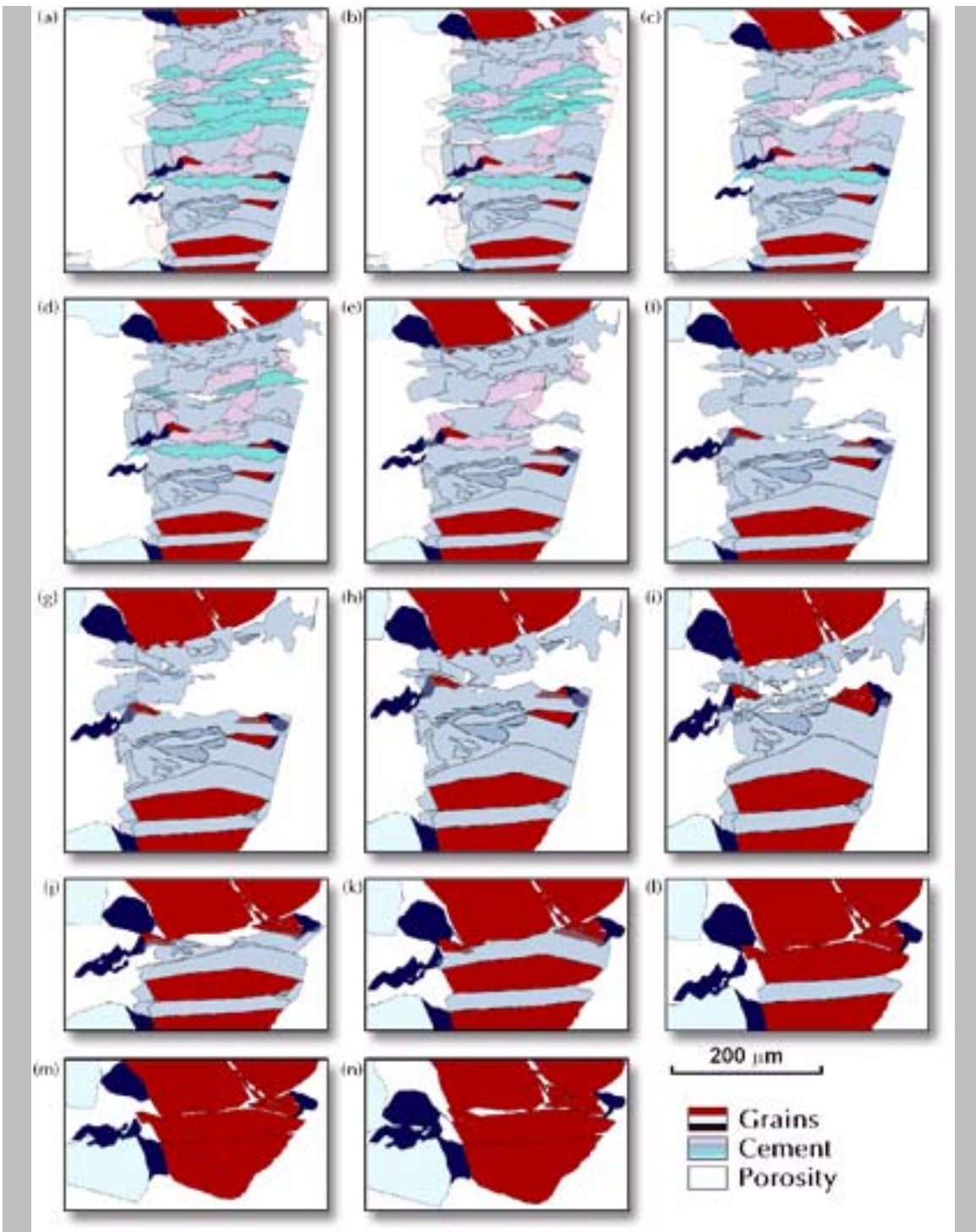


Figure 4.4. Kinematic reconstruction of fracture opening and filling with cement for a quartz bridge.

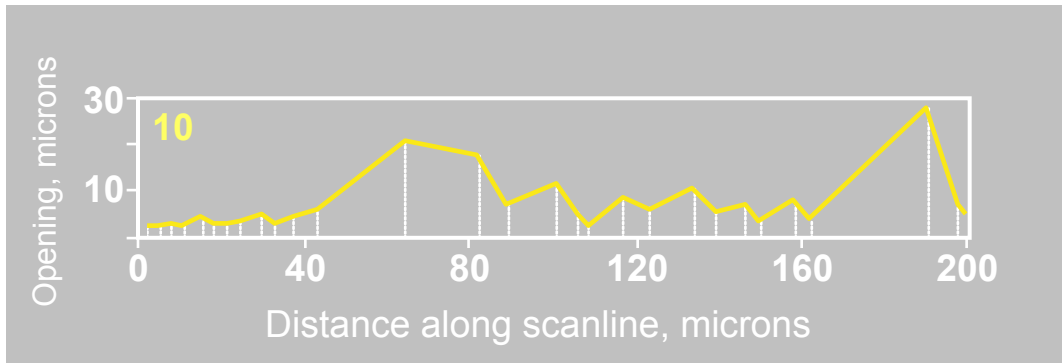


Figure 4.5. Scanline of fracture opening event magnitudes from a crack-seal texture such as that shown in Fig. 4.4.

Recently the approach toward simulation of quartz cementation in unfractured sandstones has been extended to consider quartz cementation in structurally deformed sandstones (Olson et al. 2004). Factors of particular importance for such sandstones that are considered in this model include the effects of cementation and fracturing on nucleation surface area as well as the control of crystallographic orientation and nucleation surface type on crystal growth anisotropy. Simulations of quartz cementation within the fracture zone indicate that fracture porosity is a function of the ratio of the net rate of fracture opening to the rate of quartz precipitation. The quartz precipitation rate, in turn, is a strong function of temperature and is also influenced by compositional and textural characteristics of the host sandstone.

Simulations indicate that fracture porosity increases with the ratio of fracture opening rate to quartz precipitation rate because progressively fewer crystals are able to grow across fracture apertures between fracturing events (Olson et al. 2004). When the ratio value is less than 0.5, most quartz overgrowths will seal the fracture aperture between fracturing events thereby pervasively sealing the fracture zone (Fig. 4.6). By contrast, when the ratio exceeds a value of two, no crystal will bridge across the fracture aperture and overgrowths will therefore occur exclusively as rims of euhedral crystallites along an otherwise open fracture. At intermediate ratios the cement morphology will be a mixture of euhedral crystal linings and *bridge* crystals that are pillar-like structures that span the fracture.

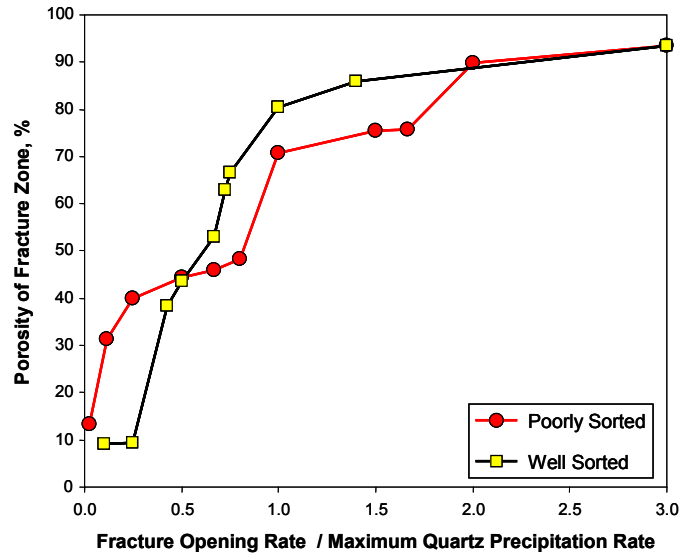


Figure 4.6. Simulated dependency in fracture zone porosity on the ratio of net rate of fracture opening to quartz precipitation rate.

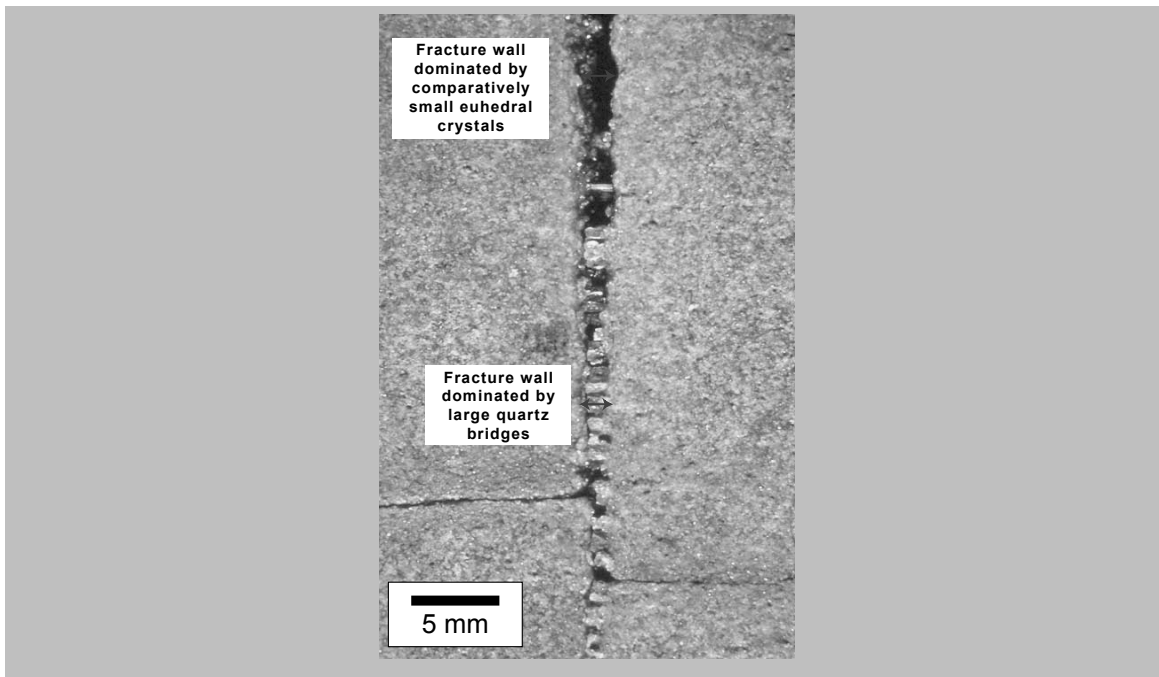


Figure 4.7. Cretaceous Travis Peak Formation core sample near tip of a vertical fracture (core photograph). Quartz cement is more abundant toward tip of fracture (bottom part of image) than where aperture widens (top part of image). Sample depth is ~9,800 ft. See (Laubach 1988) for background information.

Based on these model results we expect a transition toward greater fracture porosity in the centers of larger aperture fractures due to the faster net fracture opening rates compared to the tips. Such transitions occur in nature as illustrated for a sample from East Texas sandstone in Fig. 4.7 (Laubach 1988).

In addition to the important role that quartz cementation plays in controlling fracture porosity, it also is likely to greatly reduce the compliance of fractures. During the development of fracture systems quartz cementation occurs not only within the fracture zone itself but also within the unfractured matrix of the host sandstone. Thus the mechanical strength of the host rock will tend to increase with time. Furthermore, quartz cement that lines or bridges fractures also will decrease fracture compliance, even for fractures that have comparatively high porosities. Euhedral quartz crystals within otherwise open fractures have high spatial anisotropy and will not permit fracture porosity to go to zero even with large changes in stress orientations, and quartz bridges are likely to have an even larger strengthening effect on the fracture zone.

Precipitation of cement as a part of rock diagenesis can be divided into three stages – prekinematic, synkinematic and postkinematic, where the kinematic *event* referred to in the timing is the formation of natural, opening-mode fractures (Laubach 1988, 2003). Because quartz precipitates over a wide temperature range, it is commonly pre-, syn- and postkinematic. Other post-kinematic cements, including carbonate minerals, are commonly responsible for sealing large fractures (Laubach 2003). However, owing to the controls on quartz precipitation alluded to previously, syn- and postkinematic quartz tends to seal only small fractures, and in sandstones the phases that commonly seal large fractures are postkinematic carbonate and sulfate minerals.

Why is quartz cement so common in sandstone fractures? Quartz cementation contemporaneous with fracture may merely reflect prevalence of rock-dominated chemistry through much of a rock's burial history, including times when conditions are amenable for fracture growth. In sandstone, synkinematic quartz (and in dolostone, synkinematic dolomite), could simply be the most likely phase to precipitate through a protracted loading history (Laubach 2003).

4.2. The Importance of Subcritical Crack Growth

If we accept that fractures start to fill in with cement as soon as they start to open, it is evident that knowing the relative rates of opening versus cement precipitation is important. The diagenetic modeling of (Lander & Walderhaug 1999) and (Noh & Lake 2002) are examples of constraints on the rate of mineral accumulation in a fracture and the surrounding matrix. A complete analysis of the problem requires a rate-dependent model for fracture opening and propagation as well.

In order to analyze the simultaneous propagation of multiple fractures, both a failure criterion and a propagation velocity model are required. Brittle fracture strength is influenced by environmental factors such as relative humidity and chemical reactivity that can weaken the bonds between material grains (Atkinson 1984, Swanson 1984). For instance, most rock and ceramic material exhibit maximum fracture resistance (termed critical fracture toughness) when tested in a vacuum, and that strength is significantly reduced in the presence of water or water vapor. Fracture propagation under critical conditions is catastrophic and occurs at velocities comparable to the elastic wave speed of the material (Lawn & Wilshaw 1975). Fracture propagation below the critical toughness, termed subcritical crack propagation, occurs at lower stress levels and much lower velocities. A useful attribute of subcritical crack growth is that propagation velocity, v , can be related to opening mode stress intensity at the crack tip, K_I , with an empirically quantifiable, power-law relationship (Atkinson 1984, Olson 1993, Swanson 1984),

$$v = A \left(\frac{K_I}{K_{Ic}} \right)^n, \quad (4.1)$$

where K_{Ic} is the critical fracture toughness, n is the subcritical index, and A is a proportionality constant. The power-law exponent, n , can vary widely depending on environmental conditions (such as dry versus wet) and rock type. Reported values for carbonates and sandstones vary from 20 or less for tests done in water to greater than 100 under dry conditions (Atkinson & Meredith 1987, Holder et al. 2001).

Two dimensional, plane strain modeling of the development of fracture networks utilizing subcritical crack growth conditions has shown that the value of the subcritical index, n , exerts a strong influence on the spatial arrangement and length distribution of fractures (Olson 1993, Renshaw & Pollard 1994, Segall 1984). Results in Olson (1993) demonstrated how subcritical index controls fracture spacing to bed thickness ratio when modeling vertical fracture propagation across a bed under plane strain conditions. A very low subcritical index ($n=1$) garnered a spacing to bed thickness ratio of 0.25, while a higher index ($n=15$) resulted in a spacing/thickness ratio of 0.875. The Olson (1993) numerical results also demonstrated a mechanism for fracture cluster growth that had been postulated for joints in sandstone by Dyer (1983). The idea is that a propagating joint causes the stresses ahead of the tip to be more tensile, promoting the growth of nearby fractures in a manner similar to the process zone often observed around igneous dikes, where the intensity of dike-parallel joints is found to be very high close to the dike (Delaney et al. 1986, Pollard 1987). Olson (2004) reports qualitatively similar results to Olson (1993) except that the three-dimensional aspect of fracturing in layered formations is taken into account, resulting in fracture spacing and pattern geometries that are affected strongly by mechanical layer thickness.

4.3. Experimental Quantification of Subcritical Index

Because of the importance of the subcritical index in determining natural fracture pattern geometry, a major component of the work under this contract involved the quantification of subcritical index in different rock types from outcrop and the subsurface. Siliciclastic samples were obtained from 49 core sections and 19 outcrop locations. Carbonate samples were taken from 4 different cores and two outcrops. Crack propagation behavior was measured under nominal room conditions (dry) for all specimens, and most materials were also tested in fresh water (wet). A small fraction of the material was tested under oil- and/or brine-saturated (40,000 ppm NaCl) conditions. Brine and oil saturated conditions are representative of the environment expected to be present in the subsurface. Fresh water and air tests were predominantly performed to allow for comparison with literature values.

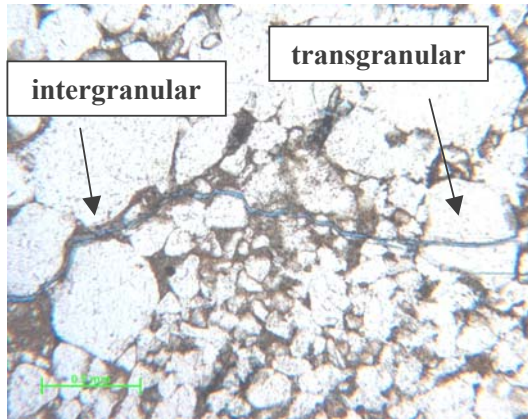
For the sub-set of samples selected for petrographic analysis, thin sections were prepared from the same specimen used for the crack propagation tests. An average of 2 thin-sections were prepared for each sample material, and 200 points were counted for each thin-section. Grain size was measured for 15 grains in each thin-section, recording both the long and short dimensions. The grain size reported is an average of the 2 thin-sections investigated. Detailed petrographic information was obtained for 32 samples in 15 formations. The point count categories are grain size (Gs, in mm), and percentages of

quartz matrix grains (Qm), quartz cement (Qc), ankerite cement (An), calcite cement (Ca), ferroan calcite cement (FeCa), potassium feldspar grains (Ks), plagioclase grains (Pl), clay (Cl), and porosity (ϕ). For dry testing the Relative Humidity (RH) is also recorded.

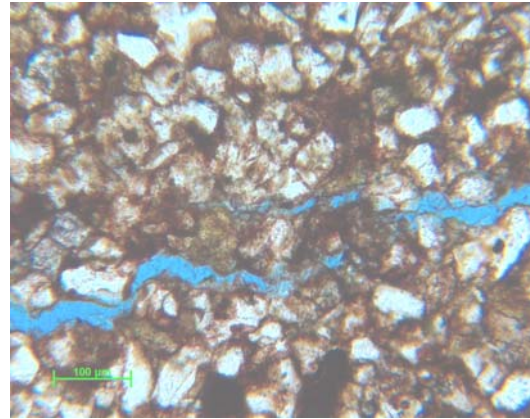
Data from the subcritical crack propagation measurements on rock are summarized in Table 4.1. Tabulated values correspond to an average from two to five different test specimens, and in many cases, one or two separate propagation sequences on the same specimen. Petrographic data for the sub-set of specimens for which thin sections were prepared are summarized in Table 4.2. The values reported are averages over two thin-sections and 400 points counted. An additional parameter is included in Table 4.1, K_a , which we term apparent toughness. This is the stress intensity factor required for a crack propagation velocity of 5×10^{-6} m/sec. This parameter provides a basis of comparison of rock strength between samples even though actual fracture toughness tests were not performed on these samples.

Thin-section images (Fig. 4.8) of the artificial cracks show the inherent complexity of fracture growth in sedimentary materials. Fractures grow predominantly through the cement between the grains (intergranular propagation), but fractures occasionally propagate through grains (transgranular propagation) (Figure 4.8A). Because of the primarily intergranular growth, the fractures tend to wander considerably (Figures 4.8A and B). En-echelon fracturing (Figure 4.8B) as well as dramatic changes in aperture (Figure 4.8C) are observed in the thin sections.

A) Sandstone (Flathead Fm.)



B) Sandstone (Moenkopi Fm.)



C) Sandstone (Scioto Fm.)

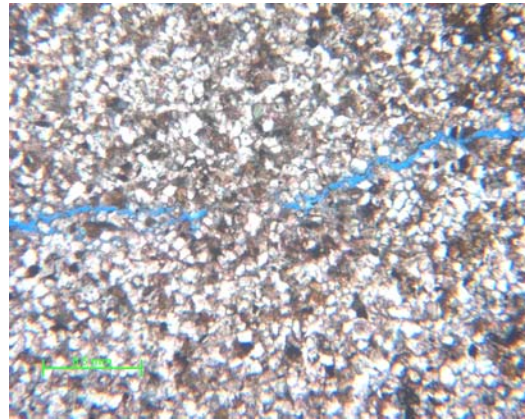


Figure 4.8: Thin-section images of 3 test specimens. A) Evidence of growth both through the grains (transgranular) as well as along the grain boundaries (intergranular). B) En echelon character of the crack. C) Changes in fracture aperture.

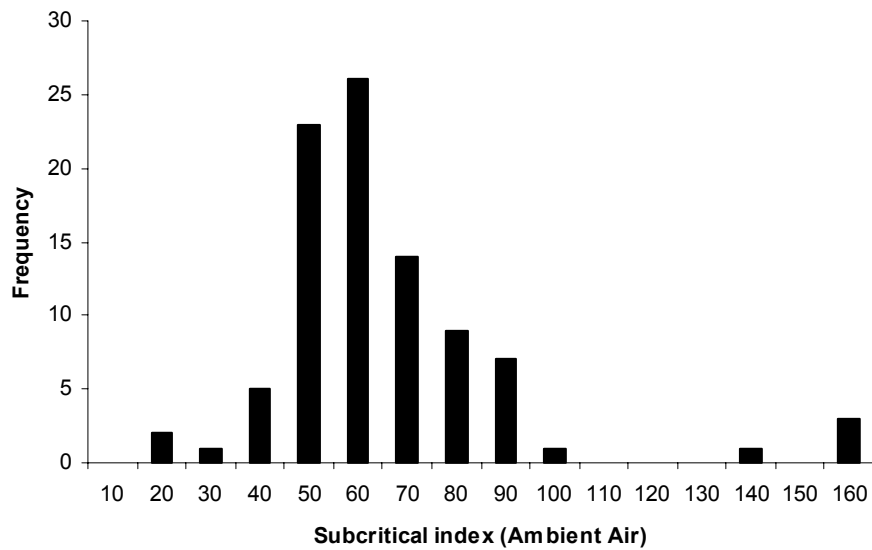


Figure 4.9. Histogram of subcritical index values determined from measurements for 92 siliciclastic rocks.

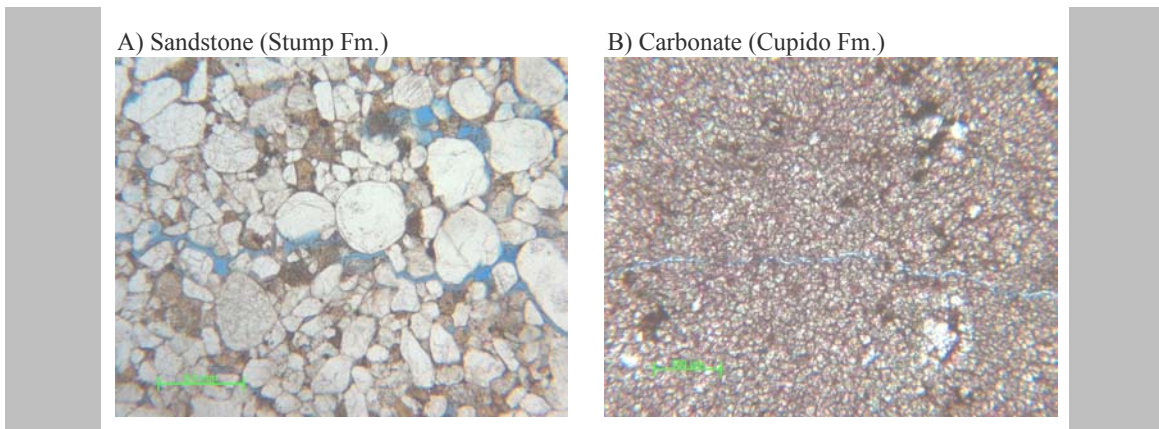


Figure 4.10: Thin-section images of a sandstone, A), and carbonate, B). The experimental crack runs from left to right through both samples in the middle of the image.

The measurements of crack behavior from 68 siliciclastic and 11 carbonate rocks provide a wide range in subcritical index and relative toughness values (Table 4.1). In siliciclastics, we measured a mean sub-critical index of 59 with a standard deviation of 20, with a relatively symmetric distribution of values with the exception of a few outliers on the high side (Fig. 4.9). Although our number of carbonate samples is much smaller, it is clear that carbonates have very different behavior, with a mean subcritical index of 194 ± 90 . Carbonate tests also show a considerably greater sensitivity to water than siliciclastics (Table 1).

Microstructural differences between carbonates and sandstones may explain the differences in subcritical index. Figure 4.10 shows two thin-section pictures of experimentally created fractures; Fig. 4.10A shows a sandstone and Fig. 4.10B shows a carbonate. The crack in the sandstone wanders more than the crack in the carbonate

sample, primarily due to a difference in grain-size. Gesing & Bradt (1983) have shown an inverse dependence of subcritical index on grain or facet size in polycrystalline ceramics, where an increase in grain size decreases the subcritical index. Although other factors are likely to play a role, the systematically higher indices in carbonates and the smaller effective grain size than sandstones is consistent with the trend predicted. Combining the grain size data of both siliciclastics and carbonates for specimens tested in air demonstrates the inverse dependence of subcritical index on grain size in sedimentary rock (Figure 4.11). However, this correlation of subcritical index with grain size is not found in water-saturated conditions.

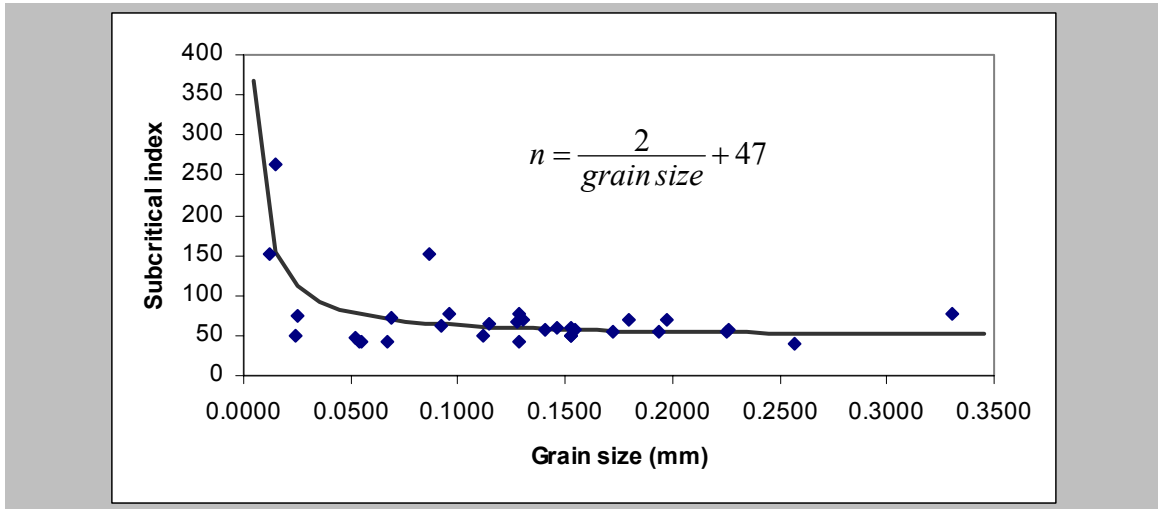
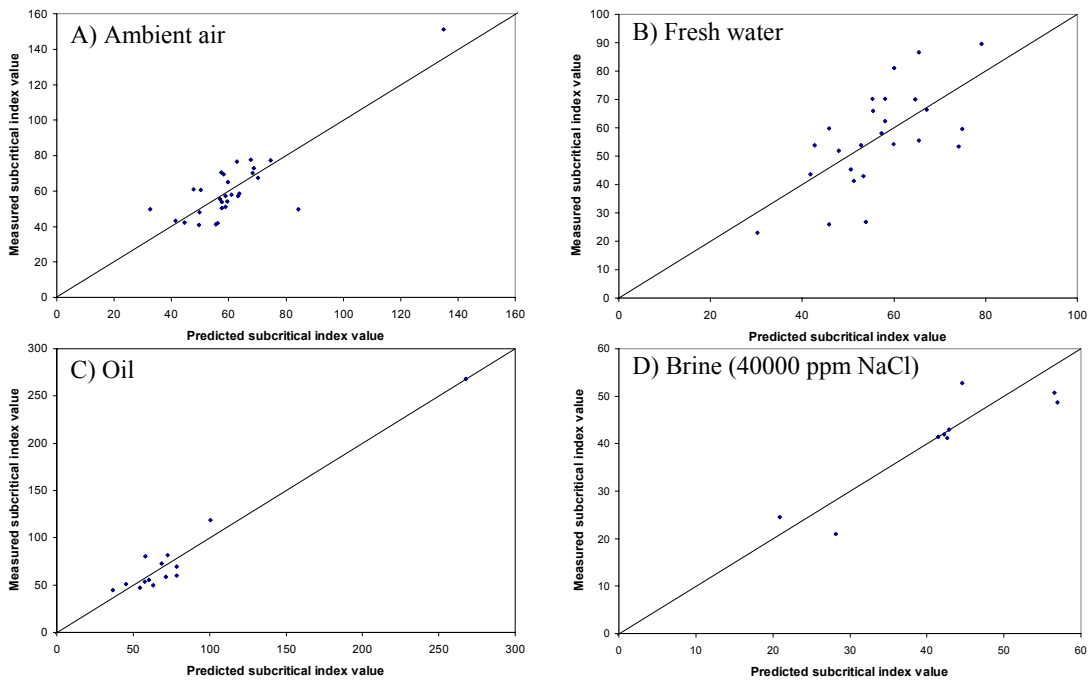


Figure 4.11: Grain size vs. Subcritical index. The inverse relationship of grain size with subcritical index as predicted by Gesing and Bradt (1983) holds for sedimentary rocks. Both siliciclastics as well as carbonate samples are included in this plot, where quartz grains are measured in the siliciclastics and “carbonate” grains are measured in the carbonates.

Looking at the siliciclastics in more detail, we assessed the control of various petrographic parameters on subcritical crack index using step-wise regression analysis (Draper & Smith 1981). The objective of this method was to select a sub-set of parameters which gave the optimum regression equation. We started by picking the petrographic variable with the highest correlation coefficient and used it to perform a regression analysis with subcritical index. We tested the significance of the regression variable using an F-test analysis with significance level, α , of 0.1 or less. If the variable was considered significant, the parameter with the next larger correlation coefficient was selected and used in the regression analysis, and the resultant fit was again tested for its significance using the F-test.

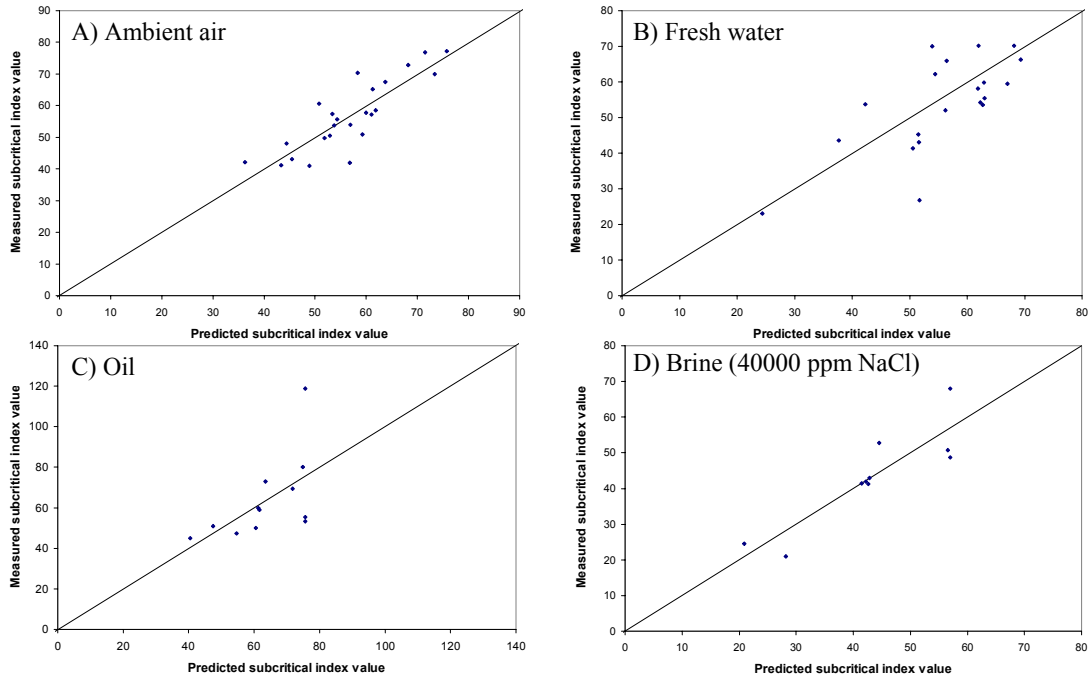


n_{air}	=	31	+	97 * FeCa	+	33 * Qc	+	15 * Ks	
n_{wet}	=	30	+	26 * FeCa					+ 45 * Qm
n_{oil}	=	35	+	219 * FeCa					+ 65 * Gs
n_{brine}	=	57							- 36 * Cl

Figure 4.12: Multivariable linear regression analysis for all sandstone samples as shown in Tables 2. Separate analyses were carried out for each of the pore fluids used during the investigation. All variables were normalized to range from 0 to 1.

A step-wise multivariable linear regression analysis was first applied to all siliciclastics for which petrographic data was collected (Fig. 4.12). Tests in the four different pore fluids were analyzed separately. All the petrographic data was normalized such that the coefficients indicate the relative importance of each parameter to the fit. The multivariable equations (Fig. 4.12) show that the most important parameter for specimens tested in air, fresh water and oil is ferroan calcite (FeCa). This increase in n with carbonate content is consistent with the general observation that carbonates have higher subcritical indices than sandstones.

In order to examine the influence of other petrographic factors on subcritical index, the data were re-evaluated using only those samples with less than 10% carbonate. The results (Fig. 4.13) show that, for all but the ambient air tests, the subcritical index correlates well with clay content (Cl), such that an increase in clay content decreases the subcritical index. The lack of correlation between subcritical index and clay content for air tests may be a consequence of a strong dependence of fracture growth on moisture content in clay-rich sandstones.



n_{air}	$= 15$	$+ 37 * An$	$+ 29 * Qc$	$+ 21 * Ks$	$+ 15 * RH$	$+ 15 * Gs$	
n_{wet}	$= 70$	$- 46 * Cl$					$- 15 * \phi$
n_{oil}	$= 75$	$- 35 * Cl$					
n_{brine}	$= 57$	$- 36 * Cl$					

Figure 4.13: Multivariable linear regression analysis for samples with total carbonate content of less than 10%. Separate analyses were carried out for specimens with each of the four different pore fluids.

Further reducing the independent variables by eliminating samples with both high carbonate and high clay content (>10%) shows that porosity becomes the most important parameter for tests in air and water (Fig. 4.14). The subcritical index decreases as porosity increases, possibly the consequence of the increases in surface area with porosity, which provides additional access for water molecules to weaken silicate bonds. The correlation of subcritical index to porosity is not found for oil-saturated tests. This is likely a consequence of the dominant role of water in weakening silicate bonds. No water molecules are present in the oil-saturated tests to weaken the silicate bonds.

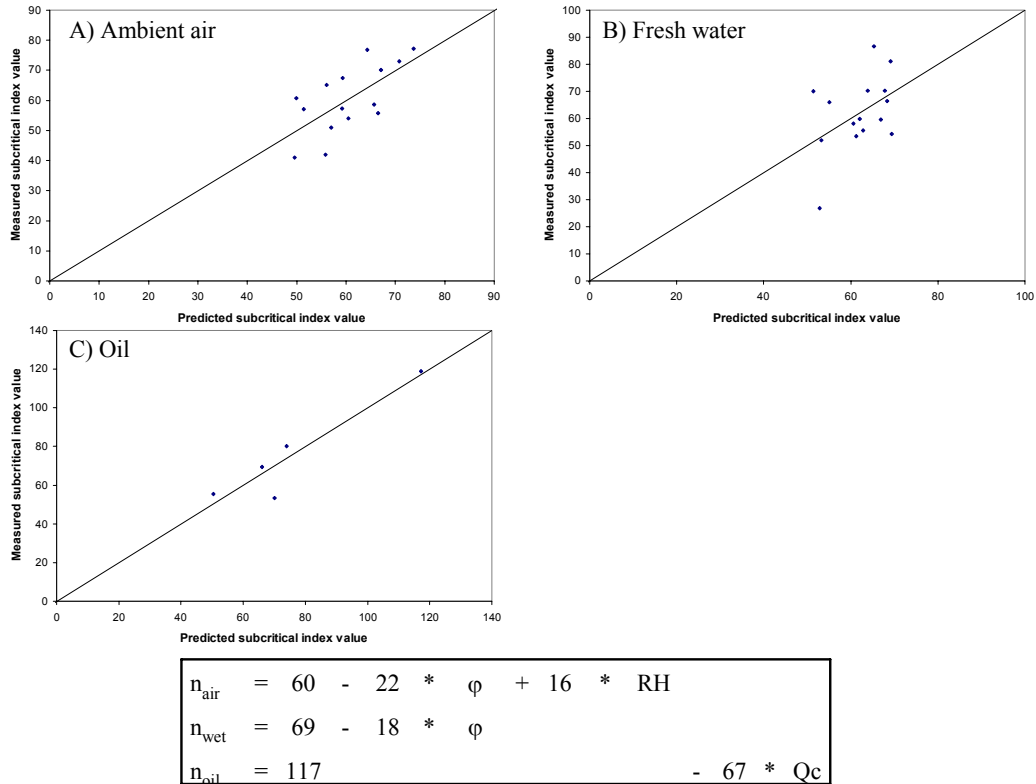


Figure 4.14: Multivariable linear regression analysis for samples with total carbonate and clay content less than 10%. Results were analyzed for three of the pore fluids used: A) Ambient air, B) Fresh water, and C) Oil. The correlations show that porosity is the dominant factor for these samples, where an increase in porosity decreases the subcritical index.

We examined whether subcritical index correlated with rock strength as measured by the relative fracture toughness. Although there is considerable scatter, siliciclastics tested with air, water, and brine showed lower subcritical indices for lower relative toughness (Fig. 4.15). This observation is consistent with that reported by Beaudoin (1987), who found that a weakening of the silicate bonds in glass by water leads to a decrease in both strength and subcritical index. Carbonates do not appear to show the same dependence, but the number of tests is small.

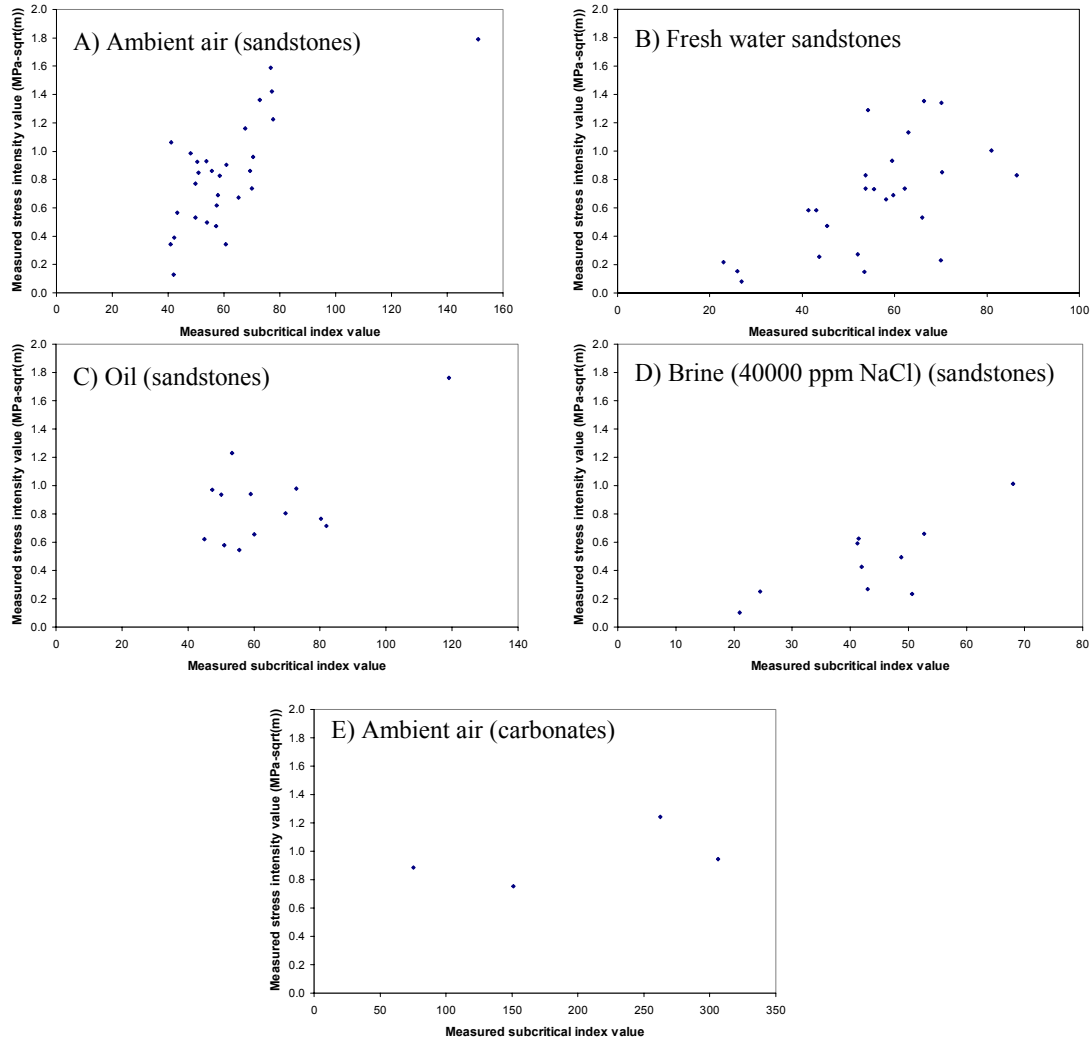


Figure 4.15: Plots of subcritical index value vs. relative fracture toughness for: A) Siliclastics in ambient air, B) Siliclastics in fresh water, C) Siliclastics in oil, D) Siliclastics in brine (40000 ppm NaCl), and E) Carbonates in ambient air.

In general we observe that the subcritical index as well as the relative fracture toughness value change as the chemical environment is altered. Both the subcritical index and the average stress intensity value are larger for oil and air tests than for fresh water and brine tests. We also observe a dependence of the decrease in the subcritical index and average stress intensity value from air to wet tests with clay and carbonate content of the rock. Specifically, an increase in the difference between the air and wet tests is observed as the clay and carbonate content increases.

Table 4.1. Summary of survey measurements of subcritical crack indices for sedimentary rock.

Formation	Depth (ft)	Subcritical index				Stress Intensity (MPa-sqrt(m)), K_a			
		dry	wet	oil	brine	dry	wet	oil	brine
Siliclastics									
Travis Peak	5,952	61 ± 8	70 ± 7			0.34± 0.05	0.23± 0.05		
"	5,962	50 ± 12	26			0.77± 0.11	0.15		
"	6,206	65 ± 3	66 ± 5			0.67± 0.08	0.53± 0.09		
"	6,244	54 ± 6	52	56 ± 8	49 ± 3	0.47± 0.07	0.27	0.54± 0.04	0.49± 0.03
"	6,270	61 ± 14	54 ± 16			0.91± 0.17	0.73± 0.08		
"	6,295	51 ± 12	58 ± 7			0.85± 0.15	0.66± 0.16		
"	6,633	78 ± 17				1.23± 0.26			
"	7,457	57 ± 17	56 ± 9			0.62± 0.21	0.73± 0.05		
"	7,506	59 ± 15	70 ± 8			0.82± 0.17	0.85± 0.08		
"	7,737	41 ± 8	63 ± 9			1.06± 0.17	1.13± 0.12		
"	9,817	56 ± 11	60 ± 15			0.86± 0.22	0.93± 0.14		
"	9,837	69 ± 8		82 ± 4		0.86± 0.10		0.71± 0.07	
"	9,880	54 ± 8	87 ± 7	70 ± 1		0.50± 0.08	0.83± 0.03	0.80± 0.07	
"	10,141	73 ± 22	54 ± 16			1.36± 0.24	1.29± 0.24		
Dakota	7,068	57 ± 12	38 ± 12						
"	7,090	47 ± 11	20 ± 4						
"	7,099	60 ± 8	41 ± 1						
"	7,112	46 ± 5	11 ± 1						
"	7,186	62 ± 9	37 ± 8						
"	7,198	44 ± 5							
"	7,205	37 ± 4							
"	7,218	41 ± 7							
"	7,225	74 ± 10	50 ± 8						
"	7,227	84 ± 11	90 ± 39						
"	7,236	138 ± 36	93 ± 30						
"	7,211	59 ± 7							
Cozzette	7,892	66 ± 17	39 ± 4						
"	7,892	64 ± 16	67 ± 18						
"	9,002	58 ± 6	45 ± 4	60 ± 2	42 ± 7	0.69± 0.09	0.47± 0.06	0.66± 0.02	0.42± 0.05
"	9,041	54 ± 16	43 ± 3	59 ± 15	41 ± 3	0.93± 0.09	0.58± 0.04	0.94± 0.06	0.59± 0.04
"	9,071	50 ± 9	41 ± 3	50 ± 7	41 ± 3	0.92± 0.12	0.58± 0.07	0.94± 0.06	0.63± 0.09
Capaya	13,449.6	62 ± 11	17						
"	13,464.1	60 ± 6	55						
"	13,468.0	59 ± 5	37						
"	13,481.5	52 ± 15	48						
"	13,497.1	66 ± 6	46						
"	13,501.0	62 ± 9	58						
"	13,502.0	48 ± 16	35						
"	13,513.0	54 ± 9	55						
San Juan	14,327	46 ± 12	59 ± 8						
"	14,547	59 ± 17	50						
Rosa Blanco	5,929	78 ± 8							
Spraberry	core	48 ± 6	54 ± 2	47 ± 12		0.98± 0.05	0.83± 0.05	0.97± 0.02	

(Table 4.1 continued)

Formation	Depth (ft)	Subcritical index				Stress Intensity (MPa-sqrt(m)), K_a			
		dry	wet	oil	brine	dry	wet	oil	brine
Siliclastics (continued)									
Stump	outcrop	41 ± 6	54 ± 12		51 ± 2	0.34± 0.07	0.15± 0.06		0.23± 0.02
"	outcrop	75 ± 16							
Moenkopi	outcrop	43 ± 5		51 ± 5	21 ± 7	0.57± 0.04		0.58± 0.03	0.10± 0.03
Flathead	outcrop	77 ± 11	66 ± 26	119 ± 16		1.59± 0.07	1.35± 0.15	1.76± 0.11	
Cloverly	outcrop	68 ± 7	81 ± 12	53 ± 16	68 ± 10	1.16± 0.06	1.01± 0.04	1.23± 0.08	1.01± 0.02
Frontier	outcrop	15 ± 5							
"	outcrop	41 ± 7							
Nugget	outcrop	77 ± 15	70 ± 11			1.42± 0.06	1.34± 0.12		
Cedar Mesa L.	outcrop	42 ± 8	27 ± 3			0.13± 0.03	0.08± 0.01		
Cedar Mesa U.	outcrop	50 ± 3	35						
Tensleep	outcrop	70 ± 8	60 ± 6	80 ± 11		0.74± 0.05	0.69± 0.02	0.77± 0.04	
Gannett (1)	outcrop	151 ± 51	90 ± 8	268		1.79± 0.22	1.90± 0.12	2.25	
Gannett (2)	outcrop	70 ± 9	62 ± 5	73 ± 11	53 ± 4	0.96± 0.11	0.74± 0.11	0.98± 0.11	0.66± 0.11
Honaker Trail	outcrop	60 ± 8	25						
Fort Union	outcrop	50 ± 6	23 ± 2	45 ± 7	25 ± 1	0.53± 0.05	0.22± 0.02	0.62± 0.03	0.25± 0.02
Ankereh	outcrop	77 ± 63							
Scioto	outcrop	35	25						
"	outcrop	52 ± 17	36						
"	outcrop	42 ± 2	44 ± 3		43 ± 3	0.39± 0.03	0.25± 0.03		0.27± 0.02
Clear Fork	6,091	43 ± 8	37 ± 9						
"	6,138	40 ±	34						
"	6,367	60 ± 18	53 ± 15						
"	6,385	81 ± 15	70 ± 4						
"	6,484	43 ± 10	37						
"	6,520	38 ± 8	30 ± 6						
Carbonates									
Unidentified 1	2,076 m	76 ± 6			29 ± 8	0.88± 0.06			0.53± 0.05
Unidentified 2	1,807 m	151 ± 40			21 ± 9	0.75± 0.20			0.52± 0.07
Kinlaw	5,585	124	42						
"	5,573	95	20						
Knox	14,516	97 ± 23	56 ± 6						
Yates	1,347*	32 ± 6	44 ± 8						
	1,427*	64 ± 13							
Cupido (1)	outcrop	262 ± 44	104 ± 7	238 ± 21		1.24± 0.12	1.18± 0.26	1.05± 0.11	
Cupido (2)	"	306 ± 33	145 ± 17			0.94± 0.09	1.13± 0.08		
Honaker Trail	outcrop	271 ± 58	41 ± 22						
"	"	250 ± 113							

* Sample contains large vugs

Table 4.2: Summary of petrographic characteristics for the sub-set of specimens for which thin sections were prepared.

Formation	Depth (ft)	Pointcount data (in % unless otherwise specified)									
		Grain size (mm)	Quartz matrix	Quartz cement	Ankerite	Calcite	Ferroan calcite	K-Spar	Plagioclase	Clay	Porosity
Siliclastics											
Travis peak	5952	0.152 ± 0.057	65.38	12.38	1.13	0	0.75	1.75	0	0.88	18
"	5962	0.152 ± 0.057	41.75	0.75	40.25	0.25	15.75	0.75	0	0.5	0
"	6206	0.114 ± 0.037	58.67	16.83	1.17	0.33	0.67	6.67	0	1.5	14
"	6244	0.14 ± 0.041	53.5	21.5	0	0	0	6.5	2.5	0	16
"	6270	0.092 ± 0.039	49	10.5	37.5	0	1	0.5	0	0.5	1
"	6295	0.111 ± 0.034	60	14	1.75	0.5	0.75	9.25	4.25	0.75	9
"	6633	0.096 ± 0.028	55	14.5	14	0.5	4.5	4.5	1.25	1.25	5
"	7457	0.155 ± 0.063	66.5	20	0	0	0	3.5	2	1.5	7
"	7506	0.146 ± 0.058	61	23	0	0.5	0	5	1.5	3.5	6
"	7737	0.067 ± 0.028	64	16	0.5	0	0.5	3.5	0	10	6
"	9817	0.172 ± 0.051	73.5	18.5	0	0	0	3.5	1	1	3
"	9837	0.197 ± 0.046	54	21	17.5	0	0	1.5	0	0	6
"	9880	0.226 ± 0.062	66.5	19.5	0	0	0	5	0	5	4
"	10141	0.069 ± 0.036	60.5	19	4	0.5	3	5	0	8	0
Cozette	9002	0.226 ± 0.114	55.5	21.5	0	0	0	4	0	19	0
"	9041	0.193 ± 0.074	57.5	18	0	0	0	5	0.5	18.5	1
"	9071	0.153 ± 0.046	56	20.5	0.5	0	0	1.5	1.5	20	0
Sprayberry	Core	0.052 ± 0.024	56	6.25	1	0	1.75	6.25	0.25	27.8	1
Stump	Outcrop	0.257 ± 0.114	72.93	7.02	0	0	0	11.53	0	0.5	8
Moenkopi	Outcrop	0.054 ± 0.026	50.75	0	1	0	0.5	10.25	0.25	37.3	0
Flathead	Outcrop	0.33 ± 0.286	67.75	13	0	0	0	18.25	0	0	1
Cloverly	Outcrop	0.128 ± 0.039	62.5	19	0	0	0	18.25	0	0	0
Nugget	Outcrop	0.128 ± 0.04	59	27	0	0	0	11.75	0	0.75	2
Cedar Mesa L.	Outcrop	0.128 ± 0.046	57.83	16.67	0.17	0	0.17	4.5	0	4.33	16
Ten sleep	Outcrop	0.13 ± 0.046	52	18.5	0	0	0	16.75	4.5	1	7
Gannett (1)	Outcrop	0.087 ± 0.03	57.5	5.25	0	0	29.5	0.75	0	7	0
Gannett (2)	Outcrop	0.18 ± 0.051	61	19	0	0	0	3.25	0.75	16	0
Forth Union	Outcrop	0.024 ± 0.013	40.33	0	9.5	0	0.17	1.17	2.17	46.7	0
Scioto (block 3)	Outcrop	0.055 ± 0.021	49	3	0.5	0	0	11.5	1	18.3	17
Carbonates											
Unidentified 1	2076 m	0.025 ± 0.009	0	0	48	0	0	0	0	52	0
Unidentified 2	1807 m	0.012 ± 0.008	0	0	45	0	0.5	0	0	54.5	0
Cupido (1)	Outcrop	0.015 ± 0.006	0	0	0.25	0	91.88	0	0	7.88	0

4.4. Modeling Diagenesis and Fracturing

The continuity of fracture-porosity is fundamental to how fractures conduct fluids. Modeling studies and comparisons to field data demonstrate that subcritical crack growth can be used to explain the presence or absence of fracture clustering and the shape of fracture length and spacing distributions (Olson 1993, Olson 2004, Renshaw 1993, Segall 1984). The fracture pattern variability illustrated in Fig. 4.16 is caused solely by the variation of the subcritical index. Figure 4.17 shows how the subcritical index controls the shape of the length distribution of the fracture population. High subcritical indices ($n > 40$) cause fractures to grow as clusters where the median fracture segment length is very low (point at which cumulative frequency is 0.5) and overall fracture intensity is low. Intermediate values ($20 < n < 40$) result in fairly regularly spaced, en echelon fracture arrays with larger median segment lengths with more fracture trace length created for a given amount of strain. Very low values of the subcritical index ($n < 20$) results in highest cumulative fracture length created for a given strain, but the pattern becomes more clustered again, with median fracture lengths between those for the high and intermediate subcritical index cases.

Fracture Permeability Estimation for Non-Percolating Networks

Standard permeability estimation procedures for fractured reservoirs (Van Golf-Racht 1984) are based on the parallel plate law,

$$k_{fm} = \frac{b^3}{12S}, \quad (4.2)$$

where k_{fm} is the permeability of a fractured media (fm) with a single fracture set parallel to the flow direction having a hydraulic (open) aperture of b and a perpendicular spacing between fractures of S . Not only does this expression imply a dominance of aperture controlling fracture permeability, but it also assumes that all fractures are through-going (i.e., they completely cross the area of interest for permeability estimation), an assumption that is unreasonable based on geologic characterizations of fracture length distributions (Olson et al. 2001, Segall 1984). Consequently, investigations of flow in populations of parallel fractures with finite lengths and varying intensity (intensity is used to refer to the total amount of fracture trace length created) suggest that fracture connectivity and network pattern geometry may be more important than hydraulic aperture in determining fracture permeability (Lough et al. 1996, Nakashima et al. 2000, Philip et al. 2002).

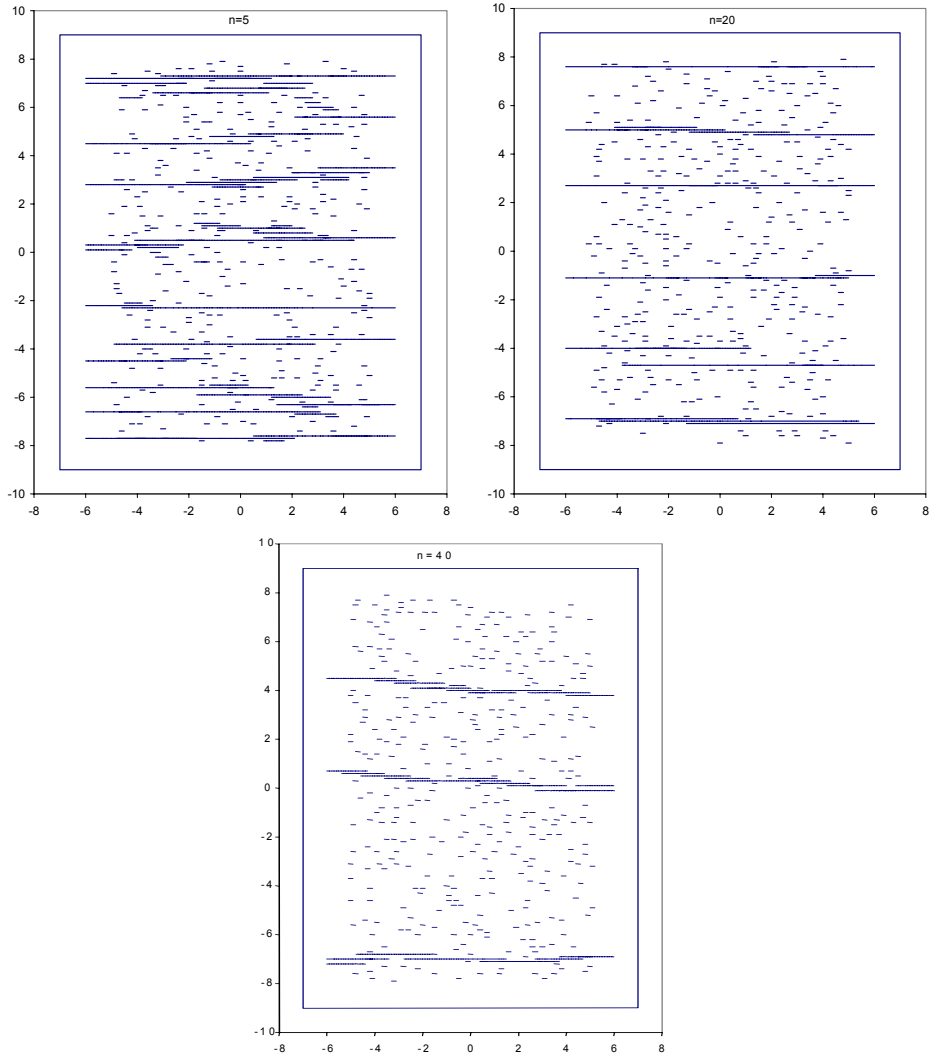


Figure 4.16. Map traces of fracture patterns for subcritical indices of $n = 5$, $n = 20$, and $n = 40$ generated by fracture-mechanics-based modeling. Top view of 3-D model volume where x and y axes refer to distance in meters. Extension magnitude in models is identical. Very short fractures in fracture patterns are seed flaws that never grew.

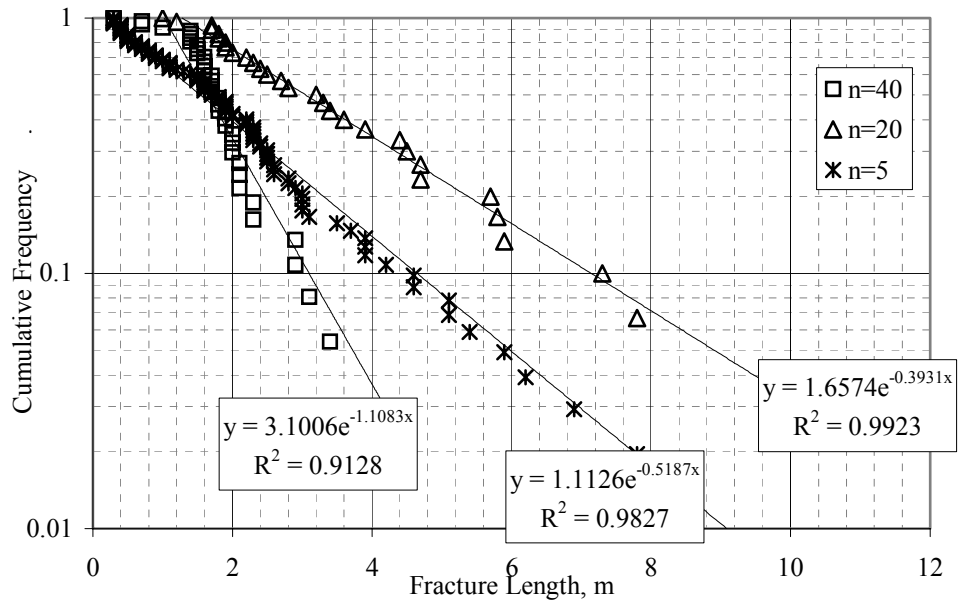


Figure 4.17. Fracture length distributions for numerical simulation of Fig. 4.16 showing the impact of varying the subcritical index on results. Total strain applied perpendicular to fracture trend was 5.6×10^{-5} .

Philip et al. (2002) estimated equivalent permeabilities for a variety of single set fracture patterns generated using a geomechanical model (Olson 1993, Olson 2004) in an attempt to discern the key fracture attributes that controlled flow in fracture networks. Local fracture permeability was computed using the parallel plate law by mapping a fine flow simulation grid (0.1 m by 0.1 m grid blocks) onto numerically generated fracture networks for a 50 m by 50 m study area. Equivalent permeability for the entire study area was computed from steady state, single phase flow rates generated by a constant pressure gradient parallel to the fracture trends. For flow to get from one side of the simulation area to the other, given the fact that the fracture network was non-percolating, at least part of the flow path included the matrix (non-fractured media). In this manner, the modeling incorporated the effects of the finite lengths of individual fractures and the variability of fracture aperture along that length. Results showed that permeability was strongly dependent on fracture intensity as measured by cumulative trace length, but it was also influenced by average fracture segment length. Fracture patterns of the same cumulative trace length but larger average segment length had higher equivalent permeability than those with smaller average segment lengths (Fig. 4.18).

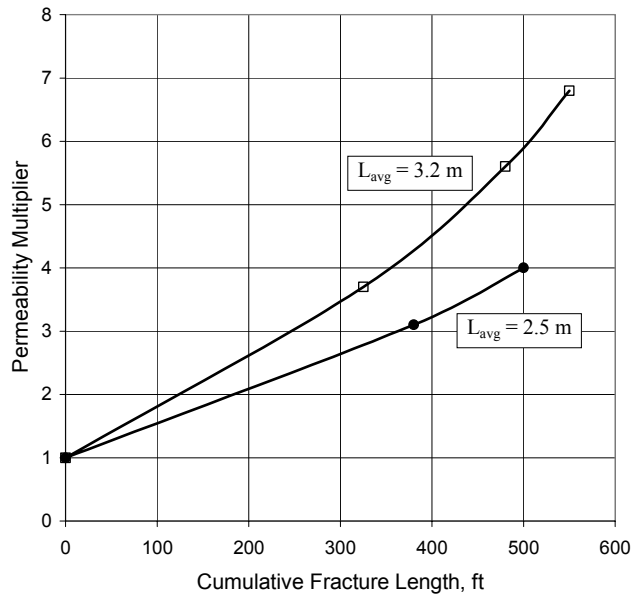


Figure 4.18. Permeability multiplier for the equivalent permeability of a fractured media versus unfractured matrix as a function of cumulative fracture length in a 50m by 50m area for fracture populations with different average segment length.

Nakashima et al. (2000) showed similar fracture permeability versus length distribution relationships for statistically generated fracture patterns, but the geologic controls on fracture pattern attributes were not investigated. Using the geomechanical approach, we can point out what geologic parameters influence fracture network characteristics and ultimately fracture permeability.

As mentioned in the previous section, cumulative fracture length and mean fracture segment lengths for a given imposed strain can be related to the subcritical index. Variations in cumulative fracture trace length, holding other conditions and properties the same, can also be related to the mechanical layer thickness. The layer thickness effect is

related to the oft observed outcrop relationship that fracture spacing is roughly proportional to layer thickness (Bai et al. 2000, Narr & Suppe 1991). Thus, for a given strain, thinner beds generate more cumulative fracture trace length, which implies greater fracture permeability according to the results in Fig. 4.18.

At first glance, this conclusion may seem consistent with the parallel plate law of equation (4.2), where decreasing fracture spacing, S , causes an increase in fracture permeability. However, the mechanical analysis of bed-bounded fractures also shows that fracture aperture is expected to be less in thin beds than in thick beds, all other things equal (Olson 2003). Since fracture permeability has a stronger dependence on aperture than spacing in equation (4.2), it seems that thicker beds might have higher permeability even though their fracture intensity is less. Interestingly, this is a point where the inadequacy of the parallel plate law for large scale permeability estimation is most pronounced. If the assumption of through-going fractures is not true (fracture flow paths are segmented and non-percolating), Philip et al. (2002) showed that a doubling of fracture aperture for identical fracture trace networks, which should have resulted in nearly an order of magnitude equivalent permeability increase according to the parallel plate law, had virtually no effect on equivalent permeability.

Diagenesis Effects on Aperture and Permeability

Although Philip et al. (2002) showed that fracture aperture did not affect permeability as implied in the parallel plate law, they did show that imposing the effects of an emergent threshold on the fracture pattern strongly influenced permeability. The geomechanical simulations for study were made up of fractures divided into multiple short patches or elements. Fracture aperture for a given fracture can vary from element to element, where the narrowest apertures are typically at and near the fracture tips. A dimensionless emergent threshold was defined as a multiple of the mean kinematic aperture of the fracture patches for a given network generated by the geomechanical model. The results of Fig. 4.18 were made assuming an emergent threshold of zero, where all of the kinematically open fracture patches were open to flow (geologically speaking, no mineral precipitation had occurred in the fractures). Increasing the emergent threshold resulted in some of the fracture patches being closed to flow, starting with those that had the smallest kinematic aperture.

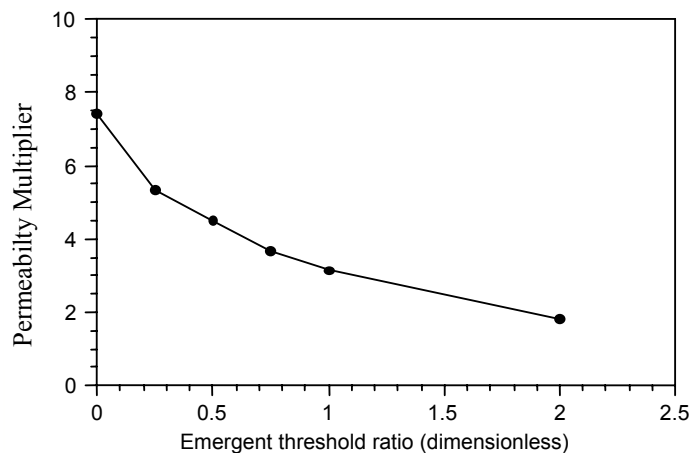


Figure 4.19: The effect of synkinematic cement on equivalent permeability for a simulated fracture pattern.

Since these are typically at the tips of the fractures, filling the fractures with cement not only reduced hydraulic aperture of the fractures but decreased their lengths. It is the diminution of length that will be most important for non-percolating networks, and equivalent fracture permeability decreases dramatically with increasing emergent threshold (Fig. 4.19).

Finally, we analyzed the emergent threshold effects on fracture continuity for more complex fracture patterns than the single parallel fracture set case of Philip et al. (2002). The simulations of Olson et al. (2001) and Philip et al. (2002) assume strong in situ stress anisotropy at the beginning of fracture propagation that forces fractures to propagate in planar, non-interacting paths. However, it is common that natural fractures interact and form curving (Olson & Pollard 1989, Pollard et al. 1982) or orthogonal, ladder-like patterns (Gross 1993, Rives et al. 1994) as shown in Fig. 4.20. Such a pattern was generated geomechanically (Fig. 4.21) by applying a constant strain rate extension in the y direction and holding the strain in the x-direction constant (zero normal displacement). Early propagation is dominated by fractures propagating in the x-direction, relieving fracture promoting stresses acting in y until the principal stresses flip to favor fracture propagation in the y-direction (in response to the fracture promoting stresses caused by the Poisson effect) (Olson 1997).



Figure 4.20. Bedding plane exposure of natural fracture pattern with good trace pattern connectivity (6 inch scale in middle of photo).

Fig. 4.21a shows the resultant fracture trace pattern, showing strong connectivity in both the x and y directions in what would be a percolating fracture network. Fig. 4.21b, however, shows how aperture varies throughout the network, where the thickness of the fracture segments is proportional to kinematic aperture (widths exaggerated for clarity). The wider, gray-filled fractures represent fracture apertures of 1 to 3 mm. The thinner black lines have apertures ranging from 0.1 to 1 mm. Based on the parallel plate law, the

flow resistance of a single fracture by itself (not accounting for surrounding matrix rock) can be characterized as the permeability k_f as

$$k_f = \frac{b^2}{12}. \quad (4.3)$$

Local permeability variations caused by an order of magnitude aperture reduction at the fracture tips from 1 to 0.1 mm would represent a 100 times reduction in local fracture permeability. Finally, if the emergent threshold for this particular fracture pattern were 1 mm, only the fatter gray fracture segments would be left open, and the black connecting fracture segments would be completely mineralized and closed. Thus, based on this qualitative assessment of permeability, analogous to the more quantitative work described in the previous section for parallel fracture sets, it is evident that the interaction of diagenetic and kinematic effects play a pivotal role in determining the flow properties of a given fracture network.

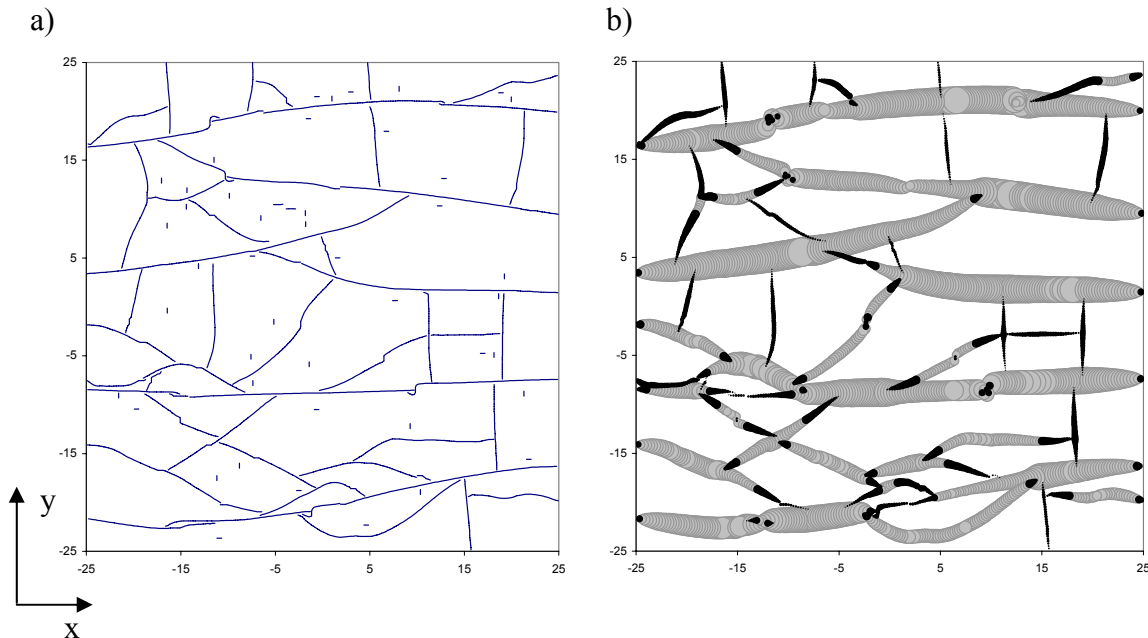


Figure 4.21. Fracture network generated by uniaxial strain in the y -direction (zero strain in x) and starting with an isotropic in situ stress. The body is 50x50 m in map view and the mechanical layer thickness is 8m. The subcritical index used was $n=20$. a) Fracture tracemap with no aperture information. b) Kinematic aperture map where apertures are exaggerated but appropriately scaled (maximum aperture is 3×10^{-3} m).

5. Conclusions

The goal of this research was to develop new technology for the reliable prediction of fracture pattern attributes related to subsurface fluid flow. We focused on predicting natural fracture connectivity, clustering and aperture, attributes that are exceedingly difficult to measure but can be the controlling factors for fluid movement (during injection or extraction) in an oil reservoir. The project involved a multi-disciplinary team, integrating geological observational techniques and modeling to the fluid flow quantification of fractured reservoir blocks. The goal of this research project was met successfully and as a result of our technology transfer effort the results are being implemented.

Nevertheless, the challenges to effective exploration and production are very great, and many remain to be overcome. The research conducted in this study has identified a new avenue for approaching these challenges. There are several issues pertaining to the fundamental processes of fracture opening and sealing that need to be addressed with basic research. The results of this study also point to several areas where additional research could quickly yield practical applications in accurate fluid flow simulation, better seismic fracture characterization, and more efficient exploration and development.

The underlying theme that sets this work apart from previous attempts at fracture characterization and permeability estimation is the integration of mechanical and diagenetic processes in the characterization and modeling effort.

High temperatures and reactive fluids in sedimentary basins dictate that interplay and feedback between mechanical and geochemical processes could significantly influence evolving rock and fracture properties. Not only does diagenetic mineralization fill in once open fractures either partially or completely, it modifies the rock mechanics properties that can control the mechanical aperture of natural fractures. In this study, we have evolved an integrated methodology of fractured reservoir characterization and we have demonstrated how it can be incorporated into fluid flow simulation. The research encompassed a wide range of work from geological characterization methods to rock mechanics analysis to reservoir simulation. With regard to the characterization of mineral infilling of natural fractures, the strong interplay between diagenetic and mechanical processes is documented and shown to be of vital importance to the behavior of many types of fractured reservoirs. Although most recent literature emphasizes Earth stress orientation, cementation in fractures is likely a critically important control on porosity, fluid flow attributes, and even sensitivity to effective stress changes. The diagenetic processes of dissolution and partial cementation are key controls on the creation and distribution of open natural fractures within hydrocarbon reservoirs.

The continuity of fracture-porosity is fundamental to how fractures conduct fluids. In this study, we have made a number of important discoveries regarding fundamental properties of fractures, in particular related to the prevalence of kinematically significant structures (crack-seal texture) within otherwise porous, opening-mode fractures, and the presence of an aperture size threshold below which fractures are completely filled and above which porosity is preserved. These observations can be linked to models of quartz cementation. Significant progress has been made as well in theoretical fracture mechanics and geomechanical modeling, allowing prediction of spatial distributions of fractures that

mimic patterns observed in nature. Geomechanical modeling shows the spatial arrangement of opening mode fractures (joints and veins) is controlled by the subcritical fracture index of the material. In particular, we have been able to identify mechanisms that control the clustering of fractures in slightly deformed rocks. Fracture mechanics testing of a wide range of clastic rocks shows that the subcritical index is sensitive to diagenetic factors. We show geomechanical simulations of fracture aperture development can be linked to diagenetic models, modifying fracture porosity as fractures grow, and affect the dynamics of fracture propagation. Fluid flow simulation of representative fracture pattern realizations shows how integrated modeling can give new insight into permeability assessment in the subsurface. Using realistic, geomechanically generated fracture patterns, we propose a methodology for permeability estimation in non-percolating networks.

6. References

- Atkinson, B. K. 1984. Subcritical Crack Growth in Geological Materials. *Journal of Geophysical Research* **89**(June 10, 1984), 4077-4114.
- Atkinson, B. K. & Meredith, P. G. 1987. Experimental Fracture Mechanics Data for Rocks and Minerals. In: *Fracture Mechanics of Rock* (edited by Atkinson, B. K.). Academic Press, London, 477-525.
- Bai, T., Pollard, D. D. & Gao, H. 2000. Explanation for fracture spacing in layered materials. *Nature* **403**, 753-756.
- Beaudoin, J. J. 1987. Subcritical crack growth in low-porosity cement systems. *Journal of Material Science Letters* **6**(2), 197-199.
- Bjørklykke, K. & Egeberg, P. K. 1993. Quartz cementation in sedimentary basins. *AAPG Bulletin* **77**, 1538-1548.
- Bjørkum, P. A., Oelkers, E. H., Nadeau, N. H., Walderhaug, O. & Murphy, W. F. 1998. Porosity prediction in quartzose sandstones as a function of time, temperature, depth, stylolite frequency, and hydrocarbon saturation. *AAPG Bulletin* **82**(4), 637-648.
- Delaney, P. T., Pollard, D. D., Ziony, J. L. & Mckee, E. H. 1986. Field Relations Between Dikes and Joints: Emplacement Processes and Paleostress Analysis. *Journal of Geophysical Research* **91**(B5), 4920-4938.
- Draper, N. R. & Smith, H. 1981. *Applied Regression Analysis*. Wiley and Sons.
- Dyer, J. R. 1983. Jointing in sandstones, Arches National Park, Utah. Unpublished Ph. D. dissertation thesis, Stanford University.
- Evans, A. G. 1972. A method for evaluating the time-dependent failure characteristics of brittle materials and its application to polycrystalline alumina. *Journal of Material Science* **7**, 1137-1146.
- Gesing, A. J. & Bradt, R. C. 1983. A microcrack model for the effect of grain size on slow crack growth in polycrystalline Al_2O_3 . In: *Fracture Mechanics of Ceramics* (edited by Bradt, R. C., Evans, A. G., Hasselman, D. P. H. & Lange, F. F.). Plenum Press, New York, 569-590.
- Gross, M. R. 1993. The Origin and Spacing of Cross Joints: Examples from the Monterey Formation, Santa Barbara Coastline, California. *Journal of Structural Geology* **15**(6), 737-751.
- Holder, J., Olson, J. E. & Philip, Z. 2001. Experimental determination of subcritical crack growth parameters in sedimentary rock. *Geophysical Research Letters* **28**(4), 599-602.
- Lander, R. H. & Walderhaug, O. 1999. Porosity prediction through simulation of sandstone compaction and quartz cementation. *AAPG Bulletin* **83**, 433-449.
- Laubach, S. E. 1988. Subsurface fractures and their relationship to stress history in East Texas Basin sandstone. *Tectonophysics* **156**(1-2), 37-49.
- Laubach, S. E. 2003. Practical Approaches to Identifying Sealed and Open Fractures. *AAPG Bulletin* **87**(4), 561-579.
- Laubach, S. E., Olson, J. E. & Gale, J. 2004a. Are open fractures necessarily aligned with maximum horizontal stress? *Earth and Planetary Science Letters* **222**(1), 191-195.

- Laubach, S. E., Reed, R. M., Olson, J. E., Lander, R. H. & Bonnell, L. M. 2004b. Coevolution of crack-seal texture and fracture porosity in sedimentary rocks: cathodoluminescence observations of regional fractures. *Journal of Structural Geology* **26**, 967-982.
- Lawn, B. R. & Wilshaw, T. R. 1975. *Fracture of Brittle Solids*. Cambridge University Press, Cambridge.
- Lough, M. F., Lee, S. H. & Kamath, J. 1996. A New Method to Calculate the Effective Permeability of Grid Blocks Used in the Simulation of Naturally Fractured Reservoirs. In: *ATCE SPE*, Denver, CO, 493-499.
- McBride, E. R. 1989. Quartz cement in sandstones: a review. *Earth-Science Reviews* **26**, 69-112.
- Nakashima, T., Sato, K., Arihara, N. & Yazawa, N. 2000. Effective permeability estimation for simulation of naturally fractured reservoirs. In: *SPE Asia Pacific Oil and Gas Conference and Exhibition*, Brisbane, Australia.
- Narr, W. & Suppe, J. 1991. Joint Spacing in Sedimentary Rocks. *Journal of Structural Geology* **13**(9), 1037-1048.
- Noh, M. H. 2003. Reactive Transport Modeling in Fractures and Two-phase Flow. Unpublished Ph.D. thesis, The University of Texas.
- Noh, M. H. & Lake, L. W. 2002. Geochemical Modeling of Fracture Filling. In: *SPE/DOE Thirteenth Symposium on Improved Oil Recovery*, Tulsa, Oklahoma, 1-11.
- Oelkers, E. H., Bjørkum, P. A. & Murphy, W. F. 1996. A petrographic and computational investigation of quartz cementation and porosity reduction in North Sea sandstones. *American Journal of Science* **296**, 420-452.
- Oelkers, E. H., Bjørkum, P. A., Walderhaug, O., Nadeau, N. H. & Murphy, W. F. 2000. Making diagenesis obey thermodynamics and kinetics: the case of quartz cementation in sandstones from offshore mid-Norway. *Applied Geochemistry* **15**, 295-309.
- Olson, J. & Pollard, D. D. 1989. Inferring paleostresses from natural fracture patterns: A new method. *Geology* **17**, 345-348.
- Olson, J. E. 1993. Joint Pattern Development: Effects of Subcritical Crack-Growth and Mechanical Crack Interaction. *Journal of Geophysical Research* **98**(B7), 12,251-12,265.
- Olson, J. E. 1997. Natural fracture pattern characterization using a mechanically-based model constrained by geologic data - moving closer to a predictive tool. In: *36th U. S. Rock Mechanics Symposium*, New York City.
- Olson, J. E. 2003. Sublinear Scaling of Fracture Aperture Versus Length: an exception or the rule? *Journal of Geophysical Research* **108**(B9), 2413.
- Olson, J. E. 2004. Predicting fracture swarms -- the influence of subcritical crack growth and the crack-tip process zone on joint spacing in rock. In: *The initiation, propagation, and arrest of joints and other fractures: A field workshop dedicated to the memory of Paul Hancock* (edited by Engelder, T. & Cosgrove, J.). Geological Society of London.
- Olson, J. E., Laubach, S. E. & Lander, R. H. 2004. Improving fracture permeability prediction by combining geomechanics and diagenesis. In: *Gulf Rocks - 6th North America Rock Mechanics Symposium*, Houston, TX.

- Olson, J. E., Qiu, Y., Holder, J. & Rijken, P. 2001. Constraining the Spatial Distribution of Fracture Networks in Naturally Fractured Reservoirs Using Fracture Mechanics and Core Measurements. In: *2001 SPE Annual Technical Conference and Exhibition*, New Orleans, LA.
- Philip, Z., Jennings, J. W., Jr., Olson, J. E. & Holder, J. 2002. Modeling Coupled Fracture-Matrix Fluid Flow in Fracture Patterns Generated using a Geo-Mechanical Crack Growth Simulator. In: *2002 SPE Annual Technical Conference and Exhibition*, San Antonio, TX.
- Pollard, D. D. 1987. Elementary fracture mechanics applied to the structural interpretation of dykes. In: *Mafic dyke swarms; a collection of papers based on the proceedings of an international conference* (edited by Halls, H. C. e. & Fahrig, W. F. e.) **34**, Mississauga, ON, Canada, 5-24.
- Pollard, D. D., Segall, P. & Delaney, P. T. 1982. Formation and Interpretation of Dilatant Echelon Cracks. *Geological Society of America Bulletin* **93**(Dec. 1982), 1291-1303.
- Renshaw, C. E. 1993. Connectivity and Fluid Flow Within Physically-Based Fracture Networks. Dept. of Applied Earth Sciences, Stanford University, Stanford, 1-29.
- Renshaw, C. E. & Pollard, D. D. 1994. Numerical Simulation of Fracture Set Formation: A Fracture Mechanics Model Consistent with Experimental Observations. *Journal of Geophysical Research* **99**(B5), 9359-9372.
- Rijken, P., Holder, J., Olson, J. E. & Laubach, S. 2002. Predictiong Fracture Attributes in the Travis Peak Formation using Quantitative Mechanical Modeling and Structural Diagenesis. In: *52 Annual Convention Gulf Coast Association of Geologic Societies*.
- Rives, T., Rawnsley, K. D. & Petit, J. P. 1994. Analogue Simulation of Natural Orthogonal Joint Set Formation in Brittle Varnish. *Journal of Structural Geology* **16**(3), 419--429.
- Segall, P. 1984. Formation and Growth of Extensional Fracture Sets. *Geological Society of America Bulletin* **95**(Apr. 1984), 454-462.
- Swanson, P. L. 1984. Subcritical Crack Growth and Other Time- and Environment-Dependent Behavior in Crustal Rocks. *Journal of Geophysical Research* **89**(B6 (June 10, 1984)), 4137-4152.
- Van Golf-Racht, T. D. 1984. Fundamentals of Fractured Reservoir Engineering. *Developments in Petroleum Science* **12**, 199-208.
- Walderhaug, O. 1994. Precipitation rates for quartz cement in sandstones determined by fluid-inclusion mircothermometry and temperature-history modeling. *Journal of Sedimentary Research* **A64**, 324-333.
- Walderhaug, O. 1996. Kinetic modeling of quartz cementation and porosity loss in deeply buried sandstone reservoirs. *AAPG Bulletin* **80**, 731-745.
- Walderhaug, O. 2000. Modeling quartz cementation and porosity loss in Middle Jurassic Brent Group sandstones of the Kvitebjørn Field, Northern North Sea. *AAPG Bulletin* **84**, 1325-1339.
- Wangen, M. 1998. Modeling porosity evolution and cementation of sandstones. *Marine and Petroleum Geology* **15**(5), 453-465.
- Williams, D. P. & Evans, A. G. 1973. A simple method for studying slow crack growth. *Journal of Testing and Evaluation* **1**, 264-270.

7. Appendix – Publications

What follows are publications for the third year of this project.

Refereed Archival Publications:

- Laubach, S. E., Olson, J. E. & Gale, J. 2004a. Are open fractures necessarily aligned with maximum horizontal stress? *Earth and Planetary Science Letters* **222**(1), 191-195.
- Laubach, S., Olson, J., Reed, R., Lander, R., & Bonnell, L., 2004. Opening histories of fractures in sandstone. In: The initiation, propagation, and arrest of joints and other fractures: A field workshop dedicated to the memory of Paul Hancock (edited by Engelder, T. & Cosgrove, J.). Geological Society of London.
- Laubach, S. E., Reed, R. M., Olson, J. E., Lander, R. H. & Bonnell, L. M. 2004. Coevolution of crack-seal texture and fracture porosity in sedimentary rocks: cathodoluminescence observations of regional fractures. *Journal of Structural Geology* **26**, 967-982.
- Olson, J. E. 2003. Sublinear Scaling of Fracture Aperture Versus Length: an exception or the rule? *Journal of Geophysical Research* **108**(B9), 2413.
- Olson, J. E. 2004. Predicting fracture swarms -- the influence of subcritical crack growth and the crack-tip process zone on joint spacing in rock. In: The initiation, propagation, and arrest of joints and other fractures: A field workshop dedicated to the memory of Paul Hancock (edited by Engelder, T. & Cosgrove, J.). Geological Society of London.

Technical meeting papers and presentations:

- Olson, J. E., Holder, J., and Rijken, P. 2002. Quantifying the Fracture Mechanics Properties of Rock for Fractured Reservoir Characterization. Arlington, TX. October 20-23.
- Olson, J. E., Laubach, S. E. & Lander, R. H. 2004. Improving fracture permeability prediction by combining geomechanics and diagenesis. In: Gulf Rocks - 6th North America Rock Mechanics Symposium, Houston, TX.
- Park, N., Holder, J., and Olson, J.E. 2004. Discrete Element Modeling of Fracture Toughness Tests in Weakly Cemented Sandstone. Gulf Rocks - 6th North America Rock Mechanics Symposium, Houston, TX.
- Rijken, Peggy, Holder, Jon, Olson, Jon E. and Laubach, Stephen E. 2002. Natural Fracture Characterization within the Travis Peak Formation, East Texas. Gulf Coast Association of Geologists Society. Austin, TX. October 30-November 1.

Theses and Dissertations

- Noh, M. H. 2003. Reactive Transport Modeling in Fractures and Two-phase Flow. The University of Texas at Austin, Ph.D. thesis.
- Philip, Zeno. 2003. Incorporating subcritical crack growth mechanics into natural fracture characterization for improved reservoir simulation. The University of Texas at Austin, Ph.D. thesis, 198 pages.



ELSEVIER

Available online at www.sciencedirect.com

SCIENCE @ DIRECT®

Earth and Planetary Science Letters 222 (2004) 191–195

EPSL

www.elsevier.com/locate/epsl

Are open fractures necessarily aligned with maximum horizontal stress?

Stephen E. Laubach^{a,*}, Jon E. Olson^{a,b}, Julia F.W. Gale^a

^a*Bureau of Economic Geology, Jackson School of Geosciences, The University of Texas at Austin, Austin, TX 78713, USA*

^b*Department of Petroleum and Geosystems Engineering, The University of Texas at Austin, Austin, TX 78713, USA*

Received 15 December 2003; received in revised form 17 February 2004; accepted 17 February 2004

Abstract

Fluid flow in fractured rock is an increasingly central issue in recovering water and hydrocarbon supplies and geothermal energy, in predicting flow of pollutants underground, in engineering structures, and in understanding large-scale crustal behaviour. Conventional wisdom assumes that fluids prefer to flow along fractures oriented parallel or nearly parallel to modern-day maximum horizontal compressive stress, or S_{Hmax} . The reasoning is that these fractures have the lowest normal stresses across them and therefore provide the least resistance to flow. For example, this view governs how geophysicists design and interpret seismic experiments to probe fracture fluid pathways in the deep subsurface. Contrary to these widely held views, here we use core, stress measurement, and fluid flow data to show that S_{Hmax} does not necessarily coincide with the direction of open natural fractures in the subsurface (>3 km depth). Consequently, in situ stress direction cannot be considered to predict or control the direction of maximum permeability in rock. Where effective stress is compressive and fractures are expected to be closed, chemical alteration dictates location of open conduits, either preserving or destroying fracture flow pathways no matter their orientation.

© 2004 Elsevier B.V. All rights reserved.

Keywords: stress; fractures; diagenesis; fluid flow; shear wave anisotropy; hydrocarbons

1. Introduction

Are vertical fractures in the Earth that are aligned with the direction of present-day maximum horizontal compressive stress preferentially open compared to their nonparallel counterparts? If they are, there are fundamental implications for crustal properties and for interpreting geophysical data. A common claim is that misaligned fractures *will* tend to close because of the

prodigious compressive normal stress they experience [1–6]. The view that S_{Hmax} and open fractures tend to align is popular for several reasons. S_{Hmax} and open fractures locally *are* aligned, in some cases because fractures formed in the contemporary stress field. Some fractures *are* sensitive to changes in effective stress [2,4]. Two decades of observations of azimuthal shear wave velocity anisotropy have been interpreted to result from open fractures preferentially aligned by the current stress field [5,6].

Here we show that, contrary to widespread expectation, opening-mode fractures misaligned with respect to modern S_{Hmax} may not close. Divergence

* Corresponding author. Tel.: +1-512-471-6303; fax: +1-512-471-0140.

E-mail address: steve.laubach@beg.utexas.edu (S.E. Laubach).

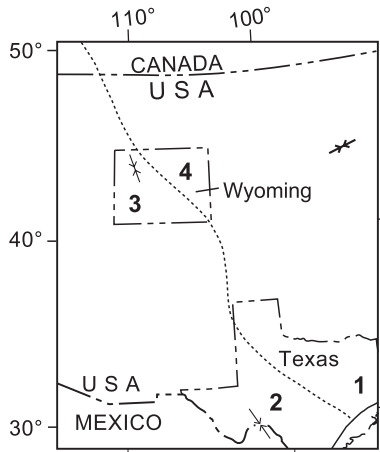


Fig. 1. Study areas in the western United States. Dotted line is the boundary between midcontinent compressional stress province and Cordilleran extensional stress province [9]. (1) East Texas Basin; (2) Val Verde Basin, West Texas; (3) Green River Basin; (4) Powder River Basin. Measurements within study wells defined orientation and magnitude of the local stress field; results show that fractures are not critically stressed (c.f. [18]).

between S_{Hmax} and open fractures that also demonstrably contribute to fluid flow ranges from a few degrees to 90° . These findings, based on high-quality fracture and stress data sets in representative areas, and new appreciation of chemical processes that accompany fracture in the Earth, suggest that instead

of being a dominant process, mechanical closure of fractures in many settings may be rare.

2. Examples

Over the past 20 years, debate on the loading conditions of opening-mode fracture *formation* led to a consensus that fractures primarily accommodating opening displacement propagate along a plane of zero shear stress in isotropic rock, specifically the plane perpendicular to the least compressive principal stress [7,8]. This pattern makes such fractures indicators of past stress orientations, inasmuch as such vertical fractures include the maximum horizontal stress direction *at the time of their formation*. Yet, many fractures in the Earth formed in the distant past. Should we expect parallelism between fractures open *now* and present-day S_{Hmax} ? The past loading configurations will match only the *contemporary* stress field (S_{Hmax}) in special circumstances. Depending on tectonic history, fractures may or may not remain aligned with maximum horizontal stress (S_{Hmax}).

Modern state of stress results primarily from gravitational and tectonic loads that define stress provinces [9] (Fig. 1). We compared S_{Hmax} indicators and open fractures in three stress provinces (Fig. 2a–h). The fractures lack evidence of shear failure. They are

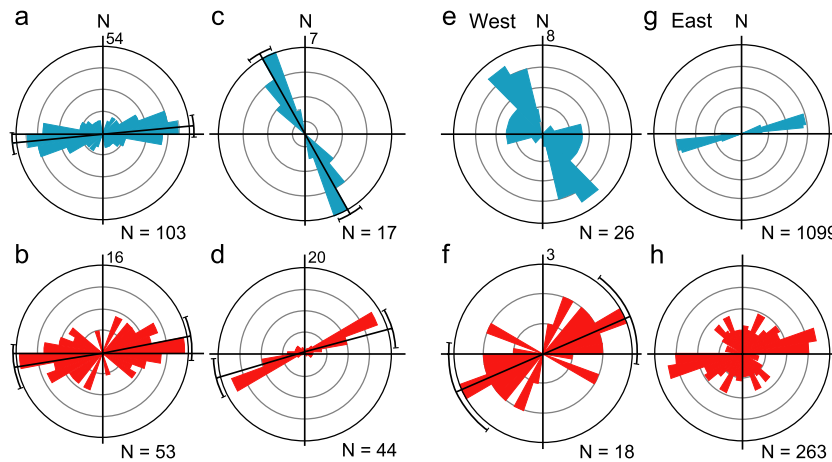


Fig. 2. Rose diagrams of maximum compressive stress (S_{Hmax}) (upper row) and open fracture strike (lower row) for study areas 1–4. (a) S_{Hmax} and (b) fracture strike, area 1. Average ENE fracture strike is similar to S_{Hmax} trends, but open fractures ($n=51$) have a spread of 130° ; (c) S_{Hmax} and (d) fracture strike, four West Texas wells, area 2. (e) S_{Hmax} and (f) fracture strike, western Green River Basin [14,15], area 3; (g) S_{Hmax} and (h) fracture strike southern Powder River Basin, horizontal well image log data [14], area 4.

nearly vertical and have apertures of as much as several millimeters. We also measured mineral deposits (cement) in fractures and host rocks. The fractures we measured are typical of low-porosity, moderately cemented (10–20% whole rock volume) sandstones but similar structures are present in other rock types [8].

We first consider an example that shows the pitfall of using alignment by itself to infer relations among in situ stress and open fractures (Fig. 2a and b). In East Texas, the approximate alignment of maximum horizontal stress and open fractures is most likely a coincidence related to the relatively simple geologic history of this region reflecting a long-lived regime of gravity-driven movement of sediments and rock toward the subsiding Gulf of Mexico. Dated faults show that S_{Hmax} during Late Cretaceous and early Tertiary time is substantially the same as the modern stress direction. Burial history and fluid inclusion data indicate that fractures in these rocks formed in the Late Cretaceous [11] when sandstones were at depths of between 900 and 1500 m.

Although delicate crystals in fractures show no evidence of abrasion, fracturing, or dissolution [10], demonstrating that fractures having apertures >5 mm were open at depths >3 km, it is doubtful that fracture apertures reflect current loading conditions. Formation pressures in intervals with open fractures are close to hydrostatic (10 MPa/km), whereas minimum horizontal stress is approximately 14 MPa/km. Thus, judging from mechanics, even favorably oriented fractures parallel to S_{Hmax} should be closed because of the large net closing stress perpendicular to fracture faces. Moreover, while *generally* paralleling S_{Hmax} , open fractures have a wide dispersion in strike, and some are misaligned with local S_{Hmax} by amounts that range from a few degrees to 40° .

Our second example illustrates the misalignment of S_{Hmax} and open fractures. Permian sandstones in West Texas contain subvertical, opening-mode fractures having ENE strikes. Borehole breakouts from the same wells show a NNW S_{Hmax} orientation (Fig. 2c). This result proves that flow is not favored along fractures that are oriented parallel or nearly parallel to the maximum horizontal stress direction, in contrast to conventional wisdom. Narrow bridges of cement within otherwise open fractures could account for their resistance to closure. Identical structures exist

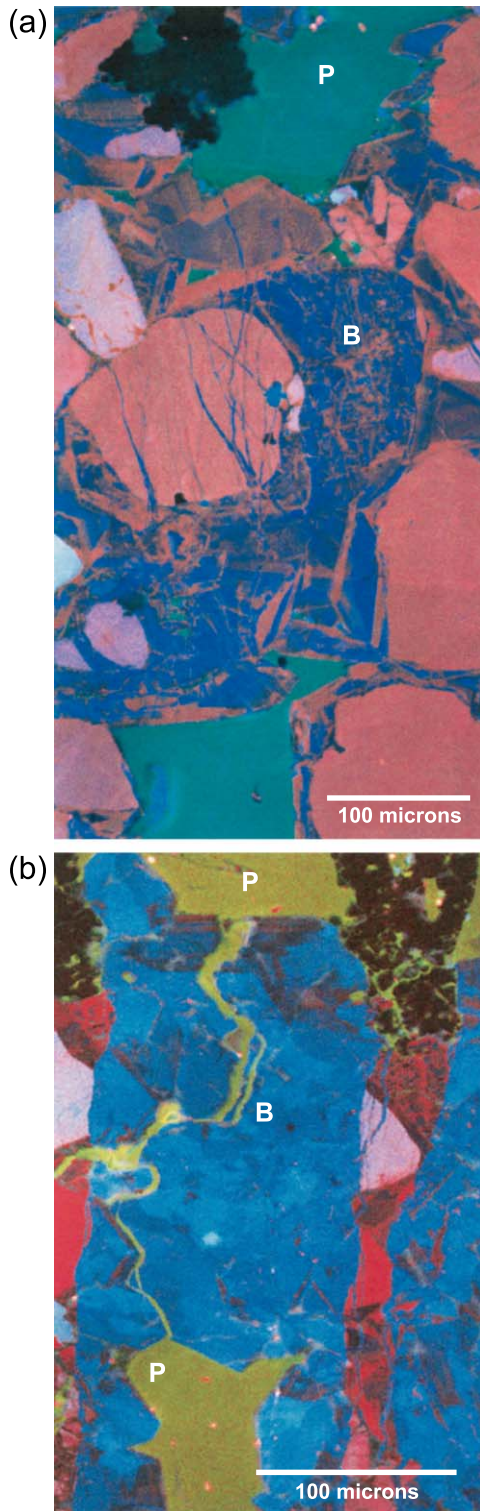
in the fractures from East Texas. Moreover, whereas some fractures are open and lined with cement, others are sealed. Effects of these cements on fluid flow can be isolated in a key well pair where engineering and geologic parameters (other than fractures) are closely similar. Gas production confirms that the well that penetrated open fractures shows enhanced flow compared with that of a second well, which penetrated sealed fractures having the same orientation.

The final example shows both aligned and misaligned open fractures and S_{Hmax} near a stress province boundary, where the maximum horizontal stress rotates 90° from one end of a transect to the other. A persistent set of natural fractures having unidirectional strike within Upper Cretaceous sandstones is open across this basin (Fig. 2e and g). In the east, conductive fractures strike ENE, nearly parallel to current S_{Hmax} . In the west, open fractures are perpendicular to current S_{Hmax} . Production data demonstrate that in the west fractures conduct fluid despite highly oblique angles between fractures and S_{Hmax} [12–14]. In both areas, fractures lacking mineral fill are essential for fluid flow.

3. Discussion and conclusions

These examples show that open fractures can have any strike relative to S_{Hmax} and that chemical processes can cause resistance to fracture closure. In all areas, stress orientation data is from high-quality borehole breakouts and other reliable stress direction measurements including drilling-induced fractures, various core tests, and overcored or remotely monitored hydraulic fractures, and results are consistent with regional stress maps. Open fractures governing fluid flow are documented in extensive core collections that include horizontal well data and associated production data. These results document a fundamental discrepancy between observation and the expectation that open fractures are necessarily oriented parallel or nearly parallel to modern-day maximum horizontal compressive stress, or S_{Hmax} .

Chemical process can account for resistance of fractures to closure. In all areas, we observe isolated cement bridges within fractures (Fig. 3) and petro-



graphic evidence that fractures formed prior to the end of cement precipitation in the rock mass [12]. Fractures at depths of 4–6 km or more form in environments where hot ($>100^{\circ}\text{C}$), mineral-laden water strongly favors precipitation of partial quartz coatings and spatially isolated, pillarlike cement bridges [11,12]. Open fractures frequently contain these bridges, which are natural byproducts of cement precipitation while fractures are opening [12]. Similar structures occur in carbonate rocks. Modelling of cement precipitation shows that at temperatures typical of sedimentary basins, these structures are likely to be ubiquitous [11] and we have found such bridges in every suite of opening-mode fractures inspected from rocks below approximately 3 km as well as in many rocks at shallower depths (which may have been uplifted from greater depth), a data set that includes most of the major basins in the continental United States and many basins in other parts of the world.

The prevalence of strong, spatially isolated mineral bridges has not been previously appreciated. Where such mineral bridges are present, they will resist fracture closure. Laboratory tests show that partial mineral fills can make fractures insensitive to changes in effective stress [15–17].

Another mechanism that can increase the resistance of natural fractures to closing is the precipitation of cement *in the host rock* while or immediately after the fractures form, essentially freezing the open fractures and their associated strain field in place. Lander et al. [11] showed that as much as 20% whole rock volume of quartz cement can precipitate in a rock's pore space after fractures form, without sealing or even bridging fractures. Such a process is likely to be widespread in sedimentary basins where temperatures are approximately 100°C or above.

Fig. 3. Cathodoluminescence images of partly mineral bridged open fractures. (a) Cretaceous sandstone, East Texas Basin (P indicates open fracture pore space, B indicates a quartz bridge, fracture walls parallel long dimension of image, bar = 100 μm). (b) Jurassic sandstone, northeastern Mexico (P indicates open fracture pore space, B indicates quartz mineral bridge). In both examples, crack seal texture in bridge, marked by cement-filled microfractures (thin lines) and wall rock inclusions, shows bridge formation was contemporaneous with fracture opening [12].

On the other side of the spectrum, cement may close fractures regardless of stress orientation by filling them with precipitate. The chemical processes that lead to sealing of large fractures apparently differ from those that produce local bridges, and are not well understood, yet empirical evidence shows that heterogeneous patterns of infilling of large fractures by late cements is widespread [12]. This heterogeneity in infilling is evident in the cases considered here. For example, not all fractures parallel to S_{Hmax} in East Texas and Wyoming are open. Core demonstrates that sealed and open fractures having identical strike can be interspersed over vertical distances that range from a few meters or less to decimeters and over lateral distances of meters to kilometers. It is only in those fractures where mineral filling is incomplete that significant permeability exists. In West Texas, production and core data demonstrate that it is the degree of cement fill in natural fractures rather than fracture orientation that governs fluid flow. Two wells intercepted fractures having identical strike in the completion interval, where matrix porosity, permeability, sandstone thickness, and facies, as well as drilling and completion practice, are indistinguishable. In both wells, S_{Hmax} is normal to fractures, but flow occurs only where fractures are not sealed with cement.

Our results show that contrary to widely held views, parallelism of modern-day stress directions and open fractures is not good evidence, by itself, that the current stress field can be used to predict the occurrence of open natural fractures. In the absence of reliable measurements of both open fracture strike and S_{Hmax} , these features should not be presumed to be parallel. Moreover, even in the most favorable mechanical environment, precipitated cements can seal any orientation fracture. Consequently, the chemical history of fractures and the surrounding rock may provide a clearer insight than stress data into which fractures are open to fluid flow.

Acknowledgements

We gratefully acknowledge comments from D. D. Pollard and support by the US Department of Energy Office of Basic Energy Sciences and the Fracture Research and Application Consortium. [VC]

References

- [1] J.H. Queen, W.D. Rizer, An integrated study of seismic anisotropy and the natural fracture system at the Conoco Borehole test facility, Kay County, Oklahoma, *J. Geophys. Res.* 95 (1990) 11255–11273.
- [2] K.J. Heffer, J. Lean, Earth stress orientation—a control on, and a guide to, flooding directionality in a majority of reservoirs, in: W. Linville (Ed.), *Reservoir Characterization III*, PennWell Books, Tulsa, 1993, pp. 799–822.
- [3] J.E. Gaiser, Stress direction hints and flow, *AAPG Explor.* 24 (2003) 36–39.
- [4] L.W. Teufel, D.W. Rhett, H.E. Farrell, Effect of reservoir depletion and pore pressure drawdown on in situ stress and deformation in the Ekofisk field, North Sea, *Proc. U.S. Rock Mech. Symp.* 32 (1991) 63–72.
- [5] S. Crampin, Geological and industrial implications of extensive-dilatancy anisotropy, *Nature* 328 (1987) 491–496.
- [6] S. Crampin, J.H. Lovell, A decade of shear-wave splitting in the Earth's crust: what does it mean? What use can we make of it? And what should we do next? *Geophys. J. Int.* 107 (1991) 387–407.
- [7] B.R. Lawn, T.T. Wilshaw, *Fracture of Brittle Solids*, Cambridge Univ. Press, Cambridge, 1975. 204 pp.
- [8] D.D. Pollard, A. Aydin, Progress in understanding jointing over the past century, *Geol. Soc. Amer. Bull.* 100 (1988) 1181–1204.
- [9] M.L. Zoback, M.D. Zoback, Tectonic stress field of the continental United States, in: L.C. Pakiser, W.D. Mooney (Eds.), *GSA Memoir*, vol. 172, 1989, pp. 523–539.
- [10] S.E. Laubach, Subsurface fractures and their relationship to stress history in East Texas basin sandstone, *Tectonophysics* 156 (1988) 37–49.
- [11] R.H. Lander, J.F.W. Gale, S.E. Laubach, L.M. Bonnell, Interaction between quartz cementation and fracturing in sandstone, *AAPG Annu. Conv. Prog.* 11 (2002) A98.
- [12] S.E. Laubach, Practical approaches to identifying sealed and open fractures, *AAPG Bull.* 87 (2003) 561–579.
- [13] L.F. Krystinik, Predicting fractures 5 km down: integrated reservoir characterization, UPR/DOE Rock Island 4-H well, *AAPG Bull.* 84 (2000) 1878.
- [14] W.L. Parks, M.S. Gale, Exploring overpressured, naturally fracture reservoirs in the Powder River Basin, Wyoming: a multi-disciplinary effort, *AAPG Powder River Basin Symp.*, (1999) 2–11.
- [15] C. Dyke, How sensitive is natural fracture permeability at depth to variation in effective stress? in: L.R. Myer, et al. (Eds.), *Fractured and Jointed Rock Masses*, Balkema, Rotterdam, 1995, pp. 81–88.
- [16] W.B. Durham, Laboratory observations of the hydraulic behaviour of a permeable fracture from 3800 m depth in the KTB pilot hole, *J. Geophys. Res.* 102 (18) (1997) 18405–18416.
- [17] N.R. Morrow, K.R. Brower, S. Ma, J.S. Buckley, Fluid flow in healed fractures, *J. Pet. Technol.* 42 (1990) 1310–1318.
- [18] C.A. Barton, D. Moos, M.D. Zoback, Fluid flow along potentially active faults in crystalline rock, *Geology* 23 (1995) 683–686.

Opening histories of fractures in sandstone

S. E. LAUBACH^{1,2}, R. H. LANDER^{1,3}, L. M. BONNELL^{1,3}, J. E. OLSON² & R. M. REED¹

¹*Bureau of Economic Geology, John A. and Katherine G. Jackson School of Geosciences,
University of Texas at Austin, Austin, TX 78713, USA*

²*Department of Petroleum and Geosystems Engineering, University of Texas at Austin, Austin,
TX 78713, USA*

(e-mail: Steve.Laubach@beg.utexas.edu)

³*Geocosm L.L.C., 3311 San Mateo, Austin, TX 78729, USA*

Abstract: High-resolution scanning electron microscope (SEM)-based cathodoluminescence images were used to reconstruct incremental fracture opening in regional opening-mode fractures in sandstone. Opening is recorded by crack–seal texture in isolated mineral bridges that span opening-mode fractures *formed* in sandstone at moderate–great depth (c. 1000–6000 m). We restored opening histories of nine representative fractures with apertures of millimetres in five sandstones from five sedimentary basins. Gaps created by fracture widening in 11 bridges range from less than 1 μm to more than 1 mm, but nearly all are less than 20 μm and most are less than 5 μm . These are the opening amounts that could be spanned by cement growth in these diagenetic environments. Our observations are the first evidence of opening amounts from mostly porous, opening-mode (joint-like) fractures formed in diagenetic environments. Patterns are consistent with a new structural diagenetic model of bridge growth that can use opening patterns to indicate rate of fracture opening as a function of time.

Cement is typically present in fractures in sedimentary rocks that have been exposed to moderate–deep burial conditions (c. 1000–>6000 m). Thickness of these cements ranges from micron deposits that line fracture walls to crystalline masses that fill fractures with apertures of centimetres and more. Cement can fill a porous, permeable fracture to block flow (Laubach 2003). An understanding of how cement precipitates in fractures has practical value for predicting bulk permeability of a fractured rock. Cements that record fracture-opening histories (crack–seal textures) can provide insight into the timing of fractures relative to a rock's cement precipitation history (Laubach 1988). Opening amounts recorded in fracture cement constrain fracture opening, propagation and arrest history.

Fracture opening

A structural association in opening-mode fractures in moderately–deeply buried sedimentary rocks includes isolated bridges of cement deposited during fracture opening (Figs 1 and 2). Bridges are cement deposits in otherwise open, joint-like fractures. They have rod or pillar-like shapes that are typically oriented normal to, and connect opposite, opening-mode fracture walls. Bridges are composed of wall-rock fragments and cement arranged in crack–seal texture that records repeated cracking and local cementing of cracks within the bridges.

Unlike crack–seal textures described from metamorphic veins, where the entire fracture is commonly filled with cement (e.g. Ramsay 1980), these fractures in sedimentary rock can have extensive porosity and only a thin veneer of contemporaneous cement on areas of fracture wall between bridges (Laubach 1988; Lander *et al.* 2002). Although typically present only in some fractures in a given area and generally small and inconspicuous, crack–seal bridges are widespread and they provide evidence of opening amounts from mostly open, joint-like fractures formed in diagenetic environments.

Recent structural diagenetic modelling and experiments clarify how isolated crack–seal bridges form. According to Lander *et al.* (2002), such bridges arise when: (1) the increase in fracture aperture is small for individual fracture events (e.g. microns); (2) the rate of aperture increase integrated over geological timescales is less than the rate of precipitation on anhedral surfaces; and (3) new anhedral nucleation surfaces are periodically created by fracturing of quartz crystals. Laboratory crystal-growth experiments show that, although crystal growth is faster in the direction of the quartz *c*-axis than precipitation in the direction of the *a*-axis, slower growth rates on euhedral crystals compared with fresh fracture surfaces is a key to whether overall cement precipitation keeps up with fracture opening (Lander *et al.* unpublished results 2000). The Lander *et al.* (2002) model is based on concepts that rock surface area and temperature

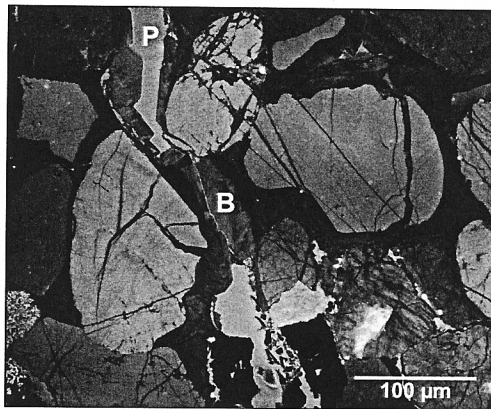


Fig. 1. Cement bridge with uniform texture marking a single opening–sealing event. Scanned-CL image: P, porosity; B, bridge. Sandstone, Venezuela, depth 4187 m. Quartz cement with red luminescence predates fracture opening; blue quartz is syn-kinematic. Note that the amount of blue quartz cement varies along fracture walls.

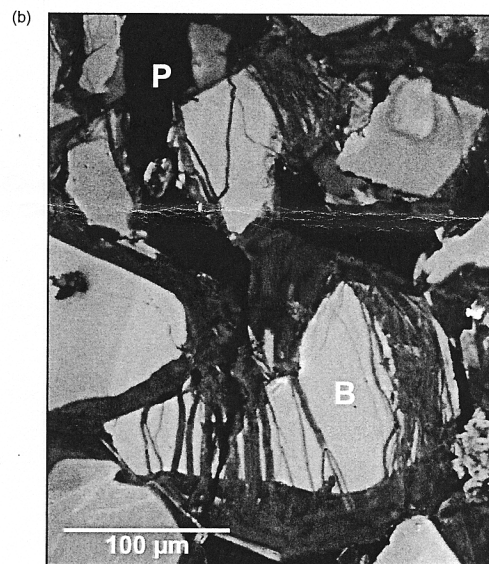
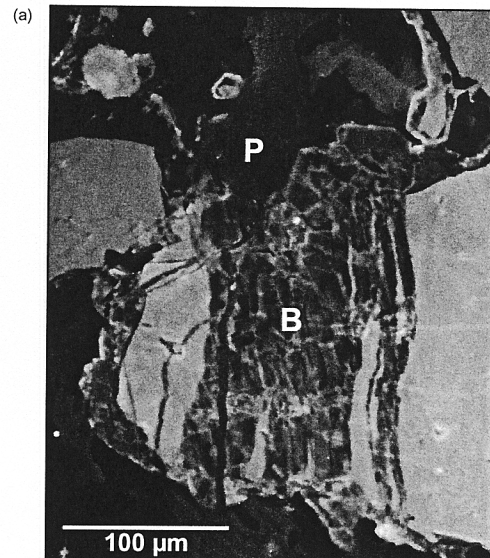


Fig. 2. Cement bridges with crack–seal textures resulting from repeated openings. Scanned-CL images: P, porosity; B, bridge. (a) Lower Cretaceous Fall River Formation, Wyoming, depth 3775 m. The orange and blue material is quartz cement. (b) Lower Cretaceous Travis Peak Formation, East Texas, depth 1865 m. The blue in the bridge is quartz cement. Note the filled fractures that extend across some cement zoning but truncate at others in (b). Crack–seal texture develops when fracture apertures are sufficiently narrow that cement can span them before any subsequent opening occurs.

fundamentally control progress of quartz precipitation (Walderhaug 1996).

Bridges grow as incremental fracture opening breaks the bridge and cement precipitates in the resulting gap. To distinguish small cement-filled fractures making up crack–seal texture in bridges from the large, mostly open fracture containing the bridges, we call the former *cement-filled gaps*. The purpose of this chapter is to quantify how bridges grow by using high-resolution scanning electron microscope (SEM)-based cathodoluminescence (scanned-CL) images to identify and measure cement-filled gaps within bridges. We demonstrate that the fine detail of fracture-widening history can be recovered from typical regional fractures formed at depth. For mostly open, joint-like fractures formed in diagenetic environments, our observations document opening amounts and patterns.

Samples

In this chapter we describe 11 bridges from nine fractures. Each of these fractures contains numerous bridges, but we only examined multiple bridges in one fracture. The examples are from five sandstones from five sedimentary basins (Table 1). We selected these samples because they span a range of burial depths and they have representative patterns of microstructure. The conclusion that these features are representative is based on a survey of more than 95 sandstone formations and more than 300 oriented thin sections. Opening-mode fractures display isolated bridges containing crack–seal texture and associated fracture porosity in rocks that have expe-

OPENING HISTORIES OF FRACTURES

3

Table 1. Sample depth and location of mineral bridges

Bridge No.	Well	Depth (m)	Unit (Age)	Basin	Aperture (μm)
1	SHCT 1	2753	Mesaverde (K)	Piceance	600
2	Gr. Valley 2 Fed.	2199	Mesaverde (K)	Piceance	450
3	Big Horn 2-3	6240	Frontier (K)	Wind River	700
4	Big Horn 3-36*	6244	Frontier (K)	Wind River	400
5	Big Horn 3-36*	6244	Frontier (K)	Wind River	400
6	Big Horn 3-36*	6244	Frontier (K)	Wind River	400
7	Big Horn 3-36	6242 [†]	Frontier (K)	Wind River	312
8	Holditch SFE 2	3008 [‡]	Travis Peak (K)	East Texas	100
9	Holdith Howell 5	1864	Travis Peak (K)	East Texas	112
10	Linares	Outcrop [‡]	Huizachtal (J)	NE Mexico	205
11	H. L. Jenkins 1	1052	Pottsville (Penn.)	Black Warrior	35

* Adjacent bridges from same fracture.

[†] Fluid-inclusion data.[‡] Estimated maximum burial c. 5km.

K, ???; J, ???; Penn., ???.

rienced moderate–deep burial (Laubach *et al.* 2004). This association is also present in some dolomites and limestones (Gale *et al.* 2004). Typically, at least part of the cement that occurs within fractures is contemporaneous with cements infilling the rock's intergranular volume, reflecting the shared diagenetic history of fracture and host rock.

Samples used in this study are from mostly low to moderate porosity rocks that are deeply buried or that have been in the past (Table 1). Quartz is the dominant cement, generally comprising >15% whole rock volume. Although bridges occur in rocks with a spectrum of burial histories and tectonic settings, the samples described here are from foreland basins, with the exception of bridges 8 and 9 (Table 1). Samples are mostly from flat-lying rocks distant from faults or from fold limbs. We interpret the opening-mode fractures to be part of regional sets that formed in response to some combination of burial and tectonic loading and pore-pressure changes. Fluid-inclusion data sets from intermediate- (3000 m) and deep-burial (6400 m) sandstones (Table 1) suggest temperatures of bridge formation ranging between 110 and 240°C, showing that bridges form under a range of burial conditions.

Methods

High-resolution microstructure imaging using SEM-based cathodoluminescence (scanned CL) allows effective high-magnification (as much as $\times 2000$) examination of silicate minerals that have low levels of luminescence over large specimen areas (Laubach 1997; Milliken & Laubach 2000; Reed & Milliken 2003) (Figs 1–3). Sensitive photomultiplier-based CL systems, high magnification and stable SEM observing conditions provide clear resolution of both

zones within cements and cement-filled microfractures that cut grains and/or cement. This imaging permits construction of accurate microstructure maps that delineate grain and fracture boundaries and cement growth textures within fractures.

The detectors and processing used for these images record CL emissions in the range of ultraviolet through visible into near infrared and convert them to grey-scale intensity values. To allow textures not evident on panchromatic images to be revealed, colour images were acquired using filters, superposition of multiple images (Reed & Milliken 2003) and image manipulation using commercial image-processing filters. Most images were acquired using an Oxford Instruments MonoCL2 system attached to a Philips XL30 SEM operating at 15 kV.

Crack–seal texture and associated cement bridges

Crack–seal texture results from repeated small increments of extension across a discontinuity and cement precipitation in the resulting gaps (Hulin 1929; Ramsay 1980) (Figs 1 and 2). Grain and cement fragments, fluid inclusions and luminescence colour bands parallel to fracture walls define the texture. In some cases, inclusion trails form at boundaries of grain fragments and tend to parallel the wall-rock displacement direction. Sharp-sided boundaries between broken grains and cement record individual opening and sealing events.

In sandstone, quartz and other phases form isolated masses, or bridges, that span fractures and that range in size from individual crystals to areas of cement with dimensions of centimetres or more. Bridges can be categorized by the presence or

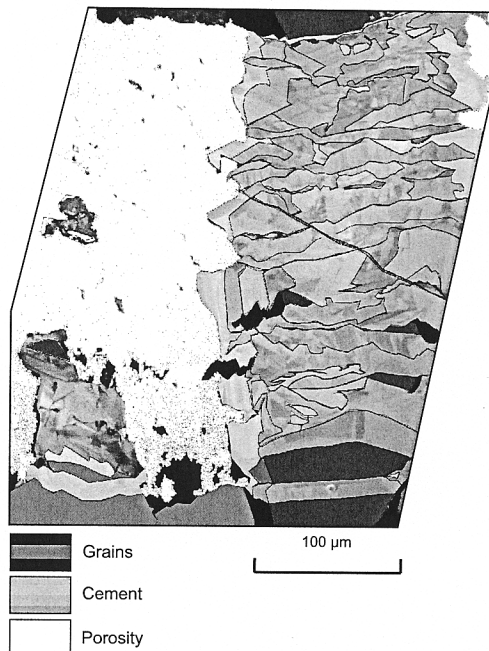


Fig. 3. Annotated scanned-CL image of bridge 7. Fracture trace is at a right angle to the long dimension of the bridge. Colour, texture, crystal outlines, and cross-cutting and overlapping relations separated cement zones and fractures. Figure 4 shows the fracture opening sequence.

absence of crack-seal texture. Bridge crystals lacking crack-seal textures either did not grow sufficiently to make a connection after fracture walls moved apart or formed in fractures that were quiescent (walls not moving). In some cases crystals merely grew across a fracture that subsequently did not widen (Fig. 1). Evidence of cement that precipitated in quiescent fractures is common. Such cements tend to overlap and locally surround bridges containing crack-seal structures (see fig. 1 in Laubach 1988). In sandstones the cements that form this latter type of bridge are frequently carbonate and sulphate minerals, not quartz.

The focus of this paper is on isolated bridges in sandstone composed of cements that precipitated while fractures were opening. These bridges are surrounded by fracture porosity or, later, post-kinematic cement. Bridges form where cement grows only locally across the fracture between widening increments. Repeated fracture creates gaps in the bridge that are subsequently filled with cement. Localization of new cement precipitation in these gaps results in much greater cement accumulation in the bridge compared with that of adjacent areas of the fracture wall. The resulting bridge structures can occupy a small footprint on the fracture wall, yet

cross from one fracture wall to the other with a nearly uniform dimension in the plane of the fracture. Because they occupy a small and discontinuous volume of the fracture, these bridges are not barriers to fluid flow.

Within bridges, quartz cement marking crack-seal texture comprises continuous-luminescence colour bands. In quartz, differences in CL intensity arise from slight variations in trace-element content or defect structure that characterize quartz of various origins (Sipple 1968). In addition to distinguishing grains entrained in crack-seal texture and cement (Fig. 2), contrasts in CL response can discriminate quartz cements deposited at different times in a rock's cementation history, helping to clarify structural events. For example, in Figure 1 early red-luminescent quartz coats grains and fills compaction fractures, whereas later blue-luminescent quartz fills tectonic microfractures and lines or, locally, bridges larger fractures.

Yet, crack-seal texture is frequently present only locally in fractures that contain bridges. A veneer of euhedrally terminated quartz overgrowths that lacks internal structure commonly lines fracture walls. The thickness of such veneers is typically a small fraction of crack-seal bridge thicknesses. Some euhedrally terminated crystals have crack-seal textures at their bases, succeeded by unfractured zoned crystals that developed after cement no longer bridged the opening fracture (see fig. 6 in Laubach 1997). As their width diminishes, many fractures show increased bridging, with partial-complete fill more prevalent near tips where apertures are smaller. Fractures that experienced episodic widening may also lack crack-seal texture if cement did not span the fracture.

Many bridges comprise quartz crystals elongated parallel to the *c*-crystallographic axis, the preferred rapid-growth direction for this mineral. The composition and crystallographic orientation of grains that make up fracture walls also influence cement patterns within fractures, locations where fracture porosity is retained and amount of fracture porosity. Residual fracture porosity tends to occur in association with rock fragments and feldspars that are not favourable substrates for quartz precipitation.

Core data show that bed-normal opening-mode fractures in sandstone have a wide range of sizes (Marrett *et al.* 1999). In terms of kinematic aperture, sizes range from microns to decimeters and more. Well-developed crack-seal texture is present in microfractures as narrow as 35 μm . Microfractures of this size and smaller tend to be sealed or to have only small, discontinuous areas of porosity. Fractures with kinematic apertures of millimetres commonly have crack-seal texture along at least part of their length. Larger fractures frequently have wide bridges with crack-seal texture and adjacent areas of porosity (Figs 1–4) or they may lack bridges entirely.

OPENING HISTORIES OF FRACTURES

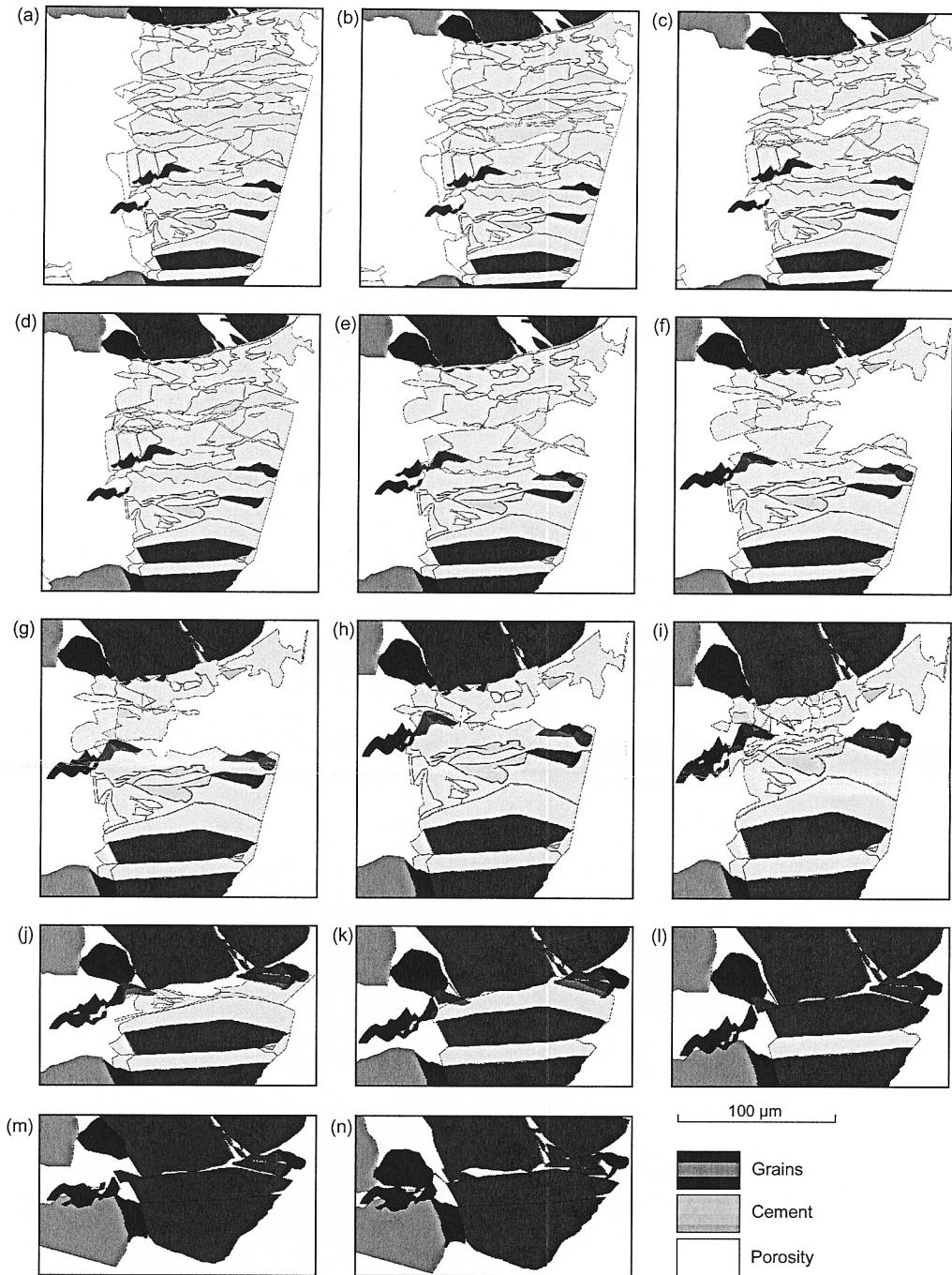


Fig. 4. Fracture opening restoration sequence (a–n) based on mapping cross-cutting cement and fractures on scanned-CL images, bridge 7, Upper Cretaceous Frontier Formation, Wind River Basin, Wyoming, depth 6242 m. Fracture trace is at a right angle to the long dimension of the bridge, which shows cement zones in (a) the present-day bridge; (n) is the prefracture, restored state. Animations of the opening sequence suggest that the fracture propagated from left to right in the reference frame of this diagram.

Bridge restoration

Of the 11 bridges examined in this study, 10 have relatively simple internal structures, exemplified by Figure 2. Visible within these bridges are wall-rock inclusions and uniform-textured luminescence bands. There are also areas, usually near or on the outer margins of bridges, with faceted crystals representing unimpeded crystal growth into pore space adjacent to the bridge. Luminescence bands may be continuous, with areas of euhedral crystal on bridge margins (upper part of bridge, Fig. 2a) marking crystal growth into open pore space from the edge of broken grains. Large, single crystal faces commonly mark outer edges of bridges. In some cases breakage of these crystal faces is evident in overlapping and cross-cutting zones of bands (Figs 2b and 3).

Within bridges, bands with uniform luminescence frequently cross-cut one another. The youngest bands may retain considerable fracture pore space lined with minute crystal faces (Fig. 2a, left side). In some cases cross-cutting relations among luminescence bands and crystal zoning along (or within) bridges give evidence of relative fracture timing (Fig. 2b, lower part of bridge). Textures in these bridges arise from repeated breakage and crystal growth on bridges with a simple initial structure, such as that shown in Figure 1. Even where bridges have broken in approximately the same location, cement accumulation leads to textural and luminescence differences that allow breaks to be recognized.

Mapping internal structures in bridges involves identifying and correlating fractures within bridges (cement-filled gaps) and determining their timing relative to other cement via cross-cutting and overlapping relations. Some patterns are readily identified because gaps are relatively isolated or they are bounded by prominent wall-rock inclusions (for example, much of Fig. 2b) or crystal faces. In areas with repeatedly broken cement and cross-cutting luminescence bands (Fig. 2a), high magnification and careful contact tracing are required for cross-cutting relations to be determined.

To identify fractures within bridges, we mapped grain and cement fragments derived from the wall rock and cement textures. We used the generally euhedral quartz cement on the bridge margin to find the latest fractures (for example, Fig. 2b). Consistent cement textures, abrupt luminescence band or crystal outline truncations, and euhedral crystal faces overlapped by later cement define cross-cutting relations. For example, in the bridge in Figure 3, areas marked in blue-green are interpreted to have formed during latest stages of bridge growth because bands with consistent texture and luminescence divide areas on the bridge margin marked by late euhedral overgrowths. However, the relative order of fracture and cements deposited during the

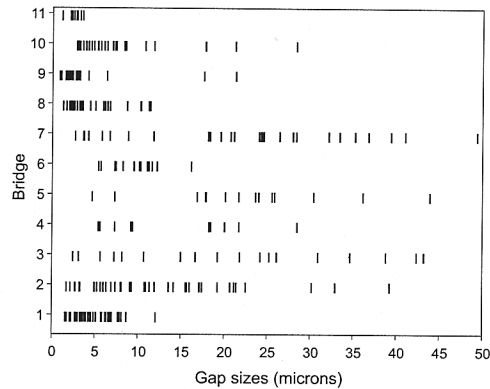


Fig. 5. Gap sizes v. bridge data set for gaps less than 50 μm . See Table 1 for sample depths. All filled gaps larger than 40 μm are from bridges 3 to 7, Frontier Formation at depths below 6242 m. Kinematic apertures are entire opening displacement spanned by the bridge.

middle stage of this bridge's growth (Fig. 4e-i) is ambiguous because repeated fracturing of cement created complex crossing relations. This ambiguity results in alternative permissible sequences of events during sequential restoration in this texturally complex cement bridge (Figs 3 and 4). However, fractures may not intersect, especially in wide bridges, leading to a lack of clear cross-cutting relations that may preclude unique identification of some relative fracture-timing relations.

As illustrated by bridge restoration (Fig. 4), gaps tend to localize in part of the bridge. However, the location of gaps does not necessarily conform to a progression from fracture wall to fracture interior or vice versa, and the locus of fracture may shift within the bridge. To trace a single rupture along a fracture would require the mapping of many bridges and the correlation of the fracture histories within each. Thus, gaps in adjacent bridges in the same fracture are not necessarily in the same position relative to the fracture wall (Fig. 5, bridges 4-6), from one bridge to the next (Fig. 6).

Restorations show that euhedral crystal terminations form and are subsequently overgrown by other cement (and dissected by later fractures) as bridges develop (Fig. 4b, h). This pattern suggests that immediately after a fracture propagated, cement in the bridge was not in contact with the opposite fracture wall and thus could not have been supporting a normal stress. We found no textural evidence that cement precipitation and fracture opening were synchronous in the sense that solid cement was in continuous contact.

Restoration of bridges suggests that their breadth does not increase greatly through time, even though their cross-fracture dimension increases markedly,

OPENING HISTORIES OF FRACTURES

7

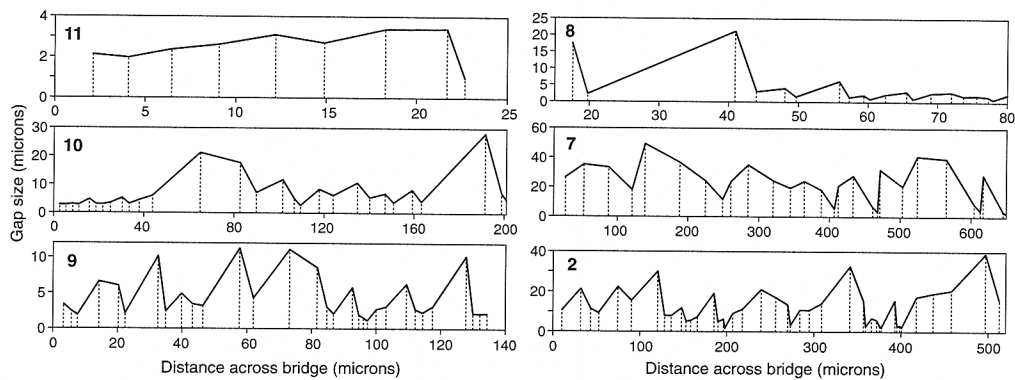


Fig. 6. Gap size v. distance across bridge. Dotted vertical lines mark the centre point of filled gap. The height of the dotted line is the width of the gap. Diagrams show spatial distribution of gap size; sequential restoration provides evidence of sequence of gap development (cement volume) that can be tied to cement history, fluid inclusion temperature and pressure data, and, thus, thermal and burial history and models of fracture growth (Lander *et al.*, 2002; Olson 2004). Numbers refer to bridges listed in Table 1. Note that scales differ for each profile.

in most cases matching the dimension of the overall fracture kinematic aperture. The main cause of increase in bridge volume is addition of cement on broken surfaces that are aligned normal to the opening direction and parallel to the main fracture trace. Accumulation of cement in the bridge is a by-product of repeated renewal of fracture surface area within bridges.

Competing fracture opening and cement-precipitation rates are responsible for patterns recorded by crack–seal textures (Fig. 6). There are several possible explanations for these contrasting opening patterns. Some may reflect the mechanics of fracture opening and the structural geology of specific fracture arrays. Others may merely represent complex breakage patterns in fractures with only small amounts of cement. For example, gap distributions may depend on bridge shape, crystal orientation, and bridge and substrate composition, as illustrated by three bridges from the same fracture that have different patterns of breakage (Fig. 5, bridges 4–6).

Bridge 7 records a history that is consistent with growth of a simple opening-mode fracture. Large initial opening increments record the propagation of the fracture tip (Figs 4I–I and 6). These are succeeded by smaller openings localized first near one wall of the fracture (upper wall in Fig. 4) and subsequently in the centre of the bridge. These smaller openings presumably track lengthening of a fracture with an opening displacement concentrated near the fracture tip. Some fractures show similar a progression (Fig. 6, bridge 8), but others have more complex patterns that might record interaction and linkage of fractures (Fig. 6, bridges 2 and 9). To test these concepts evidence is required at various positions along a fracture trace or from several fractures in an array.

Geomechanical modelling shows that fracture-

opening histories can be complex even for simple fracture patterns (Olson 2004). The record from cement bridges deciphered using scanned-CL mapping provides the evidence for documenting and interpreting these opening histories.

Opening amounts

Isolated quartz bridges that contain crack–seal texture occur in opening-mode fractures that otherwise may be open and that lack appreciable cement. Unlike previous observations of extensively mineral filled veins in metamorphic rocks, these structures provide evidence of fracture-opening amounts from diagenetic environments that was previously lacking. Crack–seal patterns in bridges show that the fractures we studied have an involved opening history. Yet, there is little or no evidence of this history outside of the bridges, where a micron-scale veneer of faceted quartz crystals lines fracture walls.

Inspection identifies individual fractures in bridges (cement-filled gaps) marked by luminescence bands created by incremental fracture opening. We also used maps of fractures and cement zones within bridges to restore bridge development sequentially (Figs 2–4). Sequential restoration helps identify individual fractures (gaps) in areas of complex texture and also reveals the timing of gap development.

Gap sizes and locations were recorded along lines parallel to bridge axes (normal to fracture walls). Although this procedure does not accurately capture the cement volumes accumulated in each gap, it minimizes possible over or undercounting of the number and size of filled gaps in texturally complex areas with ambiguous cross-cutting relations and gives an accurate measure of individual opening steps.

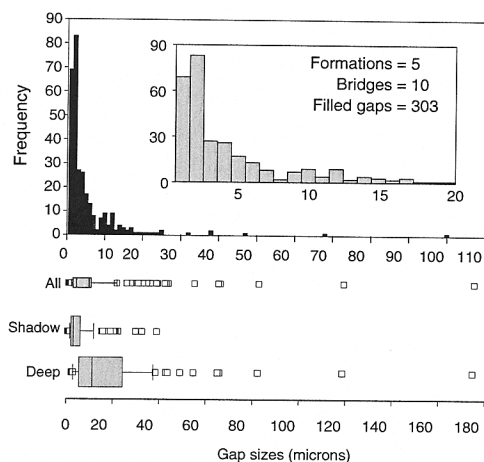


Fig. 7. Frequency distributions of gap sizes (filled opening increments) in bridges. Bridge 11, a microfracture, is included in box plots but not the histogram. The histogram shows the size distribution for gaps less than 120 μm ; the inset histogram shows the distribution for gaps less than 20 μm . The first box plot shows the mean and range for the entire data set; second and third box plots show bridge data separated into relatively shallow (bridges 1, 2, 8, 9 and 11) and deep (bridges 3–7 and 10) samples.

Gaps in bridges created by fracture widening with contemporaneous cementation range from less than 1 μm to more than 1 mm, but nearly all are less than 20 μm and most are less than 5 μm (Fig. 7). The average gap size is about 10 μm , but gap sizes appear to have a log-normal size distribution (Fig. 7). The significance of this distribution is uncertain. It is probably truncated at both small and large sizes. At small sizes, small opening increments may not produce recognizable textural features with our current imaging methods. At large sizes, bridges record only opening amounts that could be spanned by subsequent cement growth rather than the entire range of permissible opening increments.

For all sample sets, the average gap size is less than the average thickness of quartz cement on monocrystalline quartz grains within adjacent host rocks. This difference is consistent with slow, continuous cement accumulation on fracture walls outside of bridges.

The largest minimum gap sizes are in the deepest samples and in the outcrop sample of Jurassic sandstone from NE Mexico, the burial history of which suggests likely fracturing at great depth (*c.* 5 km). The opening patterns in these fractures probably record diverse strain histories, possibly in the context of changing ambient conditions. Nevertheless, although the data set is small, overall average gap

sizes are somewhat larger for deeper samples (Fig. 7). The largest filled gaps are in the deepest samples, and the average gap size for deeper samples (18.9 μm) is also larger than for shallower samples (5.4 μm). These apparent differences between deep and shallow samples are consistent with a scenario in which cement grew faster relative to fracture opening in the deeper samples, allowing larger gaps to be spanned for a given opening history. Wider cemented gaps found in deeper samples could be a result of faster precipitation rates at these depths owing to higher temperatures.

Discussion and conclusions

Our observations are the first evidence of opening amounts from joint-like fractures formed in diagenetic environments (depths of 1–6 km, temperatures of >80–200°C). Previous studies of arrest lines on fracture surfaces documented that such fractures experienced episodic growth. Our study shows that it is possible to recover fine detail of opening histories from fractures that retain little other evidence of their structural development. Fractures containing bridges may superficially even appear to lack mineralization.

Information on opening patterns for such fractures is useful for comparison with mechanical models of fracture pattern development (Olson 2004). Bridge structures also provide a link between the rock's mechanical and diagenetic histories. Cements are more readily associated with thermal and burial history than are fractures; crack–seal bridges may therefore provide a route to better dating of fracture formation and, thus, to improved models of fracture development. We found suggestive evidence that differences in the average size of fractures spanned by cement may provide an indication of the depth of fracture formation.

The patterns we observe in crack–seal texture and bridge patterns are consistent with a structural diagenetic model of bridge growth in which the chemical environment is dominated by host-rock composition, and cement accumulation on new fracture surface areas is temperature sensitive (Lander *et al.* 2002). In conjunction with diagenetic models that predict cement accumulation as a function of time and temperature (Lander & Walderhaug 1999), patterns of cement accumulation associated with fracture opening can potentially indicate rate of fracture opening as a function of time.

Partly supported by US Department of Energy Contract No. DE-FC26-00BC15308, by associates of the Fracture Research & Application Consortium: Saudi Aramco, ChevronTexaco, Devon Energy Corporation, Ecopetrol, Marathon Oil, PEMEX Exploración y Producción and IMP, Petroleos de Venezuela, Petrobras, Repsol-YPF, Shell

OPENING HISTORIES OF FRACTURES

9

International Exploration & Production, Schlumberger, Tom Brown, Inc., Williams Exploration & Production, and Geocosm LLD. We are grateful to associates for samples used in this study, to J. Gale, R. Marrett and K. Milliken for discussion, and C. Onash and T. Engelder for helpful review comments.

References

- GALE, J. F. W., LAUBACH, S. E., MARRETT, R., OLSON, J. E., HOLDER, J. & REED, R. M. 2004. Predicting and characterizing fractures in dolomite reservoirs: using the link between diagenesis and fracturing. Geological Society, London, Special Publications, ???, 000–000.
- HULIN, C. D. 1929. Structural control of ore deposition. *Economic Geology*, **24**, 15–49.
- LANDER, R. H. & WALDERHAUG, O. 1999. Predicting porosity through simulating sandstone compaction and quartz cementation. *AAPG Bulletin*, **83**, 433–449.
- , GALE, J. F. W., LAUBACH, S. E. & BONNELL, L. M. 2002. Interaction between quartz cementation and fracturing in sandstone. *American Association of Petroleum Geologists Annual Convention Program*, **11**, A98–A99.
- LAUBACH, S. E. 1988. Subsurface fractures and their relationship to stress history in East Texas Basin sandstone. *Tectonophysics*, **156**, 37–49.
- 1997. A method to detect fracture strike in sandstone. *AAPG Bulletin*, **81**, 604–623.
- 2003. Practical approaches to identifying sealed and open fractures. *AAPG Bulletin*, **87**, 561–579.
- , REED, R. M., OLSON, J. E., LANDER, R. H. & BONNELL, L. M. 2004. Co-evolution of crack–seal texture and fracture porosity in sedimentary rocks: cathodoluminescence observations of regional fractures. *Journal of Structural Geology*.
- MARRETT, R., ORTEGA, O. O. & KELSEY, C. 1999. Power-law scaling for natural fractures in rock. *Geology*, **27**, 799–802.
- MILLIKEN, K. L. & LAUBACH, S. E. 2000. Brittle deformation in sandstone diagenesis as revealed by scanned cathodoluminescence imaging with application to characterization of fractured reservoirs. In: *Cathodoluminescence in Geosciences*. Springer, New York, Chap. 9, 225–243.
- OLSON, J. E. 2004. Predicting fracture swarms – the influence of subcritical crack growth and the crack-tip process zone on joint spacing in rock. In: COSGROVE, J.W. & ENGELDER, T. (eds) *The limitation, Propagation, and Arrest of Joints and Other Fractures: Interpretations Based on Field Observations*. Geological Society, London, Special Publications, ???, 000–000.
- RAMSAY, J. G. 1980. The crack–seal mechanism of rock deformation. *Nature (London)*, **284**, 135–139.
- REED, R. M., & MILLIKEN, K. L. 2003. How to overcome imaging problems associated with carbonate minerals on SEM-based cathodoluminescence systems. *Journal of Sedimentary Research*, **73**, 326–330.
- SIPPLE, R. F. 1968. Sandstone petrology, evidence from luminescence petrography. *Journal of Sedimentary Petrology*, **38**, 530–554.
- WALDERHAUG, O. 1996. Kinetic modeling of quartz cementation and porosity loss in deeply buried sandstone reservoirs. *AAPG Bulletin*, **80**, 731–745.



ELSEVIER

Journal of Structural Geology xx (0000) xxx–xxx

**JOURNAL OF
STRUCTURAL
GEOLOGY**

www.elsevier.com/locate/jsg

Coevolution of crack-seal texture and fracture porosity in sedimentary rocks: cathodoluminescence observations of regional fractures

S.E. Laubach^{a,*}, R.M. Reed^a, J.E. Olson^b, R.H. Lander^{a,c}, L.M. Bonnell^{a,c}

^a*Bureau of Economic Geology, John A. and Katherine G. Jackson School of Geosciences, The University of Texas at Austin, Austin, TX 78713, USA*

^b*Department of Petroleum and Geosystems Engineering, The University of Texas at Austin, Austin, TX 78713, USA*

^c*Geocosm L.L.C., 3311 San Mateo Drive, Austin, TX 78738, USA*

Received 2 May 2002; accepted 16 August 2003

Abstract

This paper examines evidence of coupled diagenetic and mechanical processes within growing fractures in sandstones: crack-seal texture and associated, concurrently produced fracture porosity. Crack-seal textures in narrow mineral bridges associated with fracture porosity are common in regional fractures formed at moderate to great depth (>1000–~6000 m) in quartz-cemented sandstones that otherwise lack significant structure. Use of SEM-based cathodoluminescence systems and superposition of images collected using color filters accurately delineate crack-seal increments in fracture-bridging quartz cement. Bridges and crack-seal texture mark competition between cement precipitation and opening rates during opening-mode fracture growth. These structures document episodic fracture growth that can include tens to hundreds of widening increments in fractures having apertures of a few tens of microns to several millimeters or more. These structures are not the product of unique circumstances in burial history and fluid flow but, rather, reflect the confluence of rock-dominated geochemistry that is widespread in time and space and fracturing caused by a spectrum of loading conditions.

© 2004 Elsevier Ltd. All rights reserved.

Keywords: Fracture porosity; Diagenesis; Crack-seal texture; Fluid flow; Quartz cement

1. Introduction

Essential to progress in the understanding of fracture patterns is appreciation of chemical processes in growth of opening-mode fracture systems. For fractures in sedimentary rocks in diagenetic environments (>1000–~6000 m depth), where fractures are new rock surfaces created in the presence of high temperatures and reactive fluids, effects of mineral precipitation and dissolution (diagenesis) on fracture attributes and growth could be significant. Observations of core samples show that fractures from these settings typically contain at least some authigenic cement. Yet dynamic evolution of coupled diagenetic reactions and fracture mechanics and their effects on fracture attributes remain largely unknown. We illustrate the importance of interacting mechanical and diagenetic processes in sandstones during fracture growth by describing a widespread

but little-appreciated by-product of these linked processes, namely crack-seal texture and associated fracture porosity.

Crack-seal texture is the result of repeated fracturing during cement precipitation within fractures (Figs. 1 and 2). Thus, it is emblematic of coupled mechanical and diagenetic interaction. Although previously documented primarily in veins in low-temperature metamorphic rocks and faults (Ramsay, 1980; Anders and Wiltschko, 1994), crack-seal texture is also a common, but little appreciated, attribute of opening-mode fractures in slightly deformed and nearly flat lying sedimentary rocks. Moreover, as discussed later, owing to advances in microscopy, fine-scale observations are now possible that provide insight into the origin and development of these structures.

2. Sample suite

Our conclusions are based on documentation of definitive crack-seal textures in 24 sandstone units and observations of weakly developed or somewhat ambiguous crack-

* Corresponding author. Tel.: +1-512-471-6303; fax: +1-512-471-0140.
E-mail address: steve.laubach@beg.utexas.edu (S.E. Laubach).

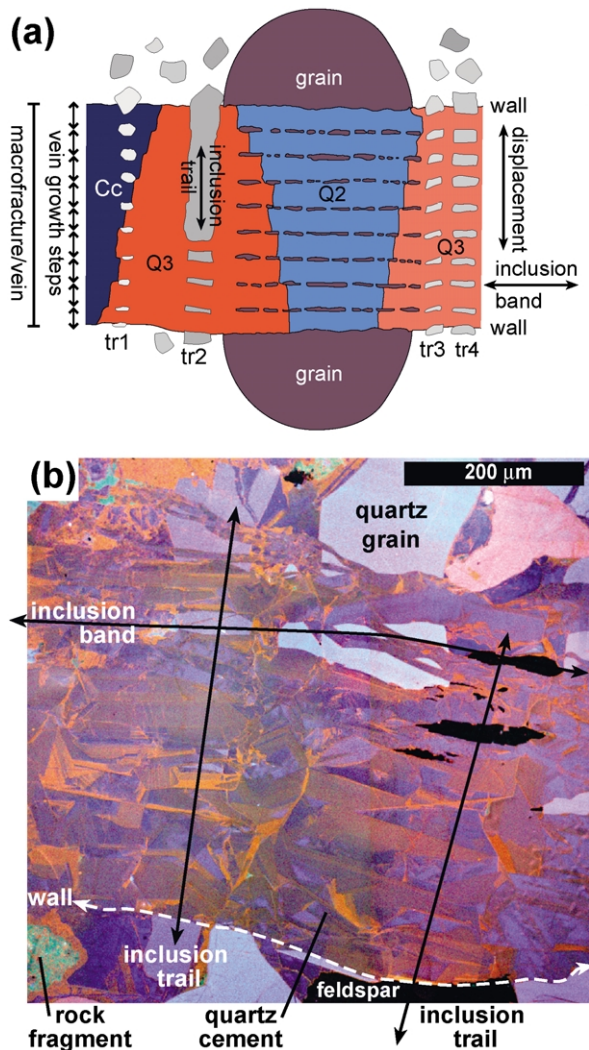


Fig. 1. Features associated with the crack-seal mechanism. (a) Inclusion trails are a series of grain fragments parallel to displacement direction. Fragments of different grains define inclusion bands, which are arranged perpendicular to displacement direction and which formed during the same growth step. Q = quartz, C = calcite, tr = trail. Spacing of inclusion bands is $\sim 50 \mu\text{m}$. Modified from Ramsay (1980). (b) Color-CL image mosaic of quartz-lined fracture in sandstone formed by numerous individual crack and cement precipitation events. Quartz grains and cement compose most of the image area; fragmented nonluminescent grain is feldspar, and green speckled areas are rock fragments. Sample is a quartz-cemented lithic arkose, Cretaceous Frontier Formation, Wind River Basin, Wyoming.

seal textures in an additional 19 formations that range in age from Archean to Tertiary. Samples are mostly from core taken from hydrocarbon reservoirs that have undergone minimal tectonic disturbance. Many samples are from horizontal to gently dipping beds of mostly low to moderate porosity (0–20 bulk volume percent) sandstone. Samples are from rock that is moderately or deeply buried (>1000 – ~ 6200 m) or that has been so in the past. Sandstones are dominantly quartz cemented, although most contain other cements. Quartz cement volumes are typically high (15– $>20\%$), suggesting that host sandstones have been exposed to temperatures more than 80°C (Lander and

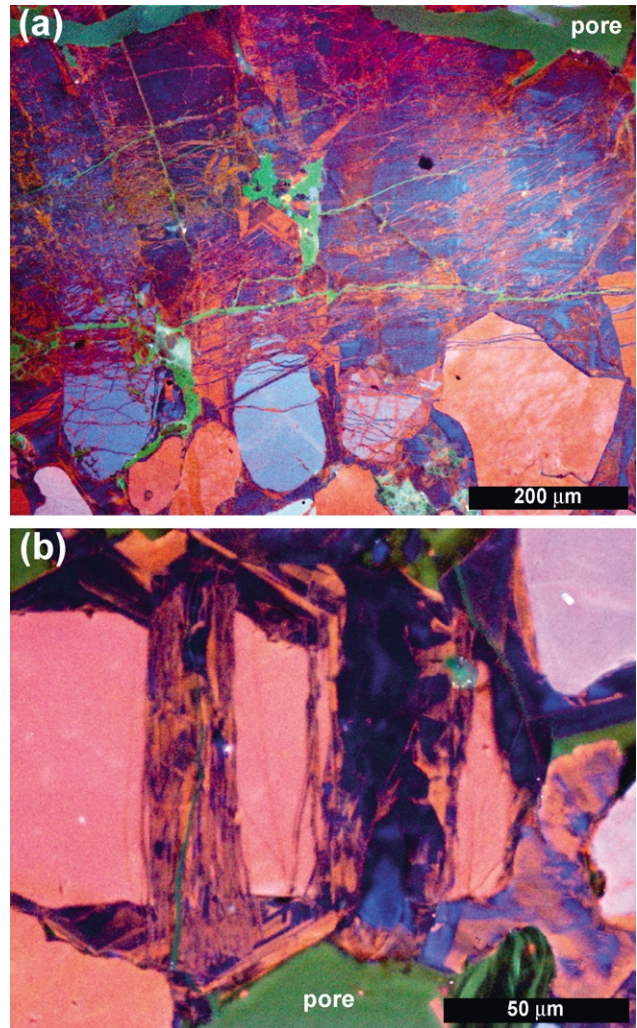


Fig. 2. (a) Color-scanned CL image showing crack-seal texture in a group of quartz bridges and associated fracture porosity. Only one side of the macrofracture is shown; fracture trend is parallel to the long axis of the image. Sample is quartzarenite from a depth of 3009 m. (b) Color-scanned CL image showing post-fracture-opening quartz overgrowths on quartz pillars having central crack-seal texture. Quartz precipitation outlasted fracture expansion. Amount of residual fracture porosity reflects progress of cementation, which depends primarily on thermal history (Lander et al., 2002). In this particular grain, the macrofracture has bifurcated into two strands; overall fracture trend is parallel to the short axis of the image. Sample is a subarkose from a depth of 1865 m. Both samples are from Cretaceous Travis Peak Sandstone, East Texas.

Walderhaug, 1999), and fluid-inclusion data from two fracture sets are consistent with temperatures during fracturing of 110 and 240°C (Laubach, 1989a; unpublished). Rock types include quartz arenites, subarkoses, sublitharenites, lithic arkoses, feldspathic litharenites and litharenites. Grain sizes range from siltstones to granule conglomerates.

The fractures sampled in this study are typical opening-mode (extension) fractures. They are arranged in sets having consistent orientation and are mostly inclined at close to right angles to bedding. Thus, they are nearly vertical in flat-lying beds. More than half the samples are from foreland

basins, and most of the rest are from passive margins and platforms. Foreland samples are from both recent, active basins, such as those of Venezuela, Colombia, Bolivia, and older, inactive foreland basins including the Appalachians, West Texas, and Rocky Mountains. We interpret these fractures to have formed in response to some combination of regional tectonic loading and burial and pore-pressure changes (regional fractures; Nelson, 1985), but it is rarely possible to uniquely relate fracture growth to loading path or to date the fractures. Some fractures in open folds may have formed partly in response to fold-related strains, but other fractures from within fold-thrust belts we interpret to predate folding. In this paper we focus primarily on representative microstructural patterns that are found in fractures in all of these diverse structural settings and ages.

3. Imaging methods

High-resolution microstructure imaging using scanning electron microscope (SEM)-based cathodoluminescence (scanned CL) allows delineation of patterns in fracture microstructure that were previously obscure (Milliken, 1994a; Laubach, 1997; Milliken and Laubach, 2000; Reed and Milliken, 2003) (Figs. 3 and 4). The sensitivity of photomultiplier-based CL systems and the high magnification and stable observing conditions of the SEM significantly enhance weak luminescence. This approach provides an advantage over conventional CL systems in that it allows efficient high-magnification (up to 2000 \times imaging) examination of silicate minerals having low levels of luminescence. We obtained digital image mosaics over large specimen areas (square millimeters) and mapped grains, porosity, cement, and fracture patterns. Our survey of sandstone microstructure used more than 325 polished, oriented thin sections and analysis of image mosaics from multiple samples.

The detectors and processing used for these images record CL emissions in the range of 185–850 nm (ultraviolet through visible into near infrared) and convert them to gray-scale intensity values. Most images in this paper were acquired using an Oxford Instruments MonoCL2 system attached to a Philips XL30 SEM operating at 15 kV. We created color images by using red, green, and blue filters and superposing multiple images. Using color filters to convert an originally panchromatic CL source to a synthetic color image commonly reveals textures not evident on panchromatic images. In some samples examined using scanned CL, imaging only part of the available spectrum of CL emissions provides a clearer picture of texture than does using the whole spectrum (Figs. 5a and c and 6). Luminescence variations most likely reflect slight differences in trace-element composition and mineral structure (Pagel et al., 2000). We used contrast between CL colors primarily to document textural patterns. For this appli-

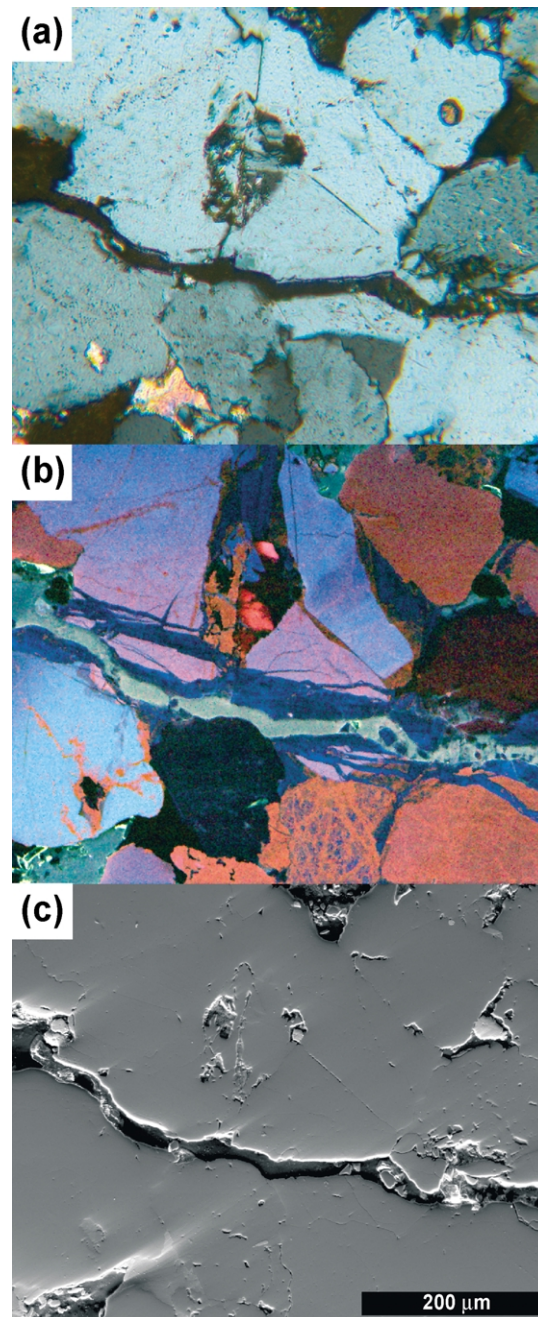


Fig. 3. Image set from a quartz-rich sandstone comparing color CL (center), secondary electron (right), and cross-polarized-light petrographic (left) views. Macrofracture with limited crack-seal texture has been broken during sampling, with reopened area now filled with epoxy. In CL image, fracture-filling epoxy is pale green, quartz grains are blue, red, and purplish red, and quartz cement is dark-blue, black, or red. Calcite cement (an isolated patch in lower-right quadrant) is nonluminescent. Altered feldspar grain in left center shows a patchwork of CL colors. Deformed quartz grain in right center shows a mixture of blue and red luminescence. Microfractures that parallel main fracture are completely filled with blue-luminescent quartz cement. Sample is from Devonian Iquiri Formation, Bolivia.

cation, neither quantitative assessment of emission intensity and color, nor the variables affecting these parameters, are critical.

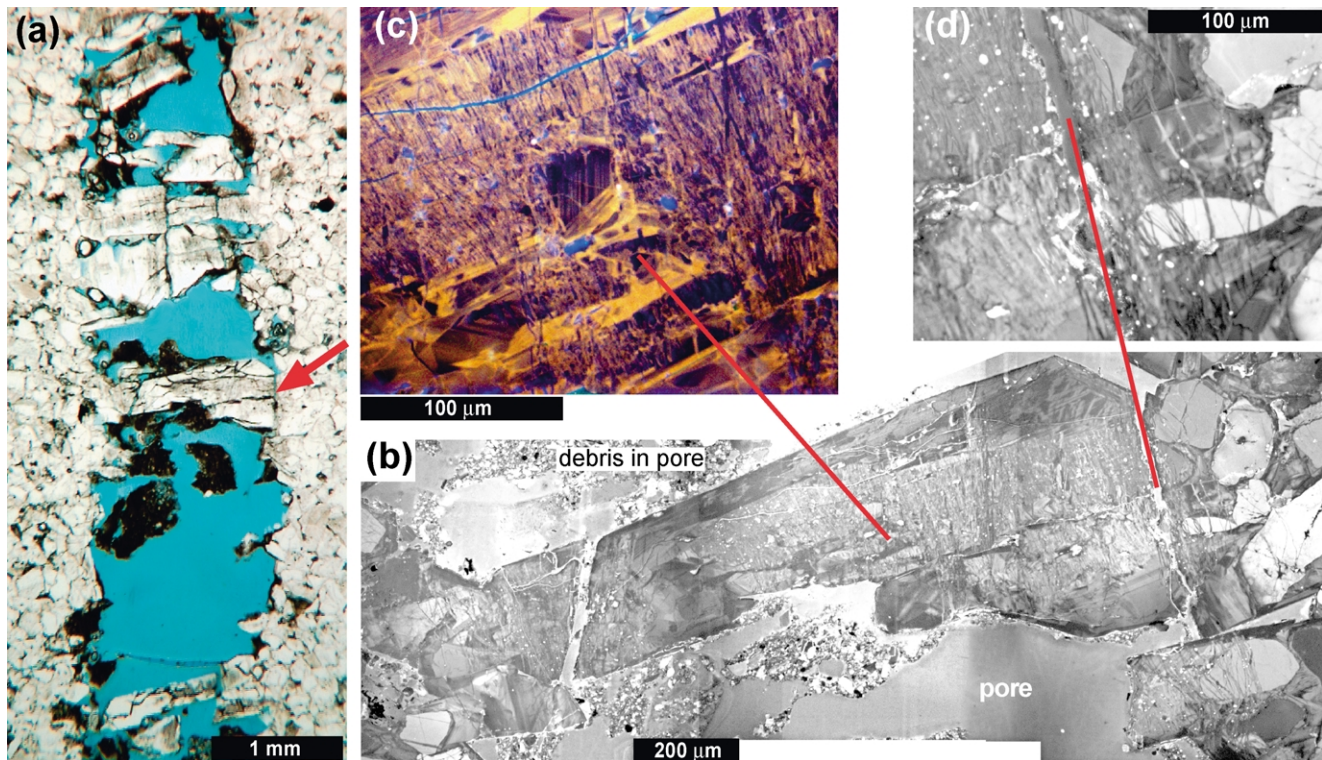


Fig. 4. Relatively simple crack-seal texture, quartz bridge spanning fracture in quartzarenite. Macrofracture strike in all images is identical. Sample depth is 3008.8 m, Cretaceous Travis Peak Formation, East Texas. Macrofracture is near vertical and is associated with subhorizontal stylolites. (a) Plane-polarized-light photomicrograph. Note fracture porosity (now filled with blue epoxy) distributed along fracture length. Red arrow indicates quartz bridge in (b). (b) Panchromatic CL mosaic of entire quartz bridge. Note dozens of smaller fractures that have broken quartz and have been sealed (crack-seal texture). (c) Color-CL image of part of (b); red lines connect corresponding points. (d) Panchromatic-CL image of part of (b), showing the fracture wall, a broken original grain, and the adjacent quartz bridge.

Scanned CL is a powerful tool for microstructural analysis. It provides hitherto inaccessible evidence of crack-seal texture in regional fractures. Applications include identification of cement-filled fringes and shadows around porphyroclasts, fibers in quartz veins in metamorphic rocks (Dietrich and Grant, 1985; Fisher and Brantley, 1992), and fault-gouge and deformation-band textures in sandstone (Fowles and Burley, 1994; Milliken, 1996; Milliken et al., 2004), delineation of grain provenance (Milliken, 1994b; Seyedolali et al., 1997), cement stratigraphy (Hogg et al., 1992), and grain-scale compaction or pressure solution features (Dickinson and Milliken, 1995).

4. Fracture internal structure

4.1. Mineral bridges

The crack-seal mechanism of vein formation has been widely described in low-grade metamorphic rocks and carbonates, mostly from significantly deformed rocks. Crack-seal texture results from repeated opening across a fracture with cement filling in the fracture between increments (Fig. 1; Hulin, 1929; Ferguson and Ganett, 1932; Ramsay, 1980). In contrast to veins in metamorphic

rocks, which are commonly filled with mineral deposits, in sedimentary sandstones fractured in diagenetic environments, cements *contemporaneous with fracture opening* rarely completely seal large (aperture > 1 mm) fractures. In these rocks, crack-seal texture is commonly found in discontinuous mineral bridges. Bridges are cement deposits that span fractures and that are surrounded by fracture porosity or by later cements (Fig. 4). Fracture volume occupied by bridges can be small and varies from absent to nearly complete fill, with smaller fractures tending to be more completely filled. These mostly inconspicuous bridges hold clear evidence of fracture-widening histories.

In sandstones, crack-seal texture is most common in mineral bridges formed of quartz cement, although examples of crack-seal texture are present in carbonate fracture fills in sandstone as well. The association of localized crack-seal texture (in dolomite cement bridges) and fracture porosity is also present in some dolomites (Gale et al., 2004).

Many quartz bridges have narrow pillar or rod shapes consisting of isolated quartz crystals or masses of crystals. Crack-seal textures occur within these isolated single crystals or clusters of crystals. Some of these crystals show dozens to hundreds of micron-scale, sealed cracks (Fig. 4b). Grain fragments and cement fragments define

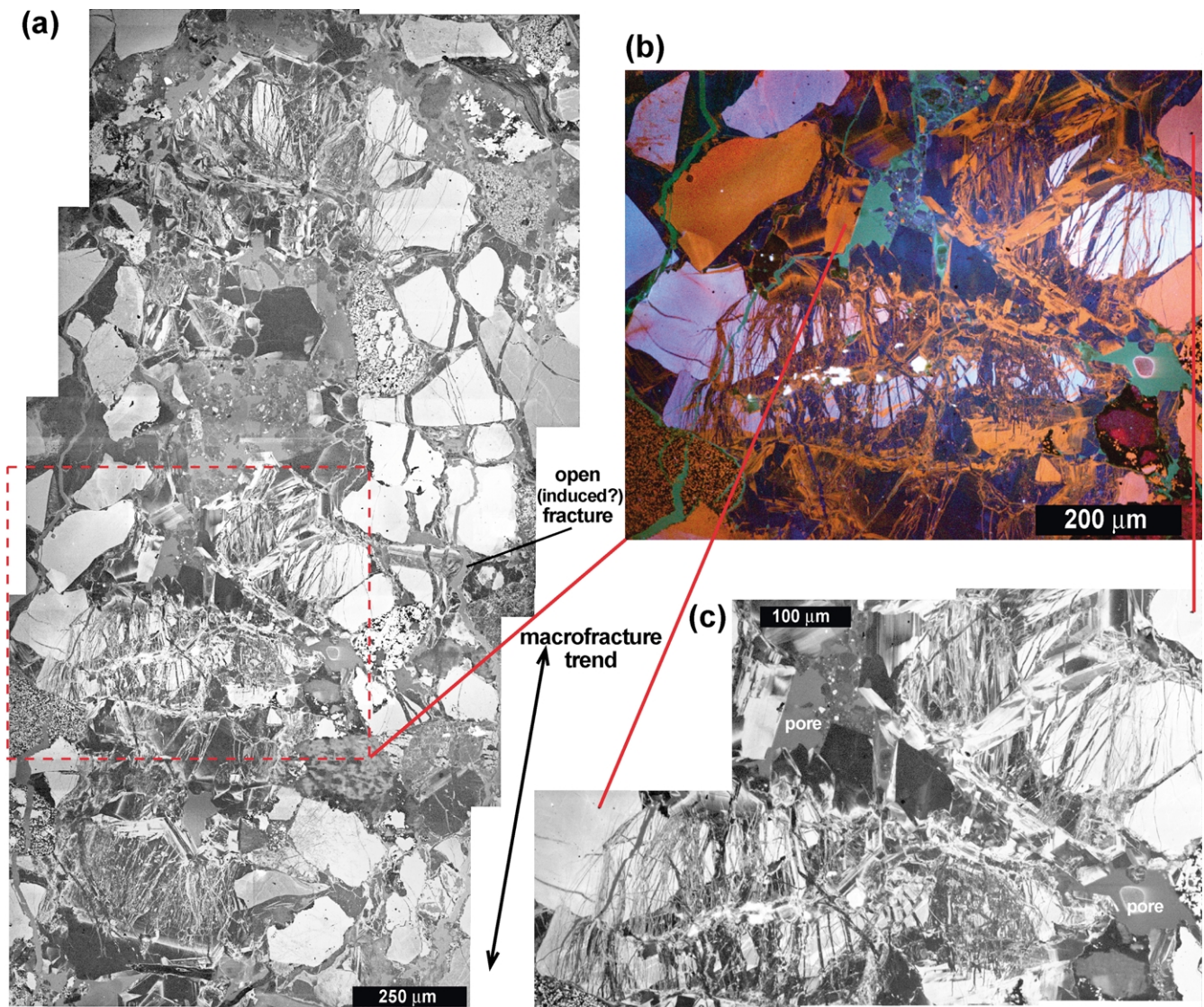


Fig. 5. Complex crack-seal texture within an almost completely quartz-filled fracture. Fracture is parallel to long axis of (a). Sample is lithic-rich, quartz-cemented sandstone of Cretaceous Cozette Sandstone (Mesaverde Group), from a depth of ~ 2417 m, Piceance Basin, northwestern Colorado. (a) Gray-scale CL-image mosaic showing segment of fracture. Images represent only CL emissions in the 600– ~ 850 nm range (red to near infrared), an emission range that shows better contrast than a more complete spectrum for this specimen. (b) Color-CL image mosaic of part of (a). Color imaging allows better determination of inclusion trails within crack-seal texture. (c) Gray-scale CL-image mosaic of red to infrared emissions showing detail within (b). (d) Plane-polarized-light photomicrograph of area shown in (a). Red lines connect corresponding points.

inclusion bands (Fig. 1) perpendicular to displacement direction. Inclusion trails (Fig. 1) form at the boundaries of grain fragments and tend to parallel the wall-rock displacement direction. Continuous-luminescence color bands shown in the CL images probably represent cement that lined or filled fracture porosity following a fracture event. Scanned-CL imaging reveals that many fractures in mineral bridges cut only earlier quartz cement (Fig. 4b). Cement bands associated with these fractures are not marked by inclusion trails, and are nearly impossible to see without scanned CL. Because crack-seal texture is developed in fracture fill that is in crystallographic continuity with grains in bridges and wall rock, in transmitted light these elongate

bridges have an appearance that has resulted in their being called *stretched crystals* (Ramsay, 1980).

Within bridges, evidence of repeated fracture includes sharp-sided boundaries, not only between broken grains and cement but also within fracture-lined cement. In many cases, scanned CL reveals micron-scale details of cross-cutting fractures and narrow cement growth zones (Figs. 4 and 5). Individual fractures are commonly less than 1 micron wide.

Crack-seal texture is typically located in the central parts of quartz mineral bridges, although in some examples cement-filled fractures extend to the outer edge of the bridge. A micron-scale veneer of unfractured quartz cement typically surrounds these areas of crack-seal texture (Figs.

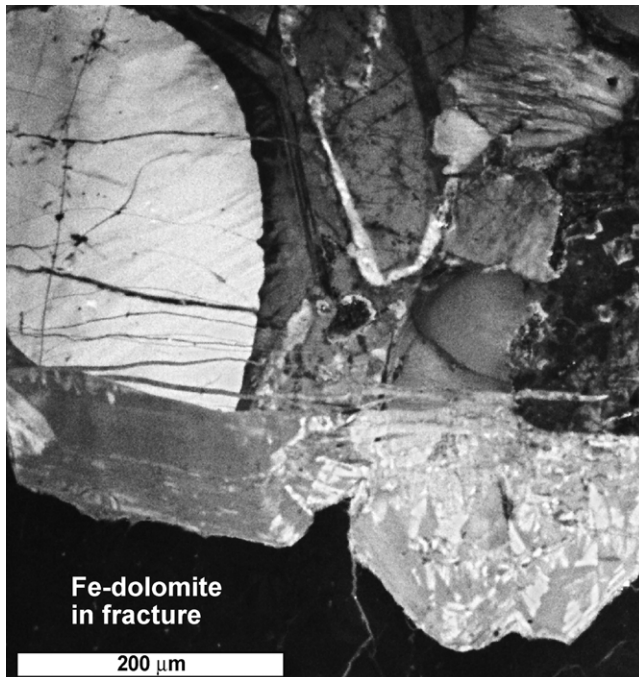


Fig. 6. Limited-wavelength (UV-blue), gray-scale-CL image showing crack-seal texture at the bases of euhedral quartz crystals growing into a macrofracture. Material on the lower part of the image is postkinematic Fe-dolomite cement. Only one side of the macrofracture is shown; opposite side shows similar textures. Sample is from Cretaceous Williams Fork Formation, northwest Colorado. Sample depth is 1748 m. Image by A. Makowitz.

2b and 4b). Where this veneer is zoned, filled fractures can be traced various distances across the zoning, apparently marking cracking and sealing within the bridge, as well as associated euhedral crystal growth on outer parts of the bridge. Where multiple crystals coalesce, complex textural patterns result from juxtaposition of these internal and external bridge textures.

Bridges reflect an unusual cement distribution along fracture walls. Quartz cement contemporaneous with fracture opening (synkinematic cement) is locally much thicker in bridges than in adjacent areas of the fracture. The ratio of cement thickness in mineral bridges spanning millimetric gaps and thin veneers of cements lining fracture walls can be 100:1 or more. Yet quartz cement on fracture walls is comparable in thickness with cement in host-rock pore space.

The concentration of synkinematic quartz cement in bridges leads to many of the features commonly associated with quartz-lined macrofractures. Areas within fractures, but between intact bridges containing crack-seal texture, may be either porous (Fig. 4) or filled to some degree by cement that postdates fracture growth (postkinematic cement) (Fig. 6; Laubach, 1988, 2003). Precipitation in static fractures is typically marked by nonquartz cements surrounding quartz bridges. Textural relations show that crack-seal texture in quartz and porosity developed at the same time. While crack-seal texture was forming in bridges,

cement did not fill in fracture pore space in adjacent parts of the fracture. As discussed later, this pattern most likely results from differences in quartz-bridge growth rate relating to substrate and orientation effects (Lander et al., 2002).

Bridges are most common in small, macroscopic fractures (apertures ~ 1 mm) and in narrow parts of wider fractures. Bridges may be absent because the fracture opened only once (and subsequently filled with cement) or opened sufficiently rapidly that cement never spanned the fracture. In some fractures, bridges are present in narrow fracture segments near fracture tips, whereas central segments may contain only euhedral crystals, presumably because quartz cement precipitation rates were insufficient to bridge the central parts of these fractures during growth (Fig. 7a). However, fractures that lack intact bridges may have relict crack-seal texture near formerly bridged fracture segments, marked by euhedral, terminated quartz crystals having crack-seal texture at their bases (Figs. 6, 7a and 8a).

The amount and location of crack-seal texture visible in a given fracture can be variable. In many cases, evidence of crack-seal processes is subtle and highly localized. Quartz can precipitate in an open fracture undergoing repeated episodic opening without recording crack-seal texture except near fracture tips and in bridges. Subsequent postkinematic cement can fill the fracture, further hiding evidence of contemporaneous deformation and cementation. Such cements will, of course, contain no record of movement. Consequently, along much of their length, many fractures will not show crack-seal texture.

4.2. Substrate effects

Wall-rock composition influences cement and porosity patterns within fractures. Materials in fracture walls that are not favorable substrates for quartz precipitation, such as lithic grains, vacuolized feldspars, and clay minerals, localize residual fracture porosity (Figs. 8 and 9). Thus, for the same fracture and burial history, small fractures in lithic and feldspathic sandstones typically are less completely filled than those in more quartzose sandstone.

Because quartz cement in fractures tends to nucleate in crystallographic continuity with host grains along fracture walls and the orientation of these grains varies, the local substrate crystallographic orientation can play a role in the details of bridge growth (Figs. 7a and 9c). An example from the Cretaceous Frontier Formation shows a quartz-lined macrofracture (Fig. 9) having four quartz grains hosting whole or partial quartz bridges, which contain dissimilar crack-seal textures. The dissimilarities result at least partly from differing growth rates along different crystallographic axes in quartz (most rapid growth is parallel to the *c*-axis).

4.3. Patterns of crosscutting fractures

Crosscutting fracture patterns (Fig. 9b) are potentially

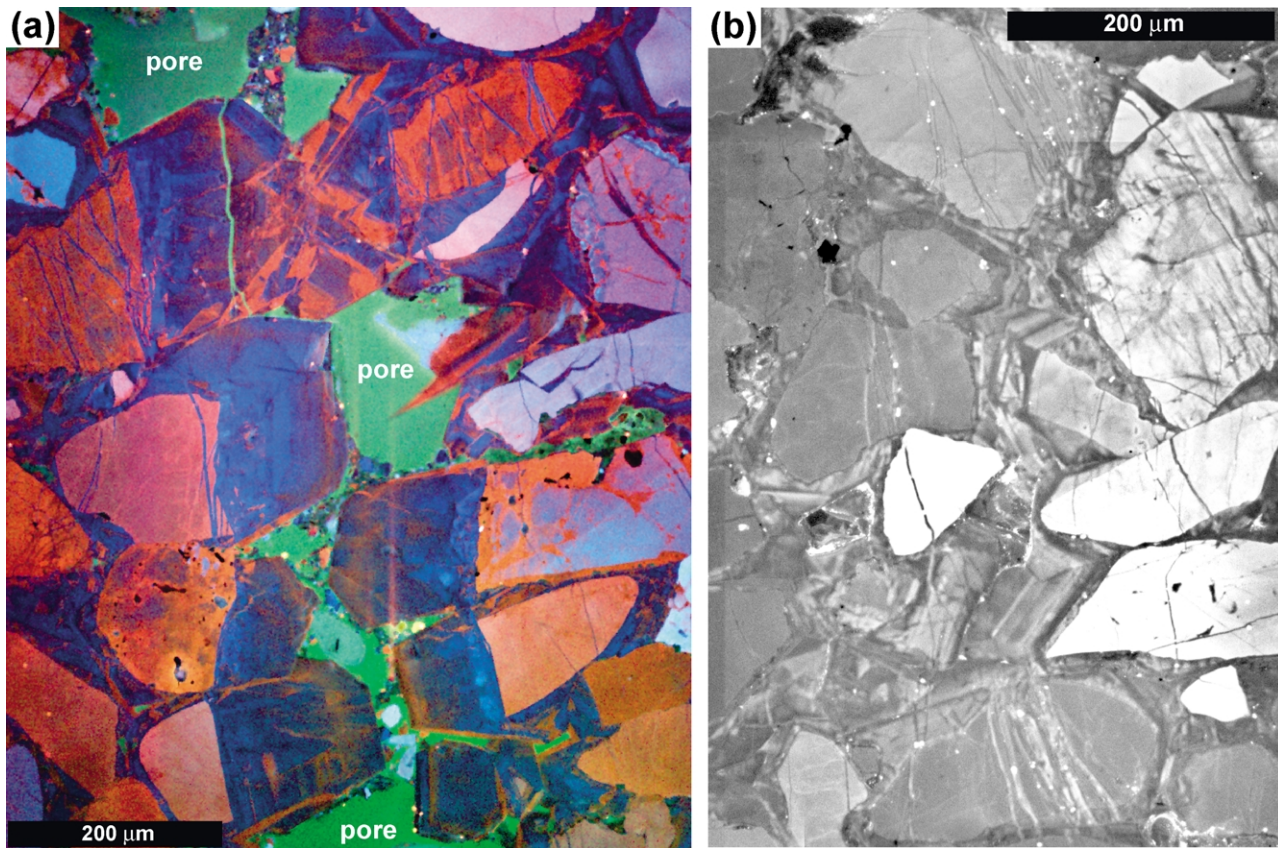


Fig. 7. Comparison of textures in central area of fracture with textures near fracture tip. Macrofracture trend is parallel to the long axis of the images. (a) Color-CL image from center of a macrofracture. (b) Panchromatic-CL image mosaic of fracture tip from same macrofracture. Image areas are approximately 12 mm apart. Both images show crack-seal texture, but note increased porosity and prevalence of unfractured, zoned, euhedral quartz in color-CL image from center of macrofracture (a). Sample is a quartz-cemented quartzarenite, depth 3008.8 m, Cretaceous Travis Peak Formation, East Texas.

significant guides for unraveling linked mechanical and cementation history. An example from Permian Wolfcamp Formation (Fig. 10) shows that in this fracture, initial cement growth was euhedral, mostly blue-luminescent, quartz cement. These crystals were cut by a set of fractures filled by orange-luminescent quartz cement. The change in cement reflects a change in precipitation conditions between early and late in the growth of the fracture.

Crack-seal patterns commonly vary along fracture traces and from one bridge to the next. These patterns mark interplay between incremental fracture widening and patterns of crystal growth into fracture cavities (Fig. 9b, #12). Some patterns, such as blunt fracture ends of quartz-filled fractures at CL-zone boundaries (Fig. 9b, #1), mark areas where porosity existed at the time fractures formed but that was subsequently destroyed by continued cement precipitation. Some structures reflect interference of simultaneous crystal growth from opposite sides of a fracture (Figs. 7a and 9b, #5).

In sandstones, fracturing occurs in both syntaxial and antitaxial positions, and these patterns may be mixed within the same fracture set or even the same fracture. Thus, in

quartz bridges, fracturing is commonly ataxial, with new fracture increments forming sequentially at various points throughout existing fracture fill (at different points within a bridge). Bridges combine aspects of both syntaxial and antitaxial fibers. Syntaxial fibers grow in optical continuity from grains in fracture walls and meet at a central seam, with the oldest parts of fibers adjacent to fracture walls. Antitaxial fibers grow incrementally from cement fill into fracture walls, lack a central seam, and are not continuous from wall grains with the youngest parts at fracture walls (Dunne and Hancock, 1994). From one quartz bridge to the next, fracture locations in bridges may be inconsistent (Figs. 5a, 8 and 9); care is thus needed in interpreting crack-seal history from fluid inclusions using optical microscopy. Scanned-CL imaging reveals that wall-rock inclusions within adjacent bridges that line up do not necessarily mark the same growth step.

In some fractures that have fills formed by the crack-seal mechanism, there is a gradation inward from closely spaced microfractures in fracture walls, to highly fractured wall-rock and cement zones, to massive, less fractured fill within fracture centers (Figs. 2a, 4d and 7a). This pattern probably results from cement precipitation, where cement initially

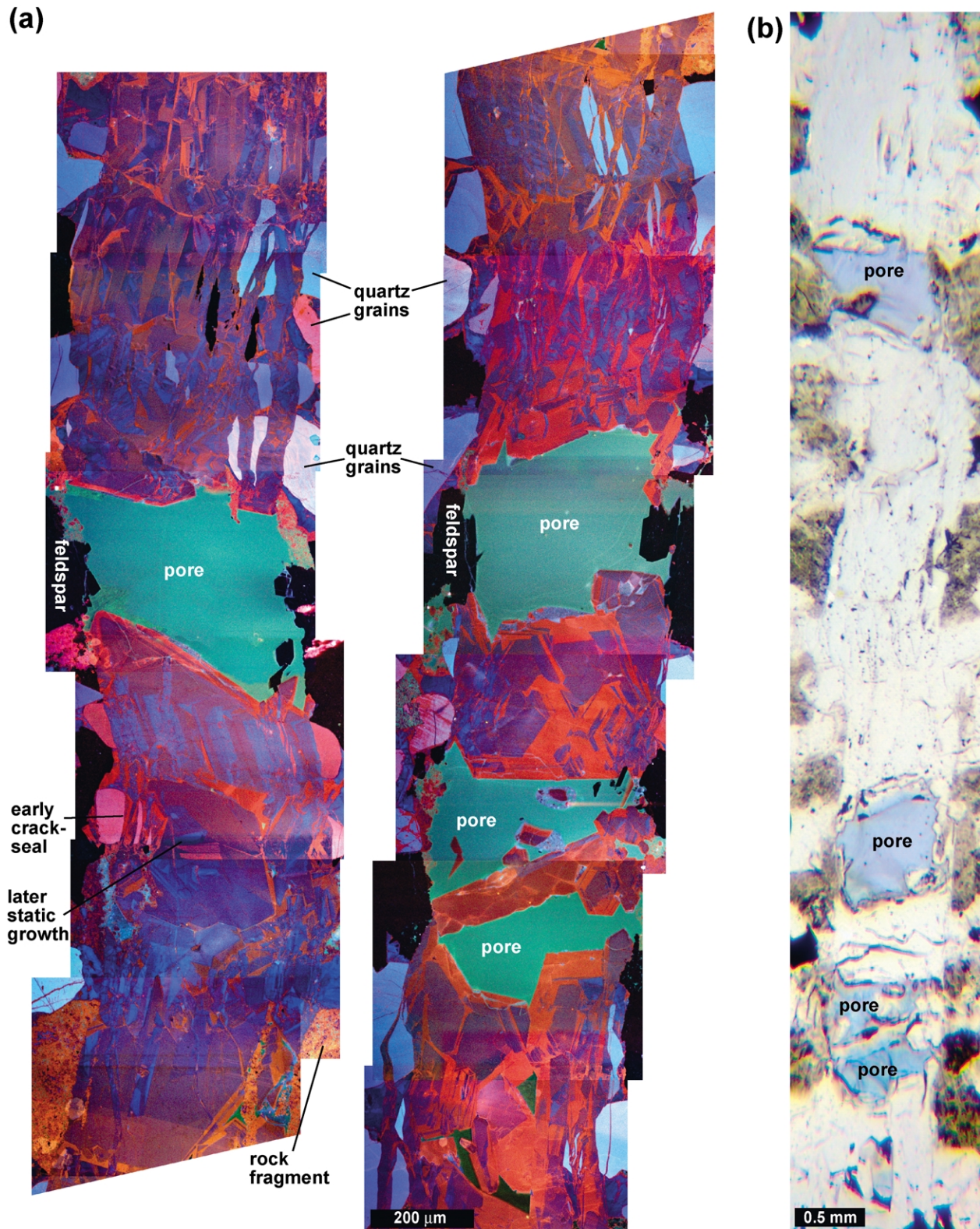
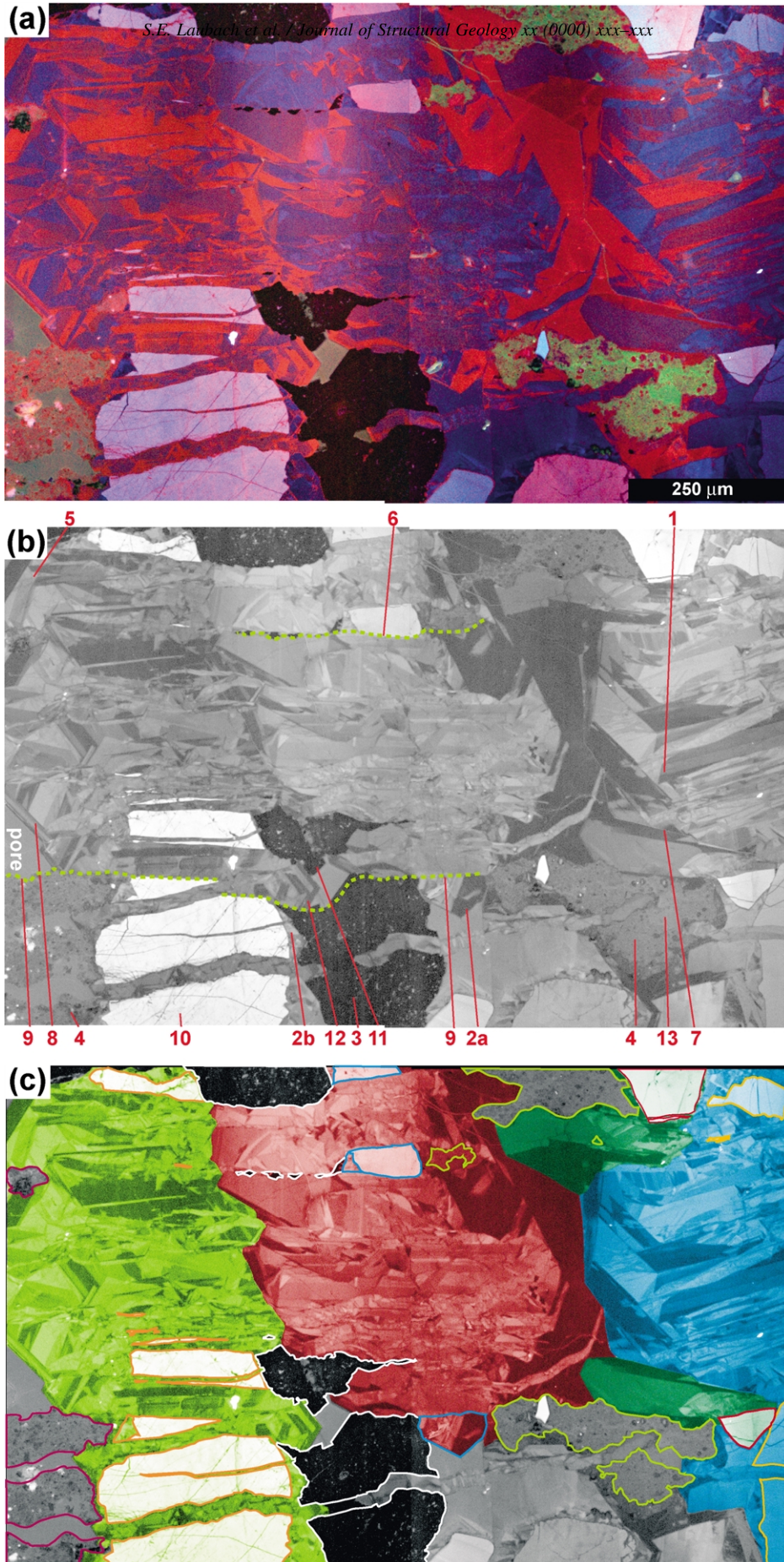


Fig. 8. Images showing variability in fracture structure along fracture plane. (a) Color-CL image mosaic along a partly open, quartz-lined macrofracture. Mosaic has been split; left image connects to the top of the right image. Bright-green, luminescent, epoxy-filled porosity is associated with nonluminescent feldspar grains. Quartz bridges adjacent to one another do not necessarily show the same patterns of breakage. (b) Plane-polarized-light photomicrograph mosaic of macrofracture shown in (a). Image shows approximately the same macrofracture area as (a). Brown grains are altered feldspars and rock fragments. Sample is lithic arkose from 6244.6 m, Cretaceous Frontier Formation, Wind River Basin, Wyoming.



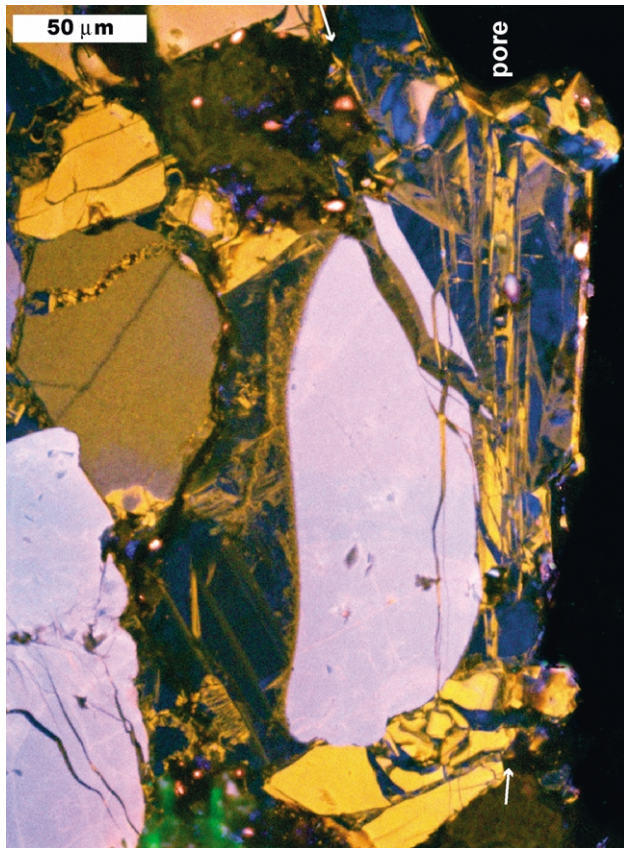


Fig. 10. Color-CL image showing one side of macrofracture rebroken during sampling. Overall macrofracture trend is parallel to the long axis of the image; arrows mark approximate fracture walls. Polyphase fracture-lining quartz cement is defined by different luminescent colors. Euhedral, mostly blue-luminescent, quartz cement in fracture is cut by incremental fractures filled with orange-luminescent quartz cement. Sample is a quartz-cemented sandstone from Permian Wolfcamp Formation, Val Verde Basin, West Texas; depth 2516.7 m.

spans a narrow fracture, but for the subsequent wider fracture the cement occurs without spanning the gap.

4.4. Fracture tips and links

Tips of macrofractures in sandstone and areas of fracture overlap and linkage show intersecting and overlapping fractures that resemble crack-seal texture formed within the main parts of fractures. These zones of fracture growth and coalescence produce distinct varieties of crack-seal texture.

Although many fractures merely taper to a tip, near their tips some fractures die out by transforming into swarms of microfractures. Transcendent or transgranular, quartz-lined microfractures are common at fracture tips (Fig. 7b). These microfractures may constitute fossilized process zones (Labuz et al., 1987). When the main fracture grows past these microfractures, they appear as a type of crack-seal texture.

Both crack-seal texture and within-fracture quartz cement tend to be more common near tips than in centers of macrofractures (Fig. 7). In many cases, the center of a macrofracture will show only early-stage crack-seal texture and euhedral quartz crystals, but fracture tips will have full-span quartz bridges that show crack-seal texture. Crack-seal texture can form only where cement can span fracture gaps before the next increment of fracture growth, so this pattern is probably a result of incomplete cement failing to span the widest parts of fractures during incremental crack growth (Fig. 7).

Some microfracture arrays near fracture tips are arranged in divergent fans of crosscutting, superposed microfractures localized at fracture tips but not elsewhere along fracture walls, as might be expected for bypassed process zones (Laubach, 1989a). Each growth increment and accompanying expansion of the main fracture result in a new quickly

Fig. 9. (a) Color-CL image mosaic of a quartz-lined macrofracture. Quartz grains and euhedral overgrowths partly filling fracture were broken repeatedly by later fracture increments. Green speckled areas within fracture are epoxy-filled fracture porosity. Macrofracture trend is parallel to the long axes of the image. (b) Panchromatic, gray-scale-CL image mosaic of same area as in (a), but labeled to show important features. (1) Note blunt termination of this quartz-filled fracture at a CL-zoning boundary. At the time the fracture formed, the blue-luminescent band was at the edge of a euhedral crystal bordered by porosity. The red-luminescent cement band grew after the fracture formed and filled. (2) Prekinematic quartz overgrowths are generally euhedral (pore-filling) and show zoned, mostly blue luminescence. 2A is an overgrowth that has been broken off its grain (see quartz grain at 6); 2B is still attached to grain on which it grew. (3) Detrital feldspar grains are not typically nonluminescent, as these are, unless they have undergone significant alteration. Authigenic feldspar cement (see 11) is typically nonluminescent. (4) Rock fragments in this sample have intermixed red and green luminescence in color CL. Green luminescence is due to epoxy filling microporosity within grain. (5) Dovetail shape defined by CL-zoning, a result of simultaneous euhedral quartz growth from both sides of a fracture meeting in the center. These structures help unravel the complex history of this macrofracture. This fracture increment occurs entirely within quartz cement, which fills a larger fracture. (6) An inclusion band defined by (top to bottom) a rock fragment, part of a quartz grain, fractured prekinematic quartz cement, and a trail of small nonluminescent feldspar grain fragments. This band marks the boundary between two microstructural provinces inside a larger macrofracture and is possibly one side of the earliest fracture increment. (7) Quartz crystallographic boundary that is also a boundary between quartz bridges with different mechanical histories. Fracture fill shown here includes four different quartz crystallographic domains, three of which span the macrofracture (Fig. 12). (8) Unfractured, late euhedral cement growing into a pore. (9) Partial trace of an early fracture surface that cuts grains and prekinematic cement but not synkinematic cement. This trace is cut by at least one later fracture. (10) Fractured quartz grain, which contributes at least seven pieces to an inclusion trail. (11) Euhedral outer zones (nonluminescent) growing into fracture porosity represents cryptic authigenic feldspar cement associated with host feldspar grains. (12) Euhedral quartz cement that grew laterally into fracture porosity adjacent to a broken feldspar grain. (13) Pore-filling epoxy typically has a speckled green luminescence in color CL. In this case, epoxy is the filling microfracture porosity inside a rock fragment. Sample is a feldspathic litharenite from the Cretaceous Frontier Formation, Wyoming, depth 6242.15 m. Thin section cut parallel to bedding. (c) Limited wavelength (ultraviolet to blue), gray-scale-CL image having other superimposed information. Margins of original sedimentary grains are outlined in a different color for grain fragments making up each inclusion trail. Color tinting delineates four optically continuous areas of quartz (areas include both grain and overgrowth cement).

sealed microfracture extending away from the main porous section of the main fracture. The fracture lengthens but subsequently shortens owing to cement deposited in fracture tips. This pattern is a type of crack-seal texture we infer to be associated with stationary crack tips. Macrofractures associated with this style of crack-seal texture tend to be unusually wide relative to their heights, having height-to-width ratios of less than 200 (Laubach, 1989b). This pattern implies feedback between cement precipitation, fracture growth, and possible decay of stress perturbation around the main fracture. Perhaps the right loading, temperature, and fluid conditions result in fracture systems that *stall*.

Evidence of repeated fracture and cementation is found where en échelon fractures link or overlap. Microfractures are common where en échelon macrofracture strands overlap (Fig. 11). Microfractures in the overlap region connecting large fracture segments can link and amalgamate into a single continuous macrofracture. Along large fractures, previous areas of overlap fossilize a variety of crack-seal textures representative of fracture linkage (similar to *vein coalescence*; Misik, 1971).

Multigenerational fracture growth near an en échelon

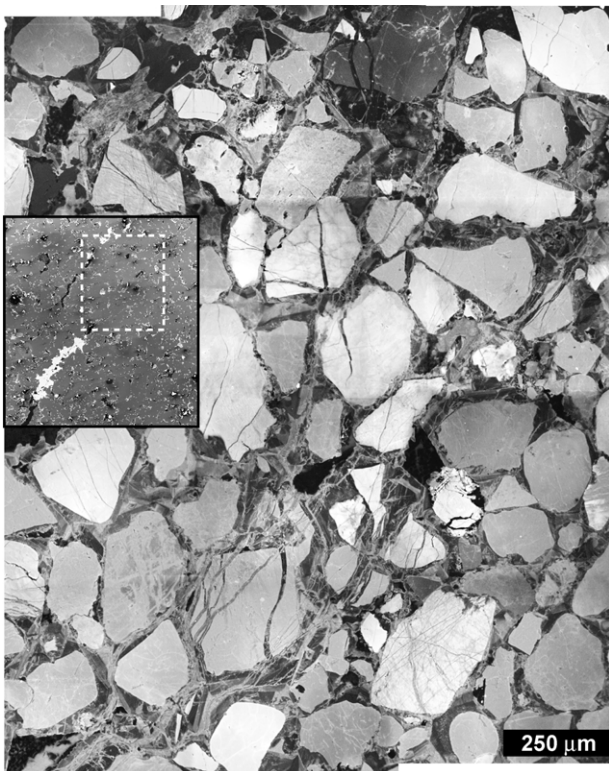


Fig. 11. Panchromatic, gray-scale-CL image mosaic showing transcement or transgranular, linking quartz-lined microfractures in the overlap zone between two macrofractures. Most visible grains are quartz. Inset shows a secondary electron image of the overlap zone; dashed square marks the approximate area of the CL mosaic. In the macrofractures, early synkinematic quartz cement is followed by postkinematic barite cement (light-colored in secondary electron image), which has partly filled the fracture porosity. Inset image is ~ 5.1 mm wide. Sample is a quartz-cemented quartzarenite of the Cretaceous Fall River Formation from the Powder River Basin, Wyoming. Sample depth is 3774.9 m.

step between two macrofractures in Cretaceous Fall River Sandstone core (Johns et al., 1995) shows in plan view early microfractures obliquely spanning the step between tips of large fractures (Fig. 11). These microfractures are crosscut by later microfractures aligned parallel to the macrofracture trend that record a growth history in the zone surrounding interacting crack tips. The transition from curved to straight traces could result from increased far-field fracture-parallel compressive stress during fracture growth (Olson and Pollard, 1989).

4.5. Variations in extension direction

Crack-seal texture can record evidence of (1) changes in incremental extension direction during deformation and (2) extension oblique to strike of the incremental fracture (Fig. 12). These are mostly examples of ataxial, as opposed to syntaxial or antitaxial, incremental fracture patterns. Graphic restoration of grain fragments in some cases shows that changes in overall extension direction are small despite changes in orientations of fracture-forming growth increments through time (Fig. 12a). However, markedly differing early and late incremental extension directions are locally evident, including one example (Fig. 12b), where the late direction differs by 65° from the early direction. In our data set, both progressive changes in extension direction and reactivation of fractures during later, separate fracturing events are attested.

Although most examples have simple patterns of opening normal to fracture walls, we have also found rare examples of textures that have a chaotic appearance compared with that of typical crack-seal texture. An example from within a fracture from the Weber Formation (Fig. 13) has grain fragments that were apparently plucked from the walls but rotated before sealing. How this structure evolved is obscure. However, this structure, and previous examples with simpler patterns, illustrates the potential for CL to track complex, kinematically significant structural patterns within quartz bridges.

4.6. Crack-seal texture in microfractures

In addition to large fractures, crack-seal texture is present in microfractures (Fig. 14). A few micron-scale microfractures have distinct crack-seal texture, indicating many increments of fracture opening. In general, however, microfractures of this size and smaller tend to be sealed and to lack distinct crack-seal texture. This situation may partly reflect the fact that these fractures are many times smaller than particles in host sandstone, making entrainment of distinct wall-rock fragments unlikely. In many cases, resolution limits of scanned CL hinder delineation of crack-seal texture in cement at this magnification. Crack-seal texture is documented in microfractures but is frequently obscure.

A spectacular example of fine-scale, crack-seal texture

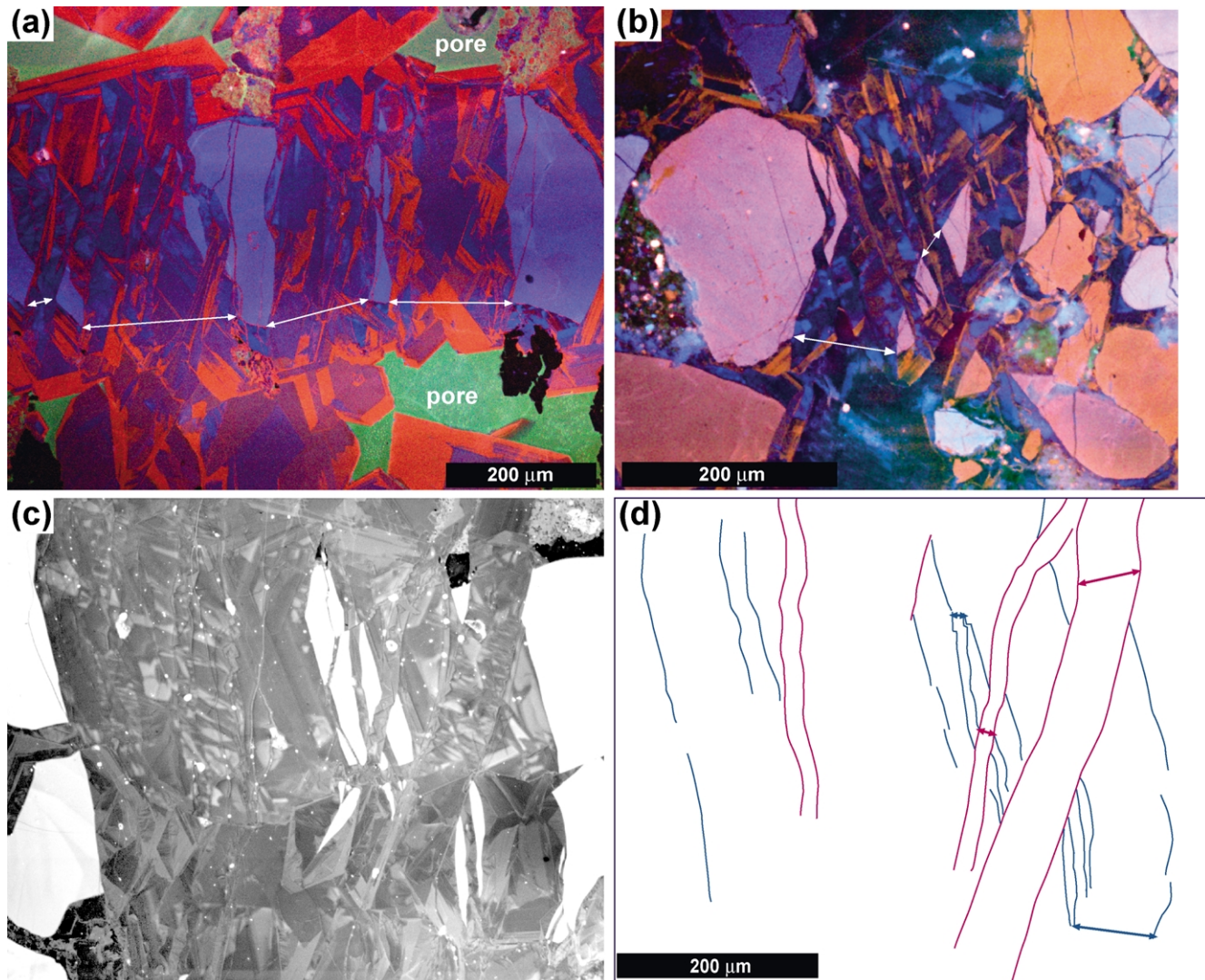


Fig. 12. Apparent variations in extension direction marked by progressive shift in fracture trends and cement-growth increments. In each image, overall fracture trend is roughly parallel to the short axis of the image. (a) Color-CL image showing crack-seal texture in a quartz bridge; reconnection of grain fragments suggests that extension direction (arrows) has not changed markedly, although the trends of early and late fractures are different. Feldspathic litharenite from Cretaceous Frontier Formation, Wyoming; 6242.1 m. (b) Fractured quartz bridge (center) surrounded by almost nonluminescent postkinematic carbonate cement. Early and late incremental extension directions differ. Color-CL image, of a sublitharenite from Permian Wolfcamp Formation, Val Verde Basin, West Texas; depth of 2386.4 m. (c) Small fractures within larger fracture showing that displacement direction of crack-seal opening steps changed with time. Panchromatic, gray-scale-CL image. Lithic arkose from Cretaceous Frontier Formation, Wyoming; depth 6244.6 m. (d) Line drawing delineating extension directions in (c). Early fractures are outlined in blue; late fractures in purple.

from the Pennsylvanian Pottsville Formation shows five to seven increments of opening in a fracture only about 35 microns wide (Fig. 14b). Microfractures of this size and smaller tend to be sealed or to have only small, discontinuous areas of porosity. Where visible, extension increments of microfractures having crack-seal texture are commonly on a submicron scale.

Progressive microfracturing and crosscutting relations among cement zoning and microfractures in host rocks also record fracture-timing information relative to cement precipitation. Microfractures that are distant from large fractures, yet are aligned with them and contain cement of the same relative age, are common (Fig. 6), suggesting that both are responding to the same far-field loads (Laubach,

1997). Moreover, consistent size distributions ranging over several orders of magnitude (Marrett et al., 1999) suggest that these disseminated microfractures are smaller versions of the fractures that contain crack-seal texture.

5. Discussion

5.1. Conditions leading to crack seal in sedimentary rocks

In folded and faulted sandstones, crack-seal texture is unsurprising because the large forcing structures probably grew incrementally. Where crack seal has been identified in sedimentary rocks, examples are mostly from fault zones

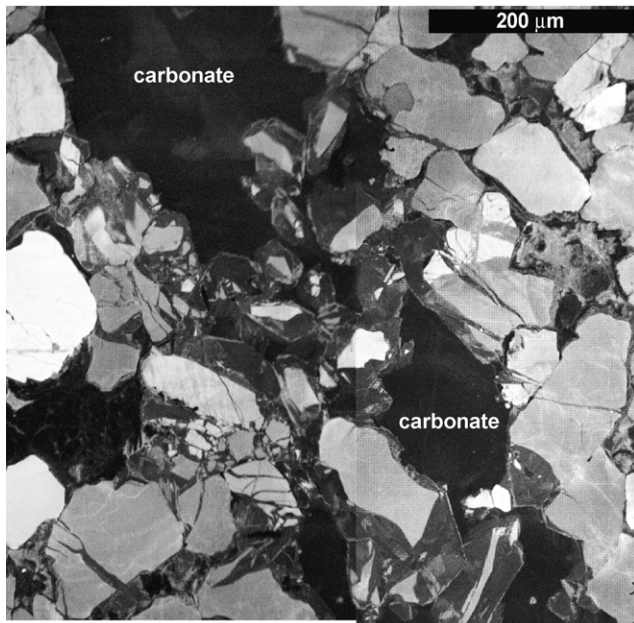


Fig. 13. Panchromatic, gray-scale-CL image showing an apparently chaotic crack-seal texture within a macrofracture, Pennsylvanian–Permian Weber Formation, Rangely field, Piceance Basin, Colorado. Grain fragments located within fracture have been torn from walls and rotated prior to sealing. Least luminescent material in macrofracture is Fe-bearing carbonate cement that surrounds and postdates euhedral quartz overgrowths. Sample depth 1738.2 m.

(Anders and Wiltchko, 1994), although a few examples were described in relatively undeformed rocks (Laubach, 1988). Our study shows that crack-seal texture is common in horizontal to subhorizontal sandstone beds distant from faults or folds, if sandstones have been subject to burial sufficiently deep and protracted for quartz cement to precipitate. These structures have never been imaged as unambiguously as they are using scanned CL. In many samples, the only structures associated with crack-seal texture are the host fractures with their flanking microfractures, and, in some cases, bed-parallel stylolites. The conditions leading to crack-seal texture must therefore be prevalent in regional fractures under a wide range of burial conditions and tectonic settings.

Qualitative evidence suggests that internal structures in fractures vary to some extent with burial depth and location. For example, fractures formed in deeper, better cemented rocks, tend to cut through, rather than around, grains and, hence, show more complex internal structures. Increased burial depth generally correlates with increased temperature and increased quartz precipitation, which can lead to better developed, more complex bridges.

In two areas where we have analyzed primary fluid inclusions trapped in cements associated with crack-seal texture, a range of temperature and salinity values is evident. Saline fluid inclusions having mean temperatures of about 110 °C but a range of more than 50 °C are present in crack-seal structures in East Texas sandstones at about 3000 m (e.g. Laubach, 1989a,b; Lander et al., 2002) and

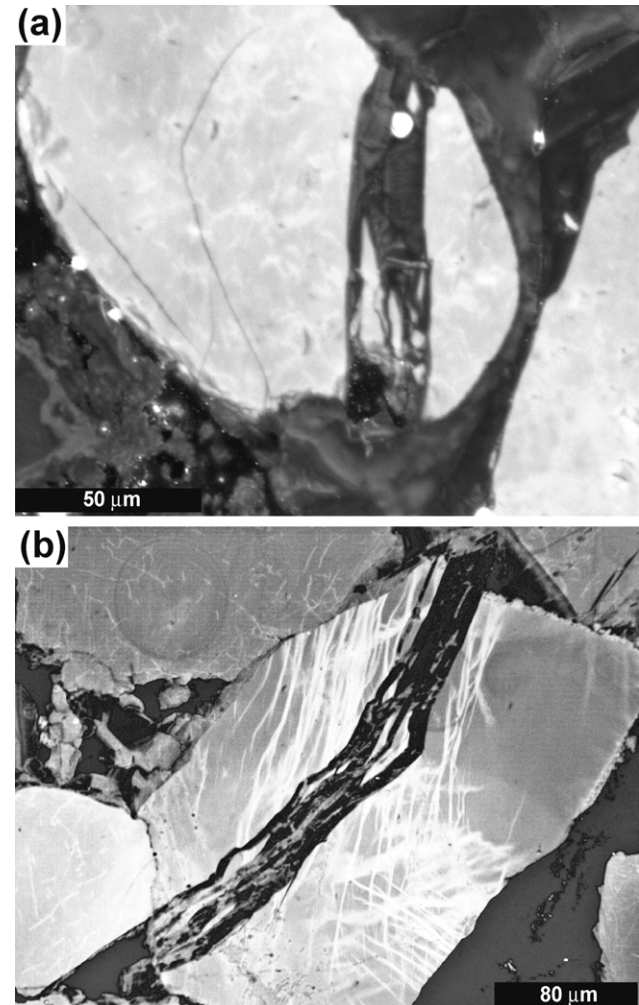


Fig. 14. Crack-seal texture in microfractures. (a) Panchromatic, gray-scale-CL image of sample from Cretaceous Dakota Formation, San Juan Basin, New Mexico; depth 2154.4 m. (b) Panchromatic, gray-scale-CL image of sample from Pennsylvanian Pottsville Formation, Black Warrior Basin, Alabama; depth 1052.5 m. Brightly luminescent linear structures in quartz grain are probably a result of plastic strain. Round structure in upper left is an imperfection in sample preparation.

low-salinity fluid inclusion having bimodal trapping temperatures of 140 and 230 °C and ranges of more than 25 °C occur in crack-seal structures in Wyoming at about 6000 m (Laubach, unpublished). These results show that a wide range of burial conditions or fluid temperatures can be associated with quartz bridges having crack-seal texture and associated fracture porosity.

Crack-seal texture is associated not only with precipitation of quartz cement but also preservation of fracture porosity for fractures of a specific size and larger. This association suggests that for the burial histories and time of fracturing of the rocks that we examined, the rate of cement precipitation for quartz is insufficient to occlude fracture porosity after fractures formed. Textures on the margins of bridges show that quartz precipitation did not stop when fracture opening ceased. Because the samples we studied represent a wide range of current burial depths and burial

histories, bridging and crack-seal textures are unlikely to result from basin-specific or rarely developed diagenetic conditions. Likewise, unusual structural conditions are probably not responsible for these structures. Repeated fracture opening marked by crack-seal texture and other evidence of episodic fracture growth, such as arrest lines, is consistent with natural hydraulic fracture mechanisms of fracture growth (Laubach, 1988; Engelder and Fischer, 1996). Such structures can arise under a wide range of tectonic, burial, and pore-pressure histories.

Crack-seal texture may be frequently associated with quartz cement precipitation in moderately to deeply buried sandstones because throughout much of a sandstone's burial history, substrate composition and rock-dominated fluid chemistry dictate that this cement is most likely to precipitate. Diagenetic modeling and high-temperature precipitation experiments show that bridges most likely result from rapid crystal precipitation on repeatedly renewed fracture surfaces (Lander et al., 2002). Multiple fracture events are required to create bridges, and the rate of fracture growth cannot greatly exceed cement precipitation rate. The size of bridges and constituent cement layers within crack-seal increments most likely depend on the time/temperature history of the fracture, the primary controls on cement precipitation rates and volumes, and fracture-opening rates. Used in conjunction with diagenetic-modeling and burial-history information, the ratio of fracture to host-rock cement volume is a potentially important metric of deformation history (Lander et al., 2002).

Because quartz frequently does not fill large fractures even in deeply buried sandstones, these structures may become cemented by other phases such as carbonate minerals. The rarity of crack-seal texture in carbonate fracture fills in sandstones suggests that mechanical conditions leading to fracture growth infrequently coincide with geochemical conditions favoring carbonate mineral precipitation in these quartzose rocks. For many types of sandstone, fluids associated with fracture growth are the same as those that precipitate quartz cement, suggesting that these are the fluids that are relevant to subcritical crack growth (cf. Holder et al., 2001).

5.2. Evidence against force-of-crystallization vein growth

The interpretation in the previous section contrasts with models of vein formation where vein and fracture growth are different processes. For example, Wiltschko and Morse (2001) assumed that veins are characteristically completely filled with cement and proposed that cement-filled veins are consistent with vein widening caused by pressure due to growing crystals. They suggested that some veins originate at sites of precipitation and then widen because of pressure exerted by crystal growth. As materials precipitate, vein walls are pushed apart. In their scenario, a nonzero remote differential stress is proposed to explain vein alignment.

Resulting veins have shapes typical of opening-mode cracks except that, mechanically, crystallization pressure replaces the role of internal fluid pressure in their propagation. Veins that formed by this mechanism involve precipitation forces driving crack growth. These researchers ascribed apparent crack-seal texture to geochemical self-organization at the vein wall driven by pressure–solution-enhanced supersaturation in pore fluid and nonlinear precipitation kinetics at the vein wall.

Sharply defined wall-rock fragments and fractured cements in narrow cement bridges are compelling evidence that cement crystallization did not drive fracture growth in the examples we studied, even though some of these fractures are now filled with cement (i.e. they are veins). The association of clearly delineated crack-seal texture and increasing fracture porosity with increasing fracture size shows that cement fills fractures passively, responding to the growing crack rather than driving it. Narrow-diameter bridges of vein-fill material having crack-seal texture are incompatible with models of fracture growth that call on cements to push fracture walls apart and call for apparent crack-seal textures to reflect geochemical self-organization. Vein-filling carbonate cements in the sandstone samples we examined are typically deposited *after* fractures ceased widening (Laubach, 2003). The force-of-crystallization mechanism for vein expansion (Wiltschko and Morse, 2001) is not a viable explanation for these widespread, open or mineral-filled fractures.

5.3. Implications for fracture growth modeling

Where regional opening-mode fractures are unrelated to faults and folds, crack-seal texture marks episodic fracture growth driven by interplay of evolving rock properties, compaction, pore pressure, burial-related temperature changes, and overburden and remote tectonic loads. Some combination of increased fluid pressure, decreased confining stress, and subcritical crack propagation is probably responsible for driving fracture growth (Engelder and Fischer, 1996; Olson et al., 2001). In these settings, cementation-related pore-pressure change is a possible mechanism for overpressure generation (Bjørkum and Nadeau, 1998; Lander et al., 1999; Walderhaug et al., 2001; Wangen, 2001). Crack-seal textures and evidence of cement accumulation rates could clarify whether local transient pore-pressure increases, associated with rapid cementation, could be a driver of fracture growth.

Together with temperature, burial history, and mineral kinetics information, crack-seal textures could provide evidence to constrain fracture-opening rates (Lander et al., 2002). By studying growth histories of individual fractures in a population and tying growth history to cement stratigraphy and other geochemical information (e.g. fluid inclusion temperature and pressure data), we can place the evolution of fracture arrays in the context of thermal and burial-history models and numerical models of fracture

growth (Lander et al., 2002; Olson, 2004). These structures could provide a useful link between mechanical and diagenetic modeling. Although the mechanics of natural opening-mode fractures has been extensively debated (Hancock, 1985; Pollard and Aydin, 1988; Engelder and Fischer, 1996; National Research Council, 1996), the potential for diagenetic reactions in fractures to influence fracture mechanics has not been widely appreciated, aside from the phenomenon of subcritical crack propagation (Atkinson, 1984; Holder et al., 2001). To the extent that cementation influences changing rock and fracture properties and pore-fluid pressure, comprehensive models of fracture systems need to account for both mechanical and chemical/cementation processes.

6. Conclusions

Crack-seal texture is present in isolated mineral bridges surrounded by fracture porosity for a wide range of sandstone rock types, tectonic settings, and burial depths. These structures document episodic fracture growth that can include tens to hundreds of growth increments in regional opening-mode fractures having apertures of a few tens of microns to several millimeters or more.

Linked crack-seal texture, bridges, and fracture porosity reflect competition between fracture growth and cement precipitation. Bridge formation probably reflects competition between fracture opening rates and cement accumulation rates (Lander et al., 2002). Most fractures never achieve the size or opening rate critical to outstripping cement precipitation and, therefore, cease growing and become sealed. As fractures widen, cement can no longer grow across open parts of the fracture before the next fracture-growth increment. Cement precipitation that falls far behind fracture expansion leads to wide, mostly open fractures having thin veneers of quartz on fracture walls. Because this association of structures is present in a range of settings, it is not the product of unique circumstances in burial history and fluid flow. We interpret them to reflect the confluence of rock-dominated geochemistry that is widespread in time and space and fracturing caused by a spectrum of loading conditions. The fine detail of cement accumulation in crack-seal texture visible using scanned CL has great potential for helping to unravel the operation of these linked diagenetic and structural processes.

Acknowledgements

Partly supported by a grant from the Office of Basic Energy Sciences, U.S. Department of Energy, Contract No. DE-FC26-00BC15308 and by industrial associates of the Fracture Research and Application Consortium: Chevron-Texaco, Devon Energy Corporation, Ecopetrol, Marathon Oil, PEMEX Exploración y Producción and IMP, Petroleos

de Venezuela, Petrobras, Repsol-YPF, Saudi Aramco, Shell International Exploration & Production, Schlumberger, Tom Brown, Inc., and Williams Exploration & Production. We are grateful to associates for sample suites used in this study, to A. Makowitz and A. Ozkan for contributions to petrography, and to J. Gale, J. Holder, O. Ortega, R. Marrett, K. Milliken, and W. Narr for valuable discussions. The manuscript benefited from comments by Jim Evans, Julia Gale, Lana Dieterich, and an anonymous reviewer. Publication approved by the Director, Bureau of Economic Geology.

References

- Anders, M.H., Wiltschko, D.V., 1994. Microfracturing, paleostress and the growth of faults. *Journal of Structural Geology* 16, 795–815.
- Atkinson, B.K., 1984. Subcritical crack growth in geological materials. *Journal of Geophysical Research* 89, 4077–4114.
- Bjørkum, P.A., Nadeau, P.H., 1998. Temperature controlled porosity/permeability reduction, fluid migration, and petroleum exploration in sedimentary basins. *APEAJ*, 453–464.
- Dickinson, W.W., Milliken, K.L., 1995. The diagenetic role of brittle deformation in compaction and pressure solution, Etjo Sandstone, Namibia. *Journal of Geology* 103, 339–347.
- Dieterich, D., Grant, P.R., 1985. Cathodoluminescence petrography of syntectonic fibers. *Journal of Structural Geology* 7, 541–553.
- Dunne, W.M., Hancock, P.L., 1994. Paleostress analysis of small-scale brittle structures. In: Hancock, P.L., (Ed.), *Continental Deformation*, Pergamon Press, pp. 102–111.
- Engelder, T., Fischer, M.P., 1996. Loading configurations and driving mechanisms for joints based on the Griffith energy-balance concept. *Tectonophysics* 256, 253–277.
- Ferguson, H.G., Ganett, R.W., 1932. Gold quartz veins of the Alleghany district, California. U.S. Geological Survey No. 172, 139pp.
- Fisher, D.M., Brantley, S.L., 1992. Models of quartz overgrowth and vein formation; deformation and episodic fluid flow in an ancient subduction zone. *Journal of Geophysical Research* 97 (13), 20043–20061.
- Fowles, J., Burley, S., 1994. Textural and permeability characteristics of faulted, high porosity sandstones. *Marine and Petroleum Geology* 11, 608–623.
- Gale, J.F.W., Laubach, S.E., Marrett, R.A., Olson, J.E., Holder, J.T., Reed, R.M., 2004. Predicting and characterizing fractures in dolomite reservoirs: using the link between diagenesis and fracturing. *Geological Society of London Special Publication, Dolomite and Dolomitization*, in press.
- Hancock, P., 1985. Brittle microtectonics: principles and practice. *Journal of Structural Geology* 7, 437–457.
- Hogg, A.J.C., Sellier, E., Jourdan, A.J., 1992. Cathodoluminescence of quartz cements in Brent Group sandstones, Alwyn South, UK North Sea. In: Morton, A.C., Haszeldine, R.S., Giles, M.R., Brown, S. (Eds.), *Geology of the Brent Group*. Geological Society Special Publication 61, pp. 421–440.
- Holder, J., Olson, J.E., Philip, Z., 2001. Experimental determination of subcritical crack growth parameters in sedimentary rock. *Geophysical Research Letters* 28, 599–602.
- Hulin, C.D., 1929. Structural control of ore deposition. *Economic Geology* 24, 15–49.
- Johns, M.K., Laubach, S.E., Milliken, K.L., 1995. New microtextural evidence of syncementation fracturing in sandstone. *Geological Society of America, Annual Meeting, Abstracts with Programs* 27 (6), 216.
- Labuz, J.F., Shah, S.P., Dowding, C.H., 1987. The fracture process zone in granite; evidence and effect. *International Journal of Rock Mechanics and Mining Sciences & Geomechanics Abstracts* 24, 235–246.

- Lander, R.H., Walderhaug, O., 1999. Predicting porosity through simulating sandstone compaction and quartz cementation. *American Association of Petroleum Geologists Bulletin* 83, 433–449.
- Lander, R.H., Helset, H.M., Bonnell, L.M., Matthews, J.C., 1999. Implications of sandstone diagenesis for fluid overpressure development and seal failure. *American Association of Petroleum Geologists Annual Convention, Abstracts* 8, A76.
- Lander, R.H., Gale, J.F.W., Laubach, S.E., Bonnell, L.M., 2002. Interaction between quartz cementation and fracturing in sandstone. *American Association of Petroleum Geologists Annual Convention, Abstracts* 11 (CD).
- Laubach, S.E., 1988. Subsurface fractures and their relationship to stress history in East Texas Basin sandstone. *Tectonophysics* 156, 37–49.
- Laubach, S.E., 1989a. Paleostress directions from the preferred orientation of closed microfractures (fluid-inclusion planes) in sandstone, East Texas Basin, U.S.A. *Journal of Structural Geology* 11, 603–611.
- Laubach, S.E., 1989b. Fracture analysis of the Travis Peak Formation, western flank of the Sabine Arch, East Texas. The University of Texas at Austin, Bureau of Economic Geology Report of Investigations No. 185, 55pp.
- Laubach, S.E., 1997. A method to detect fracture strike in sandstone. *American Association of Petroleum Geologists Bulletin* 81 (4), 604–623.
- Laubach, S.E., 2003. Practical approaches to identifying sealed and open fractures. *American Association of Petroleum Geologists Bulletin* 87 (4), 561–579.
- Marrett, R.A., Ortega, O.O., Kelsey, C., 1999. Power-law scaling for natural fractures in rock. *Geology* 27, 799–802.
- Milliken, K.L., 1994a. The widespread occurrence of healed microfractures in siliciclastic rocks: evidence from scanned cathodoluminescence imaging. In: Nelson, P.A., Laubach, S.E. (Eds.), *North American Rock Mechanics Symposium*, Austin, Texas, Balkema, pp. 825–832.
- Milliken, K.L., 1994b. Cathodoluminescence textures and the origin of quartz silt in Oligocene mudrocks, South Texas. *Journal of Sedimentary Research* A64, 567–571.
- Milliken, K.L., 1996. Deformation bands formed by interrelated cementation and brittle fracture in porous sandstones, Hickory Formation, central Texas; synkinematic diagenesis revealed by cathodoluminescence imaging. *American Association of Petroleum Geologists, Annual Convention, Abstracts* 5, 98.
- Milliken, K.L., Laubach, S.E., 2000. Brittle deformation in sandstone diagenesis as revealed by scanned cathodoluminescence imaging with application to characterization of fractured reservoirs. In: Pagel, M., Barbin, V., Blanc, P., Ohnenstetter, ? (Eds.), *Cathodoluminescence in Geosciences*. Springer-Verlag, New York, pp. 225–243, Chapter 9.
- Milliken, K.L., Reed, R.M., Laubach, S.E., 2004. Quantifying compaction and cementation within deformation bands in porous sandstones. *American Association of Petroleum Geologists Memoir, Faults and Petroleum Traps*, in press.
- Misik, M., 1971. Observations concerning calcite veinlets in carbonate rocks. *Journal of Sedimentary Petrology* 41, 450–460.
- National Research Council, 1996. *Rock Fracture and Fluid Flow*. National Academy Press.
- Nelson, R.A., 1985. *Geologic Analysis of Naturally Fractured Reservoirs*. Gulf Publishing, Houston, 320pp.
- Olson, J.E., 2004. Sublinear scaling of fracture aperture versus length: an exception or the rule? *Journal of Geophysical Research*, in press.
- Olson, J.E., Pollard, D.D., 1989. Inferring paleostresses from natural fracture patterns: a new method. *Geology* 17, 345–348.
- Olson, J.E., Holder, J., Qiu, Y., Rijken, M., 2001. Constraining the spatial distribution of fracture networks in naturally fractured reservoirs using fracture mechanics and core measurements. *Society of Petroleum Engineers Paper*, 71342.
- Pagel, M., Barbin, V., Blanc, P., Ohnenstetter ? (Eds.), 2000. *Cathodoluminescence in Geosciences*. Springer-Verlag, New York, 514pp.
- Pollard, D.D., Aydin, A., 1988. Progress in understanding jointing over the past century. *Geological Society of America Bulletin* 100, 1181–1204.
- Ramsay, J.G., 1980. The crack-seal mechanism of rock deformation. *Nature (London)* 284 (5752), 135–139.
- Reed, R.M., Milliken, K.L., 2003. How to overcome imaging problems associated with carbonate minerals on SEM-based cathodoluminescence systems. *Journal of Sedimentary Research* 73 (2), 326–330.
- Seyedolali, A., Krinsley, D.H., Boggs, S. Jr, O'Hara, P.F., Dypvik, H., Goles, G.G., 1997. Provenance interpretation of quartz by scanning electron microscope—cathodoluminescence fabric analysis. *Geology* 25, 787–790.
- Walderhaug, O., Bjørkum, P.A., Nadeau, P.H., Langnes, O., 2001. Quantitative modeling of basin subsidence cause by temperature-driven silica dissolution and reprecipitation. *Petroleum Geoscience* 7, 107–114.
- Wangen, M., 2001. A quantitative comparison of some mechanisms generating overpressure in sedimentary basins. *Tectonophysics* 334, 211–234.
- Wiltshcko, D.V., Morse, J.W., 2001. Crystallization pressure versus “crack seal” as the mechanism for banded veins. *Geology* 29, 79–82.

Sublinear scaling of fracture aperture versus length: An exception or the rule?

Jon E. Olson

Department of Petroleum and Geosystems Engineering, University of Texas at Austin, Austin, Texas, USA

Received 2 February 2001; revised 19 February 2003; accepted 20 March 2003; published 5 September 2003.

[1] Observations of natural fracture dimensions have sparked a continuing debate as to the nature of the fundamental relationship between fracture aperture (maximum opening) and length. On the basis of theoretical fracture mechanics, some have argued aperture-to-length scaling should be linear. This relationship implies that all fractures in a given population have the same driving stress regardless of fracture length, arguably a state that is difficult to reconcile with fracture propagation criteria. Also, some field observations indicate sublinear aperture-to-length scaling that is apparently inconsistent with the linear elastic fracture mechanics theory. In this work, a nonlinear aperture-to-length relationship is derived, still based on linear elastic fracture mechanics in a homogeneous body, but incorporating subcritical and critical (equilibrium law) fracture propagation criteria. The new hypothesis postulates that fractures of different lengths preserved in a body of rock are all in the same condition with respect to propagation (i.e., they all have the same stress intensity factor). This requires that fractures have driving stresses that vary inversely with the square root of fracture length, producing fracture apertures that scale with length to the 1/2 power. Under these conditions, fracture aspect ratio (aperture/length) decreases with increasing fracture length to the negative 1/2 power. Linear aperture-to-length scaling is still considered a possibility but is attributed to a relaxed, postpropagation mechanical state. Deviations in fracture aperture-to-length relationships from these idealized models can result from mechanical fracture interaction, fracture segmentation into en echelon arrays, and three dimensional effects in stratabound fractures. *INDEX TERMS:* 5104 Physical Properties of Rocks: Fracture and flow; 1829 Hydrology: Groundwater hydrology; 8010 Structural Geology: Fractures and faults; 8020 Structural Geology: Mechanics; *KEYWORDS:* fracture mechanics, joints, fracture aperture, veins

Citation: Olson, J. E., Sublinear scaling of fracture aperture versus length: An exception or the rule?, *J. Geophys. Res.*, 108(B9), 2413, doi:10.1029/2001JB000419, 2003.

1. Introduction

[2] Linear elastic fracture mechanics (LEFM) has been successfully applied to many rock fracture problems, including the analysis of dike shape [Delaney and Pollard, 1981] and process zone size [Delaney et al., 1986; Pollard, 1987], joint spacing and clustering [Pollard and Segall, 1987; DeGraff and Aydin, 1987; Olson, 1993; Renshaw, 1997; Bai and Pollard, 2000], and mixed mode fracture propagation phenomena such as en echelon array formation and crack path hooking [Pollard et al., 1982; Olson and Pollard, 1989, 1991]. The central LEFM equation used in the literature to explain the relationship between fracture aperture, d_{\max} (defined as the maximum opening displacement perpendicular to the fracture walls), and total fracture length, L , for noninteracting, opening mode fractures under two-dimensional, plane strain conditions is given by [Pollard and Segall, 1987]

$$d_{\max} = \Delta\sigma_I \frac{2(1-\nu^2)}{E} L, \quad (1)$$

where $\Delta\sigma_I$ is the opening mode driving stress, ν is Poisson's ratio and E is Young's modulus. Additional assumptions are that the body is homogeneous and isotropic. The driving stress, $\Delta\sigma_I$, is defined for a uniformly loaded crack as

$$\Delta\sigma_I = P_f - \sigma_n, \quad (2)$$

where P_f is the internal fluid pressure in the crack and σ_n is the remote normal stress perpendicular to the crack (compression is positive). In order to predict the aperture-to-length scaling in populations of cracks having different lengths, an assumption must be made about how the driving stress varies from crack to crack. The best field examples for quantifying aperture-to-length relationships are in exhumed outcrops, where the loading conditions responsible for crack opening are no longer present. However, the following two scenarios most likely bound the range of possibilities for the mechanical state preserved by filled fractures:

[3] 1. In the relaxed postpropagation state, significant time elapsed between fracture propagation and fracture filling, such that the driving stresses responsible for propagation have dissipated.

[4] 2. In the active propagation state, mineral precipitation (or magma crystallization) occurred while the fractures

were actively propagating or poised to propagate, such that the driving stresses for the cracks were at or near critical values.

[5] More complex scenarios could be imagined, but the discussion that follows is focused on these two end-member conditions.

2. Linear Aperture to Length Scaling

[6] A typical approach used implicitly in the literature is to assume that fractures of a given population all opened in response to the same driving stress (what I will call constant driving stress conditions), leading to the oft-cited prediction based on equation (1) of linear scaling between d_{\max} and L [Pollard and Segall, 1987; Renshaw and Park, 1997; Bai et al., 2000]. An interesting corollary to a linear aperture-to-length scaling is that the aspect ratio (d_{\max}/L) of the cracks should be a constant with respect to length, depending only on driving stress and elastic properties as

$$\frac{d_{\max}}{L} = \Delta\sigma_I \frac{2(1-\nu^2)}{E}. \quad (3)$$

However, the assumption of constant driving stress for all cracks in a given population is problematic when propagation is considered [Segall, 1984a].

[7] Opening mode crack propagation is controlled by the stress intensity factor at the crack tip, K_I , which for a uniformly loaded fracture depends linearly on driving stress and increases with the square root of half length ($a = L/2$) as [Lawn and Wilshaw, 1975]

$$K_I = \Delta\sigma_I \sqrt{\pi a}. \quad (4)$$

For a crack to propagate, on the basis of the energy balance of Griffith, the mechanical potential energy released during an increment of crack growth must be greater than or equal to the potential surface energy of the newly created crack increment [Atkinson, 1987; Pollard, 1987]. This occurs when K_I reaches the intrinsic fracture toughness of the material, K_{Ic} . Under constant driving stress loading, when the fracture toughness has been reached, there will be unstable, dynamic crack propagation [Lawn and Wilshaw, 1975], where propagation velocity will accelerate to approach the Rayleigh wave speed of the material [Freund, 1990]. Solving equation (4) for the critical driving stress, $\Delta\sigma_{Ic}$, required to maintain K_I at the critical value, K_{Ic} , shows the inherent instability of crack growth:

$$\Delta\sigma_{Ic} = \frac{K_{Ic}}{\sqrt{\pi a}}. \quad (5)$$

As the crack lengthens, the driving stress required to maintain the propagation condition ($K_I = K_{Ic}$) diminishes as $a^{-1/2}$. Under constant driving stress conditions, consequently, once a crack starts propagating there is more than enough driving stress available, and runaway dynamic crack growth should follow.

[8] A characteristic feature of such dynamic fracture propagation is crack tip branching [Sagy et al., 2001]. As the unstably loaded fracture reaches its limiting propagation velocity, the crack bifurcates, adding additional surface area in order to dissipate further energy and limit propagation

velocity [Kanninen and Popelar, 1985; Marder and Fineberg, 1996]. However, using published examples of systematic fracture patterns as a guide [e.g., Delaney and Pollard, 1981; Segall and Pollard, 1983; Olson and Pollard, 1989; Dunne and North, 1990; Lorenz and Finley, 1991; Cruikshank and Aydin, 1995], there is ample evidence of what Segall [1984a] terms “quasi-static growth of dilatant fractures,” where there are populations of finite length fractures that propagated stably in nominally homogeneous rock bodies with an absence of dynamic crack branching features. Consequently, long-term, constant driving stress conditions are not well supported by the fracture propagation evidence in the geologic record. It is more likely that constant driving stress conditions could develop in a postpropagation, relaxed mechanical state, where driving stress is substantially less than the critical value for all cracks and unstable dynamic growth is not an issue. In the absence of strong mechanical interactions between neighboring fractures, a relaxed state should have a population of fractures that all have the same driving stress, and linear aperture-to-length scaling would be predicted by the LEFM relationship of (1).

3. Sublinear Aperture-to-Length Scaling

3.1. Critical Crack Propagation at Constant K_I

[9] If constant driving stress conditions imply relaxed loading, what boundary conditions are likely when fractures are propagating? Textural evidence from some veins indicates that fracture mineralization may be contemporaneous with propagation [Laubach, 1988; Fisher and Brantley, 1992; Laubach, 2003]. Assuming critical crack propagation ($K_I = K_{Ic}$), it is plausible to argue that propagating fractures should all have the same, constant stress intensity factor. A constant stress intensity factor boundary condition implies that for a given population of fractures in a homogeneous material, fractures with different lengths must have different driving stresses as defined by equation (5), and aperture-to-length scaling will no longer be linear. Substituting the critical driving stress from equation (5) into equation (1) gives a new expression for the opening of cracks relative to their length:

$$d_{\max} = \frac{K_{Ic}(1-\nu^2)}{E\sqrt{\pi/8}} \sqrt{L}. \quad (6)$$

Thus, under constant stress intensity factor conditions, fracture aperture should scale with fracture length to the 1/2 power. In addition, constant stress intensity factor conditions predict that aspect ratio decreases with increasing fracture length as given by

$$\frac{d_{\max}}{L} = \frac{K_{Ic}(1-\nu^2)}{E\sqrt{\pi/8}} \frac{1}{\sqrt{L}}. \quad (7)$$

3.2. Natural Hydraulic Fracturing

[10] How might constant stress intensity factor conditions be maintained? Joint surface morphology in sedimentary rock, such as concentric rib marks or conchoidal structures [Hodgson, 1961; Engelder, 1987; Pollard and Aydin, 1988; Kulander et al., 1990], indicates episodic propagation arrest

or hesitation, implying a cyclic driving stress history. Hydraulically driven fracturing has been suggested to explain such episodic propagation; fractures advance and arrest in a cyclic process controlled by fluctuating fluid pressure in the fracture, while the remote stress field remains relatively constant [Secor, 1965; Pollard and Aydin, 1988; Engelder and Lacazette, 1990; Renshaw and Harvey, 1994]. In this scenario [Engelder and Lacazette, 1990], fluid pressures in the rock matrix and in the fracture are initially the same, and driving stress ($\Delta\sigma_I$) increases to the point required for crack growth due to either an increase in fluid pressure throughout the bed or a decrease in minimum stress, σ_n [Segall, 1984a]. It has been shown that sublithostatic pore pressure can be expected to commonly exceed the minimum principal stress at even great depths to provide the driving stress necessary for fracture growth [Secor, 1965; Engelder and Lacazette, 1990; Laubach et al., 1998]. Fracture arrest for critical propagation will occur if the driving stress falls during propagation, lowering the stress intensity factor below the fracture toughness ($K_I < K_{Ic}$). This drop in driving stress ($\Delta\sigma_I$) can occur if (1) the fracture fluid pressure (P_f) goes down as a result of propagation, (2) the stresses caused by remote extension are relieved as a result of propagation, or (3) a combination of both.

[11] Using the first scenario, where the remote normal stress acting on the crack remains constant, the feedback between fracture fluid pressure and fracture propagation can be demonstrated with a simple example. Given a fluid that is incompressible relative to the fracture volume (see Appendix A) and incremental propagation fast enough so that no appreciable fluid moves into the fracture from the rock matrix during the growth increment, the fluid volume in the fracture, and thus the fracture volume itself, will remain constant during that growth increment. In order for fracture volume to remain constant while length increases, fracture opening must reduce, which implies a decrease in driving stress. For a uniformly loaded, plane strain fracture with a unit breadth (in the out of plane dimension), fracture volume (V_f) is the integration of the elliptical fracture opening distribution [Pollard and Segall, 1987] over the entire fracture length ($-a \leq x \leq a$), given by

$$V_f = \frac{4(1-\nu^2)\Delta\sigma_I}{E} \int_a^{-a} \sqrt{a^2-x^2} dx = \frac{2\pi(1-\nu^2)}{E} \Delta\sigma_I a^2. \quad (8)$$

Constant fracture volume requires that the driving stress fall with crack propagation as a^{-2} , or

$$\Delta\sigma_I = \frac{E}{2\pi(1-\nu^2)} \frac{V_f}{a^2}. \quad (9)$$

This a^{-2} reduction in driving stress with propagation is greater than the $a^{-1/2}$ reduction required to maintain a constant stress intensity factor (see equation (5)), so propagation will arrest. By substituting equation (5) into equation (8), we can show that the fracture fluid volume required to maintain a constant stress intensity factor ($K_I = K_{Ic}$), which would keep the fracture propagating, increases with $a^{3/2}$ as

$$V_f = \frac{2\sqrt{\pi}(1-\nu^2)K_{Ic}}{E} a^{3/2}. \quad (10)$$

Thus the rate of fluid flow into the fracture would limit the propagation rate in the case of natural hydraulic fracturing, preventing runaway, dynamic crack propagation and instead promoting episodic or quasi-static fracture propagation at roughly constant stress intensity factor ($K_I = K_{Ic}$). (A complete poroelastic solution of how fluid flow in porous media affects fracture propagation rate is given by Renshaw and Harvey [1994].)

3.3. Fixed Displacement Loading

[12] The second scenario for controlled propagation at constant stress intensity assumes constant fluid pressure in the crack during propagation but with fixed displacement remote boundary conditions. Segall [1984a] proposed fixed displacement as a likely alternative to constant stress for the remote boundary conditions driving crack propagation. Consider an initial state where the pore pressure in the formation is equal to the remote minimum compressive stress. Fracture propagation can be initiated from such a state by a fixed remote displacement that causes an extensional strain perpendicular to the fractures, reducing the remote fracture-normal compression below the pore pressure. As the fractures propagate in response to the fixed extensional strain imposed on the body, the effective modulus of the material is reduced [Kemeny and Cook, 1986; Kachanov, 1992], relieving the extension-induced driving stress in the rock and ultimately arresting growth. Assuming a given uniaxial extension perpendicular to the fracture plane of $\Delta\epsilon$ and a reference state where the initial driving stress is zero and internal fluid pressure is constant, Segall [1984a] derived an expression for the driving stress in elastic plane strain as a function of applied strain and crack half length as

$$\Delta\sigma_I = \tilde{E}\Delta\epsilon = \frac{E\Delta\epsilon}{1 + (1-\nu^2)\frac{2\pi N}{A}a^2}, \quad (11)$$

where \tilde{E} is the effective Young's modulus due to a population of N parallel, noninteracting cracks of half length a in area A [Walsh, 1965]. The additional assumption is made that all of the cracks in the body are oriented perpendicular to the applied strain and have the same length, although the analysis has been generalized by Segall [1984b] to accommodate a distribution of fracture lengths. The driving stress under these conditions is linearly proportional to the imposed tectonic extension and inversely proportional to the square of fracture half length. Segall's expression for the stress intensity factor under fixed displacement loading can be written as [Olson, 1993]

$$K_I = \frac{\Delta\epsilon E \sqrt{\pi a}}{(1-\nu^2)\left(1 + \frac{2\pi N}{A}a^2\right)}. \quad (12)$$

Under these conditions, Segall [1984a] showed that a brief unstable fracture propagation period is followed by propagation at roughly constant stress intensity factor. In other words, when $2\pi Na^2/A \ll 1$, K_I increases as $a^{1/2}$, comparable to constant driving stress conditions. When $2\pi Na^2/A \gg 1$, the stress intensity factor decreases as $a^{-3/2}$, a fundamentally stable propagation condition. This stress intensity history versus crack length is depicted in Figure 1,

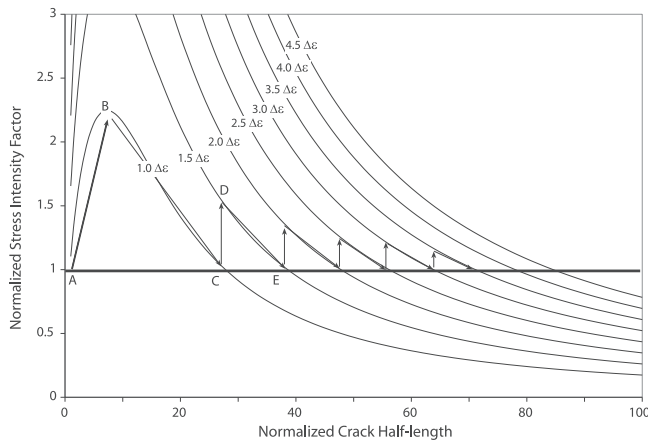


Figure 1. Normalized stress intensity factor, K_I/K_{I_0} , versus normalized crack half length, a/a_0 , where K_{I_0} is the stress intensity factor for a crack of half length a_0 with an imposed strain of $1.0\Delta\epsilon$.

where K_I is normalized by K_{Ic} and fracture half length is normalized by the initial half length. The dimensional values for (12) were computed using multiples of the initial applied strain, $E = 10$ GPa, $\nu = 0.3$, $N = 1000$, and $A = 100$ m². Assuming an initial flaw length of 0.01 m and $K_{Ic} = 1$ MPa m^{1/2}, crack growth initiation requires an initial applied strain of $\Delta\epsilon = 0.00057$ (point A, Figure 1). Under constant applied strain, early crack growth does not appreciably reduce the effective modulus, and the constant strain condition mimics constant driving stress (point A to B, Figure 1). This unstable (increasing stress intensity factor) period ends at point B when the curve rolls over (Figure 1), and the stress intensity factor falls with increasing length until crack arrest at point C, where K_I would fall below K_{Ic} if growth continued. Additional growth can be achieved by increasing the strain in a stepwise fashion, moving from point C to point D (each successive curve in Figure 1 represents an increase of strain by $0.5\Delta\epsilon$). Continued crack growth causes K_I to decrease to the point of crack arrest at E. Increasing the strain again repeats the cycle.

[13] In reality, crack propagation probably responds to both remote strain boundary loading and pore pressure that varies in response to fracture volume changes. Consequently, the initial unstable rise in K_I that exceeds K_{Ic} for fixed displacement loading (from point A to B in Figure 1) could be erased by a drop in fluid pressure in the crack as it grows, making even the early stages of fracture growth follow constant stress intensity factor conditions.

3.4. Impact of Subcritical Crack Growth

[14] The above discussion suggests that for fracture populations that are propagating critically ($K_I = K_{Ic}$), constant stress intensity factor boundary conditions may be more reasonable than constant driving stress conditions. However, much of the recent work on the growth of opening mode fracture in rock argues that systematic fracture sets are a result of subcritical fracture growth, not critical growth [Segall, 1984a, 1984b; Olson, 1993; Renshaw and Pollard, 1994; Schultz, 2000; Holder et al., 2001]. Subcritical crack growth is considered to be prevalent under many geologic conditions, where long-term

loading and chemically corrosive pore fluids weaken a rock's resistance to fracture [Anderson and Grew, 1977; Atkinson, 1984]. The propagation criterion for subcritical crack growth is

$$K_I^* < K_I < K_{Ic}, \quad (13)$$

where K_I^* is the minimum threshold below which no crack propagation will occur. We can substitute the subcritical threshold value for the fracture toughness in equation (5) and predict the initiation of subcritical fracture propagation at a driving stress of

$$\Delta\sigma_I^* = \frac{K_I^*}{\sqrt{\pi a}}. \quad (14)$$

Assuming constant stress intensity factor growth at this subcritical threshold due to natural hydraulic fracturing or fixed displacement boundary conditions, aperture can be expected to scale with fracture length to the 1/2 power as predicted by equation (6) for subcritical crack growth as well. The possible exception again is early crack growth (from point A to B in Figure 1), when nominally constant driving stress conditions could result in linear aperture-to-length scaling.

4. Comparison to Field Data

[15] The predictions of the above analysis are readily testable with field observations. Three exceptionally well-documented fracture populations were chosen to represent a wide range of scale and geologic environments. Vermilye and Scholz [1995] measured vein geometry at various locations in the eastern United States and California. Two of these data sets have veins spanning a wide range of lengths, from less than 2 cm to more than 20 m, and are discussed in detail by Vermilye and Scholz [1995] with reference to aperture-to-length scaling. One set of veins, filled with chlorite and epidote, is found in glacially polished outcrops of the Cretaceous Mount Givens Granodiorite near Florence Lake in the Sierra Nevada of California. The other set is from the Culpeper Crushed Stone Quarry in Virginia and consists of calcite-filled veins in a calcite-cemented siltstone of Triassic age. Aperture and length data from these two locations were digitized from Figures 3 and 14 of Vermilye and Scholz [1995] for the analysis presented in this paper.

[16] Delaney and Pollard [1981] mapped one of six mafic dikes that form a radial pattern around the Ship Rock volcanic plug in NW New Mexico. This dike is interpreted to have been intruded into the flat-lying Mancos Shale at a depth of at least 750 m. The dike is made up of 35 segments, ranging in length from 8 to 395 m and has a total array length of 2.9 km. The Delaney and Pollard [1981] data were extracted from their Table 2, which reports length, maximum opening, and average opening for each of the 35 segments. Delaney and Pollard [1981] noted that the maximum opening (d_{max}) measured for the segments included erosional enlargements caused by magma flow and that the average opening (d_{avg}) was probably more representative of the dilational response of the dike. In order to reduce the data scatter caused by dike wall erosion, I used the observed average opening data to estimate maximum

opening (aperture) values. Assuming the ideal dike opening distribution to be elliptical in nature, consistent with linear elastic fracture mechanics for an isolated, uniformly loaded crack [Pollard and Segall, 1987], the average opening (d_{avg}) is equal to the fracture volume per unit breadth (V_f from equation (8)) divided by the total fracture length ($2a$), or

$$d_{avg} = \frac{2\pi \frac{(1-\nu^2)}{E} \Delta\sigma_I a^2}{2a} = \pi \frac{(1-\nu^2)}{E} \Delta\sigma_I a. \quad (15)$$

Combining equations (1) and (15), we find

$$d_{max} = \frac{4}{\pi} d_{avg}. \quad (16)$$

Plotting the estimated aperture values against the actual measured values (Figure 2) shows most of the Ship Rock data are consistent with an elliptical opening distribution assumption. However, for dike segments with an average opening of 3 m or greater, the measured maximum opening values are sometimes significantly larger than would be predicted from the average opening. This suggests that the thinner dike segments were less susceptible to wall erosion than the thicker segments.

[17] Each fracture data set was described with a power law equation of the form

$$d_{max} = CL^e, \quad (17)$$

where d_{max} is the aperture, L is total fracture length, C is the preexponential constant (with units of length $^{1-e}$), and e is the power law scaling exponent. There is significant scatter in the data (Figure 3), but a linear regression analysis

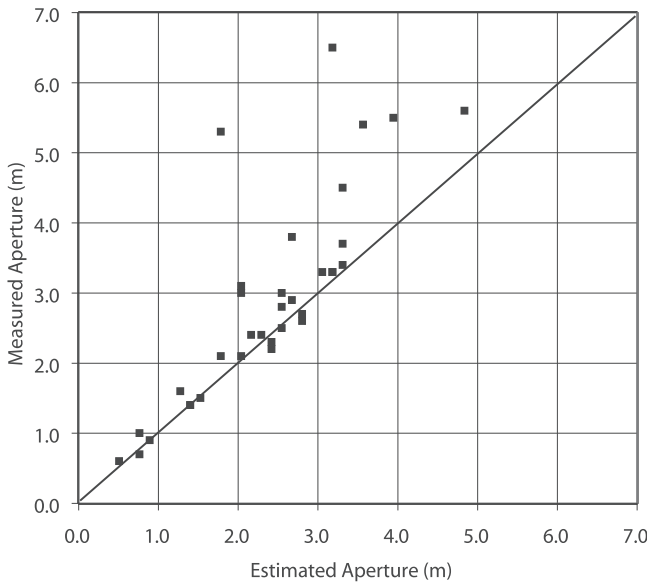


Figure 2. Measured maximum opening (aperture) data for Ship Rock dike plotted against the estimated maximum opening based on average opening data. Measured aperture exceeds that computed from average opening values because of magma erosion of the dike walls [Delaney and Pollard, 1981].

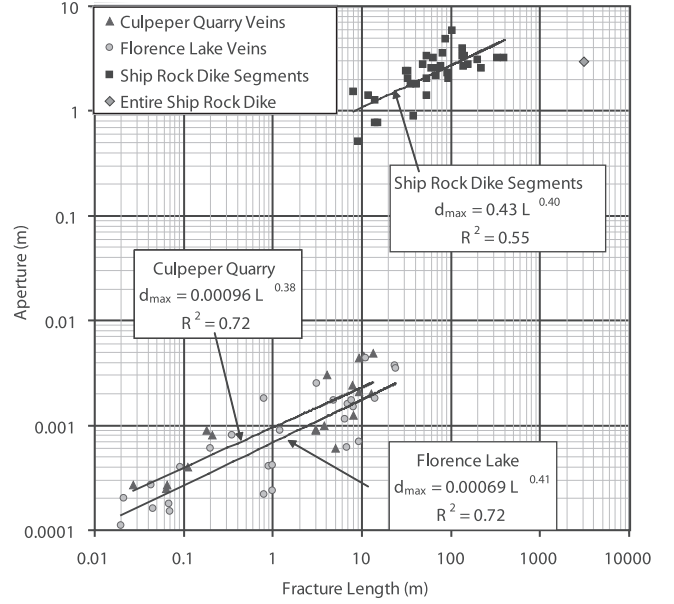


Figure 3. Aperture versus length data for NE Ship Rock igneous dike segments [Delaney and Pollard, 1981] and mineralized veins from Culpeper Quarry and Florence Lake [Vermilye and Scholz, 1995]. Apertures for Ship Rock dike were computed from average opening data (see Figure 2).

determined an exponent of ~ 0.4 to best describe each data set. The Culpeper Quarry and Florence Lake vein data were fit with power law exponents of $e = 0.38$ and $e = 0.41$, respectively, both with goodness of fit values of $R^2 = 0.72$. A similar power law exponent was fit for the Ship Rock dike data ($e = 0.40$), but the goodness of fit was not as high ($R^2 = 0.55$). Aspect ratio is computed as

$$\frac{d_{max}}{L} = \frac{CL^e}{L} = CL^{e-1}, \quad (18)$$

and Figure 4 shows the clear decrease in aspect ratio with increasing fracture half length ($e - 1 = -0.6$). The best fit power law exponent of $e \cong 0.4$ for aperture-to-length scaling from field data (Figure 3) is close to the theoretical value of $e = 0.5$ predicted by equation (6) for constant stress intensity factor conditions. The constant driving stress assumption predicts an exponent of $e = 1.0$, which is clearly not consistent with these data.

[18] Another important aspect of the aperture-to-length data is the magnitude of the preexponential constant of equation (17). Assuming constant stress intensity factor propagation is applicable, equation (6) relates the preexponential constant from (17) to the site-specific fracture toughness and elastic properties as

$$C = \frac{K_{Ic}(1-\nu^2)}{E\sqrt{\pi/8}}. \quad (19)$$

Forcing the data from Figure 3 to fit a curve with the form of equation (17) but with $e = 0.5$ in accordance with equation (6), the preexponential constants are $C = 0.00092 \text{ m}^{1/2}$ for the Culpeper Quarry veins, $C = 0.00068 \text{ m}^{1/2}$ for Florence Lake and $C = 0.27 \text{ m}^{1/2}$ for the Ship Rock dike. Solving

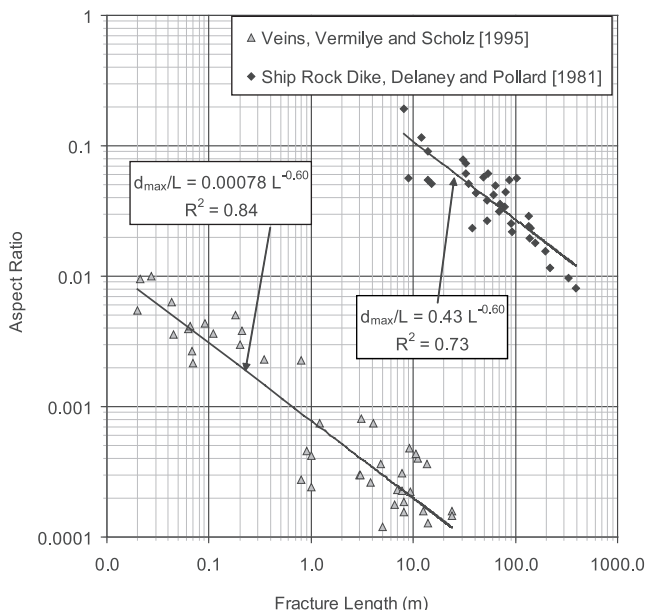


Figure 4. Aspect ratios versus fracture length for Ship Rock dike [Delaney and Pollard, 1981] and mineralized veins [Vermilye and Scholz, 1995].

equation (19) for K_{Ic} and using published values of shear modulus and Poisson's ratio for the rocks at each location, the range of effective fracture toughness for the Culpeper Quarry, Florence Lake, and Ship Rock fractures is 8–16, 12–25, and 40–4000 $\text{MPa m}^{1/2}$, respectively (Table 1). The Culpeper Quarry and Florence Lake fracture toughness values are on the high end of typical laboratory values of 1–10 $\text{MPa m}^{1/2}$ [Atkinson and Meredith, 1987], but the Ship Rock estimate is so high it suggests there are some additional factors to be addressed.

[19] The trend of increasing toughness when moving from centimeter-scale laboratory specimens to meter-scale veins to kilometer-scale dikes suggests that fracture size influences toughness. Pollard [1987] proposed the extra energy dissipated by jointing in the process zone of dikes results in higher effective fracture toughness for large (kilometer-scale) fractures. Delaney *et al.* [1986] documented joints as an expression of a process zone around dikes in multiple localities on the Colorado Plateau, including Ship Rock. Similar process zones are typically not observed in smaller, outcrop-scale veins and joints nor in laboratory specimens, and consequently the effective toughness indicated by analyzing those rocks is much smaller.

[20] Another explanation for excessive fracture toughness estimates at Ship Rock can be related to the dike geometry. As mentioned earlier, all of the dike segments are members of a single en echelon array. The mechanical interaction between the individual segments causes them to act as if they are part of a larger single-segment dike with a length approaching the length of the total en echelon array [Delaney and Pollard, 1981; Pollard *et al.*, 1982]. This interaction results in larger than expected apertures for each dike segment (as pointed out by Delaney and Pollard [1981]), inflating the preexponential constant in our aperture versus length equation, and perhaps leading to an overestimate of fracture toughness. An end-member calcu-

lation would be to assume that all of the individual dike segments can be considered as one fracture with a total mapped length of 2900 m. Coupling that with the aperture of 2.9 m estimated from the average opening of the entire dike results in a lower fracture toughness estimate of 7.9–790 $\text{MPa m}^{1/2}$. This brackets the Delaney and Pollard [1981] estimate of fracture toughness in the range of 30–110 $\text{MPa m}^{1/2}$, which was based on a comprehensive numerical analysis taking into account dike segmentation as well as including the effects of nonuniform loading along the length of the dike. Consequently, the high apparent toughness computed for Ship Rock can be partially explained by the fact that the dike segments are all part of a larger array.

[21] Increased fracture toughness for the Ship Rock dike could also be the result of heating of the country rock by the magma, resulting in near-tip plastic deformation and wider crack opening. DeGraff and Aydin [1993] summarize some of the literature related to the temperature dependence of fracture toughness, indicating that fracture toughness increases with temperature. However, Delaney and Pollard [1981] postulate the Mancos Shale surrounding the Ship Rock dike deformed in a brittle elastic manner, so it is not clear that temperature effects were important for this case.

5. Other Factors Affecting Aperture-to-Length Scaling

5.1. Single-Segment Versus Multisegment Fractures

[22] The fracture toughness estimation for the Ship Rock dike indicates that fracture segmentation can affect fracture aperture. In addition to kilometer-long dikes, meter-scale fractures observed in the field, upon closer inspection, commonly consist of closely spaced, en echelon arrays of shorter segments [Delaney and Pollard, 1981; Pollard *et al.*, 1982; Segall and Pollard, 1983; Olson and Pollard, 1989; Vermilye and Scholz, 1995]. Vermilye and Scholz [1995] categorized their vein data from Culpeper Quarry and Florence Lake into single-segment and multisegment populations (Figure 5). All the single-segment veins were shorter than the multisegment veins and had larger aspect ratios, with the transition to multisegment veins occurring at a vein length of about 1 m. They concluded the single-segment veins had linear aperture-to-length scaling, as would be predicted by LEFM for constant driving stress conditions. However, they cited tapered displacement profiles at the crack tips of many of the fractures as indication of elastic-plastic behavior, and used a Dugdale model (assuming the same driving stress for different length fractures) to explain the linear aperture-to-length scaling [Cowie and Scholz, 1992; Dugdale, 1960]. Vermilye and

Table 1. Measured and Computed Rock Properties^a

Location	E , GPa	ν	K_{Ic} , $\text{MPa m}^{1/2}$ (Computed)
Culpeper Quarry	13–26	0.22	8–16
Florence Lake	27–54	0.25	12–25
Ship Rock dike (Mancos Shale)	0.23–23	0.3	40–4000

^aPublished values of elastic constants for Florence Lake, Culpeper Quarry [Vermilye and Scholz, 1995], and Ship Rock dike [Delaney and Pollard, 1981] and calculated fracture toughness values are from this study. The wide range on the Shiprock K_{Ic} is a result of the wide range of estimates for E .

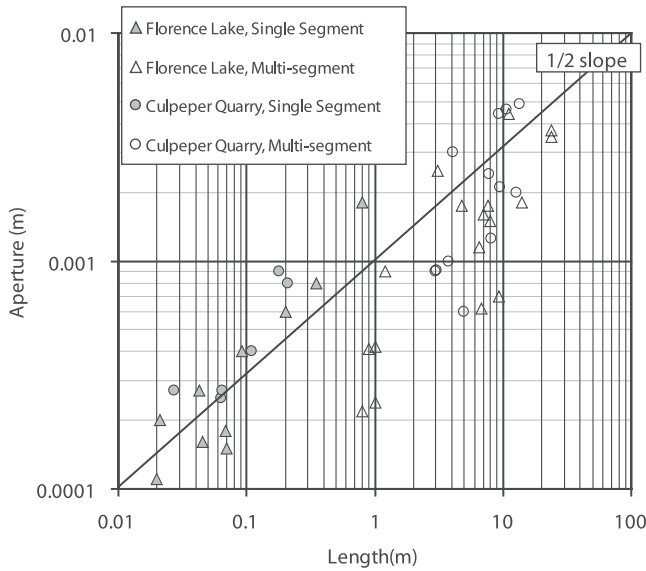


Figure 5. Aperture versus length data for Culpeper Quarry and Florence Lake from Figure 3, divided into single-segment and multisegment fractures [Vermilye and Scholz, 1995]. A scaling line with a slope of 1/2 is included for reference. Note how single-segment fractures at both localities are shorter than multisegment fractures.

Scholz [1995] interpreted their multisegment veins to have square root aperture-to-length scaling. They attributed the smaller aspect ratio and sublinear aperture-to-length scaling for multisegment fractures to the mechanical effects of an echelon arrays as described by Pollard *et al.* [1982].

[23] In my analysis, I group the single and multisegment vein data of Vermilye and Scholz [1995] into one population and propose the alternative interpretation of square root aperture-to-length scaling for fractures of all sizes, which is consistent with the observation that shorter, single-segment fractures have larger aspect ratios than the longer, multi-segment fractures. Square root aperture-to-length scaling seems to represent the entire data set fairly well (Figure 5), but the best fit for the vein data has a power law exponent of 0.4 instead of 0.5, with correlation coefficients for both Culpeper Quarry and Florence Lake of $R^2 = 0.72$ (Figure 3). Vermilye and Scholz [1995] show higher correlation coefficients for linear aperture-to-length scaling using only the single-segment fractures ($R^2 = 0.78$ for Culpeper Quarry and $R^2 = 0.96$ for Florence Lake), but their square root scaling of the multisegment data results in a poorer fit than my overall model ($R^2 = 0.45$ for Culpeper Quarry and $R^2 = 0.56$ for Florence Lake).

[24] Since Vermilye and Scholz [1995] attribute square root aperture-to-length scaling to fracture segmentation effects while I propose it as a result of constant stress intensity factor conditions, I have explored the issue of segmentation further (Figures 6 and 7). Using a linear elastic displacement discontinuity approach described by Olson [1993], I reproduced the Pollard *et al.* [1982] results (see Figure 7) for aperture in multisegment arrays of interacting fractures referenced by Vermilye and Scholz [1995]. I also investigated additional array geometries, looking at the effects of the number of fracture segments, the segment overlap and the perpendicular spacing between

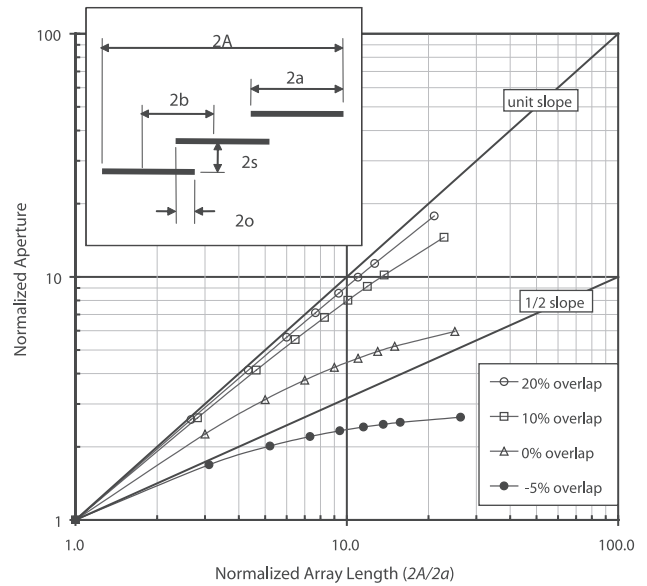


Figure 6. Calculated aperture data for an echelon fracture arrays of varying normalized segment overlap, o/b , at constant relative spacing, $s/b = 0.05$. Each fracture segment has the same length, $2a$, with segment centers spaced at $2b$ and fracture-perpendicular spacing of $2s$. The aperture for an array of length $2A$ is normalized by the aperture of a single fracture segment of length $2a$. Array length is normalized by fracture segment length as $2A/2a$.

segments on aperture-to-length scaling. Following Pollard *et al.* [1982], the results were obtained under constant driving stress conditions (all segments in an array have the same driving stress) and two-dimensional plane strain.

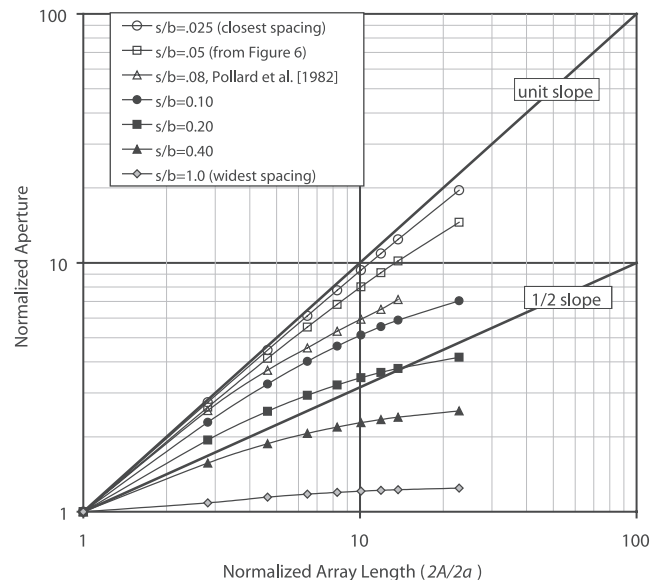


Figure 7. Calculated aperture data as shown in Figure 6 but with constant relative fracture overlap at $o/b = 0.1$ (10% overlap) and varying s/b (fracture spacing relative to crack center-to-center offset). Results for $s/b = 0.08$ match Pollard *et al.* [1982]. Aperture for array of length $2A$ normalized by aperture of a single fracture segment of length $2a$. Array length is normalized by fracture segment length as $2A/2a$.

Fracture arrays were constructed using 1 to 25 fracture segments of constant length $2a$, and array apertures were normalized by the aperture computed for a single isolated fracture of length $2a$ according to equation (1). Under these conditions, the aperture of a nonsegmented fracture should increase linearly with fracture length. If segmentation reduces aperture relative to an unsegmented fracture, the aperture-to-length scaling should plot below the unit slope line, and if that scaling is square root, it should plot parallel to the $1/2$ slope line (Figures 6 and 7). Other fracture geometry parameters are the center-to-center offset, $2b$, perpendicular spacing between segments, $2s$, and segment overlap, $2o$ (see inset of Figure 6). Segment overlap, $2o$, is a function of the difference between the segment length, $2a$, and the center-to-center offset, $2b$, where $2o = 2(a - b)$. If the segment length is equal to the center-to-center offset, the overlap is zero. Positive overlap occurs when $a > b$, and negative overlap results when $a < b$. The total array length is given by

$$2A = (N - 1) * 2b + 2a, \quad (20)$$

where N is the number of segments. Normalized array length is defined as $2A/2a$, which is approximately equal to the number of fracture segments if $a/b \cong 1$, so the plots in Figures 6 and 7 show not only how aperture varies with increasing array length but approximately how aperture varies for a constant length fracture array divided into increasing numbers of segments.

[25] The first set of results (Figure 6) come from an array with a small, constant s/b in order to demonstrate the effect of segment overlap on fracture opening for strongly interacting fractures. The aperture-to-length scaling for an array with 20% segment overlap ($o/b = 0.2$) deviates very little from single-segment fracture behavior (the curve approaches the unit slope line). This means that for this array geometry, fracture segmentation has little effect on the value of the maximum opening of the array. The case with slightly less overlap ($o/b = 0.1$) shows more aperture reduction relative to a single-segment fracture, and the magnitude of this reduction increases with array length. The cases with 0% and -5% overlap show even greater reduction in the aperture for the array relative to a single-segment fracture of the same length, and the reduction again increases strongly with array length (or number of segments). For instance, for the case of 0% overlap, the curve shows that a fracture made up of 10 segments of length $2a$ (giving a total array length of $2A = 10 * 2a$) has a normalized aperture of 4.5, while a nonsegmented fracture with the same total length ($10 * 2a$) would have a normalized aperture of 10. Consequently, segmentation for this array geometry reduces the fracture opening for the segmented array relative to an unsegmented fracture of the same total length by 55%.

[26] On the basis of fracture mechanics analyses of the propagation of an echelon fractures [Pollard *et al.*, 1982; Olson and Pollard, 1989], the mechanical interaction between nearby fractures that have a slightly negative to zero overlap enhances propagation, so it is likely that nearby echelon fractures will continue to propagate to some positive overlap before propagation arrests. Consequently, for the second set of results (Figure 7), the normalized overlap is held constant at $o/b = 0.1$ and intersegment spacing

relative to crack center-to-center offset, s/b , is varied. The wider the fracture spacing, the weaker the mechanical interaction, and the more individual segments act as if they were mechanically isolated from their neighbors. At very close relative spacing ($s/b = 0.025$), aperture-to-length scaling is nearly identical to the that for a single-segment fracture. Increasing the relative perpendicular spacing between fracture segments (i.e., increasing s/b) causes a progressive decrease of slope on the aperture-to-length plot as compared with the single-segment fracture (the slope falls below unity), indicating the dependence of aperture on array length is weakening. For $s/b = 1.0$, the segments of the array are acting almost as if they were isolated fractures, meaning the aperture of the array is controlled by the smaller segment length, $2a$, rather than the larger entire array length, $2A$. Since segment length is held constant for the range of array lengths, aperture stays almost constant.

[27] In summary, a population of multisegment fractures whose segments are closely spaced ($s/b \leq 0.05$) and have substantial tip-to-tip overlap should have aperture-to-length scaling that is indistinguishable from a population of single-segment fractures of similar length distribution. If the multisegment fracture population has segments that are more widely spaced ($s/b > 0.05$), the power law exponent for aperture-to-length scaling will be smaller than for a comparable population of single-segment fractures. Although the results show that the multisegment aperture-to-length curves are really not power law because their slopes systematically decrease with increasing length on a log-log plot (Figures 6 and 7), they can be fit with high R^2 over the range of lengths considered here (excluding the point for a normalized length of 1). The results in Figure 7 for relative segment spacings from $s/b = 0.025$ to 1.0 can be fit with power law exponents of $e = 0.94$ to 0.07, respectively (see Table 2). This wide range in values for e suggests that there is no unique power law exponent that describes multisegment aperture-to-length scaling. This dependence of aperture on the details of fracture array geometry (intersegment spacing, segment overlap and segment number) may partly explain the high degree of scatter in aperture data from the field, as no two natural fracture arrays will have the exact same geometry.

[28] Aperture-to-length scaling dependence on fracture size has also been identified in tensile fractures associated with the Krafla dike swarm by Hatton *et al.* [1993], where shorter fractures are observed to have higher power law exponents than longer fractures. However, the shorter fractures are interpreted to have superlinear aperture-to-length scaling, and the longer fractures have linear to sublinear scaling. Hatton *et al.* [1993] proposed that different fracture processes were acting at the different scales, while Renshaw and Park [1997] argued that the variation in scaling was a result of mechanical interaction.

5.2. Three-Dimensional Effects for Stratabound Fractures

[29] The analysis so far has been based on two-dimensional, plane strain elasticity. An aperture limiting scenario that might also affect scaling exponents is the three-dimensional effect of stratabound fractures in layered rock, where fracture height is restricted by the mechanical layer thickness of a formation [Helgeson and Aydin, 1991; Narr and

Table 2. Power Law Fit Results for Multisegment Arrays^a

Relative Intersegment Spacing, s/b	Power Law Fit Exponent, e	Correlation Coefficient, R^2
0.025	0.94	1.00
0.05	0.82	1.00
0.08	0.64	1.00
0.10	0.54	0.98
0.20	0.37	0.96
0.40	0.23	0.95
1.00	0.065	0.94

^aPower law curve fit data for aperture-to-length scaling of multisegment arrays under constant driving stress conditions (Figure 7).

[Suppe, 1991; Olson, 1993; Bai et al., 2000]. As a crack grows from a flaw, one idealization is that it initially has an equidimensional geometry, where the length is about equal to the height. At the layer boundary, changes in mechanical properties or stress may cause the height growth to arrest while length growth can continue. For equidimensional cracks, the aperture will vary with the crack length (equal to height) at the same rate as the 2-D plane strain crack we have already discussed. (The only difference will be that the equidimensional fracture will have an aperture that is smaller by a constant.) However, for an elastic, three-dimensional crack that is stratabound, with a length much greater than the height and no crack-tip blunting at layer boundaries due to layer-parallel slip or other nonelastic effects, aperture should depend on the fracture height and not length.

[30] Figure 8 shows the development of aperture as a function of length for a stratabound and an equidimensional fracture propagating at constant stress intensity factor. Fracture opening distributions were calculated using the program DIS3D [Erickson, 1986], a three-dimensional dislocation program in which fractures are made up of rectangular shaped elements in an elastic half-space. Because of the rectangular element shape in DIS3D, it was convenient to idealize the equidimensional crack as having a square tip line shape rather than a penny shape (a circular tip line). The stress intensity factor for these three-dimensional fractures was estimated as being linearly proportional to the crack opening displacement of the tip elements located at midheight on the lateral crack fronts. (Olson [1991] demonstrated the validity of using the opening displacement of crack tip elements to estimate the stress intensity factor for plane strain analysis.) The equidimensional fracture grows by increasing length and height simultaneously. The stratabound fracture grows by increasing its length only and keeping the height constant. Both fracture types start the simulation with the same size and shape, with their height and length equal to the magnitude of the layer thickness (T), which is the height growth limit for the stratabound fracture. (The layer boundary in these simulations is imaginary and is arbitrarily imposed to limit fracture height. There is no variation in mechanical properties or stress in the body and the layer boundary cannot slip.) The aperture results for increasing fracture length are normalized to the initial aperture of the equidimensional fracture. Fracture length is scaled to the height of the stratabound fracture ($H = T$).

[31] Comparing the aperture development for the two different fracture geometries (Figure 8), the equidimensional fracture shows an approximate square root aperture-to-length scaling for constant stress intensity factor conditions,

but the stratabound fracture shows aperture approaching an asymptotic limit. This asymptotic value can be computed using the 2d aperture formula, (1), by substituting the fracture height, H , for length, L . Therefore, for stratabound fractures propagating under constant stress intensity conditions, the aperture should not increase appreciably with increasing fracture length beyond $L/T \cong 4$ (Figure 8).

6. Discussion

[32] If the shapes of veins and dikes in outcrop preserve an active subcritical or critical propagation state, fracture apertures should nominally scale with $L^{1/2}$ as predicted for constant stress intensity factor conditions. An exception to this square root rule for the case of actively propagating fractures would be if mineralization (or crystallization) occurred during the early stages of subcritical growth, where the boundary conditions are essentially constant driving stress, resulting in linear aperture-to-length scaling. On the other hand, if fractures do not mineralize until after loading conditions have relaxed, such that all the stress intensities have fallen significantly below propagation values, the square root aperture-to-length scaling may be lost under certain circumstances. If the driving mechanism for propagation is primarily fluid pressure, the constant stress intensity factor conditions require that cracks of different lengths have different internal fluid pressures. Depending on formation permeability, the pressure gradients required in the formation to maintain different driving stresses for different cracks may be relatively short-lived, as they can be erased by flow [Secor, 1965; Renshaw and Harvey, 1994]. If fracture propagation is dormant long enough prior to mineralization and there is little mechanical interaction between neighboring fractures, the inevitable equalization

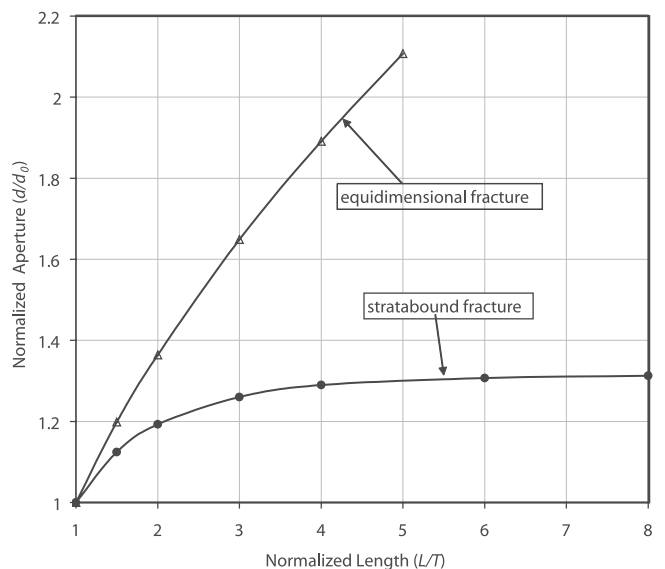


Figure 8. Fracture aperture versus length for stratabound and equidimensional fractures. For the stratabound fracture, height (H) is constant and equal to the layer thickness (T). For the equidimensional fracture, $L = H \geq T$. Fracture length is normalized by the layer thickness, and aperture is normalized by the aperture of the initial equidimensional fracture ($L = H = T$).

of fluid pressure throughout the fractured bed would result in constant driving stress conditions and linear aperture-to-length scaling.

[33] If the driving mechanism for fracture growth is primarily remote tectonic extension, and fracture propagation is slow enough such that significant fluid pressure gradients do not develop in the fracture, the variability in driving stress from fracture to fracture may result from the mechanical interaction and effective modulus effects [Segall, 1984a; Olson, 1993]. Under these conditions, the driving stress heterogeneity will be defined by the geometry of the fracture network, and will likely persist even if the stress induced by the remote tectonic extension is relaxed. Thus, whether the fractures are mineralized while on the verge of propagation or in a somewhat relaxed loading state, apertures may still scale with length in the same way. The idealized analysis presented here suggests that such constant stress intensity factor conditions result in square root aperture scaling, but in the case of high fracture density, where mechanical interaction is significant, the assumption of a uniformly loaded, isolated fracture is no longer met. The added complication of fracture interaction may be common for fairly dense fracture networks (where fracture spacing is small relative to the mechanical interaction distance), and this complication may explain some of the considerable scatter in natural data. *Renshaw and Park* [1997] come to this conclusion based on the numerical analysis of dike data, stating that both aperture data scatter and superlinear aperture-to-length scaling are a consequence of mechanical fracture interaction. In addition to mechanical interaction, other complicating effects such as material heterogeneity, stress gradients and crack tip plasticity [Burgmann *et al.*, 1994] may also account for the wide scatter in the natural scaling data. *Bai et al.* [2000] examine many of these effects on fracture aperture and aspect ratio for the case of layered rocks.

7. Conclusions

[34] Previous work using LEFM principles to predict linear aperture-to-length scaling for noninteracting fractures has implicitly assumed that all fractures within a population, regardless of their length, have the same driving stress at the time of fracture filling. I suggest this linear aperture-to-length scaling may be limited to cases of fracture mineralization under relaxed loading conditions or during the early, unstable stages of displacement-driven propagation. An alternative relationship, based on LEFM for a population of fractures where all the fractures have the same stress intensity factor, predicts that apertures will scale with the square root of length. I argue that this relationship is most appropriate for fractures that become mineralized while actively propagating or while poised to propagate. An interesting outcome of a square root (or any sublinear) aperture-to-length relationship is the fact that longer cracks should have smaller aspect ratios (aperture/length) than shorter cracks, whereas linear relationships imply constant aspect ratio over all fracture sizes. Selected data from the literature [Delaney and Pollard, 1981; Vermilye and Scholz, 1995] are consistent with the hypothesis of square root aperture-to-length scaling predicted by constant stress intensity factor conditions for noninteracting fractures. There

are also published data with superlinear aperture-to-length scaling [Hatton *et al.*, 1993] which has been attributed to populations with strong mechanical interaction [Renshaw and Park, 1997].

[35] Aperture-to-length scaling can be complicated by fracture segmentation and three-dimensional effects. Both of these factors can result in scaling exponents that vary with fracture length, where shorter fractures may exhibit higher aperture-to-length power law scaling exponents than the longer fractures in a population. The importance of fracture segmentation on aperture-to-length scaling depends on the spacing between en echelon segments and the amount of overlap of the tips. For intersegment spacing that is small relative to segment length (on the order of 5 to 10%) and for tip overlaps on the order of 20% of the segment length or greater, the aperture in a multisegment array will be nearly the same as for a single-segment fracture with the same total length. For larger intersegment spacing and for arrays with little or no segment overlap, the aperture for a multisegment fracture can be significantly less than for a single-segment fracture of the same length.

[36] For the three-dimensional case of fracture height constrained by bed thickness, aperture effectively stops increasing when fracture length exceeds about four times the fracture height. Thus shorter fractures are expected to have higher aperture-to-length scaling exponents than longer fractures (i.e., shorter fractures have larger aspect ratios), and the overall aperture-to-length scaling for an entire population depends on the maximum length fracture included in the analysis.

Appendix A

[37] When discussing natural hydraulic fracturing and its implication of constant fracture volume during a growth increment, I state that the fluid should be incompressible relative to the fracture volume. The definition of the isothermal rock pore volume compressibility, c_p , is [Earlougher, 1977]

$$c_p = \frac{1}{V_p} \frac{\partial V_p}{\partial P}, \quad (\text{A1})$$

where V_p is the pore volume and P is the pore fluid pressure. Treating the fracture volume as equivalent to pore volume, and using the definition of fracture volume from equation (10), the fracture compressibility, c_f , is simply

$$c_f = \frac{1}{V_f} \frac{\partial V_f}{\partial P} = \frac{1}{\Delta \sigma_1}. \quad (\text{A2})$$

Delaney and Pollard [1981] and *Vermilye and Scholz* [1995] estimated driving stresses on the order of 10 to 100 MPa from their dike and vein data, which would result in fracture compressibilities on the order of 10^{-1} to 10^{-2} /MPa, respectively. If the subsurface fluid is assumed to be water, it has a much smaller compressibility than a fracture, with values on the order of 5×10^{-4} /MPa over the temperature range of 0–100°C [Weast, 1970].

[38] **Acknowledgments.** This work greatly benefited from discussions with Javier Moros and Randy Marrett concerning aperture versus length scaling. I am also very grateful for the helpful review comments of M. Bonafede, S. Martel, and Associate Editor T. Yamashita. This material is

based in part on work supported by the U.S. Department of Energy under Award DE-FC26-00BC15308 (any opinions, findings, conclusions, or recommendations expressed herein are those of the author and do not necessarily reflect the views of the DOE) and the Fracture Research and Application Consortium (FRAC) of the University of Texas at Austin.

References

- Anderson, O. L., and P. C. Grew, Stress corrosion theory of crack propagation with applications to geophysics, *Rev. Geophys.*, 15, 77–104, 1977.
- Atkinson, B. K., Subcritical crack growth in geological materials, *J. Geophys. Res.*, 89, 4077–4114, 1984.
- Atkinson, B. K., Introduction to fracture mechanics and its geophysical applications, in *Fracture Mechanics of Rock*, edited by B. K. Atkinson, pp. 1–26, Academic, San Diego, Calif., 1987.
- Atkinson, B. K., and P. G. Meredith, Experimental fracture mechanics data for rocks and minerals, in *Fracture Mechanics of Rock*, edited by B. K. Atkinson, pp. 477–525, Academic, San Diego, Calif., 1987.
- Bai, T., and D. D. Pollard, Fracture spacing in layered rocks: A new explanation based on the stress transition, *J. Struct. Geol.*, 22(1), 43–57, 2000.
- Bai, T., D. D. Pollard, and M. R. Gross, Mechanical prediction of fracture aperture in layered rocks, *J. Geophys. Res.*, 105, 707–721, 2000.
- Burgmann, R., D. D. Pollard, and S. J. Martel, Slip distributions on faults: Effects of stress gradients, inelastic deformation, heterogeneous host-rock stiffness, and fault interaction, *J. Struct. Geol.*, 16(12), 1675–1690, 1994.
- Cowie, P. A., and C. H. Scholz, Physical explanation for the displacement-length relationship of faults using a post-yield fracture mechanics model, *J. Struct. Geol.*, 14(10), 1133–1148, 1992.
- Cruikshank, K. M., and A. Aydin, Unweaving the joints in the Entrada Sandstone, Arches National Park, Utah, U.S.A., *J. Struct. Geol.*, 17(3), 409–421, 1995.
- DeGraff, J. M., and A. Aydin, Surface morphology of columnar joints and its significance to mechanics and direction of joint growth, *Geol. Soc. Am. Bull.*, 99, 605–617, 1987.
- DeGraff, J. M., and A. Aydin, Effect of thermal regime on growth increment and spacing of contraction joints in basaltic lava, *J. Geophys. Res.*, 98, 6411–6430, 1993.
- Delaney, P. T., and D. D. Pollard, Deformation of host rocks and flow of magma during growth of minette dikes and breccia-bearing intrusions near Ship Rock, New Mexico, *U.S. Geol. Surv. Prof.*, 1202, 1981.
- Delaney, P. T., D. D. Pollard, J. L. Ziony, and E. H. McKee, Field relations between dikes and joints: Emplacement processes and paleostress analysis, *J. Geophys. Res.*, 91, 4920–4938, 1986.
- Dugdale, D. S., Yielding of steel sheets containing slits, *J. Mech. Phys. Solids*, 8, 100–104, 1960.
- Dunne, W. M., and C. P. North, Orthogonal fracture systems at the limits of thrusting: An example from Southwestern Wales, *J. Struct. Geol.*, 12(2), 207–215, 1990.
- Earlougher, R. C., Jr., *Advances in Well Test Analysis*, 264 pp., Soc. of Pet. Eng., Dallas, Tex., 1977.
- Engelder, T., Joints and shear fractures in rock, in *Fracture Mechanics of Rock*, edited by B. K. Atkinson, pp. 27–69, Academic, San Diego, Calif., 1987.
- Engelder, T., and A. Lacazette, Natural hydraulic fracturing, in *International Symposium on Rock Joints*, pp. 35–43, A. A. Balkema, Brookfield, Vt., 1990.
- Erickson, L. L., A three-dimensional dislocation program with applications to faulting in the Earth, M.S. thesis, 167 pp., Stanford Univ., Stanford, Calif., 1986.
- Fisher, D. M., and S. L. Brantley, Models of quartz overgrowth and vein formation: Deformation and episodic fluid flow in an ancient subduction zone, *J. Geophys. Res.*, 97, 20,043–20,061, 1992.
- Freund, L. B., *Dynamic Fracture Mechanics*, 563 pp., Cambridge Univ. Press, New York, 1990.
- Hatton, C. G., I. G. Main, and P. G. Meredith, A comparison of seismic and structural measurements of scaling exponents during tensile subcritical crack growth, *J. Struct. Geol.*, 15(12), 1485–1495, 1993.
- Helgeson, D. E., and A. Aydin, Characteristics of joint propagation across layer interfaces in sedimentary rocks, *J. Struct. Geol.*, 13(8), 897–911, 1991.
- Hodgson, R. A., Classification of structures on joint surfaces, *Am. J. Sci.*, 259, 493–502, 1961.
- Holder, J., J. E. Olson, and Z. Philip, Experimental determination of subcritical crack growth parameters in sedimentary rock, *Geophys. Res. Lett.*, 28, 599–602, 2001.
- Kachanov, M., Effective elastic properties of cracked solids: Critical review of some basic concepts, *Appl. Mech. Rev.*, 45(8), 304–335, 1992.
- Kanninen, M. F., and C. H. Popelar, *Advanced Fracture Mechanics*, 563 pp., Oxford Univ. Press, New York, 1985.
- Kemeny, J., and N. G. W. Cook, Effective moduli, non-linear deformation and strength of a crack elastic solid, *Int. J. Rock Mech. Min. Sci.*, 23(2), 107–118, 1986.
- Kulander, B. R., S. L. Dean, and B. J. Ward Jr., Fractured core analysis: interpretation, logging, and use of natural and induced fractures in core, *Methods Explor. Ser.* 8, 88 pp., Am. Assoc. of Pet. Geol., Tulsa, Okla., 1990.
- Laubach, S., R. Marrett, J. Olson, and A. R. Scott, Characteristics and origins of coal cleat: A review, *Int. J. Coal Geol.*, 34, 175–207, 1998.
- Laubach, S. E., Subsurface fractures and their relationship to stress history in East Texas Basin sandstone, *Tectonophysics*, 156(1–2), 37–49, 1988.
- Laubach, S. E., Practical approaches to identifying sealed and open fractures, *AAPG Bull.*, 87(4), 561–579, 2003.
- Lawn, B. R., and T. R. Wilshaw, *Fracture of Brittle Solids*, 204 pp., Cambridge Univ. Press, New York, 1975.
- Lorenz, J. C., and S. J. Finley, Regional fractures II: Fracturing of Mesa-verde reservoirs in the Piceance Basin, Colorado, *AAPG Bull.*, 75(11), 1738–1757, 1991.
- Marder, M., and J. Fineberg, How things break, *Phys. Today*, 49, 24–29, 1996.
- Narr, W., and J. Suppe, Joint spacing in sedimentary rocks, *J. Struct. Geol.*, 13(9), 1037–1048, 1991.
- Olson, J., and D. D. Pollard, Inferring paleostresses from natural fracture patterns: A new method, *Geology*, 17, 345–348, 1989.
- Olson, J. E., Fracture mechanics analysis of joints and veins, dissertation thesis, Stanford Univ., Stanford, Calif., 1991.
- Olson, J. E., Joint pattern development: Effects of subcritical crack-growth and mechanical crack interaction, *J. Geophys. Res.*, 98, 12,251–12,265, 1993.
- Olson, J. E., and D. D. Pollard, The initiation and growth of en echelon veins, *J. Struct. Geol.*, 13(5), 595–608, 1991.
- Pollard, D. D., Elementary fracture mechanics applied to the structural interpretation of dykes, in *Mafic Dyke Swarms: A Collection of Papers Based on the Proceedings of an International Conference*, edited by H. C. Halls and W. F. Fahrig, *Geol. Assoc. Can. Spec. Pap.*, 5–24, 1987.
- Pollard, D. D., and A. Aydin, Progress in understanding jointing over the past century, *Geol. Soc. Am. Bull.*, 100, 1181–1204, 1988.
- Pollard, D. D., and P. Segall, Theoretical displacements and stresses near fractures in rock: With applications to faults, joints, veins, dikes and solution surfaces, in *Fracture Mechanics of Rock*, edited by B. K. Atkinson, pp. 277–350, Academic, San Diego, Calif., 1987.
- Pollard, D. D., P. Segall, and P. T. Delaney, Formation and interpretation of dilatant echelon cracks, *Geol. Soc. Am. Bull.*, 93, 1291–1303, 1982.
- Renshaw, C. E., Mechanical controls on the spatial density of opening-mode fracture networks, *Geology*, 25, 923–926, 1997.
- Renshaw, C. E., and C. F. Harvey, Propagation velocity of a natural hydraulic fracture in a poroelastic medium, *J. Geophys. Res.*, 99, 21,659–21,677, 1994.
- Renshaw, C. E., and J. C. Park, Effect of mechanical interactions on the scaling of fracture length and aperture, *Nature*, 386, 482–484, 1997.
- Renshaw, C. E., and D. D. Pollard, Numerical simulation of fracture set formation: A fracture mechanics model consistent with experimental observations, *J. Geophys. Res.*, 99, 9359–9372, 1994.
- Sagy, A., Z. E. Reches, and I. Roman, Dynamic fracturing: Field and experimental observations, *J. Struct. Geol.*, 23(8), 1223–1239, 2001.
- Schultz, R. A., Growth of geologic fractures into large-strain populations: review of nomenclature, subcritical crack growth, and some implications for rock engineering, *Int. J. Rock Mech. Min. Sci.*, 37(1–2), 403–411, 2000.
- Secor, D. T., Jr., Role of fluid pressure in jointing, *Am. J. Sci.*, 263, 633–646, 1965.
- Segall, P., Formation and growth of extensional fracture sets, *Geol. Soc. Am. Bull.*, 95, 454–462, 1984a.
- Segall, P., Rate-dependent extensional deformation resulting from crack growth in rock, *J. Geophys. Res.*, 89, 4185–4195, 1984b.
- Segall, P., and D. D. Pollard, Joint formation in granitic rock of the Sierra Nevada, *Geol. Soc. Am. Bull.*, 94, 563–575, 1983.
- Vermilye, J. M., and C. H. Scholz, Relation between vein length and aperture, *J. Struct. Geol.*, 17(3), 423–434, 1995.
- Walsh, J. B., The effect of cracks on the uniaxial elastic compression of rock, *J. Geophys. Res.*, 70, 399–411, 1965.
- Weast, R. C., *Handbook of Chemistry and Physics*, Chem. Rubber Co., Cleveland, Ohio, 1970.

J. E. Olson, Department of Petroleum and Geosystems Engineering, University of Texas at Austin, 1 University Station C0300, Austin, TX 78712, USA. (jolson@mail.utexas.edu)

Predicting fracture swarms – the influence of subcritical crack growth and the crack-tip process zone on joint spacing in rock

JON E. OLSON

*Petroleum and Geosystems Engineering Department, University of Texas at Austin,
1 University Station C0300, Austin, TX 78746, USA (e-mail: jolson@mail.utexas.edu)*

Abstract: Swarms or clusters represent an exception to the widely accepted idea that fracture spacing in sedimentary rock should be proportional to mechanical layer thickness. Experimental studies and static stress analysis do not provide adequate explanation for fracture swarm occurrence. The problem is re-examined numerically, accounting for the dynamics of pattern development for large populations of layer-confined fractures. Two crucial aspects of this model are: (1) the inclusion of three-dimensional effects in calculating mechanical interaction between simultaneously propagating fractures; and (2) the use of a subcritical crack-propagation rule, where propagation velocity during stable growth scales with the crack-tip stress intensity factor. Three regimes of fracture spacing are identified according to the magnitude of the subcritical index of the fracturing material. For low subcritical index material ($n=5$) numerous fractures propagate simultaneously throughout a body resulting in irregular spacing that is, on average, much less than layer thickness. For intermediate subcritical index ($n=20$) one fracture propagates at a time, fully developing its stress shadow and resulting in a pattern with regular spacing proportional to layer thickness. For high subcritical index cases ($n=80$) fractures propagate in a fashion analogous to a process zone, leaving a fracture pattern consisting of widely spaced fracture clusters.

A common attribute of opening-mode fractures or joints (Pollard & Aydin 1988) in sedimentary rock is that observed fracture spacing is proportional to layer thickness (Ladeira & Price 1981; Narr & Suppe 1991; Gross *et al.* 1995; Wu & Pollard 1995; Bai & Pollard 2000a). Two dimensional, plane-strain, static analysis demonstrates how the stress relief around a pre-existing joint can create a propagation 'exclusion' zone (Pollard & Segall 1987). The distance to which stress relief (or stress perturbation) extends from a joint can also be termed its 'mechanical interaction distance'. Any joints within another joint's area of perturbed stress will be mechanically influenced in some way, enhancing or hindering propagation as well as modifying the opening distribution (Pollard *et al.* 1982; Olson & Pollard 1989, 1991). Olson (1993) showed how this stress perturbation can develop in an areal sense as multiple joints grow in length and their stress shadows overlap, diminishing the stress available for additional parallel fractures to grow. Recent work (Bai & Pollard 2000) has shown that in well-bonded, layered materials under crack-normal extensional loading (Fig. 1) the crack-normal stress between closely spaced, parallel joints (spacing less than or equal to layer thickness) actually becomes compressive. This surprising result dictates that increasing the remotely applied extensional strain will not promote the propagation of additional joints between the pre-existing ones, but will only cause the existing joints to open more to accommodate the added extension. Thus, a minimum spacing approximately

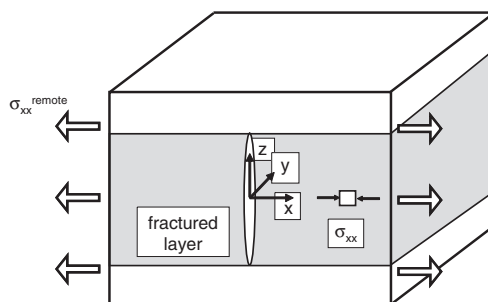


Fig. 1. A three-layer composite, where the middle layer is fractured. Typical plane-strain analysis for fracture spacing examines the variation of the crack-normal stress (σ_{xx}) with distance, x , from the fracture in the vertical x - z plane. The size of the stress relief or stress shadow scales with the height of the fracture, which is assumed to be equivalent to the mechanical layer thickness (Pollard & Segall 1987).

equal to layer thickness is expected for parallel opening-mode fractures, and such a joint set is termed 'saturated', as there is no room for additional joints to grow (Rives *et al.* 1992; Wu & Pollard 1995).

The explanation that joint spacing scales with stress relief explains much of what is observed in fracture patterns in rock and other layered materials, but it cannot explain fracture swarms or other situations where local joint spacing is significantly less than layer thickness (Fig. 2). Bai & Pollard (2000)

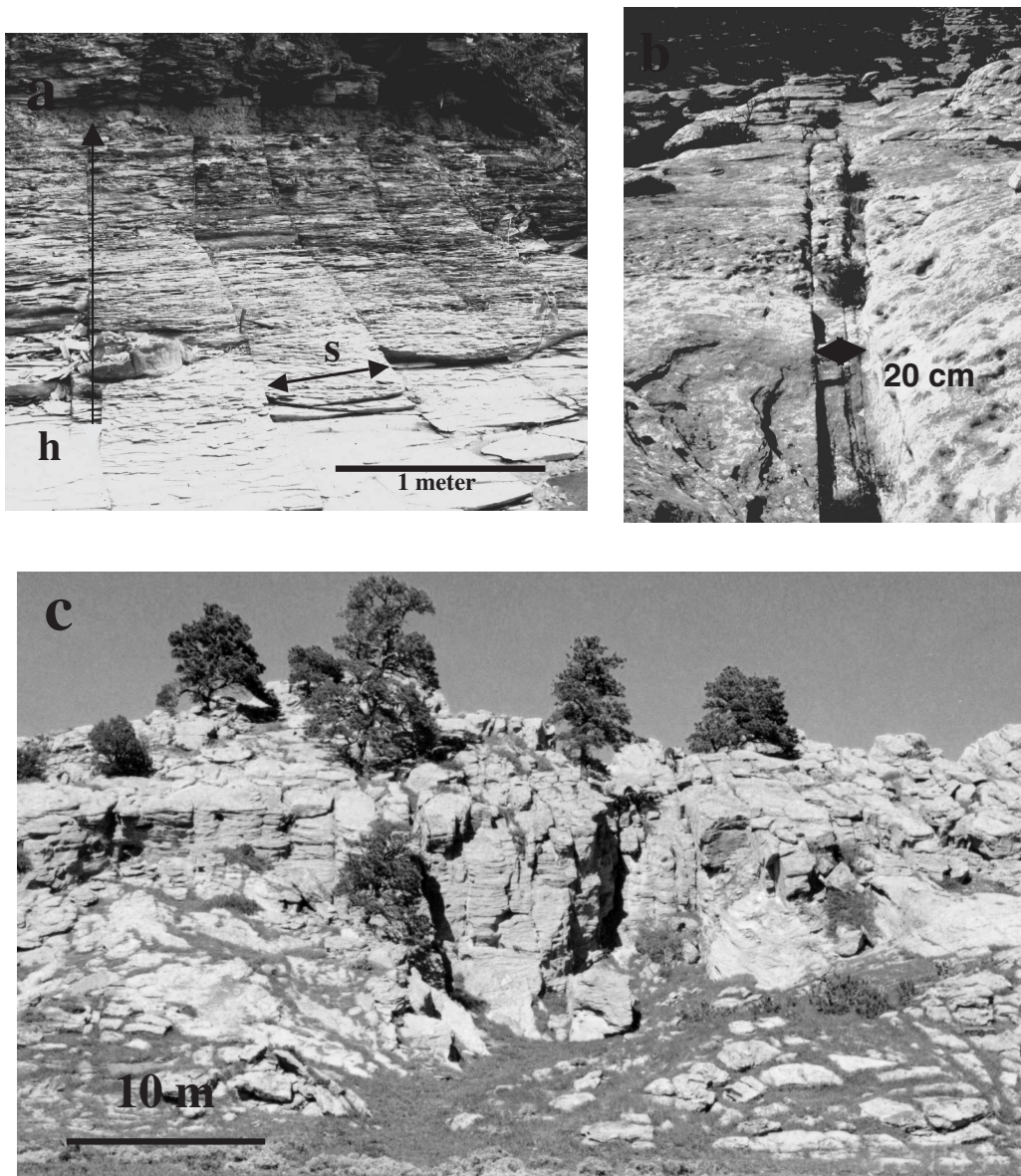


Fig. 2. Examples of fractures in rock with a spacing much less than layer thickness. **(a)** Regularly spaced joints in Devonian Huron Shale, NE Ohio, USA, where the average spacing, s , is less than one-third of the minimum fracture height, h . **(b)** A fracture cluster in the Triassic Wingate Sandstone on Comb Ridge, Utah, USA, where between three and five long fractures lie within a 20 cm-wide zone. The intercluster spacing is approximately 10 m, which is also the thickness of the fractured layer. **(c)** A large fracture swarm in the Cretaceous Frontier Sandstone at Oil Mountain, Wyoming, USA. These are cross-fold fractures with a spacing of less than 10% of layer thickness (Hennings *et al.* 2000).

proposed that joint spacing closer than bed thickness can be attributed to the vertical growth of flaws located near the intersection of fractures with layer boundaries. Their model predicted a minimum spacing to layer thickness ratio of approximately 0.3 based on the static analysis of a vertical cross-

section. The description in this chapter is a slightly different approach analogous to the conceptualization of Wu & Pollard (1995), emphasizing the role of lateral fracture growth in the plane of bedding (propagation along the bed rather than vertically through it) as well as the time sequence of the growth

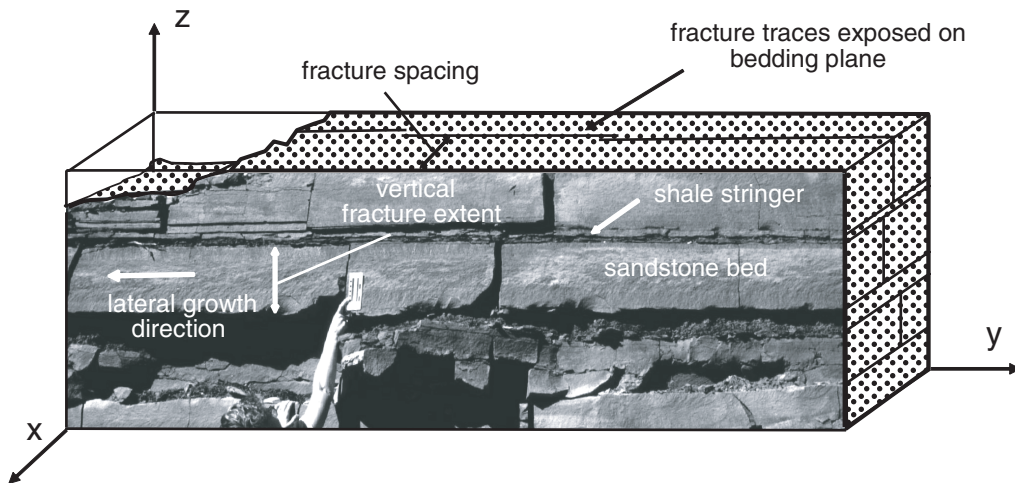


Fig. 3. Three-dimensional representation of a fractured roadcut exposure in the Triassic Chinle Formation at Hite Crossing, Utah, USA. The sandstone beds are separated by thin shale stringers that stopped the vertical growth of the fractures (see middle sandstone with a 10 cm scale). The plumose markings on the fracture surface for the middle bed indicate the fracture grew from right to left, reaching a length many times the height, indicating the dominance of lateral v. vertical fracture propagation.

process. The growth of all fractures from the flaw size to the macroscale is explicitly modelled using a subcritical crack-growth mechanism. The model addresses the mechanics of fracture swarms (and other closely spaced fractures) and shows how subcritical crack growth can be used to predict swarm occurrence. The modelling of time-dependent joint propagation and three-dimensional effects generates a wide range of spacing distributions, including spacing proportional to layer thickness spacing much less than layer thickness and the clustering of joints into swarms.

Fracture propagation in layered rocks

The importance of the lateral propagation of joints in layered rocks has been demonstrated by field observations (Pollard & Aydin 1988; Lacazette & Engelder 1992) and in the laboratory (Wu & Pollard 1995). Figure 3 represents a typical joint geometry from a roadcut example of interbedded sandstone and shale from the Triassic of SE Utah, USA. The photograph depicts the vertical outcrop face, which is a composite fracture surface made up of coplanar but non-continuous segments. The central brittle sandstone bed is bounded by thin, more ductile shale layers. The plumose structure on the joint can be used to determine that it propagated from right to left and was bounded in its propagation between the shale stringers indicated in the figure (Kulander & Dean 1995). The joint breached the entire thickness of the sandstone bed early in its growth history, and

most of the subsequent propagation involved increasing the fracture length within the bed (lateral propagation), resulting in a fracture length that greatly exceeds the height.

A two-dimensional, cross-sectional analysis (that would be carried out in the $x-z$ plane) would be inadequate for analysing the more dominant lateral fracture propagation along the y -direction. Only propagation in the vertical (z) direction can be adequately represented in such a cross-sectional geometry. However, most theoretical models in the literature that explain joint spacing are from the plane-strain perspective of a vertical, bedding-perpendicular cross-section, where length is assumed to be infinite, and the only variable fracture dimensions are height and opening (Hobbs 1967; Pollard & Segall 1987; Narr & Suppe 1991; Gross *et al.* 1995; Bai *et al.* 2000). The modelling approach described in this chapter, with the goal of understanding the variability of joint spacing and the occurrence of fracture swarms, presupposes that the fractures have already propagated vertically across a layer and focuses on the synchronous lateral propagation of numerous vertical fractures confined to a given bed, where bedding would be parallel to the $x-y$ plane of Figure 3.

Subcritical crack growth

In order to analyse the simultaneous propagation of multiple opening-mode fractures, both a failure criterion and a propagation velocity model are required. Brittle fracture strength is influenced by

environmental factors, such as relative humidity and chemical reactivity, that can weaken the bonds between material grains (Atkinson 1984; Swanson 1984). For instance, most rock and ceramic material exhibit maximum fracture resistance (termed critical fracture toughness or K_{Ic}) when tested in a vacuum, and that strength is significantly reduced in the presence of water or water vapour. Fracture propagation under critical conditions is unstable and occurs at velocities comparable to the elastic wave speed of the material (Lawn & Wilshaw 1975). Fracture propagation below the critical toughness, termed subcritical crack propagation, occurs at lower stress levels and much lower velocities. An important parameter from linear elastic fracture mechanics that quantifies the concentration of stress at the crack tip and the tendency for an opening-mode fracture to propagate is called the opening-mode stress intensity factor, K_I (Lawn & Wilshaw 1975). The K_I dependence of propagation velocity for subcritical growth is typically divided into three regions (Anderson & Grew 1977) (Fig. 4). In Region I, the log of propagation velocity varies linearly with the log of stress intensity factor, and this relationship is thought to be controlled by chemical reaction kinetics at the crack tip. In Region II, propagation velocity is roughly constant and is limited by the rate of delivery of the corrosive reactants to the crack tip. In Region III, propagation velocity accelerates to rupture speeds as the stress intensity factor approaches the fracture toughness of the material.

The importance of subcritical crack growth for geological situations is that it is a stable propagation mechanism (Segall 1984; Schultz 2000; Olson 2003) and, in Region I, the propagation velocity, v , is related to the opening-mode stress intensity factor at the crack tip, K_I , with an empirically quantifiable, power-law relationship (Atkinson 1984; Swanson 1984)

$$v = A \left(\frac{K_I}{K_{Ic}} \right)^n \quad (1)$$

where K_{Ic} is the critical fracture toughness, n is the subcritical index and A is a proportionality constant. The power-law exponent, n , can vary widely depending on rock type and environmental conditions (such as dry v. wet). The higher the value of the subcritical index, the less important subcritical growth becomes, as very little propagation occurs before the fracture toughness is reached. For a given rock type, the subcritical index in Region I typically decreases with increasing water content in the environment (Atkinson 1984). Reported values vary from 20 or less for tests carried out on sandstone submerged in water (Atkinson 1984) to greater than 250 under dry conditions in carbonate (Olson *et al.* 2002). Work in clastic sedimentary rocks (Atkinson

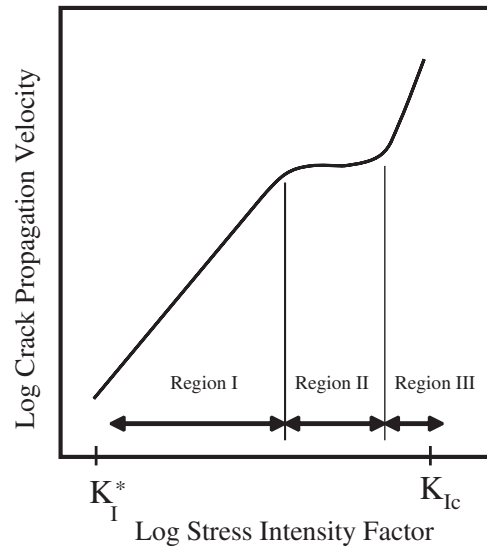


Fig. 4. A log–log plot of propagation velocity v vs. stress intensity factor (K_I) for subcritical crack growth. K_I^* is the minimum stress intensity factor below which there is no propagation. K_{Ic} is the fracture toughness of a material, at which propagation becomes critical. (See text for explanation of the three regions of behaviour.)

1987; Olson *et al.* 2002) suggests that grain size, grain mineralogy, cement type and porosity can influence the value of the subcritical index for a given environmental condition.

Two-dimensional, plane-strain modelling of the development of joint networks utilizing the mechanism of subcritical crack growth has shown that the value of the subcritical index, n , exerts a strong influence on the spatial arrangement and length distribution of fractures (Segall 1984; Olson 1993; Renshaw & Pollard 1994). Results in Olson (1993) demonstrated how the subcritical index controls the joint spacing to bed thickness ratio when modelling vertical propagation across a bed under plane-strain conditions. A very low subcritical index ($n = 1$) garnered a spacing to bed thickness ratio of 0.25, while a higher index ($n = 15$) resulted in a spacing to thickness ratio of 0.875. The Olson (1993) numerical results also demonstrated a mechanism for the growth of widely spaced clusters that had originally been postulated by Dyer (1983) for jointing in sandstone at Arches National Park in Utah, USA. The idea was that a propagating joint causes the stresses ahead of the tip to be more tensile, promoting the growth of nearby fractures in a manner similar to the process zone often observed around igneous dykes, where the intensity of dyke-parallel joints is found to be very high close to the dyke (Delaney *et al.* 1986; Pollard 1987).

Fracture propagation model

Fracture-pattern development is strongly influenced by the mechanical interaction between neighbouring fractures throughout the fracture growth history. This interaction is manifested by the opening or shearing of one fracture perturbing the stress field acting on other nearby fractures. Mathematically, the normal stress acting on an i th fracture element (σ_n^i) due to shearing and opening displacement discontinuities on the j th fracture element (D_s^j and D_n^j , respectively) can be represented by the equation (modified after Crouch 1976)

$$\sigma_n^i = \sum_{j=1}^N G^{ij} C_{ns}^{ij} D_s^j + \sum_{j=1}^N G^{ij} C_{nn}^{ij} D_n^j \quad (2)$$

where C_{ns}^{ij} are the plane-strain, elastic influence coefficients giving the normal stress at element i due to a shear displacement discontinuity at element j , and C_{nn}^{ij} gives the normal stress at element j due to an opening displacement discontinuity at element j . An analogous equation can be written for shear stresses. The fundamental integral for determining the influence coefficients C is presented by Crouch (1976).

G^{ij} is a three-dimensional correction factor by which the plane-strain influence functions are multiplied, and it is given by

$$G^{ij} = 1 - \frac{d_{ij}^\beta}{[d_{ij}^2 + (h/\alpha)^2]^{\beta/2}} \quad (3)$$

where d_{ij} is the distance between the centres of elements i and j , h is the fracture height (assumed equal to mechanical layer thickness), and β and α are empirically determined constants. The form of equation (3) was modelled after the analytical plane-strain equation for the normal stress, σ_{xx} , acting perpendicular to a uniformly loaded, isolated, vertical crack of finite height and infinite length (Pollard & Segall 1987). The solution for the fracture-induced σ_{xx} along the x -axis (at the mid-height point of the fracture where $z=0$) can be written as

$$\sigma_{xx}(x) = \Delta\sigma_1 \left[\left(\frac{|x|^\beta}{(x^2 + (h/2)^2)^{3/2}} - 1 \right) \right] \quad (4)$$

where $\Delta\sigma_1$ is the mode I driving stress. The relationship between the correction factor in equation (3) and σ_{xx} is made evident by substituting G^{ij} into equation (4) with $\beta=3$, $\alpha=2$ and $d_{ij}=x$, resulting in

$$\sigma_{xx}(x) = \Delta\sigma_1(-G^{ij}). \quad (5)$$

G^{ij} imparts a three-dimensional aspect to calculations in that it represents an influence of fracture height on fracture-induced stress, and the plane-strain influence functions, C , preserve the length dependency of the mechanics, resulting in an

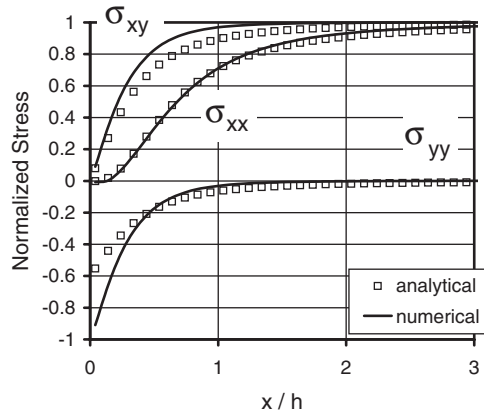


Fig. 5. Crack-induced stress components v. normalized distance, x/h , perpendicular to the fracture trend (see Fig. 1 for fracture orientation with respect to the coordinate system). Stress magnitudes are normalized by the magnitude of the mode I driving stress, $\Delta\sigma_1$, for σ_{xx} and σ_{yy} , and normalized by σ_{xy}^{remote} for σ_{xy} . The open squares represent the analytical solution for a plane-strain fracture with infinite length in the y -direction and finite height, h , in the z -direction. The solid curve is the approximate numerical solution for a three-dimensional crack that is very long in the y -direction and has a finite height, h .

approximate three-dimensional solution. The best values for β and α were empirically derived by comparing σ_{xx} from the plane-strain analytical solution to the boundary-element model result based on equation (3). Using $\beta=2.3$ and $\alpha=1$, the numerical approximation for the crack-normal stress component from a finite-height fracture is almost a perfect match to the analytical solution given in equation (4) (Fig. 5). The plane-strain solution for the crack-parallel stress component in the x - y plane, σ_{yy} , is a function of vertical stress and Poisson's ratio (Pollard & Segall 1987)

$$\sigma_{yy} = \nu(\sigma_{xx} + \sigma_{zz})$$

where

$$\sigma_{zz} = \Delta\sigma_1 \left[\frac{|x|^3 + 2|x|(h/2)^2}{(x^2 + (h/2)^2)^{3/2}} - 1 \right].$$

The approximate numerical solution for σ_{yy} is less accurate than for σ_{xx} , although the general trend is reasonable. Finally, the shear stress in the x - y plane for the plane-strain configuration is given by (Pollard & Segall 1987)

$$\sigma_{xy} = \sigma_{xy}^{remote} \left[\frac{x}{(x^2 + (h/2)^2)^{1/2}} - 1 \right]$$

where σ_{xy}^{remote} is the shear stress acting on the fracture at a distance. The numerical approximation of the

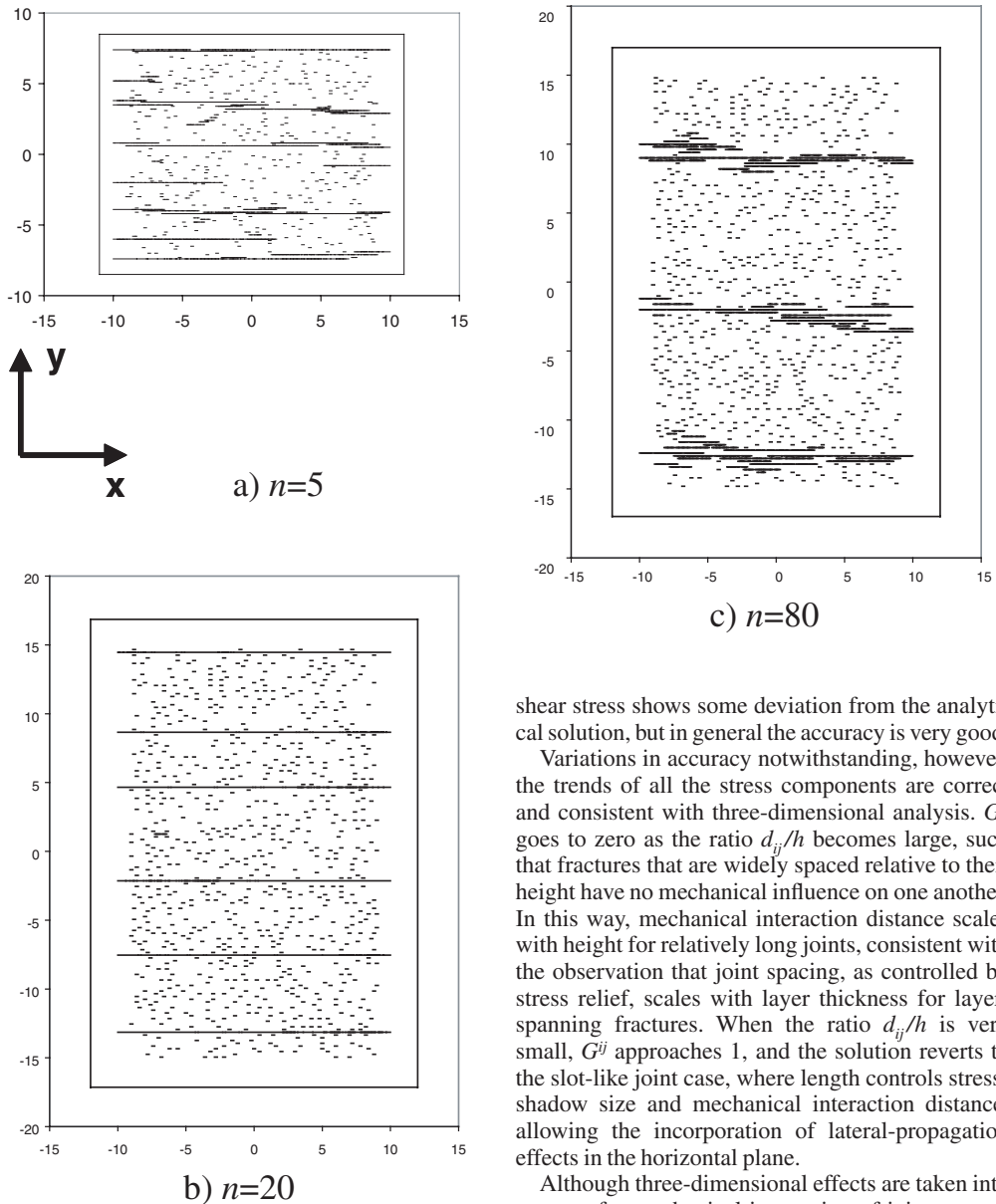


Fig. 6. Examples of subcritical fracture growth for subcritical indices of (a) $n=5$, (b) $n=20$ and (c) $n=80$. All simulations started with the same randomly located parallel flaws, a layer thickness of 8.0 m, a Young's modulus of 20 GPa and a Poisson's ratio of 0.25. Strain was imposed by normal displacement in the y -direction at a strain rate of $2.0 \times 10^{-20}/s^{-1}$ to an ultimate extension of 9×10^{-5} . The boundary conditions on the right and left boundaries of the body have zero normal displacement and all boundaries have zero shear stress. To reduce the computing burden for the $n=5$ case, a smaller representative body was simulated, changing all parameters appropriately to keep simulations equivalent.

shear stress shows some deviation from the analytical solution, but in general the accuracy is very good.

Variations in accuracy notwithstanding, however, the trends of all the stress components are correct and consistent with three-dimensional analysis. G^{ij} goes to zero as the ratio d_{ij}/h becomes large, such that fractures that are widely spaced relative to their height have no mechanical influence on one another. In this way, mechanical interaction distance scales with height for relatively long joints, consistent with the observation that joint spacing, as controlled by stress relief, scales with layer thickness for layer-spanning fractures. When the ratio d_{ij}/h is very small, G^{ij} approaches 1, and the solution reverts to the slot-like joint case, where length controls stress-shadow size and mechanical interaction distance, allowing the incorporation of lateral-propagation effects in the horizontal plane.

Although three-dimensional effects are taken into account for mechanical interaction of joints propagating in a given layer, height growth is not modelled. It is assumed that the initial starter flaws, no matter how short, extend across the full thickness of the layer. However, the mechanical influence of these microcracks is controlled by their shortest dimension (Olson 1993), which will be the length until considerable growth has occurred. As described in Olson (1993), individual fractures are represented by a series of equi-length boundary elements connected end to end. The boundary elements for these simulations were all 0.1 m long, and fracture propagation was based on the computed propa-

gation velocity, as determined using equation (1). The time-step for each iteration was computed as the shortest amount of time required to add an entire element's worth of length to the fastest propagating crack. The growth increments of the more slowly propagating cracks in that same iteration typically represent only a fraction of the total element length. These partial growth increments are tracked and are treated as cumulative, so that after many iterations if a particular crack tip has accumulated enough growth to equal an entire boundary element, an element is added. No more than one element is added to any crack tip during any program iteration.

Numerical results

The simulation results demonstrate the role of sub-critical index, layer thickness and initial flaw density on opening-mode fracture spacing and length. The initial set of simulations were run with 800 starter flaws, all with a length of 0.2 m and a height equal to the layer thickness. (There is no variation in fracture pattern from the top to the bottom of the layer, and fracture heights are constant and equal to layer thickness throughout the simulations.) The flaws were randomly located in a finite body with an x -dimension of 24 m, a y -dimension of 34 m and a layer thickness of 8 m. To prevent unwanted edge effects between the propagating fractures and the boundaries of the finite body, initial flaws were excluded from a 2 m-thick border around the body perimeter, and subsequent growth was excluded from a slightly thinner 1 m-thick border. Straight-crack propagation was imposed to simplify calculations, but such a geometry is reasonable if a strong horizontal stress anisotropy is assumed (Olson & Pollard 1989). Crack growth was induced by 10 equal increments of extension in the y -direction, spaced equally in time with a final strain magnitude of 9×10^{-5} . The strain was imposed at an average strain rate of $2 \times 10^{-20} \text{ s}^{-1}$. (Because of the greater amount of fracture propagation for the $n = 5$ case, it was run for a body of half the area and half the flaws to reduce computing time and memory requirements. However, the strain history and initial areal flaw intensity were exactly the same.)

At the beginning of a simulation, each flaw has a slightly different value of K_I due to the random spatial locations of neighbouring flaws that mechanically interact with it. Side by side juxtapositions diminish K_I while en echelon, or tip-to-tip, arrangements enhance K_I (Olson & Pollard 1991). The flaw with the highest K_I propagates first, and the magnitude of the propagation velocity contrast between the higher and lower stress intensity cracks is defined by the power-law relationship of equation (1). Previous work has shown that for very low sub-critical index values ($n < 10$) (Olson 1993; Holder *et*

al. 2001; Olson *et al.* 2001) many cracks propagate simultaneously and at roughly the same velocity. Even flaws that are initially close together relative to the layer thickness increase in length at a comparable rate, penetrating one another's propagation exclusion zones prior to the stress relief being fully developed.

Figure 5 shows the trace maps of the simulated fracture patterns and the boundary of the finite body, on which the loading was imposed. The numerous shorter fracture segments in the plots represent starter flaws that did not grow. Fracture length and spacing can be inferred from these trace maps, but length can be misleading as modelled fractures sometimes meet tip to tip, thus merging into a single trace. In particular, the length distribution for the case of $n = 20$ (Fig. 7) appears inconsistent with the trace map of Figure 6b, as the trace map apparently shows only six different fractures, all with a length of about 20 m, while Figure 7 indicates a distribution of more than 30 fractures ranging in length from 0.3 to 12 m. In reality, each of the 20 m-long fractures in Figure 6b are made up of several shorter segments that meet tip to tip. The initial flaws were not placed entirely randomly, but their initial locations were rounded to the closest 0.1 m, forcing the starter crack centres to fall onto nodes of a 200×300 grid for the $20 \text{ m} \times 30 \text{ m}$ fractured body. The reason for this constraint on starter flaw locations was to prevent numerical instabilities in the boundary element program arising from two crack elements coming too close to one another (Crouch & Starfield 1982). A more quantitative representation of fracture pattern is found in Figures 7 and 8, where the cumulative frequency of length and perpendicular spacing are reported. These statistics are only compiled for fractures that grew – non-propagated starter flaws were removed from the analysed population. The length data include all fractures that propagated within the modelled area, while spacing is measured along a single scanline running perpendicular to the fracture direction in the middle of the fracture area.

Using $n = 5$, an irregularly spaced fracture pattern was generated with a large variety of fracture lengths and an average spacing much less than the bed thickness (Figs 6a, 7 and 8). Using a higher subcritical index of 20 significantly reduced the number of fractures that propagated and the amount of total fracture length created, but more longer fractures grew (Figs 6b and 7). The spacing became more regular and systematic, with an average spacing of almost 6 m – about 75% of the bed thickness (Fig. 8). This pattern development was characterized by fractures that grew one at a time as a consequence of a large contrast in relative velocity (as defined by equation 1) between fractures of even slightly different K_I values.

Finally, the subcritical index case of $n = 80$ gave some surprising results (Figs 6c, 7 and 8). Based on

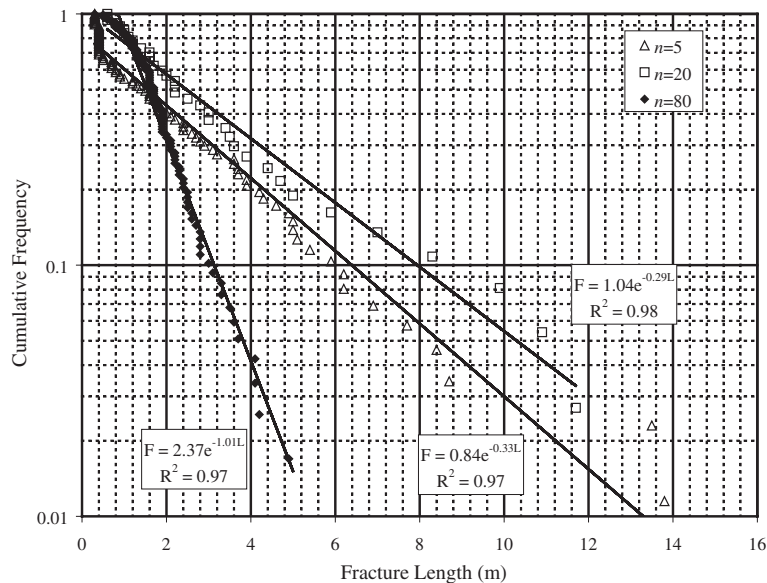


Fig. 7. Cumulative frequency of fracture length for the patterns from Figure 6. Each case can be well described with a negative exponential curve.

previous work (Olson 1993; Renshaw & Pollard 1994), it was expected that for very high values of n the propagation velocity contrast between neighbouring cracks would be even stronger than for $n=20$, and the fracture pattern would be more sparse but still regularly spaced, developed by one fracture propagating at a time. Instead, fracture clusters formed that were made up of many closely spaced short fractures. The development of this pattern through time involved clusters of smaller fractures propagating simultaneously in the tip region of larger fractures, in a fashion similar to a process zone. These fracture clusters appear to reflect the same propagation mechanism as other geological examples of process-zone fracturing, such as m-scale joints in the process zone of km-scale dykes (Delaney *et al.* 1986; Pollard 1987) and mm-scale microcracks in the process zone of m-scale joints (Labuz *et al.* 1987; Nolen-Hoeksema & Gordon 1987). The main difference seems to be that in the joint/dyke and microcrack/joint cases, the process-zone fractures are orders of magnitude smaller than the main crack around which they form. In the simulations described in Figure 6 for $n=80$, the 'process-zone' fractures and the 'main' crack are all about the same length.

A feature common to all of the length distributions from these simulations is that the cumulative frequency, F , is well described by a negative exponential function (Fig. 7). It has been proposed that a negative exponential distribution is theoretically required if fracture length is limited by crack-crack mechanical interaction (Olson *et al.* 2001), and these

results lend support to that idea. The fracture-length distributions for different subcritical indices show that the $n=5$ case is significantly different from the $n=20$ case. They both have approximately the same negative slope on the semi-log plot (-0.33 for $n=5$ and -0.29 for $n=20$), with the main difference being that the $n=20$ distribution is slightly shifted toward longer fractures. The clustered case of $n=80$, however, shows a significant reduction in fracture lengths achieved, exemplified by the much steeper negative slope of -1.01 . The conclusion is that clusters are made up of a large number of short fractures in an echelon arrangement spanning the width of the body.

The cumulative frequency distribution of spacing values (Fig. 8) shows significant and systematic differences between each of the subcritical index cases. Although the data are too sparse to make definitive statistical statements, there is a small degree of clustering (indicated by very small spacing values) for $n=5$ that is not present in the data for $n=20$. Also, the pattern for $n=20$ has substantially higher fracture-spacing values on average than the $n=5$ case, with median values of 6 and 2 m, respectively. The maximum spacing value for $n=20$ is almost 7 m, close to the layer thickness, while the maximum spacing for $n=5$ is only 3 m, less than half the layer thickness. For the $n=80$ case, spacing is bimodal, with an average spacing of less than 0.5 m, dominated by intracluster spacings, and a maximum spacing of about 10 m representing the distance between clusters.

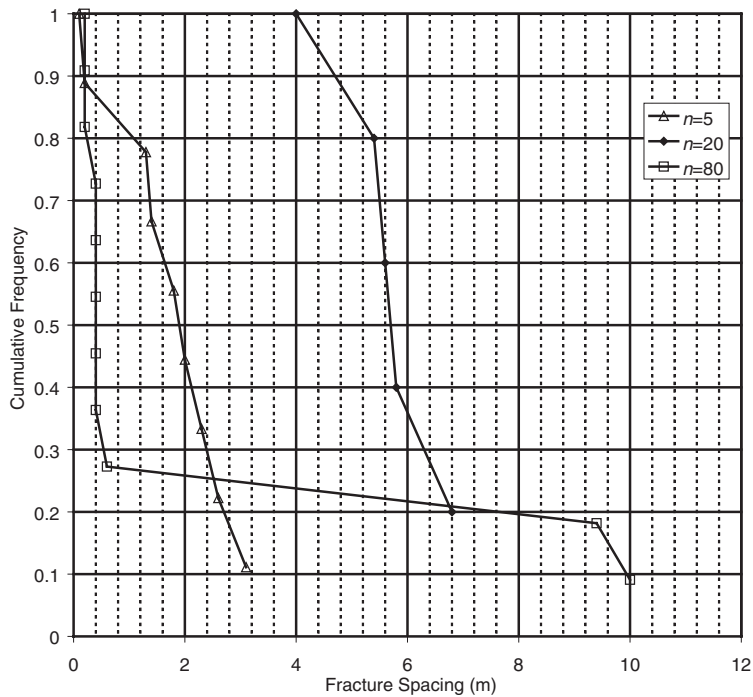


Fig. 8. Cumulative frequency of fracture spacing for the fracture patterns in Figure 6 based on a scanline at $x=0.05$ m.

Based on these simulation results, three different types of fracturing were identified based on subcritical index value. (1) Materials with very low subcritical index can be expected to develop spacing that is substantially less than layer thickness. Because numerous fractures propagate simultaneously for low subcritical index, they can penetrate into one another's stress shadow before it becomes fully developed, resulting in fracture spacing that appears too close given final fracture height and length magnitudes. (2) Intermediate subcritical index values are most likely to result in fracture spacing roughly proportional to bed thickness. As one fracture grows at a time at this subcritical index, each fracture can fully develop its stress shadow before neighbouring fractures get a chance to compete for propagation energy, and the spacing scales with the size of the fully developed fracture's stress perturbation (Pollard & Segall 1987). (3) Finally, materials with very high subcritical index are likely to generate widely spaced clusters, and the spacing between clusters appears to scale with mechanical layer thickness.

Additional simulations were run for the case of $n=80$ to demonstrate the effects of varying bed thickness and initial flaw density on fracture clustering (Figs 9–11). These simulations were run under the same strain boundary conditions used for Figure 6

but with only half the initial flaw density (400 instead of 800 flaws) and with bed thickness varying from 2 to 8 m. All of the trace maps show some degree of fracture clustering (Fig. 9), but clustering appears weakest for the thinnest bed ($h=2$ m). However, even for the layer thickness of 8 m, the clustering is not as strong as the case of $n=80$ using 800 initial flaws (Fig. 6c).

Even though the trace maps for the different bed thickness cases look substantially different, the fracture-length cumulative frequency data for all cases are very similar, again appearing to follow a negative exponential trend (Fig. 10). This suggests that subcritical index has a stronger effect on length distribution than does mechanical layer thickness. However, comparing the exponent for the negative exponential fit in Figure 11 (-0.3678) to the exponent for the $n=80$ case in Figure 7 (-1.011) shows that the initial flaw density has a very strong influence on fracture-length distribution. The steeper slope for the higher fracture density case (Fig. 7) implies that more flaws cause additional hindrance to length growth, and the result is shorter fractures. The maximum fracture length for the higher flaw density case was 5 m, while for the lower density case it was almost 10 m. This strong dependence of length development on flaw density is similar to that found in Olson *et al.* (2001).

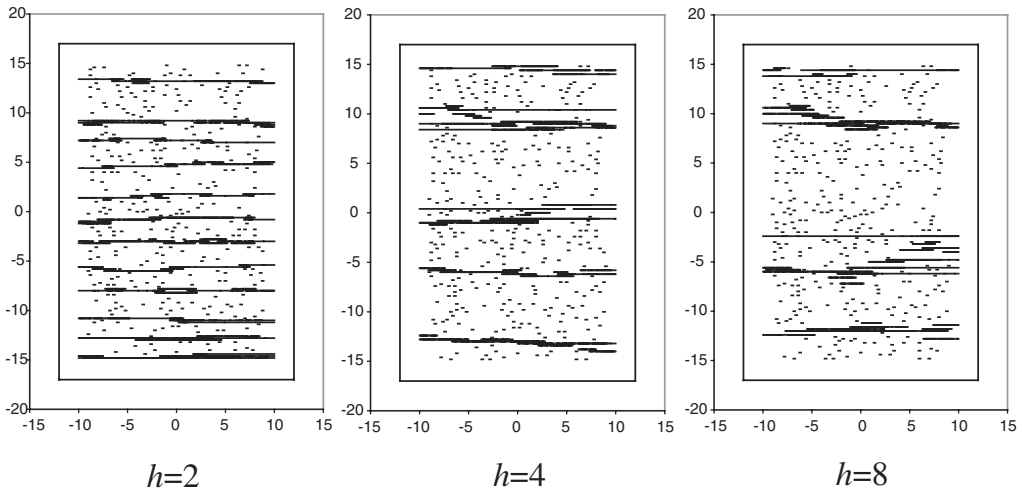


Fig. 9. Fracture trace maps for simulations run under similar conditions to those for Figure 6, except that all cases have a subcritical index of 80, there are 400 starter flaws instead of 800 and the bed thickness is varied from 2 to 4 to 8 m.

As expected, fracture-spacing distributions (Fig. 11) are strongly affected by bed thickness, even though the fracture-length distribution is relatively independent of it (Fig. 10). The maximum spacing increases with increasing layer thickness, but the median spacing has the reverse relationship. The low median value is interpreted to be an outgrowth of the effect of clustering on the spacing distribution. There is a strong change in slope of the cumulative frequency curves of fracture spacing for the cases of different bed thicknesses. From inspecting the trace maps in conjunction with the spacing data, it is evident that the larger spacings represent the distance between clusters (intercluster spacing) and the smaller values represent the distance between fractures within a cluster (intracluster spacing). For example, for the thin-bedded case ($h=2$), the data at a cumulative frequency of $F=0.78$ and above represent intracluster spacings of 0.2 m, while the data at cumulative frequency of $F=0.72$ and below, valued at 1.8 m or higher, are intercluster spacings (or in some instances the spacing between non-clustered fractures). Interpolating, the population break can be picked at a cumulative frequency of $F=0.75$. Thus, for the $h=2$ case, about 25% of the spacings represent measurements within a cluster. For the cases of $h=4$ and $h=8$, the break in the population can be picked at cumulative frequencies of $F=0.41$ and $F=0.45$, respectively. The thicker beds exhibit stronger clustering, with between 55% (for $h=4$) and 60% (for $h=8$) of the spacing measurements coming from within clusters.

Reiterating, the maximum spacing values in the distributions indicate the distance between clusters, and the dependence of intercluster spacing on

mechanical layer thickness suggests it is related to the stress shadow around fractures. The spacing within clusters (intracluster) is most probably related to crack-tip-process zone and initial flaw spacing.

Process-zone mechanics and joint clusters

As noted in the discussion of the $n=80$ simulation, the mechanism of fracture clustering can be likened to a process zone propagating across the body. The reason for clustering to occur in the high subcritical index cases is related to the magnitude of the stress intensity factor when propagation occurs. As fracture-propagation velocities for material with very high n are initially very low due to the power-law nature of equation (1), propagation is delayed until more strain has accumulated. Consequently, when fracture growth finally occurs, it can be at stress intensity factor values that approach or exceed critical values. Because fracture-induced stress scales linearly with stress intensity factor in the near-tip region (Lawn & Wilshaw 1975), the tensile stress perturbation around the crack tip is increased by high K_I values and the propagation of flaws in the crack-tip region is enhanced for high n cases. The clusters or fracture swarms essentially record the movement of a process zone across the rock body and, because of the higher stress intensity factor values, the propagation mechanism is no longer described by subcritical region I, but by region II, III or critical propagation ($K_I \geq K_{Ic}$). However, even if fracture growth approaches critical conditions, high propagation velocities are not reached under typical

PREDICTING FRACTURE SWARMS

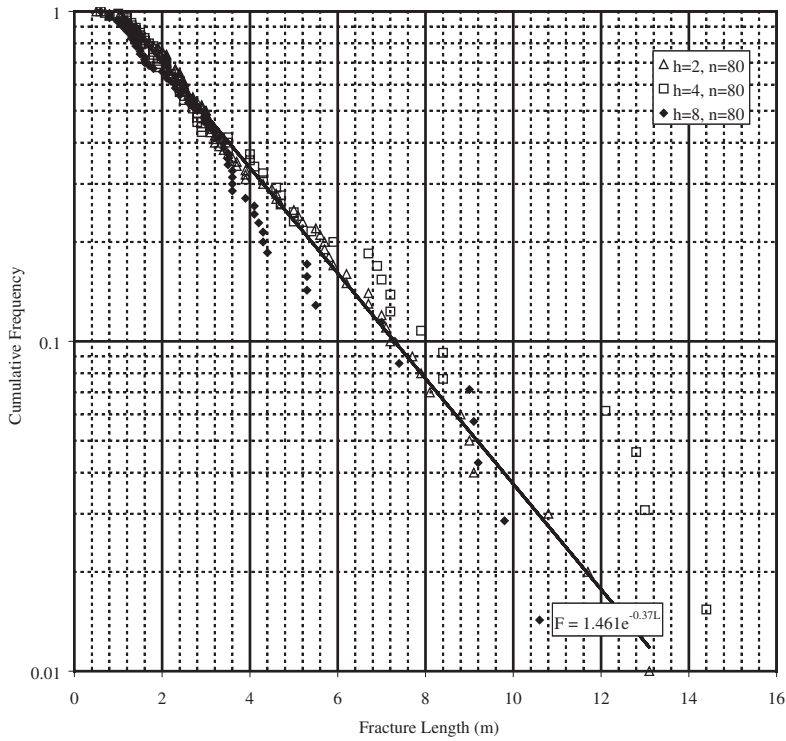


Fig. 10. Cumulative frequency of fracture length for the patterns of Figure 9. Note that all three patterns have markedly similar length distributions that follow a negative exponential shape.

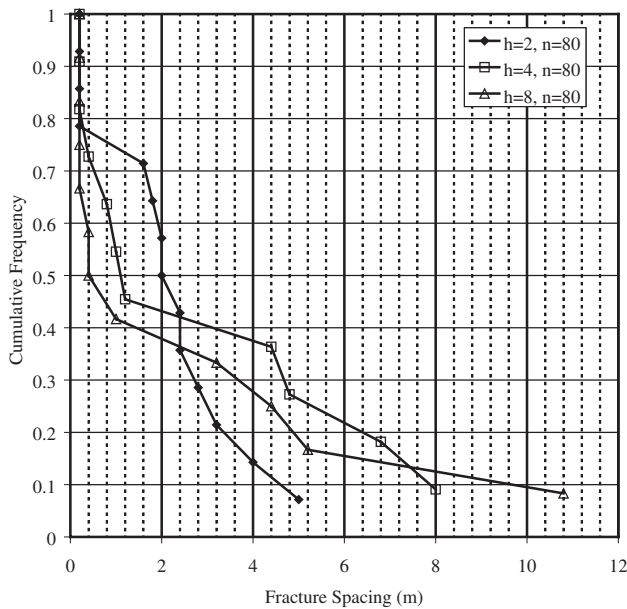


Fig. 11. Cumulative frequency of fracture spacing for the fracture patterns in Figure 9 based on a scanline at $x = 0.05$ m.

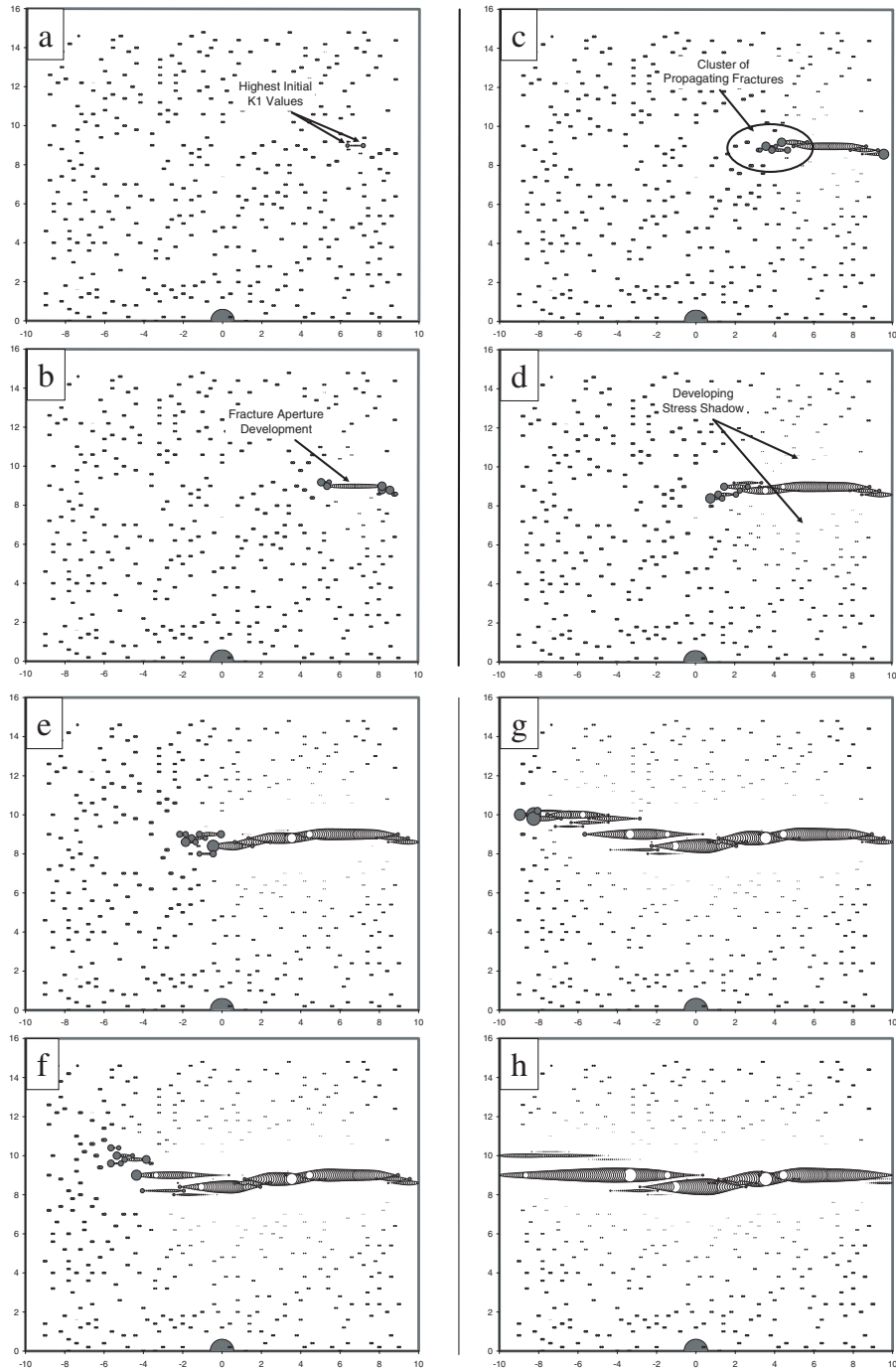


Fig. 12. Sequence of fracture aperture and stress intensity factor development for the cluster from Fig. 6 (case $n = 80$) in the vicinity of $y = 8$ m. The circle centred at $(0, 0)$ is the scale for K_I , showing the diameter appropriate for a value of $10 \text{ MPa}\cdot\text{m}^{1/2}$. Each fracture segment modelled has an opening represented by a open circle with a proportionate diameter. The fracture-tip elements have a shaded circle representing the magnitude of K_I . Frames (a) – (h) show the propagation of a cluster across the body, the stress-shadow effects of growing fractures on other nearby fractures and the tapered fracture opening shape approaching the crack tips for interacting fractures.

geological conditions (Olson 2003) because strain-softening effects (Segall 1984) or fluid-flow restrictions (Engelder & Lacazette 1990; Lacazette & Engelder 1992; Renshaw & Harvey 1994) reduce the stress intensity factor with propagation, resulting in a quasi-stable process. The apparent increase in cluster size with increased mechanical layer thickness inferred from the spacing data of Figure 11 suggests that thicker beds also allow for stronger mechanical crack interaction and more stress elevation in the crack-tip region, which may cause the growth of more fractures over a wider area in the 'process zone'.

Looking at the sequence of development of fracture aperture and stress intensity factor in a growing cluster helps illustrate the cluster growth mechanism. Figure 12 shows the time sequence of fracture growth for the cluster located around $y=8$ m from the $n=80$ case in Figure 6, mapping fracture opening at each boundary element in the simulation and stress intensity factor at every crack tip. Fracture opening is represented by the diameter of the open circles located at each fracture patch centre. (Fracture aperture exaggeration is approximately $\times 450$ —the maximum aperture in the final plot of the sequence, Fig. 12h, is approximately 1.75 mm located at $x=0$ m, $y=8.4$ m.) The stress intensity factor is proportional to the diameter of the shaded circles that are located at the centre of every crack-tip element. The scale for stress intensity factor magnitude is the large, dark circle centred at (0, 0) on each plot, whose size represents a stress intensity factor value of $10 \text{ MPa}\cdot\text{m}^{1/2}$. (There is no crack element at this location, it is merely a scale.)

In Figure 12a, only a small amount of fracture growth has occurred, starting at the cracks with the largest initial K_I values. None of the cracks in the simulation have any visible fracture aperture except for the cracks whose tips are indicated to have the highest K_I on the plot. After additional growth has occurred (Fig. 12b), the fracture aperture for the main crack is clearly visible, and the K_I values are rising for this growing crack as well as for some of its close neighbours. The fracture cluster growth (or the process zone) is well developed by Figure 12c, where several cracks are propagating ahead of the left tip of the main crack. It is interesting to note that the cracks in the cluster have elevated K_I values at both tips, suggesting that they are both propagating out ahead of the main crack (to the left) as well as back towards it (to the right). Eventually, the crack interaction of the overlapping en echelon crack tips hinders growth of the clustered fractures towards the right and the main crack towards the left, causing arrest at some tips and providing a limitation on length growth (Pollard *et al.* 1982; Olson & Pollard 1989).

Another aspect of crack interaction can be seen by comparing Figure 12a with Figure 12d. While there

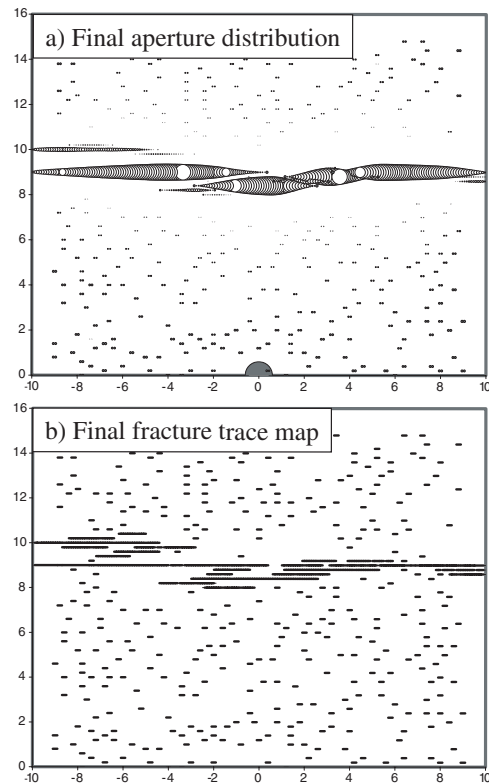


Fig. 13. Comparison of the final fracture aperture distribution and trace map of fractures that grew, showing that some fractures grow and then subsequently close or never reach an observable aperture.

is fracture-propagation enhancement ahead of the tip of the main propagating cracks, there is propagation hindrance to either side of the main body of the crack, as noted in Figure 12d. The propagation hindrance is exemplified by the diminished K_I values of the pre-existing flaws in that area compared to their initial state. Further propagation of the fracture cluster completely across the body is shown in Figure 12e–h. Further development of the stress-shadow or propagation-suppression zone is evident, as well as the tapered, non-elliptical displacement profiles at the tips for many of the overlapping, en echelon fractures.

Comparing the final fracture aperture map with a trace map (Fig. 13) shows that not all of the fractures that propagated have an appreciable aperture at the end of the deformation cycle. The figure clearly shows that, although there are many fractures that propagated in the cluster (Fig. 13b), there are a few dominant ones that have the largest aperture, and these are typically the longest fractures. Also, exaggerating the K_I scale for the initial and final

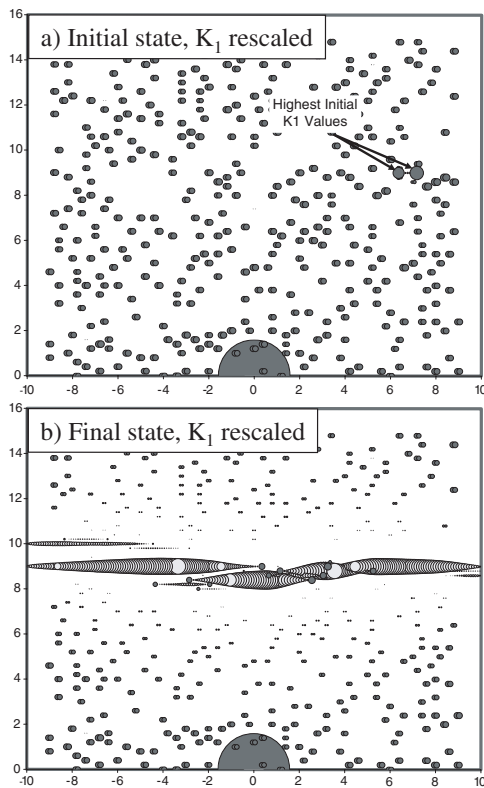


Fig. 14. Rescaled versions of Figure 12a and b, emphasizing the heterogeneity of K_1 throughout the fractured body.

states emphasizes the stress-shadow or propagation-suppression effects around the propagated cluster (Fig. 14). This K_1 suppression extends 4–6 m to either side of the open fracture zone ($h = 8$ m).

Conclusion

This work shows that the spacing of opening-mode fractures constrained to a single layer in a homogeneous elastic body depends not only on the static-stress distribution around the fractures but also on fracturing dynamics and the three-dimensional nature of lateral fracture propagation. These numerical fracture-propagation results are proposed to be analogous to the lateral propagation of joints confined to by sedimentary layering. The plane strain, static analysis of stress relief or stress-shadow effects around a fracture imply a minimum fracture spacing approximately equal to layer thickness, but that static analysis represents only one of three newly identified fracture-propagation regimes delineated by variations in subcritical crack properties.

Regular fracture spacing approximately equal to mechanical layer thickness is attributed to subcritical crack propagation in rock with subcritical indices of intermediate magnitude ($n \cong 20$). Another regime of propagation behaviour exists for very low subcritical index materials ($n \cong 5$), where fractures tend to have spacing that is very irregular and much less than bed thickness. This spacing regime may be responsible for very large fracture swarms, such as pictured in Figure 2c. Finally, at very high subcritical index ($n \cong 80$), fracturing is also very clustered, but the clusters are widely spaced and the fracture growth probably occurs at critical stress intensity factor values. The fracture pattern for this high subcritical index regime resembles the fracture clustering in Figure 2b.

Although fracture height (as constrained by bed thickness) has an influence on fracture spacing, simulations show little impact of bed thickness on the cumulative frequency of fracture-length. The key parameters controlling fracture-length development appear to be subcritical index and flaw density in the body. Another unusual result related to bed-thickness effects was found in the high subcritical index cases ($n = 80$). Although increasing bed thickness increased the maximum observed spacing between fractures for a given pattern, which seems to be consistent with stress-shadow ideas, the average spacing of the distribution actually decreased as bed thickness was increased. This behaviour is attributed to the stronger mechanical-crack interaction for larger bed thickness cases, causing more intense fracturing in the near-tip region of a propagating crack. For a thin bed, the zone of elevated stress is less well developed around the propagating crack tip, and thus fracture clusters are less significant and median spacing is broader.

This material is based in part on work supported by the US Department of Energy under Award No. DE-FC26-00BC15308, the Texas Advanced Technology Program, and by the Fracture Research and Application Consortium (FRAC) of The University of Texas at Austin. The author thanks T. Engelder for helpful review comments.

References

- ANDERSON, O. L. & GREW, P. C. 1977. Stress corrosion theory of crack propagation with applications to geophysics. *Reviews of Geophysics and Space Physics*, **15**, 77–104.
- ATKINSON, B. K. 1984. Subcritical crack growth in geological materials. *Journal of Geophysical Research*, **89**, 4077–4114.
- BAI, T. & POLLARD, D. D. 2000a. Fracture spacing in layered rocks: a new explanation based on the stress transition. *Journal of Structural Geology*, **22**, 43–57.
- & POLLARD, D. D. 2000b. Closely spaced fracture in layered rocks: initiation mechanism and propagation

- kinematics. *Journal of Structural Geology*, **22**, 1409–1425.
- BAI, T., POLLARD, D. D. & GAO, H. 2000. Explanation for fracture spacing in layered materials. *Nature*, **403**, 753–756.
- COWIE, P. A. & SCHOLZ, C. H. 1992. Displacement–length scaling relationship for faults: data synthesis and discussion. *Journal of Structural Geology*, **14**, 1149–1156.
- CROUCH, S. L. 1976. Solution of plane elasticity problems by the displacement discontinuity method. *International Journal for Numerical Methods in Engineering*, **10**, 301–343.
- & STARFIELD, A. M. 1982. *Boundary Element Methods in Solid Mechanics: With Applications in Rock Mechanics and Geological Engineering*. Allen and Unwin, London.
- DELANEY, P. T., POLLARD, D. D., ZIONY, J. L. & MCKEE, E. H. 1986. Field relations between dikes and joints: emplacement processes and paleostress analysis. *Journal of Geophysical Research*, **91**, 4920–4938.
- DYER, J. R. 1983. *Jointing in sandstones, Arches National Park, Utah*. PhD thesis, Stanford University.
- GROSS, M. R., FISCHER, M. P., ENGELDER, T. & GREENFIELD, R. J. 1995. Factors controlling joint spacing in interbedded sedimentary rocks; integrating numerical models with field observations from the Monterey Formation, USA. In: AMEEN, M. S. (ed.) *Fractography: Fracture Topography as a Tool in Fracture Mechanics and Stress Analysis*. Geological Society, London, Special Publications, **92**, 215–233.
- HOBBS, D. W. 1967. The formation of tension joints in sedimentary rocks: an explanation. *Geological Magazine*, **104**, 550–556.
- HOLDER, J., OLSON, J. E. & PHILIP, Z. 2001. Experimental determination of subcritical crack growth parameters in sedimentary rock. *Geophysical Research Letters*, **28**, 599–602.
- KULANDER, B. R. & DEAN, S. L. 1995. Observations on fractography with laboratory experiments for geologists. In: AMEEN, M. S. (ed.) *Fractography: Fracture Topography as a Tool in Fracture Mechanics and Stress Analysis*. Geological Society, London, Special Publications, **92**, 59–82.
- LABUZ, J. F., SHAH, S. P. & DOWDING, C. H. 1987. The fracture process zone in granite; evidence and effect. *International Journal of Rock Mechanics and Mining Sciences & Geomechanics Abstracts*, **24**, 235–246.
- LACAZETTE, A. & ENGELDER, T. 1992. Fluid-driven cyclic propagation of a joint in the Ithaca Siltstone, Appalachian Basin, New York. In: EVANS, B. & WONG, T.-F. (eds) *Fault Mechanics and Transport Properties of Rock*. Academic Press, London, 297–324.
- LADEIRA, F. L. & PRICE, N. J. 1981. Relationship between fracture spacing and bed thickness. *Journal of Structural Geology*, **3**, 179–187.
- LAWN, B. R. & WILSHAW, T. R. 1975. *Fracture of Brittle Solids*. Cambridge University Press, Cambridge.
- NARR, W. & SUPPE, J. 1991. Joint spacing in sedimentary rocks. *Journal of Structural Geology*, **13**, 1037–1048.
- NOLEN-HOEKSEMA, R. C. & GORDON, R. B. 1987. Optical detection of crack patterns in the opening-mode fracture of marble. *International Journal of Rock Mechanics and Mining Sciences & Geomechanics Abstracts*, **24**, 135–144.
- OLSON, J. E. 1993. Joint pattern development: effects of subcritical crack-growth and mechanical crack interaction. *Journal of Geophysical Research*, **98**, 12251–12265.
- 2003. Sublinear scaling of fracture aperture versus length: an exception or the rule? *Journal of Geophysical Research*, **108**, 2413.
- & POLLARD, D. D. 1989. Inferring paleostresses from natural fracture patterns: A new method. *Geology*, **17**, 345–348.
- & POLLARD, D. D. 1991. The initiation and growth of en echelon veins. *Journal of Structural Geology*, **13**, 595–608.
- , HOLDER, J. & RIJKEN, P. 2002. Quantifying the fracture mechanics properties of rock for fractured reservoir. In: *SPE/ISRM Rock Mechanics Conference, Irving, Texas*, 1–12.
- , QIU, Y., HOLDER, J. & RIJKEN, P. 2001. Constraining the spatial distribution of fracture networks in naturally fractured reservoirs using fracture mechanics and core measurements. In: *2001 SPE Annual Technical Conference and Exhibition, New Orleans, LA*.
- POLLARD, D. D. 1976. On the form and stability of open hydraulic fractures in the Earth's crust. *Geophysical Research Letters*, **3**, 513–516.
- 1987. Elementary fracture mechanics applied to the structural interpretation of dykes. In: HALLS, H. C. e & FAHRIG, W. F. e. (eds) *Mafic Dyke Swarms; A Collection of Papers Based on the Proceedings of an International Conference, Mississauga, ON, Canada*, **34**, 5–24.
- & AYDIN, A. 1988. Progress in understanding jointing over the past century. *Geological Society of America Bulletin*, **100**, 1181–1204.
- & SEGALL, P. 1987. Theoretical displacements and stresses near fractures in rock: with applications to faults, joints, veins, dikes and solution surfaces. In: ATKINSON, B. K. (ed.) *Fracture Mechanics of Rock*. Academic Press, London, 277–350.
- , SEGALL, P. & DELANEY, P. T. 1982. Formation and interpretation of dilatant echelon cracks. *Geological Society of America Bulletin*, **93**, 1291–1303.
- RENSHAW, C. E. & POLLARD, D. D. 1994. Numerical simulation of fracture set formation: a fracture mechanics model consistent with experimental observations. *Journal of Geophysical Research*, **99**, 9359–9372.
- RIVES, T., RAZACK, M., PETIT, J. P. & RAWNSLEY, K. D. 1992. Joint spacing: analogue and numerical simulations. *Journal of Structural Geology*, **14**, 925–937.
- SEGALL, P. 1984. Formation and growth of extensional fracture sets. *Geological Society of America Bulletin*, **95**, 454–462.
- SWANSON, P. L. 1984. Subcritical crack growth and other time- and environment-dependent behavior in crustal rocks. *Journal of Geophysical Research*, **89**, 4137–4152.
- VERMILYE, J. M. & SCHOLZ, C. H. 1995. Relation between vein length and aperture. *Journal of Structural Geology*, **17**, 423–434.
- WU, H. & POLLARD, D. D. 1995. An experimental study of the relationship between joint spacing and layer thickness. *Journal of Structural Geology*, **17**, 887–905.



SPE/ISRM 78207

Quantifying the Fracture Mechanics Properties of Rock for Fractured Reservoir Characterization

Jon E. Olson, SPE, Jon Holder, and Peggy Rijken, SPE, The University of Texas at Austin

Copyright 2002, Society of Petroleum Engineers Inc.

This paper was prepared for presentation at the SPE/ISRM Rock Mechanics Conference held in Irving, Texas, 20-23 October 2002.

This paper was selected for presentation by an SPE/ISRM Program Committee following review of information contained in an abstract submitted by the author(s). Contents of the paper, as presented, have not been reviewed by the Society of Petroleum Engineers or International Society of Rock Mechanics and are subject to correction by the author(s). The material, as presented, does not necessarily reflect any position of the Society of Petroleum Engineers, International Society of Rock Mechanics, its officers, or members. Papers presented at SPE/ISRM meetings are subject to publication review by Editorial Committees of the Society of Petroleum Engineers. Electronic reproduction, distribution, or storage of any part of this paper for commercial purposes without the written consent of the Society of Petroleum Engineers is prohibited. Permission to reproduce in print is restricted to an abstract of not more than 300 words; illustrations may not be copied. The abstract must contain conspicuous acknowledgment of where and by whom the paper was presented. Write Librarian, SPE, P.O. Box 833836, Richardson, TX 75083-3836, U.S.A., fax 01-972-952-9435.

Abstract

Natural fractures are important conduits for fluid-flow and can control the deformational behavior of rock. The accurate evaluation of natural fracture geometry in the subsurface is difficult because of the sampling problems inherent to wellbores and indirect investigation methods such as seismic. Because of these limitations in observational capability, predictive models are needed to provide more constraint on natural fracture characteristics. One approach is to look at the mechanics of fracture propagation in sedimentary rock as controlled by subcritical crack growth (also known as stress-corrosion cracking). We have measured the subcritical fracture properties of numerous sedimentary rocks, including core samples from petroleum reservoirs, in conjunction with detailed petrographic analysis. Our preliminary results suggest that carbonates and sandstones tend to have very different subcritical fracture properties, and the variation in sandstone properties can be linked to grain and cement mineralogy and volume fractions.

Introduction

The direct characterization of natural fracture network attributes such as length, spacing, aperture, orientation and intensity in most reservoirs is very difficult, primarily because of the low probability of intersecting vertical fractures with vertical wellbores.^{1,2} Accordingly, various predictive schemes based on geostatistics,^{3,4} or geomechanical models⁵⁻⁷ are used to estimate subsurface fracture attributes.

Statistical approaches fit distributions of fracture characteristics to available data. The statistical fit can treat different fracture attributes independently, or it can

incorporate interdependences into the fit,⁸ but in either case, the result is dependent on available direct fracture observations. Alternatively, geomechanics-based simulations of fracture attributes combine a physical understanding of the fracturing process with measurements of a small set of rock properties and geologic boundary conditions to predict fracture network properties, even in the absence of direct observations. This approach provides for the determination of physically reasonable fracture attributes, and of relationships between different fracture attributes.^{6,9-11}

The geomechanical model used here is based on subcritical crack growth. Although subcritical fracture velocities are several orders of magnitude slower than rupture velocities,¹² natural fracture growth can be significant in tectonically strained crustal rocks.¹²⁻¹⁴ A number of studies have demonstrated subcritical crack growth controls of fracture spacing and length distributions,^{9,13,15,16} connectivity^{17,18} and fracture aperture.^{16,19}

Subcritical crack growth can be described by the empirical relationship^{9,20}

$$V = A \left(\frac{K_I}{K_{Ic}} \right)^n, \quad (1)$$

where V is the crack propagation velocity, K_I is the mode I stress intensity factor, K_{Ic} is the fracture toughness, and A is a constant. The exponent n is called the subcritical fracture index. The influence of this parameter on fracture pattern geometry is illustrated in Figure 1.¹⁶ The fracture sets were generated using the same stress environment and number of starter flaws, but using a range in values of the subcritical index. For low values of n (less than 10), computed natural fracture patterns exhibit small spacing relative to bed thickness. At high values of the subcritical index ($n = 80$), fractures are spatially arranged in widely spaced swarms or clusters. Intermediate values (between 20 and 40) result in more regular fracture spacing that is roughly proportional to layer thickness. Discrete fracture flow modeling of geomechanically-generated fracture patterns indicates effective permeability will vary with subcritical index, primarily through its influence on fracture length distributions.²¹

The subcritical index can be measured in the laboratory,^{12,20} and subcritical index values for a wide range of rocks have been reported,^{22,23} although no systematic variation with petrographic properties has been reported for sedimentary rocks. For the purpose of natural fracture pattern interpretation and prediction, present-day subcritical index values may be problematic as fractures may have developed when the rock was in a different diagenetic state. Although grain size and grain mineralogy are unlikely to change significantly with sediment burial and lithification, porosity and intergranular cementation are likely to continuously change with time. If the impact of variations in specific microstructural elements such as cement on subcritical crack behavior can be quantified, extrapolation of present-day properties to fracture formation episodes can be carried out using diagenetic models.

In the following, we discuss measurements of the subcritical crack index in various rock types from outcrop and subsurface samples. Additionally, subcritical crack measurements and detailed thin section analyses were carried out on core material from two gas-producing formations, and the analysis is based on concepts derived from stress corrosion cracking of polycrystalline metals and ceramics.²⁴ The laboratory test procedures and measurement results are described in the following section, and a brief review of the theoretical analysis of microstructure controls of subcritical crack growth is given in the next section.

Laboratory Tests of Subcritical Crack Growth

Subcritical crack growth measurements were carried out with a constant-displacement, double-torsion testing procedure,^{25,26} using thin-section sized rock specimens. In this configuration, stress intensity is independent of fracture length, and a complete propagation velocity vs. stress intensity factor curve can be obtained from a single load decay measurement on opaque samples. Total crack propagation during a single load decay is often much less than the length of the specimen, and multiple tests can often be carried out on the same test specimen. Special measurement techniques²³ designed for compliant and heterogeneous sedimentary rocks were used.

Measured subcritical indices from a wide range of rock types are summarized in Table 1. Although we do not have detailed petrographic information on these samples, some basic trends appear in the data:

1. Subcritical indices for sandstones measured under dry conditions vary from 35 to 80, with most values being in the 50's and 60's. The values tend to be higher for lower-porosity material.
2. Subcritical indices for carbonates are considerably higher (100-300 for dry conditions) than for sandstones.
3. Tests carried out under water-saturated conditions reduce the subcritical index measured compared to dry conditions as expected,²² but the effect is much stronger for the high index carbonates. For oil-stained specimens, the effect of water is minimal.

Clearly, rock type exerts an important control on subcritical crack behavior, but a more detailed investigation was performed on two sandstone formations in hopes of identifying links between specific petrographic properties and subcritical index value. For this study, we chose two tight-gas sandstone formations where natural fractures are considered contribute significantly to producibility.²⁷ The first set was selected from the Dakota Formation of the San Juan Basin, New Mexico. A second set of measurements was carried out on samples selected from the Travis Peak Formation of East Texas.

Dakota Sandstone. Results from the subcritical crack and point count measurements on the Dakota Sandstones samples are summarized in Table 2. Suites of 5-10 test specimens were prepared for each of 12 cores extracted from different depth intervals. Some of the data are repeated from Rijken et al.,²⁸ but the table now includes petrographic analyses for all the depth intervals used for the subcritical crack measurements. The petrographic properties listed in the table are: porosity, framework grains (quartz, plagioclase, and potassium feldspar), rock fragments (chert, clay clasts, carbonate rock fragments, volcanic rock fragments), matrix (pyrite, associated clays, pseudomatrix), and cement type (quartz, dolomite, and iron dolomite).

All tests results shown were carried out under nominal room conditions of approximately 22°C and 70% relative humidity. Subcritical crack growth processes such as stress corrosion cracking are chemically driven, and weakening of silicate bonds by hydroxyl ions is what causes the lowering of subcritical crack indices in the presence of water.^{20,29,30} Unfortunately, the presence of substantial amounts of clay in these specimens led to mechanical failure of most specimens in the presence of water. No well-defined subcritical indices appropriate for water-saturated conditions could be determined for the Dakota Sandstones.

After the subcritical crack measurements, one thin section was prepared from each of the depth intervals for petrographic analysis using either a conventional thin section or a cathodoluminescence (CL) image.³¹ Secondary electron (SE) images and CL images were also used to examine the nature of the created subcritical crack (Figures 2 and 3). A secondary electron (SE) mosaic for one of the Dakota specimens, with SE and CL close-ups (Figure 2), shows the wandering, sometimes en echelon nature of the fracture produced in the subcritical tests. The close-ups show that the fractures break through grains (such as the indicated carbonate grains) as well as cut cement between grains (such as between the quartz and feldspar grains indicated). Figure 3 shows another example of both transgranular and intergranular fracture for quartz grains. This type of fracture morphology, particularly the fracturing between grains, is very similar to that found in microscopic examination of natural fractures in low porosity sandstones.³²

The identification of systematic subcritical index dependence on petrographic properties in the Dakota Sandstones is complicated by the simultaneous variation of numerous features for a relatively small (12) number of

samples (Table 1). Several attempts at simultaneous fits to various combinations of petrographic parameters were attempted. An example result (Figure 4) is described by the equation

$$n = 39 G_{qtz} + 22 G_{cht} + 82 G_{cly} + 33 C_{qtz} + 33 C_{Fed} \quad (2)$$

where G_{qtz} , G_{cht} , and G_{cly} are normalized volume percentages of quartz, chert and clay clasts, respectively, and C_{qtz} and C_{Fed} are the normalized volume percentages of quartz and ferroan-dolomite cement, respectively. Each parameter was normalized so that its minimum to maximum measured value ranged from 0 to 1 for the regression fit. Under these conditions, the magnitude of the coefficient before any variable indicates its relative importance in the regression. Using this principle, the original 14 parameters describing the Dakota petrography were narrowed to the five in equation (2). In equation (2), the coefficient for both quartz and ferroan-dolomite cement are equal, showing that further simplification of the regression model is possible by combining C_{qtz} and C_{Fed} into one parameter with no loss in goodness of fit.

This regression produces a good fit, but it is unclear whether equation (2) would be predictive for new samples given the limited dataset used to produce the model. It is possible that much of the regression is dominated by the extreme values in the data. In general, however, the regression fit and the detailed results suggest the following hypotheses:

1. Larger volume percentages of quartz grains result in higher subcritical indices. The samples from the depths of 7090, 7205 and 7218 ft (Table 2) show that the lowest quartz grain percentage samples have the lowest subcritical indices.
2. Increasing cement volume (quartz and ferroan dolomite) increases the subcritical index. The sample with the largest amount of ferroan dolomite has the lowest subcritical index (7205 ft), but it also has a very low quartz cement volume, so the sum of the two cements is not as extreme.
3. Plotting subcritical index against quartz cement fraction (fraction of the total cement volume that is made up of quartz) shows a fairly strong trend, although the slope changes sign at around 10% quartz cement fraction (Figure 5).
4. There is a strong dependence on clay clast percentage (it has the highest coefficient), but this is a result of the fact that the highest subcritical index sample (7236 ft) has the highest clay clast percentage, with no strong trend for the other depths. This may be a real effect that clay has on fracture behavior or a mere coincidence.

Travis Peak Sandstone. This sand-rich, lower Cretaceous fluvial-deltaic deposit has a wide range of grain size and cement types but lacks the variety in lithic fragments found in the Dakota Formation samples.³³ Thin section images (Figure 6) illustrate the simple mineralogy of the material. The two images show representative examples of quartz overgrowth cement and intergranular carbonate cement.

Multiple test specimens were prepared for each of 10 depths from several Travis Peak wells (Table 3). Sample depths were selected on the basis of variations in cement, porosity, and grain size. Test specimens were prepared by polishing thin slabs that were cut using a petroleum-based oil as coolant. For most of the specimens, two to three subcritical growth tests were carried out. Several different test conditions were used for the measurements on Travis Peak Sandstones, including the introduction of artificial cements into some of the specimens. Most of the specimens from each depth were bathed in toluene to remove oil and other impurities from the pore space, but five specimens were tested without cleaning. Of the cleaned specimens, six were additionally tested under water-saturated conditions to assess the effect of water content on subcritical crack behavior.

The average subcritical index for the fourteen cleaned specimens tested under dry conditions was 59, with most specimens falling with ± 10 of that value. Considering these samples were all from different depths with varying grain size and cement content, the lack of variation was surprising. Nine of those specimens were tested additionally under water-saturated conditions with very little effect. This lack of susceptibility to water was also unexpected and has not been explained. We have only seen such behavior previously in oil-stained specimens.

We again attempted a multiple-parameter, linear regression on the Travis Peak data (Figure 7). Using five parameters picked using the same normalization and elimination scheme described for the Dakota samples resulted in the equation

$$n = 74 (G_{qtz} + G_{feld}) + 37 C_{carb} + 30 \Phi + 5 C_{qtz} + 3 D_{grain} \quad (3)$$

where G_{feld} is the normalized volume percentage of feldspar grains, C_{carb} is the normalized volume percentage of carbonate cement, Φ is normalized porosity, and D_{grain} is the normalized mean grain diameter. Again, the predictive capability of this expression is not clear, but it does suggest that grain mineralogy, cement content, and in this case, porosity and grain size, appear to have some influence on the subcritical index (grain size was not measured for the Dakota samples). Although the details of the Travis Peak regression results are not the same as the Dakota results in detail, they do demonstrate similar dependencies. The amount of framework grains (both quartz and feldspar) has the strongest influence, the amounts of carbonate cement and porosity have roughly equal but lesser influence, and quartz cement and grain size follow.

Artificial, Pore-filling Cement. An organic compound, phenyl salicylate (Salol), was used to bond test specimens to a backing plate for purpose of pre-test specimen polishing. We discovered that this procedure resulted in the unintentional partial saturation of the specimens with Salol. The behavior for tests indicated as untreated (Table 3) shows this remnant Salol tends to reduce the subcritical index compared to samples that were cleaned with Toluene (Salol is highly soluble in Toluene). Although not reported in the table,

fracture initiation in the altered samples required a larger load than the unaltered samples, showing that the additional cementation increased the rock's fracture strength, once fracture growth began, the slope of the power-law dependency of the propagation velocity on stress intensity factor (equation 1) was weaker, illustrated by the drop in subcritical index values. We further investigated this secondary cementation effect by intentionally saturating samples with Salol (under molten conditions) and sodium silicate (in aqueous solution). While the cleaned specimens had an average subcritical index of 59 (none lower than 42), the subcritical index for the three tests intentionally saturated with Salol ranged from 13 to 17 and averaged 15.

We interpreted this change in subcritical index due to artificial modification of our samples to be a proxy for secondary pore-filling cementation of a sandstone. Since the effect might be sensitive to the type of secondary cement introduced to the specimen, we also saturated one sample with sodium silicate via an aqueous solution (Table 3, sample depth 9817 ft). The subcritical index was reduced from 53 for the dry, unaltered specimen to 25 for the sodium silicate saturated one, very similar to the Salol-induced reduction of the subcritical index to 13.

Discussion and Conclusions

A rock goes through a long history of diagenetic changes, and there can be substantial rock property changes after natural fracture propagation. The need to "age" or adjust the properties of rock through geologic time to better predict mechanical response was the motivation for much of this work. Diagenetic modeling can predict the progression of compaction and cementation through time with a high degree of reliability.³⁴ Fracture timing can be determined through fluid inclusion work on vein filling by estimating a temperature for fracture initiation. For instance, based on East Texas burial and temperature history, fracture initiation in the Travis Peak is estimated to be approximately 52 Ma.³²

Combining diagenetic modeling, structural history data and the knowledge of the relationship between diagenetic state and subcritical crack index (as well as other mechanical properties) can move us toward a more accurate prediction (or diagnosis) of natural fracture network characteristics. Our current understanding of the influence of the subcritical fracture index on natural fracture is based on geomechanical modeling.^{9,16} The fracture pattern implications of the described experimental work are that, given the same loading history in the presence of non-corrosive fluids (driven by gas or other hydrocarbons), sandstones (with their lower subcritical index values) would have higher fracture intensity and less fracture clustering than low porosity carbonates (such as the Austin Chalk, Honaker Trail and Cupido Formations which tend to have higher indices). Higher porosity carbonates (such as the Clear Fork Dolomite and Yates Field formations) will act more like the sandstones. However, the high subcritical index carbonates will behave more like sandstones under water-saturated conditions. Published fracture data appears to be

consistent with our interpretations - the Cozzette³⁵ ($n \approx 65$ dry) has somewhat clustered fracture spacing, while the Austin Chalk³⁶ ($n \approx 100$ dry) and the Honaker Trail Formations⁵ ($n \approx 250$ dry) show very strong clustering. However, more precise interpretations of fracture pattern geometry require detailed knowledge of geologic basin history and fracture timing.

It is clear from our testing and analysis results that linking subcritical fracture behavior to the petrographic properties of rock is a difficult task. Multiple parameters vary simultaneously from sample to sample, making it difficult to isolate any particular process, such as quartz cementation, to improve our understanding of subcritical crack behavior. However, the kinds of parameters that show up in the linear regression analysis presented seem consistent with our microscopic observations of both transgranular and intergranular fracture propagation, which would be controlled by grain and cement mineralogy, respectively. Further progress in understanding the dependency of subcritical fracture properties on rock petrography will be gained through larger natural sample database analysis as well as testing artificial samples with precisely controlled mineralogy. The clear and consistent results of adding secondary, pore-filling cement to our natural sandstone samples suggests a high potential for success under simpler, controlled experimental conditions.

Nomenclature

V = crack propagation velocity, m/s

K_I = mode I stress intensity factor, MPa*m^{1/2}

K_{Ic} = fracture toughness, MPa*m^{1/2}

A = constant of proportionality, m/s

n = the subcritical fracture index

G_{qtz} = normalized volume percentage of quartz grains

G_{feld} = normalized volume percentage feldspar grains

G_{cht} = normalized volume percentage of chert grains

G_{cly} = normalized volume percentage of clay clasts

C_{qtz} = normalized volume percentage of quartz cement

C_{Fed} = normalized volume percentages ferroan-dolomite cement

C_{carb} = normalized volume percentages carbonate cement

Φ = normalized porosity

D_{grain} = normalized mean grain diameter

Acknowledgements

We acknowledge the support of the Fracture Application and Research Consortium (FRAC) of The University of Texas at Austin and the U.S. Department of Energy under Award No. DE-FC26-00BC15308. Any opinions, findings, conclusions, or recommendations expressed herein are those of the authors and do not necessarily reflect the views of the DOE. We also want to thank Julia Gale, Steve Laubach and Rob Reed of FRAC for their help with sampling, petrographic analysis and imaging.

References

1. Narr, W. and I. Lerche: "A Method for Estimating Subsurface Fracture Density in Core," *The American Association of Petroleum Geologists Bulletin* (1984) **68**, No. 5 (May 1984), 637-648.
2. Laubach, S., R. Marrett, and J.E. Olson: "New directions in fracture characterization," *The Leading Edge* (2000), 704-711.
3. Kulatilake, P.H.S.W., D.N. Wathugala, and O. Stephansson: "Joint Network Modelling with a Validation Exercise in Stripa Mine, Sweden," *Int. J. Rock Mech. Min. Sci. and Geomech. Abstr.* (1993) **30**, No. 5, 503-526.
4. La Pointe, P.R. and J.A. Hudson: *Characterization and Interpretation of Rock Mass Joint Patterns*, Geological Society of America Special Paper 199 (1985) 37.
5. Olson, J. and D.D. Pollard: "Inferring paleostresses from natural fracture patterns: A new method," *Geology* (1989) **17**, 345-348.
6. Rives, T., M. Razack, J.P. Petit, and K.D. Rawnsley: "Joint Spacing: Analogue and Numerical Simulations," *Journal of Structural Geology* (1992) **14**, No. 8/9, 925-937.
7. Lyakhovskiy, V.: "Scaling of Fracture Length and Distributed Damage," *Geophysical Journal International* (2001) **144**, 114-122.
8. Dershowitz, W.S. and H.H. Einstein, *Characterizing Rock Joint Geometry with Joint System Models*, in *Rock Mechanics and Rock Engineering*. 1988, Springer-Verlag: Redmond/Cambridge. p. 21-51.
9. Olson, J.E.: "Joint Pattern Development: Effects of Subcritical Crack-Growth and Mechanical Crack Interaction," *Journal of Geophysical Research* (1993) **98**, No. B7, 12,251-12,265.
10. Renshaw, C.E. and D.D. Pollard: "Numerical Simulation of Fracture Set Formation: A Fracture Mechanics Model Consistent with Experimental Observations," *Journal of Geophysical Research* (1994) **99**, No. B5 (May 10, 1994), 9359-9372.
11. Vermilye, J.M. and C.H. Scholz: "Relation Between Vein Length and Aperture," *Journal of Structural Geology* (1995) **17**, No. 3, 423-434.
12. Atkinson, B.K., and Meredith, P.G., *The theory of subcritical crack growth with applications to minerals and rocks*, in *Fracture Mechanics of Rock*, B.K. Atkinson, Editor. 1989, Academic Press Geology Series: London. p. 111-166.
13. Segall, P.: "Formation and Growth of Extensional Fracture Sets," *Geological Society of America Bulletin* (1984) **95**, No. Apr. 1984, 454-462.
14. Schultz, R.A.: "Growth of geologic fractures into large-strain populations: review of nomenclature, subcritical crack growth, and some implications for rock engineering," *Int. J. of Rock Mech. and Min. Sci.* (2000) **37**, No. 1-2, 403-411.
15. Renshaw, C.E. and C.F. Harvey: "Propagation velocity of a natural hydraulic fracture in a poroelastic medium," *Journal of Geophysical Research* (1994) **99**, No. 11, 21,659-21,677.
16. Olson, J.E., Y. Qiu, J. Holder, and P. Rijken: "Constraining the Spatial Distribution of Fracture Networks in Naturally Fractured Reservoirs Using Fracture Mechanics and Core Measurements," presented at the 2001 SPE Annual Technical Conference and Exhibition, New Orleans, LA, Sept. 30 - Oct. 3, 2001.
17. Renshaw, C.E.: "Influence of Subcritical Fracture Growth on the Connectivity of Fracture Networks," *Water Resources Research* (1996) **32**, No. 6 (June 1996), 1519-1530.
18. Olson, J.E.: "Natural fracture pattern characterization using a mechanically-based model constrained by geologic data - moving closer to a predictive tool," presented at the 1997 36th U. S. Rock Mechanics Symposium, New York City.
19. Renshaw, C.E. and J.C. Park: "Effect of mechanical interactions on the scaling of fracture length and aperture," *Nature (London)* (1997) **386**, No. 6624, 482-484.
20. Atkinson, B.K.: "Subcritical Crack Growth in Geological Materials," *Journal of Geophysical Research* (1984) **89**, No. June 10, 1984, 4077-4114.
21. Philip, Z., J.W. Jennings, Jr., J.E. Olson, and J. Holder: "Modeling Coupled Fracture-Matrix Fluid Flow in Fracture Patterns Generated using a Geo-Mechanical Crack Growth Simulator," presented at the 2002 SPE Annual Technical Conference and Exhibition, San Antonio, TX, September 29 - October 2, 2002.
22. Atkinson, B.K. and P.G. Meredith, *Experimental Fracture Mechanics Data for Rocks and Minerals*, in *Fracture Mechanics of Rock*, B.K. Atkinson, Editor. 1987, Academic Press: London. p. 477-525.
23. Holder, J., J.E. Olson, and Z. Philip: "Experimental determination of subcritical crack growth parameters in sedimentary rock," *Geophysical Research Letters* (2001) **28**, No. 4, 599-602.
24. Gesing, A.J. and R.C. Bradt, *A microcrack model for the effect of grain size on slow crack growth in polycrystalline Al_2O_3* , in *Fracture Mechanics of Ceramics*, R.C. Bradt, et al., Editors. 1983, Plenum Press: New York. p. 569-590.
25. Evans, A.G.: "A method for evaluating the time-dependent failure characteristics of brittle materials and its application to polycrystalline alumina," *Journal of Material Science* (1972) **7**, 1137-1146.
26. Williams, D.P. and A.G. Evans: "A simple method for studying slow crack growth," *Journal of Testing and Evaluation* (1973) **1**, 264-270.
27. Dutton, S.P., S.J. Clift, D.S. Hamilton, H.S. Hamlin, T.F. Hentz, W.E. Howard, M.S. Akhter, and S.E. Laubach: Major low-permeability-sandstone gas reservoirs in the continental United States. 1993, The University of Texas, Bureau of Economic Geology: Austin, TX. p. 221.
28. Rijken, P., J. Holder, J.E. Olson, and S. Laubach: "Predicting Fracture Attributes in the Travis Peak Formation using Quantitative Mechanical Modeling and Structural Diagenesis," presented at the 2002 52 Annual Convention Gulf Coast Association of Geologic Societies.

29. Scholz, C.H.: "Static Fatigue of Quartz," *Journal of Geophysical Research* (1972) **77**, No. 11, 2104-2114.
30. Martin, R.J., III: "Time-Dependent Crack Growth in Quartz and its Applications to the Creep of Rocks," *Journal of Geophysical Research* (1972) **77**, No. 8, 1406-1419.
31. Laubach, S.E., K.L. Milliken, S.J. Clift, S. Burns, R.M. Reed, and M.c. Cloos: "New subsurface characterization methods for fractured siliciclastic rocks," presented at the 1996 30th annual meeting of the Geological Society of America, South-Central Section and associated societies, Austin, TX, United States, Mar. 11-12, 1996.
32. Laubach, S.E.: "Subsurface fractures and their relationship to stress history in East Texas Basin sandstone," *Tectonophysics* (1988) **156**, No. 1-2, 37-49.
33. Dutton, S.P. and L.S. Land: "Cementation and Burial History of a Low-Permeability Quartzarenite, Lower Cretaceous Travis Peak Formation, East Texas," *Geological Society of America Bulletin* (1988) **100**, No. 8, 1271-1282.
34. Lander, R.H. and O. Walderhaug: "Porosity prediction through simulation of sandstone compaction and quartz cementation," *AAPG Bulletin* (1999) **83**, 433-449.
35. Lorenz, J.C. and S.J. Finley: "Regional fractures II: Fracturing of Mesaverde reservoirs in the Piceance Basin, Colorado," *The American Association of Petroleum Geologists Bulletin* (1991) **75**, No. 11, 1738-1757.
36. Gale, J.F.W.: "Specifying length of horizontal wells in fractured reservoirs," *Reservoir Evaluation and Engineering* (2002) **SPE 78600**, 266-272.
37. Philip, Z., J.W. Jennings, Jr., J.E. Olson, and J. Holder: "Modeling Coupled Fracture-Matrix Fluid Flow in Fracture Patterns Generated using a Geo-Mechanical Crack Growth Simulator," presented at the 2002 Conference on Naturally Fractured Reservoirs, Oklahoma City, OK, September 29 - October 2, 2002.

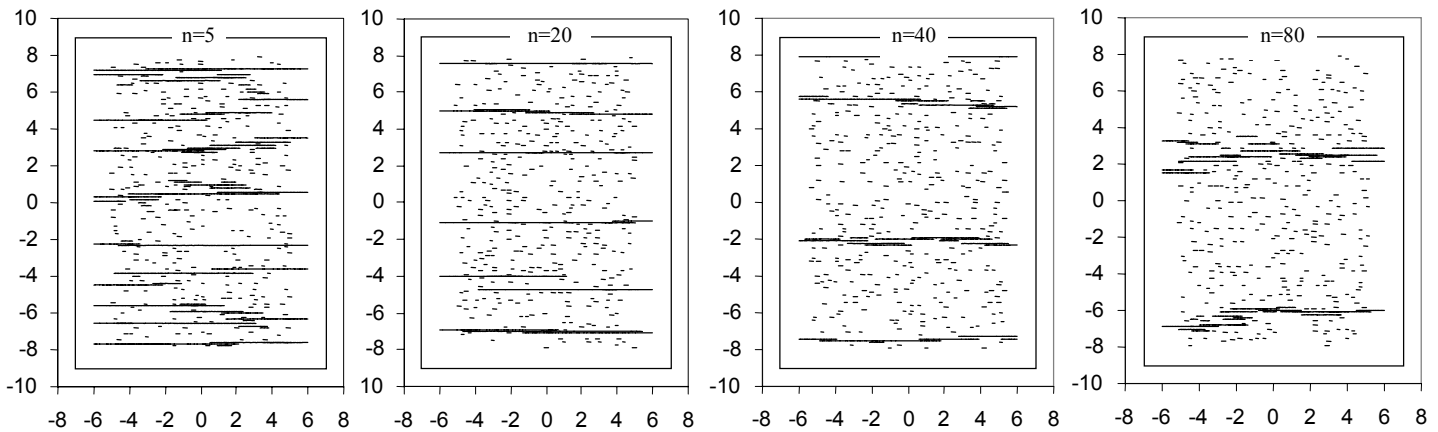


Figure 1: Fracture trace maps for numerical subcritical crack propagation simulations for different subcritical crack indices, using 400 initial flaws. Each case used an identical crack-perpendicular extensional strain rate. Note increasing fracture density with decreasing n , and fracture clustering for $n=40$ and $n=80$. From Olson et al.¹⁶

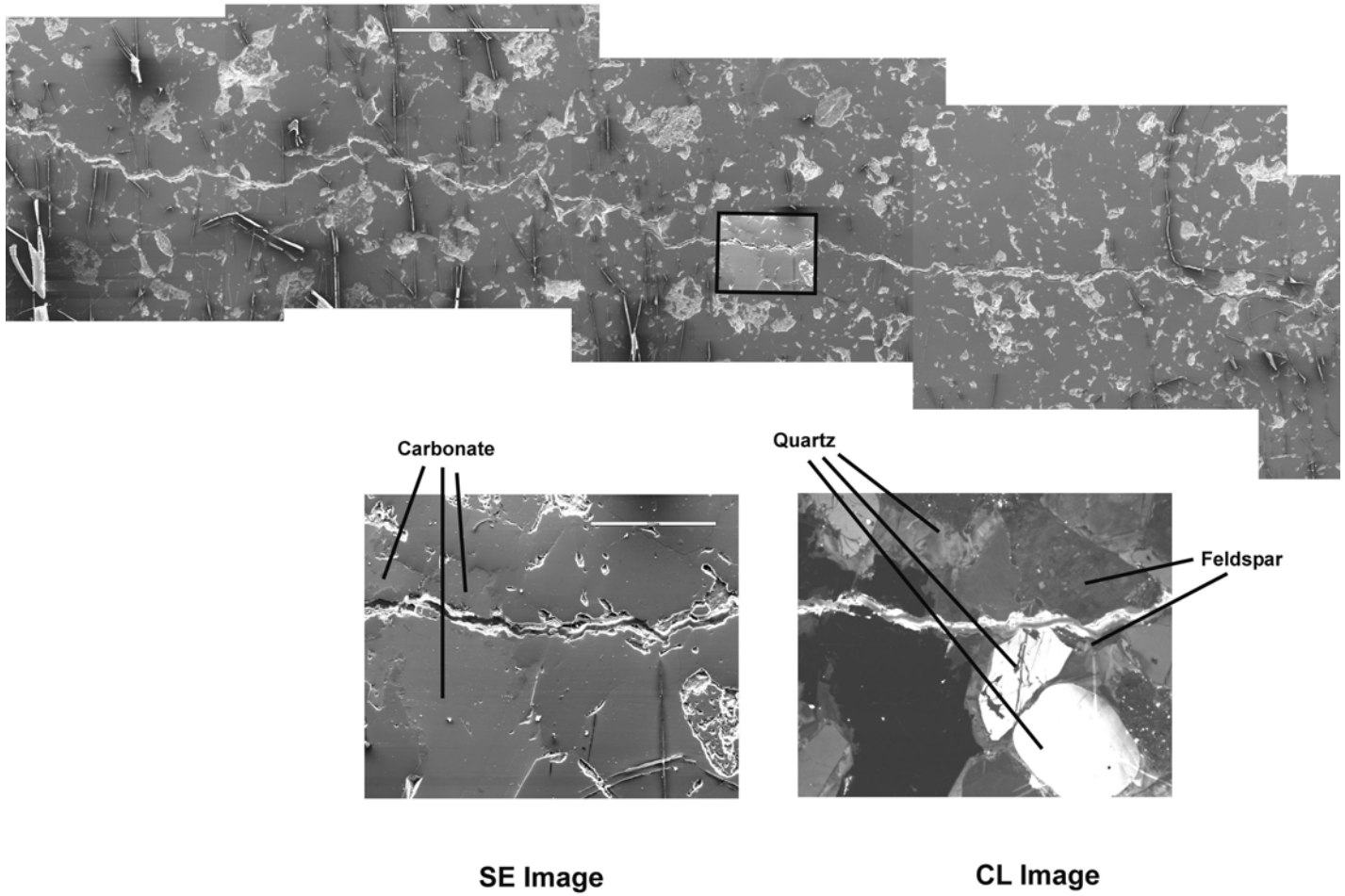


Figure 2. Mosaic of secondary electron (SE) images of Dakota Sandstone from depth 7217 ft, showing mostly intergranular subcritical crack, with enlarged SE and cathodoluminescence (CL) images of highlighted area. Note elucidation of grains in CL image, showing transgranular fracture of carbonate grain and intergranular fracture between quartz and feldspar.

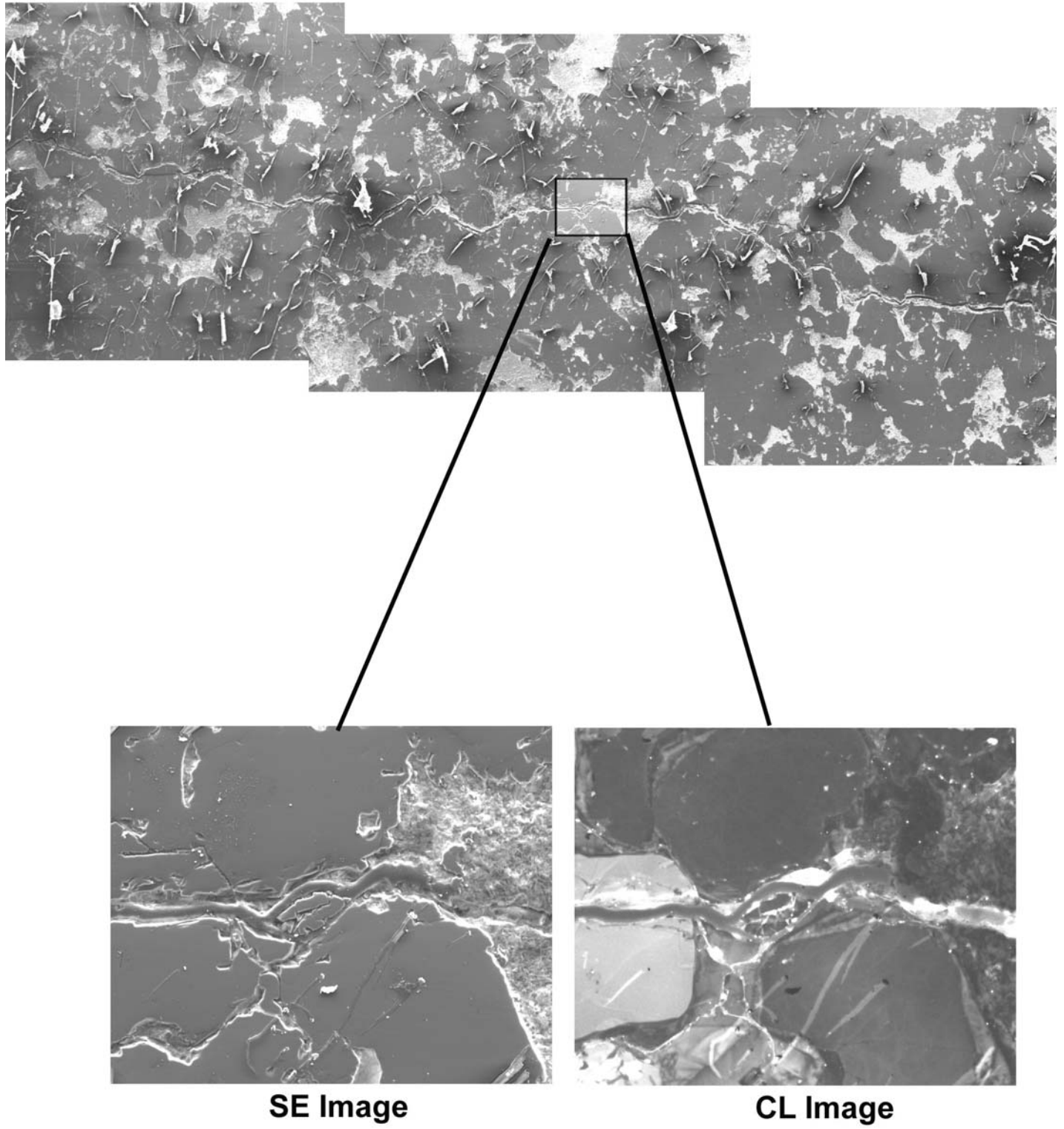


Figure 3. Another mosaic of secondary electron (SE) images of Dakota Sandstone from depth 7217 ft. In the enlarged SE and cathodoluminescence (CL) images, the quartz grain on the left has a transgranular fracture, while to the right, the fracture runs between grains and through the quartz cement.

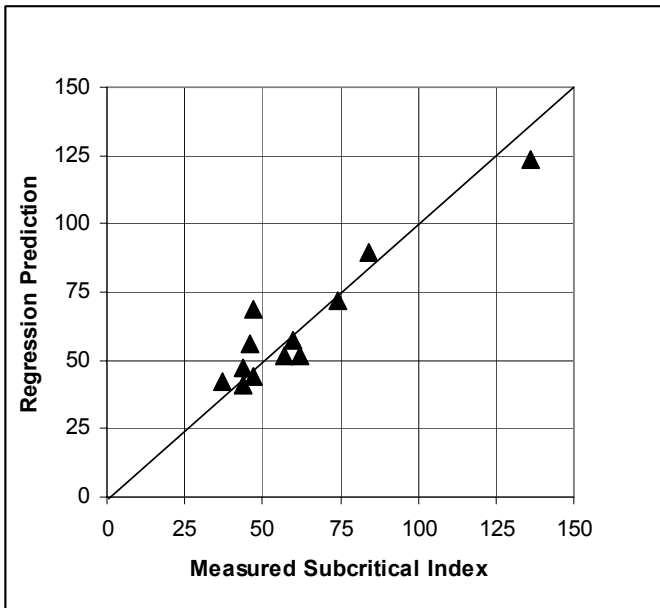


Figure 4. Linear multivariant regression fit of subcritical index to fractional contents of five Dakota Sandstone constituents.

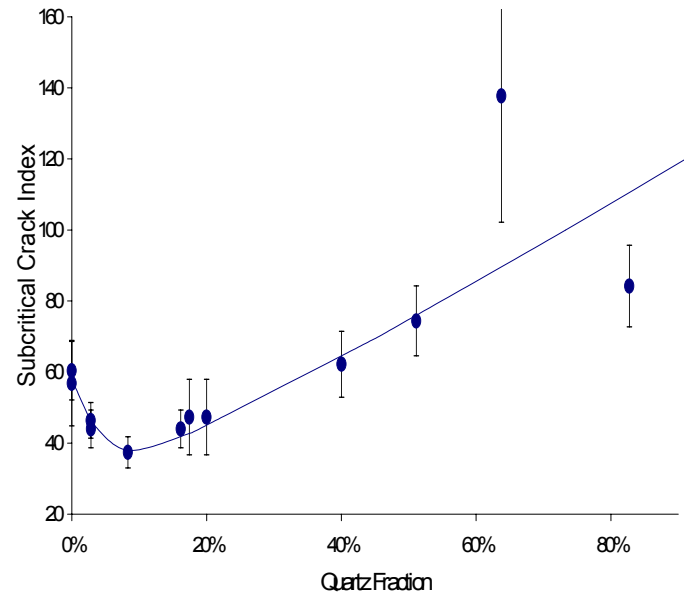


Figure 5. Variation of measured subcritical crack (SC) index with fraction of quartz cement in Dakota Sandstone.

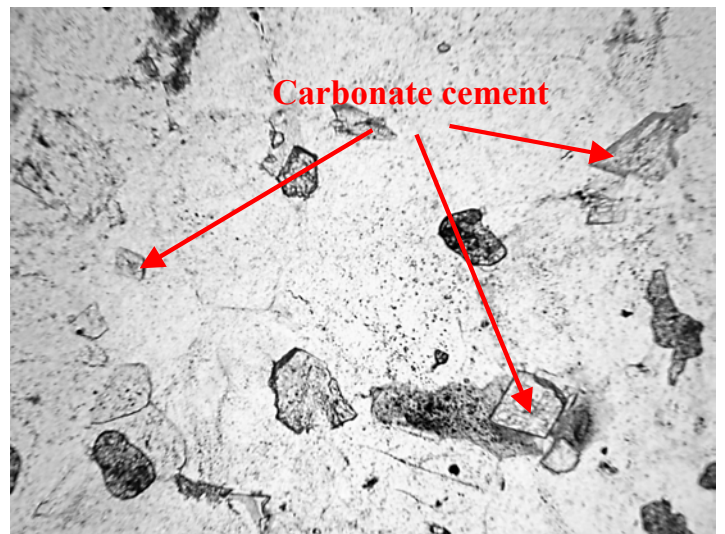
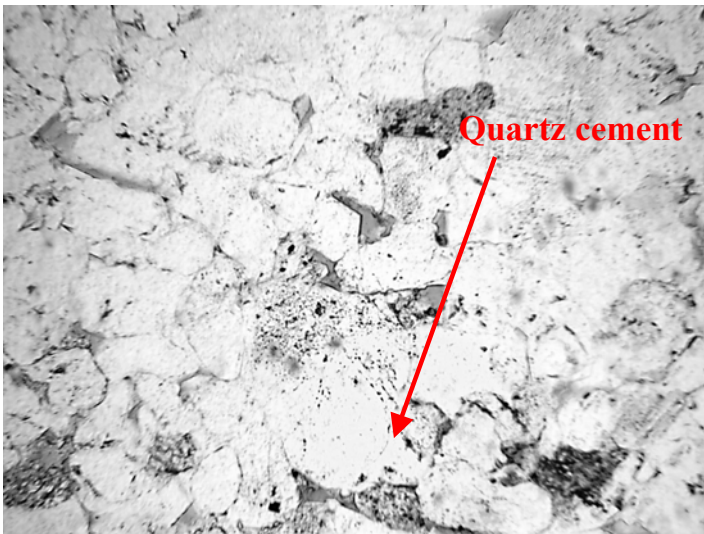


Figure 6. Optical images from thin section of specimens from core at 7,506 feet (left side), and 9,330 feet (right side).

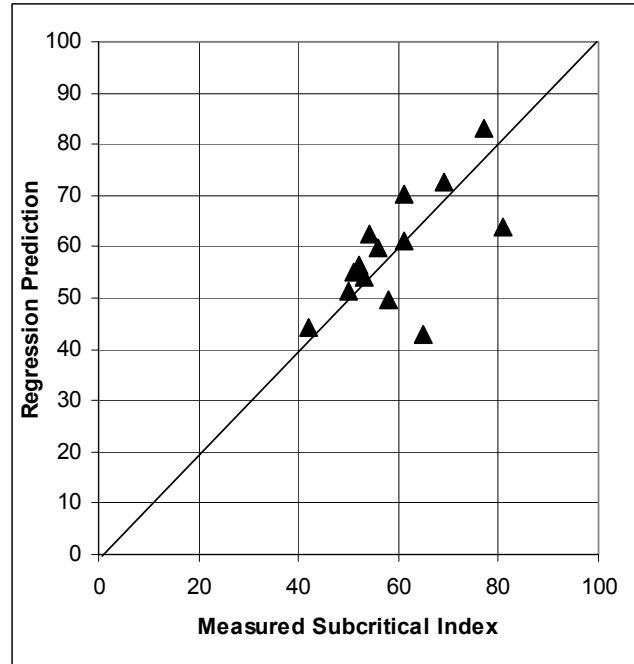


Figure 7. Best fit linear regression for subcritical crack index based on 5 petrographic properties of the Travis Peak Formation from 14 tests.

Table 1. Summary of survey measurements of subcritical crack indices for sedimentary rock.

Material	Depth (feet)	Subcritical Index	
		Dry	Wet
<i>Sciota, Ohio</i> ²³			
Quartz-rich sandstone	quarry (#1)	35	25
	quarry (#2)	52	36
<i>Cupido Fm, Mexico</i>			
Dolostone	outcrop	400	
<i>Honaker Trail Fm, Utah</i>			
Low-porosity limestone	outcrop (#1)	271±58	
	outcrop (#2)	250±113	41±10
<i>Austin Chalk</i> ²³			
	5,585	124	42
	5,573	95	20
<i>Clear Fork</i> ^{23,37}			
Grain-dominated dolopackstone	6,091	43	
Dolomitic sandstone	6,138	40	
Grain-dominated dolopackstone	6,367	60	
Dolowackestone	6,385	81	
Grain-dominated dolopackstone	6,484	43	
Grain-dominated dolopackstone	6,520	38	
<i>Yates Field, West Texas</i>			
Porous limestone	1,347	33± 6	
	1,427	64± 14	30± 11
<i>San Juan Formation, Venezuela</i>			
Sandstone	14,327	46±12	59±8
	14,547	59±17	50
<i>Cozette Formation, Colorado</i>			
Tight gas ss	Well MWX-1	7,892	66±17
	Well MWX-2	7,892	64±16
			39±4
			67±1718
<i>Rosa Blanco Fm, Tobasco Mexico</i>			
Sandstone	5,929	78±8	

Table 2. Petrographic and subcritical crack indices for Dakota Sandstone specimens. See text for Descriptions of headings.

Depth (ft)	SC Index	Porosity (%)	Framework Grains			Rock Fragments				Matrix			% Cement		
			Qtz (%)	Plag (%)	Kspar (%)	Chrt (%)	CIClst (%)	CRF (%)	VRF (%)	Pyrite (%)	AsstCl (%)	PsMat (%)	QOG (%)	Dol (%)	FeD (%)
7068	57±12	3.3	69.0	0.3	1.0	1.7	1.3	1.0	0.3	2.3	0.0	13.0	0.0	6.7	0.0
7089	47±11	3.1	77.6	0.0	1.7	0.0	2.1	0.7	0.4	0.7	0.4	8.6	1.4	3.5	0.0
7090	47±11	10.0	59.0			2.5	0.0			14.0			4.0	0.0	6.0
7099	60±8	30.0	48.0			0.5	1.5	0.5	0.0	6.5			0.0	0.0	11.0
7112	46±5	3.7	62.6	0.0	2.0	0.8	2.0	0.8	1.6	1.6	0.0	14.2	0.4	9.4	0.8
7186	62±9	0.7	85.7	1.0	2.3	0.0	0.3	0.0	0.3	0.7	0.3	2.7	2.7	1.7	1.7
7198	44±5	3.3	78.7	1.7	1.0	0.3	0.3	0.7	1.3	1.0	0.7	4.0	1.7	5.0	0.3
7205	37±4	20.0	52.5			0.0	0.0	7.5	0.0	1.5			3.0	0.5	12.5
7218	44±5	29.5	55.5			0.0	1.5	0.0	0.0	6.0			1.0	0.0	4.5
7225	74±10	3.7	71.3	2.3	3.7	1.0	1.3	0.3	2.3	0.0	0.7	0.0	8.7	1.3	3.3
7227	84±11	2.5	58.0			5.0	1.0	4.5	0.0	0.5			24.0	0.0	2.5
7236	138±36	3.2	65.4	2.2	3.0	1.2	4.7	1.0	3.7	1.2	0.8	1.0	10.0	0.5	2.0

Table 3. Test results for the Travis Peak Formation. (See text for explanation of headings.)

Well	Depth (ft)	Subcritical Index					Framework Grains			Cements			porosity count (%)
		Untr't'd	Clean'd	Salol	Water	Other	Quartz (%)	size (mm)	Feld/other (%)	Qtz (%)	Carb (%)	clay (%)	
1	5,962		50±12				59	0.105	1.5/1	20	10	0.5	9
1**	6,206		65±4		66±5		60.5	0.097	8.5/0	16.5	2.5	1.5	9.5
1	6,270		61±14		54±16		72	0.102	0/0	10.25	14.5	1	2.25
1	6,295		51±12				52	0.097	1.5/0	19	18	1	7
1**	7,457	43±25	56±16		56±9		76.25	0.150	0/0	14.25	0	1	8.5
1**	7,506	26±6	58±15	17±2	70±8		72.75	0.155	0/0	18.75	0	0.5	7
2**	5,952		61±8		70±7		68.5	0.208	0/2.5	12	1.5	0.5	14.5
2**	6,244		54±7		52		68.25	0.129	0/0	13.75	0.75	1	16.25
3	6,633		81±17				67	0.108	2/3.5	10.5	11.5	4	0
4	7,737		42±7		63±9		70.3	0.058	3.5/1.5	17.3	1	3.5	0
5**	10,141	19±2	77±19		54±16		74.75	0.094	0/0	11.75	3.25	10.25	0
6**	9,817	47±9	53±11	13±3	60±15	25±3(a)	73.7	0.186	0/0	17.3	0	0.7	7.8
6	9,837	17±3	69±8			82±4(b)	73.5	0.222	0/0	9.5	12.5	0.5	4
6**	9,880		52±10	16±1		70±1(b)	74.75	0.262	0/0	18	0	1.25	6

Wells: 1) Holditch Howell #5; 2) Mobil Cargill #14; 3) Marshall Werner Sawmill #5; 4) Arkla #1 J.O. Pate; 5) Ashland #1 SFOT; and 6) Holditch SFE #2.

Specimen Treatments: (a) sodium silicate cement; (b) oil-saturated

**Samples used for grain size correlation.

Improving fracture permeability prediction by combining geomechanics and diagenesis

Olson, J. E. and Laubach, S. E.

The University of Texas, Austin, TX USA

Lander, R. H.

Geocosm, Austin, TX USA

Copyright 2004, ARMA, American Rock Mechanics Association

This paper was prepared for presentation at Gulf Rocks 2004, the 6th North America Rock Mechanics Symposium (NARMS): Rock Mechanics Across Borders and Disciplines, held in Houston, Texas, June 5 – 9, 2004.

This paper was selected for presentation by a NARMS Program Committee following review of information contained in an abstract submitted earlier by the author(s). Contents of the paper, as presented, have not been reviewed by ARMA/NARMS and are subject to correction by the author(s). The material, as presented, does not necessarily reflect any position of NARMS, ARMA, CARMA, SMMR, their officers, or members. Electronic reproduction, distribution, or storage of any part of this paper for commercial purposes without the written consent of ARMA is prohibited. Permission to reproduce in print is restricted to an abstract of not more than 300 words; illustrations may not be copied. The abstract must contain conspicuous acknowledgement of where and by whom the paper was presented.

ABSTRACT: High temperatures and reactive fluids in sedimentary basins dictate that interplay and feedback between mechanical and geochemical processes could significantly influence evolving rock and fracture properties. In this paper, we propose an integrated methodology of fractured reservoir characterization and show how it can be incorporated into fluid flow simulation. In recent years, there have been a number of important discoveries regarding fundamental properties of fractures, in particular related to the prevalence of kinematically significant structures (crack-seal texture) within otherwise porous, opening-mode fractures, and the presence of an aperture size threshold below which fractures are completely filled and above which porosity is preserved. Significant progress has been made as well in theoretical fracture mechanics and geomechanical modeling, allowing prediction of spatial distributions of fractures that mimic patterns observed in nature. Geomechanical modeling shows the spatial arrangement of opening mode fractures (joints and veins) is controlled by the subcritical fracture index of the material. Fluid flow simulation of representative fracture pattern realizations shows how integrated modeling can give new insight into permeability assessment in the subsurface. Using realistic, geomechanically generated fracture patterns, we propose a methodology for permeability estimation in non-percolating networks.

1. INTRODUCTION

The continuity of fracture-porosity is fundamental to how fractures conduct fluids. One approach to predicting the spatial arrangement of opening mode fracture networks is through geomechanical modeling. We utilize a model based on subcritical crack growth to generate fracture trace patterns and mechanical opening distributions for various boundary conditions and material properties [1,2]. An important capability of such modeling is the ability to predict the presence or absence of fracture clustering, as well as the shape of the fracture length distribution. Another aspect of the problem is how diagenesis modifies fracture porosity and effective length distribution and may affect the dynamics of fracture propagation. Cements may also alter the compliance of fractures and host rock, tending to preserve fracture pore space under changing load conditions. Although most recent literature emphasizes Earth stress orientation [3,4], cementation in fractures and host rock is likely a critically important control on porosity, fluid flow

attributes, and even sensitivity to effective stress changes [5-7].

Little is known of the evolution of fracture networks in the context of the diagenetic pathway followed by the host rock or of the influence on fracture growth of diagenetic processes within fractures. Yet the high temperatures and reactive fluids in sedimentary basins suggest that interplay and feedback between mechanical and geochemical processes could have significant influence on evolving rock and fracture properties. In this paper we show how coupling fracture mechanics and diagenesis considerations can lead to improved predictions of flow performance in fractured reservoirs.

2. CEMENT IN SANDSTONE FRACTURES

Here we focus on the effects of quartz cement because diagenetic modeling can be used to predict the distribution and abundance of this phase [8,9]. Quartz is the most abundant and widespread cement in sandstones exposed to temperatures in excess of

~90 °C for geologically significant periods [10,11]. It is therefore not surprising that virtually all transgranular fractures in such sandstones show at least some degree of porosity loss due to quartz cementation. However, not all fractures are occluded by quartz cement. In a wide range of sandstones, there is a threshold kinematic fracture opening (separation between two previously adjacent points across the fracture regardless of later mineral filling) above which fracture porosity is preserved and below which fractures are completely filled. This fracture aperture size is the *emergent threshold* [12].

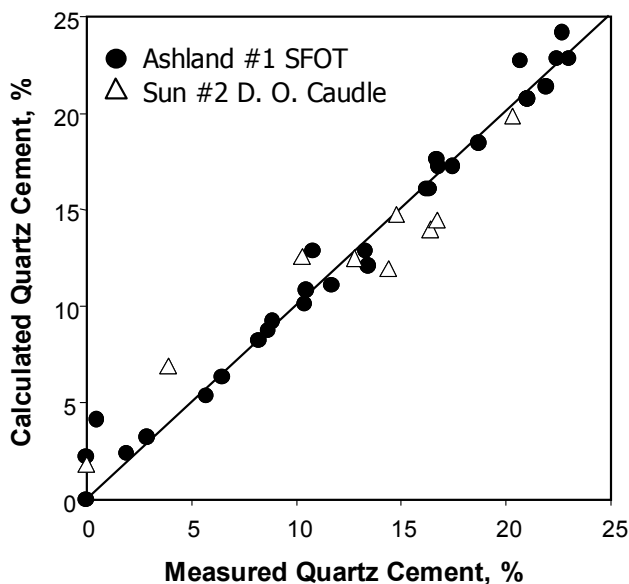


Fig. 1. Correspondence between measured and calculated quartz cement abundances for unfractured matrix of Travis Peak Formation sandstones, demonstrating effectiveness of quartz cementation modeling [18].

Quartz cement in sandstones generally occurs as *overgrowths* that nucleate on detrital quartz grains. The concept that the kinetics of quartz crystal precipitation is the rate limiting process for the overall growth rate in many types of sandstone [13-17] represents an important milestone in understanding the controls on quartz cement abundances. Using this concept, quartz cementation rates are a function of temperature and nucleation surface area. Computer simulators incorporating this concept accurately reproduce measured quartz cement abundances in sandstones from diverse geologic settings (Fig. 1)[18] and have been used to (1) reconstruct the diagenetic evolution of sandstones and to predict reservoir quality when coupled with compaction models (e.g., 18-20), (2)

constrain thermal histories [21], and (3) evaluate how the magnitudes and rates of pore volume loss associated with quartz diagenesis influence fluid overpressure development [22-25].

High-resolution cathodoluminescence imaging of fracture zones in sandstones reveals that fracture kinematic apertures represent the cumulative expression of hundreds or thousands of micron scale fracturing events [26]. In some cases quartz cement may bridge across the fracture zone between microfracturing events. Thus the nucleation surface area for quartz cement within fracture zones may vary significantly through time as cementation reduces surface area by partial or complete sealing of fractures and micro fracturing events increase surface area by crystal breakage.

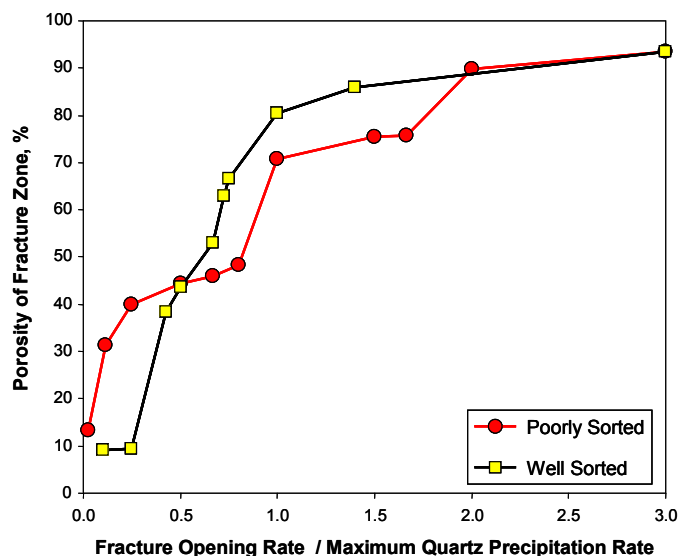


Fig. 2. Simulated dependency in fracture zone porosity on the ratio of net rate of fracture opening to quartz precipitation rate. From [9].

Recently the approach toward simulation of quartz cementation in unfractured sandstones has been extended to consider quartz cementation in structurally deformed sandstones [8,9]. Factors of particular importance for such sandstones that are considered in this model include the effects of cementation and fracturing on nucleation surface area as well as the control of crystallographic orientation and nucleation surface type on crystal growth anisotropy. Simulations of quartz cementation within the fracture zone by Lander et al. [8,9] indicate that fracture porosity is a function of the ratio of the net rate of fracture opening to the rate of quartz precipitation. The quartz precipitation rate, in turn, is a strong function of temperature and

is also influenced by compositional and textural characteristics of the host sandstone.

Lander et al. [9] simulated the controls on fracture porosity in fine-grained litharenite sandstones assuming constant rates of fracture opening at a constant temperature. Simulations indicate that fracture porosity increases with the ratio of fracture opening rate to quartz precipitation rate because progressively fewer crystals are able to grow across fracture apertures between fracturing events. When the ratio value is less than 0.5, most quartz overgrowths will seal the fracture aperture between fracturing events thereby pervasively sealing the fracture zone (Fig. 2). By contrast, when the ratio exceeds a value of two, no crystal will bridge across the fracture aperture and overgrowths will therefore occur exclusively as rims of euhedral crystallites along an otherwise open fracture. At intermediate ratios the cement morphology will be a mixture of euhedral crystal linings and *bridge* crystals that are pillar-like structures that span the fracture.

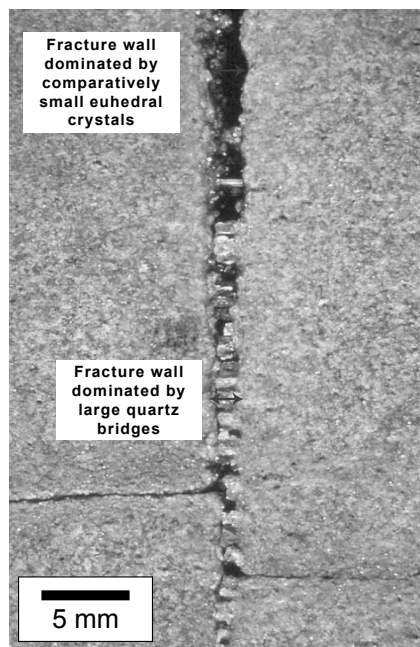


Fig. 3. Cretaceous Travis Peak Formation core sample near tip of a vertical fracture (core photograph). Quartz cement is more abundant toward tip of fracture (bottom part of image) than where aperture widens (top part of image). Sample depth is ~9,800 ft. See [27] for background information.

Based on these model results we expect a transition toward greater fracture porosity in the centers of larger aperture fractures due to the faster net fracture opening rates compared to the tips. Such

transitions occur in nature as illustrated for a sample from East Texas sandstone in Fig. 3.

In addition to the important role that quartz cementation plays in controlling fracture porosity, it also is likely to greatly reduce the compliance of fractures. During the development of fracture systems quartz cementation occurs not only within the fracture zone itself but also within the unfractured matrix of the host sandstone. Thus the mechanical strength of the host rock will tend to increase with time. Furthermore, quartz cement that lines or bridges fractures also will decrease fracture compliance, even for fractures that have comparatively high porosities. Euhedral quartz crystals within otherwise open fractures have high spatial anisotropy and will not permit fracture porosity to go to zero even with large changes in stress orientations, and quartz bridges are likely to have an even larger strengthening effect on the fracture zone.

Precipitation of cement as a part of rock diagenesis can be divided into three stages – prekinematic, synkinematic and postkinematic, where the kinematic *event* referred to in the timing is the formation of natural, opening-mode fractures [27, 12]. Because quartz precipitates over a wide temperature range, it is commonly pre-, syn- and postkinematic. Post-kinematic cements, including carbonate minerals, are commonly responsible for sealing large fractures [12]. However, owing to the controls on quartz precipitation alluded to previously, syn- and postkinematic quartz tends to seal only small fractures, and in sandstones the phases that commonly seal large fractures are postkinematic carbonate and sulfate minerals.

Why is quartz cement so common in sandstone fractures? Quartz cementation contemporaneous with fracture may merely reflect prevalence of rock-dominated chemistry through much of a rock's burial history, including times when conditions are amenable for fracture growth. In sandstone, synkinematic quartz (and in dolostone, synkinematic dolomite), could simply be the most likely phase to precipitate through a protracted loading history [12].

3. GEOMECHANICAL FRACTURE PATTERN MODELING

Modeling studies and comparisons to field data demonstrate that subcritical crack growth can be used to explain the presence or absence of fracture clustering and the shape of fracture length and spacing distributions [1, 2, 29, 34]. The fracture pattern variability illustrated in Fig. 4 is caused solely by the variation of the subcritical index, a material property that is postulated to depend on grain size, porosity, and mineralogy [35-37]. As expected, for a given rock layer, increasing strain applied to a body increases the total amount of fracture trace length created (or cumulative fracture length).

However, for the case of similar layers (same mechanical thickness, elastic moduli and fracture toughness) all experiencing the same amount of strain, Olson et al. [2] showed that the subcritical index controls the shape of the length distribution making up the fracture population and the cumulative length created (Fig. 5). High subcritical indices ($n > 40$) cause fractures to grow as clusters where the median fracture segment length is very low (point at which cumulative frequency is 0.5) and overall fracture intensity is low. Intermediate values ($20 < n < 40$) result in fairly regularly spaced, en echelon fracture arrays with larger median segment lengths with more fracture trace length created for a given amount of strain. Very low values of the subcritical index ($n < 20$) results in

highest cumulative fracture length created for a given strain, but the pattern becomes more clustered again, with median fracture lengths between those for the high and intermediate subcritical index cases.

4. FRACTURE PERMEABILITY ESTIMATION FOR NON-PERCOLATING NETWORKS

Standard permeability estimation procedures for fractured reservoirs [28] are based on the parallel plate law,

$$k_{fm} = \frac{b^3}{12S}, \quad (1)$$

where k_{fm} is the permeability of a fractured media (fm) with a single fracture set parallel to the flow direction having a hydraulic (open) aperture of b and a perpendicular spacing between fractures of S . Not only does this expression imply a dominance of aperture controlling fracture permeability, but it also assumes that all fractures are through-going (i.e., they completely cross the area of interest for permeability estimation), an assumption that is unreasonable based on geologic characterizations of fracture length distributions [29, 2, 30]. Consequently, investigations of flow in populations of parallel fractures with finite lengths and varying intensity (intensity is used to refer to the total amount of fracture trace length created) suggest that fracture connectivity and network pattern geometry may be more important than hydraulic aperture in determining fracture permeability [30-33].

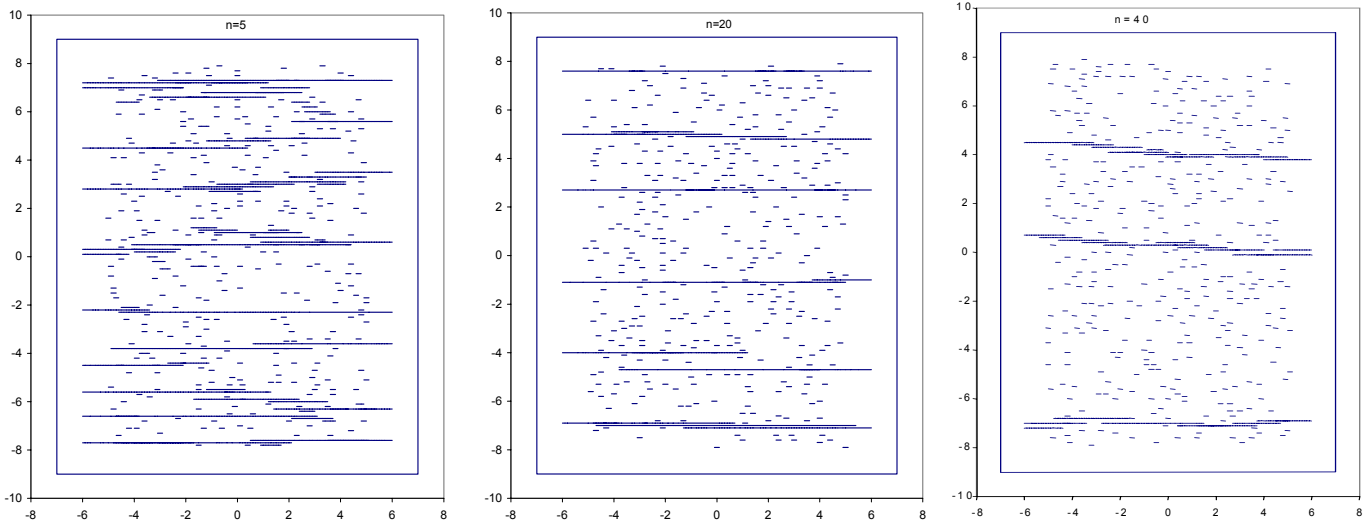


Fig. 4. Map traces of fracture patterns for subcritical indices of $n = 5$, $n = 20$, and $n = 40$ generated by fracture-mechanics-based modeling. Top view of 3-D model volume where x and y axes refer to distance in meters. Extension magnitude in models is identical. Very short fractures in fracture patterns are seed flaws that never grew [2].

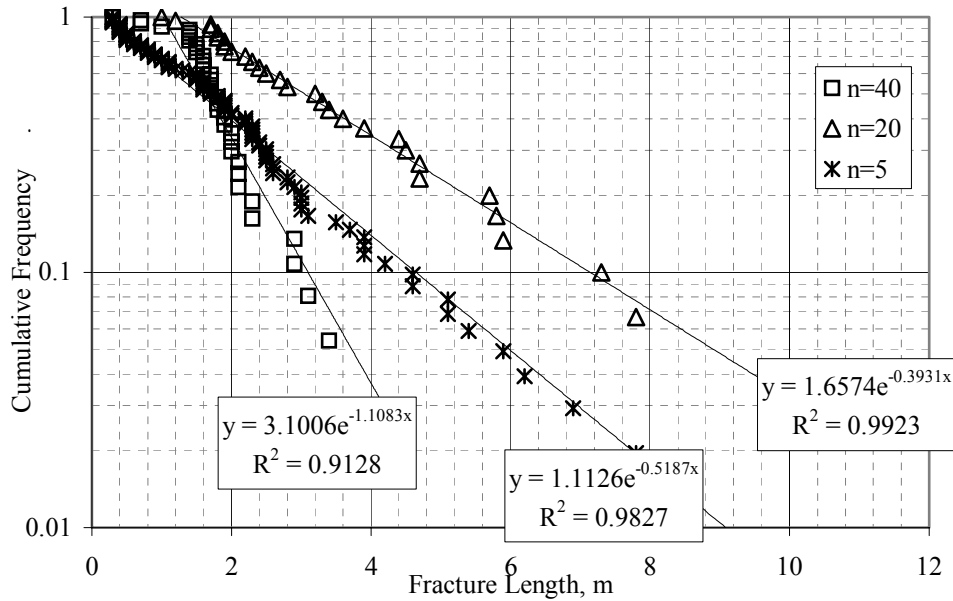


Fig. 5. Fracture length distributions for numerical simulation of Fig. 4 showing the impact of varying the subcritical index on results. Total strain applied perpendicular to fracture trend was 5.6×10^{-5} [2].

Philip et al. [30] estimated equivalent permeabilities for a variety of single set fracture patterns generated using the geomechanical model of Olson et al. [2] in an attempt to discern the key fracture attributes that controlled flow in fracture networks. Local fracture permeability was computed using the parallel plate law by mapping a fine flow simulation grid (0.1 m by 0.1 m grid blocks) onto numerically generated fracture networks for a 50 m by 50 m study area. Equivalent permeability for the entire study area was computed from steady state, single phase flow rates generated by a constant pressure gradient parallel to the fracture trends. For flow to get from one side of the simulation area to the other, given the fact that the fracture network was non-percolating, at least part of the flow path included the matrix (non-fractured media). In this manner, the modeling incorporated the effects of the finite lengths of individual fractures and the variability of fracture aperture along that length. Results showed that permeability was strongly dependent on fracture intensity as measured by cumulative trace length, but it was also influenced by average fracture segment length. Fracture patterns of the same cumulative trace length but larger average segment length had higher equivalent permeability than those with smaller average segment lengths (Fig. 6).

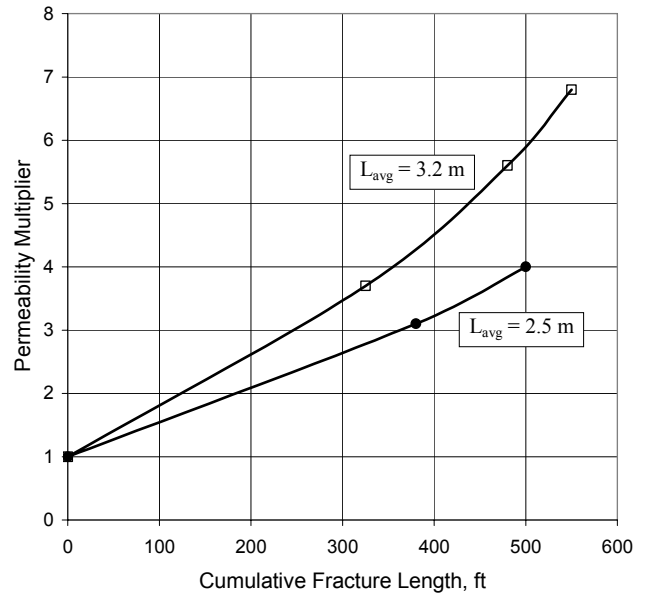


Fig. 6. Permeability multiplier for the equivalent permeability of a fractured media versus unfractured matrix as a function of cumulative fracture length in a 50m by 50m area for fracture populations with different average segment length. After [30].

Nakashima et al. [33] showed similar fracture permeability versus length distribution relationships for statistically generated fracture patterns, but the geologic controls on fracture pattern attributes were not investigated. Using the geomechanical approach, we can point out what geologic parameters influence fracture network characteristics and ultimately fracture permeability.

As mentioned in the previous section, cumulative fracture length created and mean fracture segment lengths for a given imposed strain can be related to the subcritical index. Variations in cumulative fracture trace length, holding other conditions and properties the same, can also be related to the mechanical layer thickness. The layer thickness effect is related to the oft observed outcrop relationship that fracture spacing is roughly proportional to layer thickness [38, 39]. Thus, for a given strain, thinner beds generate more cumulative fracture trace length, which implies greater fracture permeability according to the results in Fig. 6.

At first glance, this conclusion may seem consistent with the parallel plate law of equation (1), where decreasing fracture spacing, S , causes an increase in fracture permeability. However, the mechanical analysis of bed-bounded fractures also shows that fracture aperture is expected to be less in thin beds than in thick beds, all other things equal [40]. Since fracture permeability has a stronger dependence on aperture than spacing in equation (1), it seems that thicker beds might have higher permeability even though their fracture intensity is less. Interestingly, this is a point where the inadequacy of the parallel plate law for large scale permeability estimation is most pronounced. If the assumption of through-going fractures is not true (fracture flow paths are segmented and non-percolating), Philip et al. [30] showed that a doubling of fracture aperture for identical fracture trace networks, which should have resulted in nearly an order of magnitude equivalent permeability increase according to the parallel plate law, had virtually no effect on equivalent permeability.

5. DIAGENESIS EFFECTS ON APERTURE AND PERMEABILITY

Although Philip et al. [30] showed that fracture aperture did not affect permeability as implied in the parallel plate law, they did show that imposing the effects of an emergent threshold on the fracture pattern influenced permeability. The geomechanical simulations were performed using a boundary element program [41], where each individual fracture is made up of multiple short patches or elements. Fracture aperture for a given fracture can vary from element to element, where the narrowest apertures are typically at and near the fracture tips. A dimensionless emergent threshold was defined as a multiple of the mean kinematic

aperture of the fracture patches for a given network generated by the geomechanical model. The results of Fig. 6 were made assuming an emergent threshold of zero, where all of the kinematically open fracture patches were open to flow (geologically speaking, no mineral precipitation had occurred in the fractures). Increasing the emergent threshold resulted in some of the fracture patches being closed to flow, starting with those that had the smallest kinematic aperture.

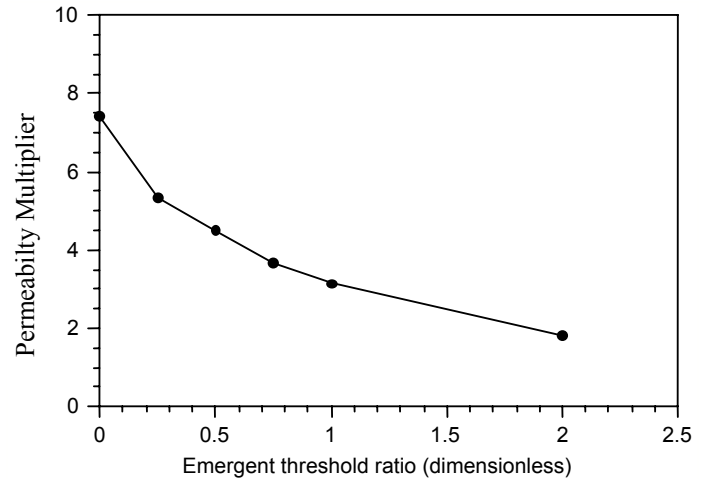


Fig. 7: The effect of synkinematic cement on equivalent permeability for a simulated fracture pattern. From [30].

Since these are typically at the tips of the fractures, filling the fractures with cement not only reduced hydraulic aperture of the fractures but decreased their lengths. It is the diminution of length that will be most important for non-percolating networks, and Philip et al. [30] showed how equivalent fracture permeability decreases dramatically with increasing emergent threshold (Fig. 7).

Finally, we analyzed the emergent threshold effects on fracture continuity for more complex fracture patterns than the single parallel fracture set case of Philip et al. [30]. The simulations of Olson et al. [2] and Philip et al. [30] assume strong in situ stress anisotropy at the beginning of fracture propagation that forces fractures to propagate in planar, non-interacting paths. However, it is common that natural fractures interact and form curving or orthogonal, ladder-like patterns [42-44] as shown in Fig. 8. Such a pattern was generated geomechanically (Fig. 9) by applying a constant strain rate extension in the y direction and holding the strain in the x-direction constant (zero normal displacement). Early propagation is dominated by fractures propagating in the x-direction, relieving

fracture promoting stresses acting in y until the principal stresses flip to favor fracture propagation in the y-direction (in response to the fracture promoting stresses caused by the Poisson effect) [45].



Fig. 8. Bedding plane exposure of natural fracture pattern with good trace pattern connectivity (6 inch scale in middle of photo).

Fig. 9a shows the resultant fracture trace pattern, showing strong connectivity in both the x and y directions in what would be a percolating fracture network. Fig. 9b, however, shows how aperture varies throughout the network, where the thickness of the fracture segments is proportional to kinematic aperture (widths exaggerated for clarity). The wider, gray-filled fractures represent fracture apertures of 1 to 3 mm. The thinner black lines have apertures ranging from 0.1 to 1 mm. Based on the parallel plate law, the flow resistance of a single fracture by itself (not accounting for surrounding matrix rock) can be characterized as the permeability k_f as

$$k_f = \frac{b^2}{12}. \quad (2)$$

Local permeability variations caused by an order of magnitude aperture reduction at the fracture tips from 1 to 0.1 mm would represent a 100 times reduction in fracture permeability.

Finally, if the emergent threshold for this particular fracture pattern were 1 mm, only the fatter gray

fracture segments would be left open, and the black connecting fracture segments would be completely mineralized and closed. Thus, based on this qualitative assessment of permeability, analogous to the more quantitative work described in the previous section for parallel fracture sets, it is evident that the interaction of diagenetic and kinematic effects play a pivotal role in determining the flow properties of a given fracture network.

6. CONCLUSIONS

Natural fractures are complex structures formed by mechanical breaking of rock and the diagenetic alteration of those broken surfaces. Numerical modeling of diagenesis occurring simultaneously with fracture opening shows how some fractures can be completely filled with cement while others may only be partially filled (bridged) or largely open. Analysis of cement patterns in fracture networks shows that fracture aperture variability can have a strong influence on flow continuity and ultimately permeability. Diagenetic effects can be imprinted during development of these more complex fracture patterns or after the fact. Permeability estimation through modeling shows that systematic changes can be expected where fracture length distributions are modified by variable thermal aging histories experienced by the fracture network, in other words varying emergent threshold values (minimum kinematic aperture this is hydraulically open). Both the rock properties that govern fracture pattern development and the cementation process that modify effective fracture porosity are amenable to accurate prediction using diagenetic modeling. Based on the concepts presented in this paper, future progress on permeability modeling of fractured reservoirs will require a coupling of geomechanically-based fracture network generation and diagenetic processes in both the fracture and matrix pore space.

7. ACKNOWLEDGMENTS

Supported by the Chemical Sciences, Geosciences and Biosciences Division, Office of Basic Energy Sciences, Office of Sciences, U.S. Department of Energy, and by industry sponsors of fracture and diagenesis research at The University of Texas at Austin and Geocosm.

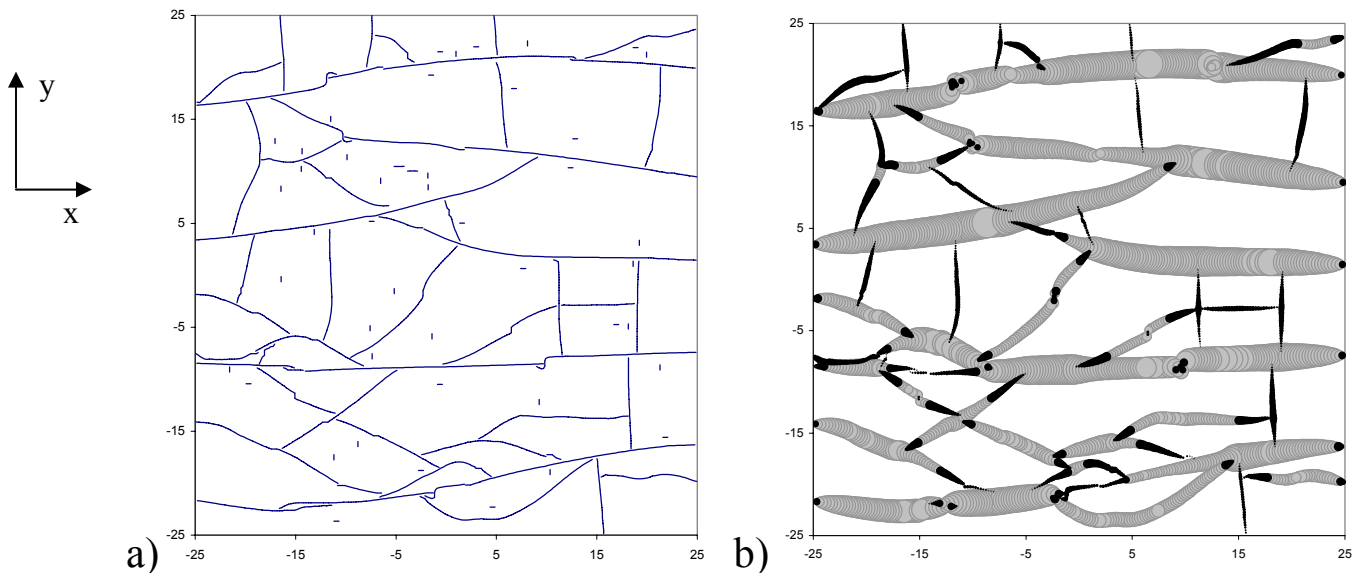


Fig. 9. Fracture network generated by uniaxial strain in the y -direction (zero strain in x) and starting with an isotropic in situ stress. The body is 50x50 m in map view and the mechanical layer thickness is 8m. The subcritical index used was $n=20$. a) Fracture tracemap with no aperture information. b) Kinematic aperture map where apertures are exaggerated but appropriately scaled (maximum aperture is 3×10^{-3} m).

8. REFERENCES

- Olson, J.E., 1993, Joint pattern development: effects of subcritical crack-growth and mechanical crack interaction: *Journal of Geophysical Research*, 98, p. 12,251-12,265.
- Olson, J.E., Y. Qiu, J. Holder, and P. Rijken, 2001, Constraining the spatial distribution of fracture networks in naturally fractured reservoirs using fracture mechanics and core measurements, in *SPE Annual Technical Conference and Exhibition*: New Orleans, LA.
- Crampin, S., 1987, Geological and industrial implications of extensive-dilatancy anisotropy: *Nature*, 328, p. 491-496.
- Heffer, K.J., and J.C. Lean, 1993, Earth stress orientation - a control on, and guide to, flooding directionality in a majority of reservoirs: *Reservoir Characterization III*, Tulsa, PennWell Publishing.
- Dyke, C., 1995, How sensitive is natural fracture permeability at depth to variation in effective stress? in Myer, L.R., Cook, N.G.W., Goodman, R.E., and Tsang, C.-F., eds., *Fractured and Jointed Rock Masses*: Balkema, p. 81-88.
- Durham, W.B., 1997, Laboratory observations of the hydraulic behavior of a permeable fracture from 3800-m depth in the KTB pilot hole: *Journal of Geophysical Research*, 102, p. 18405-18416.
- Laubach, S.E., J.E. Olson, and J.F.W. Gale, 2004, Are open fractures necessarily aligned with maximum horizontal stress?: *Earth & Planetary Science Letters*.
- Lander, R.H., J.F.W., Gale, S.E. Laubach, and L.M. Bonnell, 2002, Interaction of quartz cementation and fracturing in sandstones (abs.): *AAPG Conference and Exhibition*, Houston, Texas, p. A98-A99.
- Lander, R. H., L. M. Bonnell, and S. E. Laubach, in preparation, Theory for quartz cementation in fractured sandstones.
- McBride, E. F., 1989, Quartz cement in sandstones: a review: *Earth-Science Reviews*, 26, p. 69-112.
- Björklykke, K., and P.K. Egeberg, 1993, Quartz cementation in sedimentary basins: *AAPG Bulletin*, 77, p. 1538-1548.
- Laubach, S.E., 2003, Practical approaches to identifying sealed and open fractures: *AAPG Bulletin*, 87, p. 561-579.
- Walderhaug, O., 1994, Precipitation rates for quartz cement in sandstones determined by fluid-inclusion microthermometry and temperature-history modeling: *Journal of Sedimentary Research*, A64, p. 324-333.
- Walderhaug, O., 1996, Kinetic modeling of quartz cementation and porosity loss in deeply buried sandstone reservoirs: *AAPG Bulletin*, 80, p. 731-745.
- Walderhaug, O., 2000, Modeling quartz cementation and porosity loss in Middle Jurassic Brent Group Sandstones of the Kvitebjørn Field, Northern North Sea: *AAPG Bulletin*, 84, p. 1325-1339.
- Oelkers, E. H., P. A. Bjørkum, and W. M. Murphy, 1996, A petrographic and computational investigation of quartz cementation and porosity reduction in North Sea sandstones: *American Journal of Science*, 296, p. 420-452.
- Oelkers, E. H., P. A. Bjørkum, O. Walderhaug, N. H. Nadeau and W. M. Murphy, 2000, Making diagenesis obey thermodynamics and kinetics: the case of quartz cementation in sandstones from offshore min-Norway: *Applied Geochemistry* 15, p. 295-309.
- Lander, R.H., and O. Walderhaug, 1999, Porosity prediction through simulation of sandstone compaction and quartz cementation: *AAPG Bulletin*, 83, p. 433-449.

19. Bonnell, L.M., R. H. Lander and J. C. Matthews, 2000, Probabilistic prediction of reservoir quality in deep water prospects using an empirically calibrated process model (abs.): 2000 AAPG Conference and Exhibition, New Orleans, Louisiana.
20. Walderhaug, O., R. H. Lander, P. A. Bjørkum, E. H. Oelkers, K. Bjørlykke, and P. H. Nadeau, 2000, Modelling quartz cementation and porosity in reservoir sandstones - Examples from the Norwegian continental shelf. in R. H. Worden and S. Morad, eds., *Quartz Cementation in Sandstones: International Association of Sedimentologists Special Publication No. 29*, p. 39-49.
21. Lander, R. H., V. Felt, L. Bonnell, and O. Walderhaug, 1997, Utility of sandstone diagenetic modeling for basin history assessment, 1997 AAPG Conference and Exhibition, Dallas, p. A66.
22. Bjørkum, P. A., and P. H. Nadeau, 1998, Temperature controlled porosity/permeability reduction, fluid migration, and petroleum exploration in sedimentary basins: *Australian Petroleum Production and Exploration Association Journal*, 38, p. 453-465.
23. Lander, R. H., 1998, Effect of sandstone diagenesis on fluid overpressure development (abs.): 1998 AAPG Conference and Exhibition, Salt Lake City, Utah.
24. Wangen, M., 1998, Modeling porosity evolution and cementation of sandstones: *Marine and Petroleum Geology*, 15, p. 453-465.
25. Helset, H. M., R. H. Lander, J. C. Matthews, P. Reemst, L. M. Bonnell, and I. Frette, 2002, The role of diagenesis in the formation of fluid overpressures in clastic rocks: in A. G. Koestler and R. Hunsdale, eds., *Hydrocarbon Seal Quantification, Norwegian Petroleum Society Special Publication 11*, p. 1-15.
26. Laubach, S.E., R. M. Reed, J.E. Olson, R.H. Lander, and L.M. Bonnell, 2004, Coevolution of crack-seal texture and fracture porosity in sedimentary rocks: cathodoluminescence observations of regional fractures: *Journal of Structural Geology*, 26, p. 967-982.
27. Laubach, S.E., 1988, Subsurface fractures and their relationship to stress history in East Texas basin sandstone: *Tectonophysics*, 156, p. 37-49.
28. Van Golf-Racht, T. D., 1984, *Fundamentals of Fractured Reservoir Engineering*, Elsevier.
29. Segall, P. 1984. Formation and growth of extensional fracture sets. *Geological Society of America Bulletin*, 95, p. 454-462.
30. Philip, Z., J. Jennings, J.E. Olson, and J. Holder, 2002, Modeling coupled fracture-matrix fluid flow in fracture patterns generated using a geo-mechanical crack growth simulator, in 2002 SPE Annual Technical Conference and Exhibition, San Antonio, TX, September 29 – October 2.
31. Chirlin, G. R., 1985, Flow through a porous medium with periodic barriers or fractures. *SPEJ*, p. 358-362.
32. Lough, M.F., S.H. Lee, and J. Kamath, 1996, A new method to calculate the effective permeability of grid blocks used in the simulation of naturally fractured reservoirs, in *ATCE SPE: Denver*, p. 493-499.
33. Nakashima, T., K. Sato, N. Arihara, and N. Yazawa, 2000, Effective permeability estimation for simulation of naturally fractured reservoirs, in *SPE Asia Pacific Oil and Gas Conference and Exhibition: Brisbane, Australia*.
34. Renshaw, C.E., 1996, Influence of subcritical fracture growth on the connectivity of fracture networks: *Water Resources Research*, 32, p. 1519-1530.
35. Holder, J., J.E. Olson, and Z. Philip, 2001, Experimental determination of subcritical crack growth parameters in sedimentary rock: *Geophysical Research Letters*, 28, p. 599-602.
36. Olson, J. E., Holder, J. and Rijken, P., 2002, Quantifying the fracture mechanics properties of rock for fractured reservoir, in *SPE/ISRM Rock Mechanics Conference*, Irving, Texas, 1-12.
37. Rijken, P., J. Holder, J. E. Olson, and S. E. Laubach, 2003, Predicting fracture attributes in the Travis Peak Formation using quantitative mechanical modeling and structural diagenesis: in *Gulf Coast Association of Geological Societies Transactions*.
38. Narr, W. and J. Suppe, 1991. Joint spacing in sedimentary rocks. *Journal of Structural Geology* 13, p. 1037-1048.
39. Bai, T., and Pollard, D.D., 2000, Fracture spacing in layered Rocks: A new explanation based on the stress transition: *Journal of Structural Geology*, 22, p. 43-57.
40. Olson, J. E., 2003, Sublinear scaling of fracture aperture versus length: an exception or the rule? *Journal of Geophysical Research*, 108, Art. No. 2413.
41. Crouch, S. L. & A. M. Starfield, 1982. *Boundary element methods in solid mechanics: with applications in rock mechanics and geological engineering*. Allen and Unwin, London.
42. Olson, J. and D. D. Pollard, 1989, Inferring paleostresses from natural fracture patterns: A new method, *Geology*, 17, p. 345-348.
43. Gross, M. R., 1993, The origin and spacing of cross joints: Examples from the Monterey Formation, Santa Barbara Coastline, California, *Journal of Structural Geology*, 15, p. 737-751.
44. Rives, T., M. Razack, J. P. Petit, and K. D. Rawnsley, 1992. Joint spacing: analogue and numerical simulations. *Journal of Structural Geology*, 14, p. 925-937.
45. Olson, J. E., 1997, Natural fracture pattern characterization using a mechanically-based model constrained by geologic data - moving closer to a predictive tool, in *36th U.S. Rock Mechanics Symposium*, New York City.

Discrete Element Modeling of Fracture Toughness Tests in Weakly Cemented Sandstone

Park, N., Holder, J., and Olson, J. E.

Department of Petroleum and Geosystems Engineering, The University of Texas at Austin, Austin, TX, USA

Copyright 2004, ARMA, American Rock Mechanics Association

This paper was prepared for presentation at Gulf Rocks 2004, the 6th North America Rock Mechanics Symposium (NARMS): Rock Mechanics Across Borders and Disciplines, held in Houston, Texas, June 5 – 9, 2004.

This paper was selected for presentation by a NARMS Program Committee following review of information contained in an abstract submitted earlier by the author(s). Contents of the paper, as presented, have not been reviewed by ARMA/NARMS and are subject to correction by the author(s). The material, as presented, does not necessarily reflect any position of NARMS, ARMA, CARMA, SMMR, their officers, or members. Electronic reproduction, distribution, or storage of any part of this paper for commercial purposes without the written consent of ARMA is prohibited. Permission to reproduce in print is restricted to an abstract of not more than 300 words; illustrations may not be copied. The abstract must contain conspicuous acknowledgement of where and by whom the paper was presented.

ABSTRACT: Linear elastic fracture mechanics is widely used to describe fracture behavior in hard rock, and fracture toughness values for many such rocks are in the literature. The main application has been in hydraulic fracturing. However, hydraulic fracturing operations are now widely performed in unconsolidated and weakly-cemented sandstones or "soft rocks." Soft rocks can have significantly different mechanical behavior than hard rocks, but typically linear elastic models are still applied in these rocks for fracture design purposes. Because of the difficulty of coring and preparing of samples, fracture toughness testing of soft sandstone samples from the subsurface is very challenging. In the study reported here, we assess the fracture mechanics behavior of weakly cemented sandstone numerically with the Discrete Element Method (DEM), in which input parameters are evaluated by comparison with selected elastic and fracture properties. The first step in the study was to carry out the assessment for well cemented Berea sandstone. Mode I fracture toughness was determined using the semi-circular specimen under three-point bending (SCB) test. Further DEM simulations were then run by progressively weakening the bond strength from the reference values determined for Berea sandstone in order to estimate the behavior of weakly-cemented sandstones. The variation of fracture toughness with particle size, notch length, and specimen size is presented and discussed. The assessments of fracture behavior in this study provide a framework of guidelines for fracture mechanics testing and characterization in weakly cemented sandstones.

1. INTRODUCTION

In hard rock, Linear Elastic Fracture Mechanics (LEFM) is generally used for the analysis of fracture propagation. In weakly cemented and poorly consolidated rocks, fracture propagation mechanisms may be complex, including inelastic deformation, disaggregation, and near-tip shear failure. The mechanical behavior of weakly cemented granular materials is strongly influenced by the amount or characteristic of the cement between particles, and several studies have been conducted on the effect of cement on the deformation and failure behavior of sandstones [1, 2].

Bernabè et al. [3] created well-consolidated artificial sandpacks using sand and cement material, and measured the variations in strength, dilation and stress-strain behavior with cement content. They

observed that small amounts of cement deposited at grain-to-grain contacts had a significant effect on mechanical behavior and strength. Nakagawa and Myer [4] showed that load-displacement paths for samples with constant porosity were identical for different cement saturation ratios until the grains achieved a certain level of intergranular cohesion. After the critical cohesion was achieved, deformation due to intergranular slip decreased and the deformation behavior became more rock-like than soil-like.

Continuum modeling of inelastic deformation and brittle fracturing of rocks can be classified as an indirect method, where damage is represented by its effect on constitutive relations [5]. The present study employs the Discrete Element Method (DEM), which can be categorized as a direct method, where deformation is represented by explicitly introducing cracks and tracking grain

motion. DEM has several advantages over continuum based numerical methods. Instead of the complex constitutive relationships that must be characterized to use continuum methods, DEM traces the motion and interactions of individual particles based on the direct application of Newton's second law. Particles interact through contacts and bonds with other particles. Cracks are a natural consequence of exceeding the bond strength between particles, and do not require special meshing or slip surface algorithms. Because of its micro-mechanical foundations, DEM can be a useful simulation tool to understand the factors and mechanisms that control the behavior of granular materials, even when experimental data is limited.

In the present study, suites of numerical mode I fracture toughness tests were conducted to learn more about laboratory characterizations of fracture in weak sandstones. For these simulations, three-dimensional DEM models representing well cemented sandstones were generated, and the appropriate grain and bond stiffness, and bond strength were determined by comparison with experimental values of selected material properties. An initial assessment of the viability of this process was carried out for Berea sandstone, which is a well-cemented sandstone for which published fracture toughness values are consistent. Numerical fracture toughness tests were then performed using semi-circular specimens in three-point bending (SCB) tests. Following the initial simulation, the amount of cement was systematically reduced to represent progressively weaker sandstones, and the changing nature of fracture propagation was characterized using the SCB test. Other parameters that were investigated were particle size, notch length, and specimen size.

2. LINEAR ELASTIC FRACTURE MECHANICS

In linear elastic fracture mechanics (LEFM), the mode I stress intensity factor, K_I , is a measure of the tensile stress field near the tip of an ideal crack in a linear-elastic solid. It is a function of load, crack geometry, and boundary conditions [6]. A fracture propagates critically when K_I is greater than a critical value denoted by the fracture toughness, K_{IC} . Fracture toughness is a material property that can be measured in the laboratory, and LEFM has been applied to many areas of rock engineering [7]. In petroleum engineering, fracture toughness is

primarily applied in the area of hydraulic fracturing [8, 9, 10, 11].

2.1. *Fracture toughness of soft rocks*

Experimental testing of fracture toughness in a variety of rock types has shown that the values can depend on sample size and whether or not a substantial process zone develops. A process zone represents a volume around the crack tip where energy is dissipated by ductile strain (typically in metals) or micro-cracking and shear (more typical for rocks) [12]. It is our hypothesis that this process zone will become more substantial as the inter-granular bonding between sand grains in a sandstone weakens, causing behavior that progressively deviates from what is expected for LEFM analysis.

Experimental fracture toughness results for tests in weak rock have been published for synthetic mudstones [13, 14, 15], synthetic sandstones [4], and a weak natural sandstone [16]. Haberfield and Johnston [13] used a Single Edge Cracked Beam (SECB) and a Single-Edge Cracked Round Bar Bend (SECRBB) specimen under three point bending and showed that fracture toughness for a specific saturated water content was dependent on the rate of loading, initial crack length, and the overall specimen size, but that the specimen thickness and sharpness of the crack tip had no significant effect. Lim et al. [13, 14] conducted mode I, mode II, and mixed mode fracture toughness tests using SCB specimens. They concluded that fracture toughness is independent of the specimen thickness and that neither the specimen size nor the notch length has an appreciable effect on the measured value of fracture toughness. Nakagawa and Myer [4] also used SCB specimens, and showed that the mode I fracture toughness decreases with a decrease in cement, but weakly cemented samples failed in the same manner as strong sandstones. Krishnan et al. [16] reported mode I, II, and mixed mode fracture toughness of a natural weakly cemented Antler sandstone using Straight Edge Notch Brazilian Disk (SENBD) specimens, and developed an empirical failure envelope under both tension-shear and compressive-shear conditions.

2.2. *SCB test*

As indicated in the previous paragraph, a number of methods can be used to determine the fracture toughness of rock materials [12, 17, 18, 19].

Thiercelin and Roegiers [20] found that applying compression normal to the crack face in the specimen resulted in a smaller process zone. Because of this, most rock fracture toughness tests utilize compressive loads. Lim et al. [21] advocated the use of SCB test because it uses half the sample size of the conventional Brazilian tensile test specimen, making it cost effective and easy to handle. They demonstrated equally reliable results as the more established SECB and SECRBB techniques using synthetic soft mudstone.

Since Chong and Kuruppu [22] proposed the SCB test in 1984, it has been used for broad range of rock types, such as Colorado oil shale [23], Welsh limestone [24], Berea sandstone and eastern basalt [25], synthetic soft mudstone [14, 15], limestone from Saudi Arabia [26], Keochang granite and Yeosan Marble [27]. The schematic diagram of test setup is shown in Fig. 1. Fracture toughness, K_{IC} , is calculated as a function of peak load from

$$K_{I} = \frac{P\sqrt{\pi a}}{DB} Y_I, \quad (1)$$

where P is the maximum load, a is the crack length, D is the specimen diameter, B is the specimen thickness, and Y_I is a dimensionless coefficient.

Several different equations for the coefficient, Y_I , have been proposed [28, 29, 30]. The present study uses the equation based on the work of Lim et al. [14, 15, 30], who demonstrated its applicability to soft rock:

$$Y_I = 4.782 - 1.219 \frac{a}{r} + 0.063 \exp\left(7.045 \left(\frac{a}{r}\right)\right), \quad (2)$$

where $0.03 \leq a/r \leq 0.8$ and $s/r = 0.8$. The SCB specimens used in this study are constrained to a normalized notch length of $0.1 \leq a/r \leq 0.5$ and support span of $s/r = 0.8$.

3. NUMERICAL METHODS

Three-dimensional models representing cemented sandstones were generated using PFC3D (Particle Flow Code 3D) by Itasca Consulting Group, Inc. This code has been widely used for numerical modeling of granular geo-material [2, 31, 32, 33, 34]. The behavior of a rock can be simulated by the interaction between particle assemblies using three

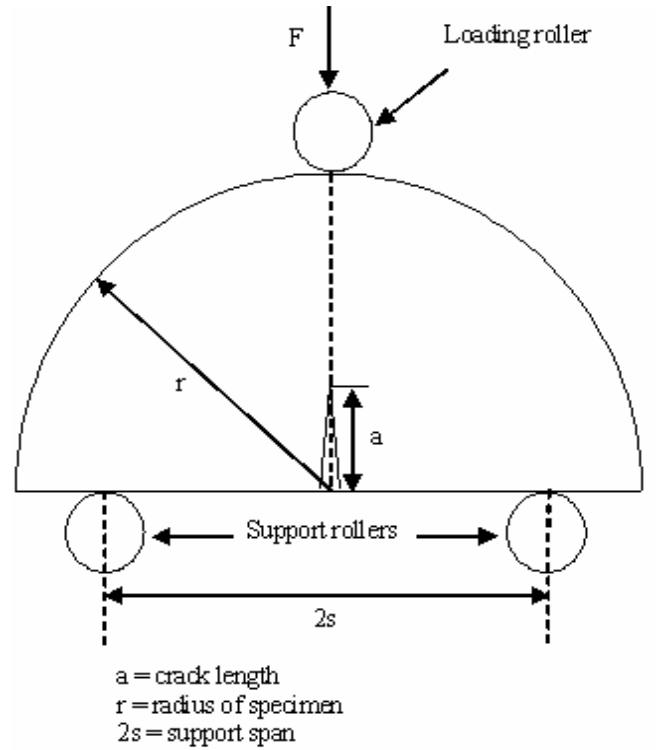


Fig. 1. Schematic view of semi-circular bend (SCB) test specimen

basic models in PFC: the stiffness model, the slip model, and the parallel bonding model. The stiffness model uses elastic spring constants to simulate contact forces between overlapping particles, and particle displacements are computed by Newton's second law. For un-bonded particles, slip on contacts occur when the resolved shear force exceeds the frictional strength. The effects of interparticle cementation is simulated by "parallel bonds" which have their own stiffness with respect to normal and shear loads and have a specified strength [5].

The stiffness model uses only two basic material properties that must be quantified: the normal and shear stiffness, k_n and k_s [35]. Particles do not deform or change shape when they interact, they merely overlap. The normal force between particles is calculated as

$$F_n = k_n U_n, \quad (3)$$

where U_n is the overlap between contacting particles. Shear force on a particle is related to incremental displacement tangent to the particle boundaries, ΔU_s , over each timestep as

$$\Delta F_s = -k_s \Delta U_s \quad (4)$$

The slip model compares the shear force on the particle to the frictional strength of the contact, and if the strength is exceeded, slip will occur (in the absence of bonding).

Inter-particle cementation can be described in PFC using a parallel bond with normal and shear stiffness per unit area, $k_{n,p}$ and $k_{s,p}$, and tensile and shear strength, σ_p and τ_p . The area of the bond is computed based on its radius, which is given by

$$R_p = \lambda_p R_{A,B}^{\min}, \quad (5)$$

where λ_p is the bond radius multiplier and $R_{A,B}^{\min}$ is the smaller of the two contacting particle radii. Parallel bonds act in parallel with the particle-particle interaction. A crack propagates as a parallel bond breakage when either the tensile or shear strength of the parallel bond is exceeded.

The numerical specimens were generated in the following sequence [36]:

1. *Particle generation* - A uniformly or normally distributed array of particles with half their final radii are randomly located inside of a boundary created by three sets of mutually perpendicular confining walls. Then, particle radii are increased to the final values and result in a densely packed assembly.

2. *Isotropic stress installation* - In order to reduce the magnitude of locked-in forces, particles and the boundaries are allowed to move with no inter-particle friction, and the assembly of unbonded, frictionless particles is stabilized for a specified low value of isotropic stresses acting on the assembly.

3. *Floating particle elimination* - Particles which have less than three contacts are eliminated by increasing the radii of the floating particles. As a result, a densely packed and well-connected assemblage of particles is created.

4. *Parallel bond installation* - Parallel bonds are installed at the contact between particles to mimic the cementation. Initial values of parallel bond stiffness, strength, and radius are specified, and the system is allowed to stabilize.

5. *Parameter determination* - PFC simulations of selected mechanical deformation tests are generated, and the magnitudes of model input parameters are adjusted to replicate measured material parameters.

4. RESULTS AND DISCUSSION

4.1. Determining micro-mechanical properties

The initial micro-mechanical parameters for the DEM model (contact stiffness, bond stiffness bond strengths, and friction coefficient) were determined by matching measured values of selected macroscopic mechanical properties of Berea sandstone from the literature [37].

The laboratory tests simulated were a Brazilian tensile test, a uniaxial compression test, and triaxial compression tests under confining pressures of 10, 20, and 30 MPa. The contact and bond stiffnesses were constrained by the macroscopic Young's modulus and internal friction. The bond strength was constrained by the uniaxial compressive strength and cohesion. Fig. 2 shows the comparison between experimental triaxial test specimen and the PFC3D simulation. For the uniaxial and triaxial compression tests, specimen size was 54mm by 54mm by 108mm. A 21.46mm thick specimen was 'cut' from the middle of compression test specimen for the Brazilian test. Microscopic input parameters are listed in Table 1.

The comparison of the elastic properties and strengths for the experimental and numerical tests are listed in Table 2. The stress-strain behavior of Berea sandstone was matched successfully except for tensile strength. In the current version of PFC3D, matching both uniaxial compressive strength and Brazilian tensile strength at the same time is not possible. In general, material strength is dependent on specimen size due to the increase of pre-existing microcracks, and tensile strength is more size dependent than compressive strength. Uniaxial compressive strength is more representative of strength than tensile strength, and the present study focused on matching uniaxial compressive strength.

4.2. Fracture toughness test of Berea sandstone

Many of the rock fracture mechanics concepts have been adopted from that of metals. However, several studies [20, 38, 39] have shown that the size, shape and mechanics of rock fracture process zones are significantly different from those of metal. Schmidt [40] introduced a specimen size criterion for rocks, modified from that for metals.

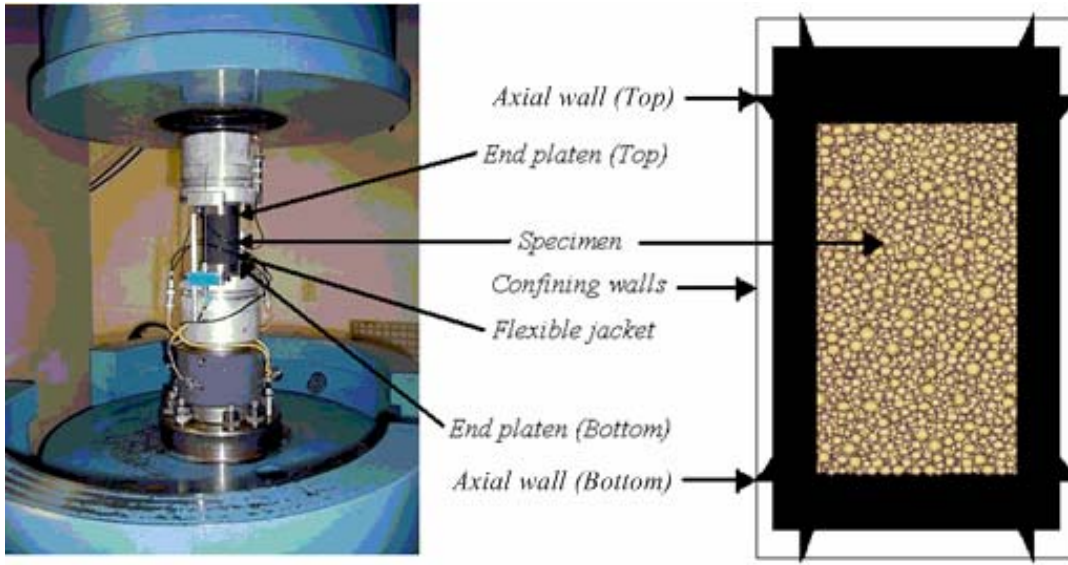


Fig. 2. Comparison of laboratory specimen and a corresponding numerical model

Table 1. Microscopic input parameters for PFC

Items	Values
Particle Properties	
R_{min}	1.5
R_{max} / R_{min}	1.65
Density (kg/m^3)	2650
Friction Coefficient, μ	0.5
Contact Modulus, E_c (GPa)	17.5
Normal / Shear Stiffness, k_n/k_s	1.0
Parallel Bond Properties (Cement Effect)	
Modulus, E_p (GPa)	17.5
Normal / Shear Stiffness Ratio, $k_{n,p}/k_{s,p}$	1.0
Radius Multiplier, λ_p	1.0
Mean Normal Strength, σ_p (MPa)	40
Mean Shear Strength, τ_p (MPa)	400
Strength Standard Deviation (MPa)	5

Table 2. The measured and simulation value of mechanical properties of Berea sandstone

Properties	Experiment	PFC3D
Young's Modulus, E (GPa)	19.26	20.2
Poisson's Ratio, ν	0.38	0.35
Internal Friction Angle, ϕ	32.8	33.0
Cohesion, c (MPa)	15.4	19.8
Uniaxial Compressive Strength, UCS (MPa)	73.8	72.5
Tensile Strength, S_t (MPa)	1.17	7.6

Several studies [12, 13, 23, 41] have shown that criteria for metals provide too conservative requirements for specimen size. So far, no standard criterion has been established for rock, and Lim et al. [14] concluded that the minimum size criteria

depend on both the type of rocks and the testing methods. To investigate the effect of various geometric parameters, several different specimen geometries were tested in the present study. All these specimens satisfied the criteria suggested by Chong et al. [23] and Barton [41]:

$$D \geq 0.269 \left(\frac{K_{IC}}{\sigma_t} \right)^2 \quad (6) [23]$$

$$a \geq 0.269 \left(\frac{K_{IC}}{\sigma_t} \right)^2 \quad (7) [41]$$

The present investigation of fracture toughness is based on numerical simulations of SCB tests. After determining the micro-mechanical properties of the numerical rock, the input parameters were used in a simulation of a fracture toughness test on Berea sandstone. The specimen was tested at a loading rate of 0.005 mm/s and had a diameter, D of 55mm. The thickness, B , was 14mm, and the notch length was 6.875mm, which corresponds to a normalized notch length (a/r) of 0.25. The distribution of computed contact forces and displacements in the SCB specimen is shown in Fig. 3. Compressive force is acting on the loading and supporting balls and the displacement is symmetrically acting outwards. As a result, a crack propagates from top of the notch along the loading axis. Using the Berea properties constrained by the compressive tests, the resultant fracture toughness was $K_{IC} = 1.45 \text{ MPa}\sqrt{m}$. This is in good agreement with the laboratory value of K_{IC} of 1.31 – 1.36 $\text{MPa}\sqrt{m}$

reported by Thiercelin and Roegiers [22], although others have reported lower values [42, 43].

4.3. Effects of the amount of cement

The effect of cementation on fracture toughness was simulated by reducing the area of the cement between grains while holding the bond strength and stiffness per area at the values determined using Berea sandstone. In this way a cement with constant mechanical properties is used, and the reduction in bond radius is analogous to reducing the volume of a specific type of cement. The parallel bond radius multiplier was varied from a maximum value of $\lambda_p=1.0$ for the well cemented sandstone to a minimum of $\lambda_p=0.25$ for the least cemented case.

The evolution of fractures compared for these levels of cementation is shown in Fig. 4, and the corresponding force-displacement behavior of fracture toughness tests are compared in Fig. 5. The fracture for the weakly cemented case still propagates along the loading axis, but is fatter and more dispersed than that for the well cemented case.

In Fig. 5, the effect of cement weakening is clearly shown. The specimen fails at a much lower force and displacement in weakly cemented case, which results in low value of K_{IC} . The applied force decreases gradually after the peak load for the weakly cemented sandstone, showing an increasing effect of friction with decreasing cement. This behavior contrasts sharply with the very brittle behavior shown for the well cemented sandstone in which there is an instantaneous drop in loading force after its peak value.

Similar behavior is observed in the crack abundance. The number of cracks abruptly increases immediately after the peak load in the well cemented case, while the number of cracks gradually increases in a relatively wide range of displacement in the weakest cementation case.

The variations in cement have a large effect on fracture toughness as shown in Fig. 6. K_{IC} decreases with the weakening of cementation, in agreement with the observation of Nakagawa and Myer [4]. This quantitative linear relationship between K_{IC} and cement content for weak sandstones would be difficult to determine from laboratory measurements.

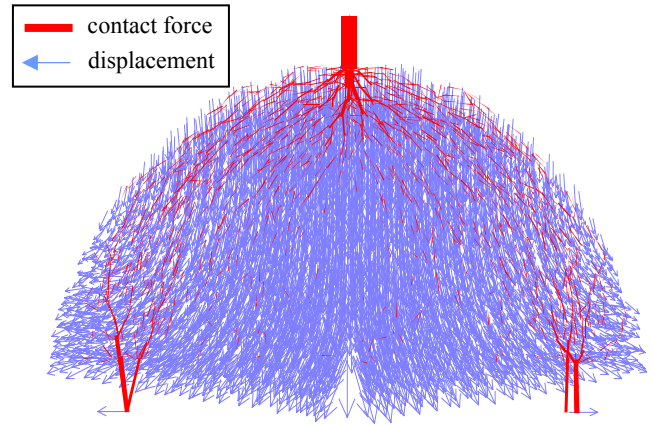


Fig.3. Force and displacement distribution in SCB specimen

4.4. Effects of other parameters

4.4.1. Particle size

The effects of variations in particle size on K_{IC} were investigated by numerical simulations in which the minimum particle radius, R_{min} , was changed from 0.65 mm to 1.0 mm in the sample with a diameter of 55 mm for four different cases of cementation ($\lambda_p=0.25, 0.5, 0.75$ and 1.0). All other microscopic input parameters kept the same. The results are shown in Fig. 7.

In well cemented sandstones ($\lambda_p=1.0$), K_{IC} increased from a minimum value at $R_{min}=0.8$ by approximately $0.15 MPa\sqrt{m}$ for both lower and higher radii. This is not a substantial change and no significant variation is found for the weaker cemented sandstones.

Singh and Sun [44] found much larger variation in experimental value of K_{IC} in fine and coarse grained sandstone using SCB tests. They reported a 35% increase of K_{IC} for fine grained sandstones. The grain sizes tested in the present study are all in the range of coarse sand where no significant effect of particle size was found. Further studies in broader range of particle size including finer grains are needed to establish trends in particle size effects.

4.4.2. Notch length

The effects of notch length were investigated by varying its size from 2.75mm to 13.75mm, which corresponds to a normalized notch length (a/r) of 0.1 to 0.5, in a 55 mm diameter specimen. Tests were also conducted on four different cases of cementation. The results are plotted in Fig. 8.

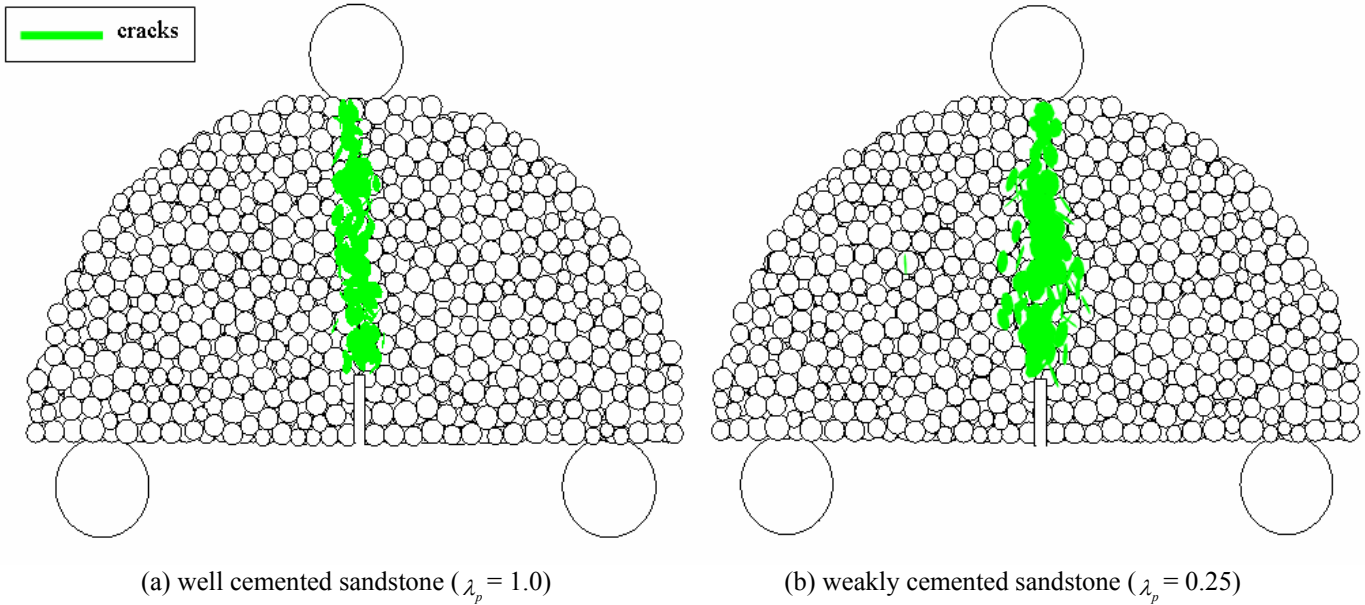


Fig. 4. The comparison of fracture propagation in well ($\lambda_p = 1.0$) and weakly cemented sandstones ($\lambda_p = 0.25$).

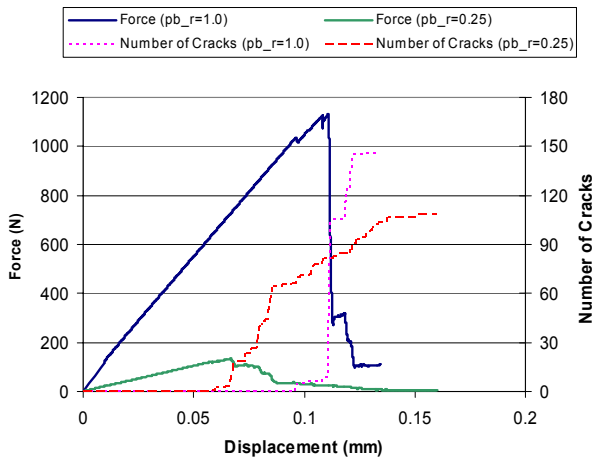


Fig. 5. The effect of cementation weakening on force-displacement behavior

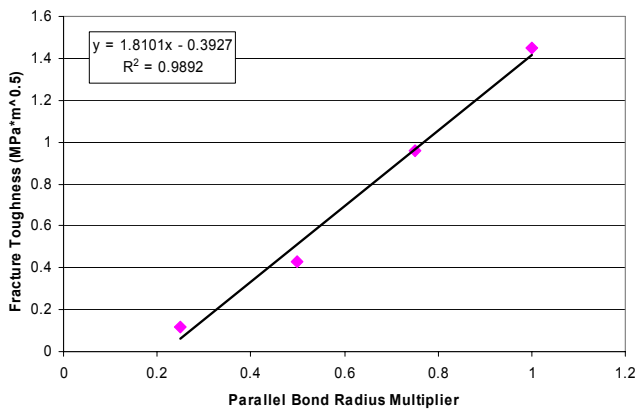


Fig. 6. The effect of cementation on fracture toughness

In well cemented sandstones, K_{IC} slightly increased with increasing normalized notch length, but it only by 5% and it is difficult to tell that it is due to the notch length effect. Notch length does not have a significant effect on K_{IC} regardless of the amount of cementation in the range tested here.

Experimentally, Lim et al. [14] concluded that notch lengths between 3mm and 0.8 times the specimen diameter are valid for SCB tests in weak rocks, and Singh and Sun [24] suggested normalized notch length greater than 0.25 for Welsh limestone. In the present study, normalized notch length between 0.1 and 0.5 (notch length between 2.75mm and 13.75mm) appear to provide valid K_{IC} values. This result supports the work of Lim et al. [14]. They tested only on soft mudstones, but in the present study, a similar range of notch length has been found to be satisfactory for valid K_{IC} determinations in both weakly and well cemented sandstones.

4.4.3. Specimen thickness

Three different specimen thicknesses, from 10.5mm to 17.5mm, were used in numerical simulations of SCB tests with a diameter of 55mm, for four different ranges of cementation. As shown in Fig. 9, K_{IC} slightly increased only in the well cemented case, but generally there is no significant effect of thickness throughout all cementation cases.

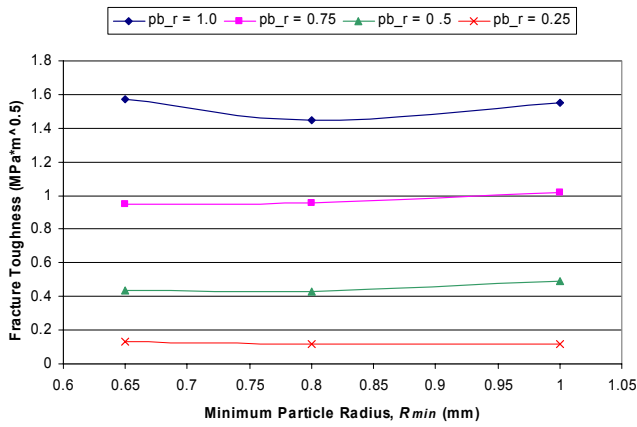


Fig. 7. Effects of particle size on K_{IC}

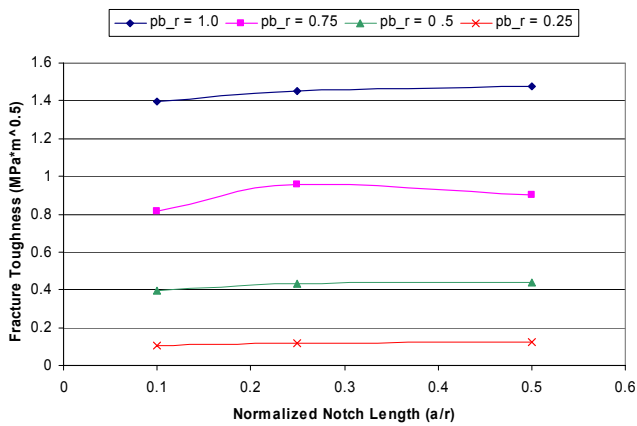


Fig. 8. Effects of notch length on K_{IC}

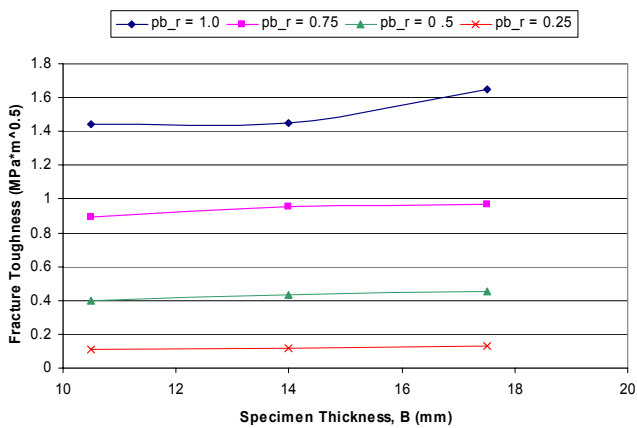


Fig. 9. Effects of specimen thickness, B , on K_{IC}

Lim et al. [14] conducted a series of experiments on the effect of specimen thickness using specimens with thickness from 13mm to 48.4mm and reached

this same conclusion. Singh and Sun [24] also reported the independence of SCB behavior to specimen thickness.

5. CONCLUSIONS

As an initial step towards understanding the fracture propagation behavior of weakly cemented sandstones, a number of numerical DEM simulations of mode I fracture toughness tests were conducted using SCB specimens. The fracture toughness of well cemented Berea sandstone was successfully determined using the micro-mechanical parameters for DEM which were determined by matching the macroscopic mechanical properties of Berea sandstone. The weakening of cementation was simulated by the systematic reducing of the volume of cement with a decrease in parallel bond radius. The K_{IC} decreased in a linear fashion as the intergranular cementation weakens, and based on this strong linear trend, the K_{IC} of very weakly cemented sandstones, which can not be determined in laboratory tests, was predicted.

The effects of particle size, notch length, and specimen thickness on K_{IC} were assessed, but no significant effects were observed in the range tested here. Due to the limited range of test parameters, it is difficult to extrapolate trends observed to other type of rocks. Results from this study are generally consistent with the previous experimental studies.

The assessments of fracture behavior in this study provide a framework of guidelines for fracture mechanics testing and characterization in weakly cemented sandstones. Additional study will provide a better understanding of the behavior of weakly cemented sandstones. Future studies should involve: 1) the quantitative examination of the non-linearity effect caused by fracture process zone using level II fracture toughness test, 2) tests of the validity of parameters which control K_{IC} in a broader range, and 3) the investigation of the applicability of different types of tests to the determination of fracture toughness of weakly cemented sandstones.

ACKNOWLEDGEMENTS

Support for this project was provided by the National Science Foundation through grant No. CMS-9978662. Additional support was provided by the U.S. Department of Energy project number. DE-FC26-00BC15308 and the Fracture Application and Research Consortium (FRAC) of The

University of Texas at Austin. Any opinions, findings, conclusions, or recommendations expressed herein are those of the authors and do not necessarily reflect the views of the DOE or NSF.

REFERENCES

1. Yu, A.-B. 2002. DEM – An effective method for particle scale research of particulate matter. In *Proceedings of the Third International Conference on Discrete Element Methods; Numerical Modeling of Discontinua, Santa Fe, 23 – 25 September 2002*, eds. B.K. Cook and R.P. Jensen : 17-22. ASCE.
2. Bruno, M.S., A. Dorfmann, K. Lao, and C. Honeger. 2001. Coupled particle and fluid flow modeling of fracture and slurry injection in weakly consolidated granular media. In *Proceedings of the 38th Annual U.S. Rock Mechanics Symposium: Rock mechanics in the national interest, Washington D.C., 7 – 10 July 2001*, eds. D. Elsworth et al., 1, 173-180: Balkema.
3. Bernabè, Y., D.T. Fryer, J.A. Hayes. 1992. The effect of cement on the strength of granular rocks. *Geophysical Research Letters*. 19, 14:1511-1514.
4. Nakagawa, S. and L.R. Myer. 2001. Mechanical and acoustic properties of weakly cemented granular rocks. In *Proceedings of the 38th Annual U.S. Rock Mechanics Symposium: Rock mechanics in the national interest, Washington D.C., 7 – 10 July 2001*, eds. D. Elsworth et al., 1, 3-10: Balkema.
5. Potyondy, D.O., P.A. Cundall, and C.A. Lee. 1996. Modelling rock using bonded assemblies of circular particles. In *Proceedings of the Second North American Rock Mechanics Symposium: NARMS 96, Montreal, PQ, Canada, 19-21 June 1996*, eds. M. Aubertin et al., 1937-1944. Rotterdam: Balkema.
6. Lawn, R. and Wilshaw R. 1975. Review indentation fracture: Principles and applications. *J. Mat. Sci.* 10, 6: 1049-1081.
7. Ouchterlony, F. 1988. Suggested methods for determining the fracture toughness of rock. *Int. J. Rock Mech. & Min. Sci. & Geomech. Abstr.* 25, 1: 71-96.
8. Cleary, M.P. 1983. Modelling and developing hydraulic fracturing technology. In *Rock Fracture mechanics, CISM Courses and Lectures. No. 275*, ed. Rossmanith, 383-476.
9. Roegiers, J.-C., J.D. McLennan, and D.L. Murphy. 1982. Influences of pre-existing discontinuities on the hydraulic fracture propagation process. In *Proceedings of The First Japan-U.S.A. Symposium on Fracture Mechanics Approach, Hydraulic Fracture and Geothermal Energy*. Sendia, Japan. 217-240.
10. Rummel, F. 1987. Fracture mechanics approach to hydraulic fracturing stress measurements. In *Fracture Mechanics of Rocks*, ed. B.K. Atkinson, 217-240.
11. Thiercelin, M. 1989. Fracture toughness and hydraulic fracturing. *Int. J. Rock Mech. & Min. Sci. & Geomech. Abstr.* 26, 3: 177-183.
12. Whittaker, B.N., R.N. Singh, and G. Sun. 1992. *Rock fracture mechanics – principles, design and applications*. Amsterdam: Elsevier
13. Haberfield, C.M. and I.W. Johnston. 1990. Determination of the fracture toughness of a saturated soft rock. *Can. Geotech. J.* 27, 6: 276-284
14. Lim, I.L., I.W. Johnston, S.K. Choi, and J.N. Boland. 1994. Fracture testing of a soft rock with semi-circular specimens under three point bending, part 1: mode-I. *Int. J. Rock Mech. & Min. Sci. & Geomech. Abstr.* 31, 3: 185-197.
15. Lim, I.L., I.W. Johnston, S.K. Choi, and J.N. Boland. 1994. Fracture testing of a soft rock with semi-circular specimens under three point bending, part 2: mixed mode. *Int. J. Rock Mech. & Min. Sci. & Geomech. Abstr.* 31, 3: 199-212.
16. Krishnan, G.R., X.L. Zhao, M. Zaman, and J.C. Roegiers. 1998. Fracture toughness of a soft sandstone. *Int. J. Rock Mech. & Min. Sci. & Geomech. Abstr.* 35, 6: 695-710.
17. Atkinson, B.K. 1987. *Fracture mechanics of rock*. 1st ed. San Diego: Academic Press.
18. Zhang, Z.X. 2002. An empirical relation between mode I fracture toughness and the tensile strength of rock. *Int. J. Rock Mech. & Min. Sci.* 39: 410-406.
19. Kahraman, S. and R. Altindag. 2003. A brittleness index to estimate fracture toughness. *Int. J. Rock Mech. & Min. Sci.* 41: 343-348.
20. Thiercelin, M. and Roegiers, J.-C. 1986. Toughness determination with the modified ring test. In *Proceeding of the 27th U.S. Symposium on Rock Mechanics: Key to Energy Production, Tuscaloosa, 23-25 June 1986*, eds. H.L. Hartman 615-622. Rotterdam: Balkema.
21. Lim I.L., I.W. Johnston, and S.K. Choi. 1994. Assesment of mixed-mode fracture toughness testing methods for rocks. *Int. J. Rock Mech. & Min. Sci. & Geomech. Abstr.* 31: 265-272.
22. Chong, K.P. and M.D. Kuruppu, 1984. New specimen for fracture toughness determination of rock and other materials. *Int. J. Frac.* 26: R59-R62.
23. Chong, K.P., M.D. Kuruppu, and J.S. Kuszmaul. 1987. Fracture toughness determination of layered materials. *Eng. Frac.Mech.* 28, 1: 43-54.
24. Singh, R.N. and G. Sun. 1989. A numerical and experimental investigation for determining fracture toughness of Welsh limestone. *Min. Sci. and Tech.* 10: 61-70.
25. Basham, K.D., K.P. Chong, and A.P. Borezi. 1993. A new method to compute size independent fracture toughness values for brittle materials. *Eng. Frac. Mech.* 46, 3: 357-363.

26. Khan, K. and N.A. Al-Shayea. 2000. Effect of specimen geometry and testing method on mixed mode I-II fracture toughness of a limestone rock from Saudi Arabia. *Rock Mech. and Rock Eng.* 33, 3: 179-206.
27. Chang, S.-H., C.-I. Lee, and S. Jeon. 2002. Measurement of rock fracture toughness under mode I and II and mixed-mode conditions by using disc-type specimens. *Engineering Geology.* 66: 79-97.
28. Chong, K.P., M.D. Kuruppu, and J.S. Kuzmaul. 1987. Fracture toughness determination of layered materials. *Eng. Frac. Mech.* 28, 1: 43-54.
29. Basham, K.D. 1989. *Nonlinear fracture mechanics using semi-circular specimens and tension softening behavior. Ph.D Dissertation.* Department of Civil Engineering, University of Wyoming.
30. Lim, I.L. , I.W. Johnston, and S.K. Choi. 1993. Stress intensity factors for semi-circular specimens under three-point bending. *Eng. Frac. Mech.* 44, 3: 363-382.
31. Ruisteun, H. and L.W. Teufel. 1996. Analysis of the influence of stress path on compressibility of weakly cemented sandstones using laboratory experiments and discrete particle models”, In *Proceedings of the Second North American Rock Mechanics Symposium: NARMS 96, Montreal, PQ, Canada, 19-21 June 1996*, eds. M. Aubertin et al. , 1525-1531. Rotterdam: Balkema.
32. Jensen, R.P., P.J. Bosscher, M.E. Plesha, and T.B. Edil. 1999. DEM simulation of granular media – structure interface: effects of surface roughness and particle shape. *Int. J. Num. and Anal. Meth. in Geomech.* 23: 531-547.
33. Holt R.M., T. Brandshaug, and P.A. Cundall. 2000. Discrete particle and laboratory modelling of core mechanics. In *Proceedings of the Fourth North American Rock Mechanics Symposium: Pacific Rocks 2000, Seattle, 31 July – 3 Aug 2000*, eds. J.M. Girard et al., 1937-1944. Rotterdam: Balkema.
34. Li, L. and R.M. Holt. 2001. Simulation of granular material using particle model with non-circularly shaped super-particles. In *Proceedings of ISRM Regional Symposium: Eurock 2001, Espoo, Finland*, 511-516.
35. Cundall, P.A. and D.L. Strack. 1979. A discrete numerical model for granular assemblies. *Geotechnique.* 29: 47-65.
36. Wang, C., D.D. Tannant, and P.A. Lilly. 2003. Numerical analysis of the stability of heavily jointed rock slopes using PFC2D. *Int. J. Rock Mech. & Min. Sci.* 40, 415-424.
37. Goodman, R.E. 1989. *Introduction to Rock Mechanics.* 2nd ed. New York: John Wiley & Sons.
38. Labuz, J.F., S.P. Shah, and C.H. Dowding. Experimental analysis of crack propagation in granite. *Int. J. Rock Mech. & Min. Sci.* 22: 85-98.
39. Ingraffea, A.R. and W.H. Gerstle. 1984. Non-linear fracture models for discrete crack propagation. *Application of Fracture Mechanics to Cementitious Composites.* eds. Shah, S.P. 247-285.
40. Barton, C.C. 1982. Variables in fracture energy and toughness testing of rock. In *Proceedings of the 23rd Annual U.S. Rock Mechanics Symposium: Issues in Rock Mechanics, Berkeley, 25 – 27 August 1982*, eds. R.E. Goodman and Heuze, F.E.449-462: Balkema.
41. Schmidt, R.A. 1976. Fracture-toughness testing of limestone. *Exp. Mech.* 16: 161-167.
42. Zoback, M.D. 1978. A simple hydraulic fracturing for determining rock fracture toughness In *Proceedings of the 19th Annual U.S. Rock Mechanics Symposium* Stateline, May 1978, 83-85.
43. Thiercelin, M. 1989. Fracture toughness and hydraulic fracturing. *Int. J. Rock Mech. & Min. Sci. & Geomech. Abstr.*26: 177-183.
44. Singh, R.N. and G.X. Sun. 1989. Relationships between fracture toughness, hardness indices and mechanical properties of rocks. *Mining Department Magazine.* 49-62. Department of Mining Engineering, University of Nottingham, England.

Reference: Rijken, Peggy, Holder, Jon, Olson, Jon E. and Laubach, Stephen E. 2002. Natural Fracture Characterization within the Travis Peak Formation, East Texas. Gulf Coast Association of Geologists Society. Austin, TX. October 30-November 1.

Predicting fracture attributes in the Travis Peak Formation using quantitative mechanical modeling and structural diagenesis

Peggy Rijken¹, Jon Holder¹, Jon E. Olson¹, and Stephen E. Laubach²

¹Department of Petroleum and Geosystems Engineering, The University of Texas at Austin, Austin, Texas 78712

²Bureau of Economic Geology, The University of Texas at Austin, Austin, Texas 78758

Abstract

Fluid flow prediction in naturally fractured reservoirs is challenging, since fracture pattern attributes such as aperture, filling, spacing, length and connectivity are difficult to obtain from core samples and logs. We combine two methods that circumvent this sampling problem to predict fracture characteristics within the Travis Peak Formation. Firstly, a geomechanical approach is employed to estimate aperture, spacing, length and connectivity of the fracture pattern. This model uses subcritical fracture index, a rock property, and geological boundary conditions as input. Secondly, micro-fractures are used to estimate conductivity and orientation of macro-fractures.

The relationship between micro-fractures and macro-fractures has been established in previous studies. Likewise, subcritical fracture index has been shown to influence natural fracture pattern characteristics such as length, spacing and connectivity. However, the dependence of subcritical index on petrologic features is still largely unknown. In this study, suites of subcritical fracture growth experiments were performed on the Travis Peak Formation to investigate systematic variations in subcritical fracture index. Observations show that subcritical fracture index increases with decreasing grain size. Preliminary testing also suggests that subcritical index varies with carbonate cement. Additional tests were carried out in which artificial cement was added to samples. The added cement resulted in increased strength, but decreased subcritical index. We postulate that this kind of artificial cementing of the sample can be equated to secondary carbonate cementation. Using these techniques and understanding the depositional and diagenetic history of a reservoir provides for natural fracture pattern prediction without extensive sampling.

Introduction

Fractures control fluid flow in low permeability formations. The prediction of fracture patterns and fracture attributes has been the subject of many studies (e.g. La Pointe and Hudson, 1985; Rives et al., 1992). Conventional studies gather data on fracture attributes and use geostatistics to obtain fracture distributions (e.g. Rives et al., 1992; Marrett, 1997). A wide range in distributions has been reported, from negative exponential, exponential, log normal to power law for fracture spacing and length, and from log normal to power law for fracture aperture (e.g. Snow, 1970; Panek, 1985; Rives et al., 1992; Marrett, 1997). However, significant data collection and correlation are required to estimate fracture pattern distributions within a region. The correlations are limited not only to the region under investigation, but also to surface formations. Subsurface fracture data are sparse; vertical wellbores do not often intersect vertical fractures because of large fracture spacing and small borehole size (Laubach et al., 2000). Hence the use of conventional data gathering techniques to predict subsurface fracture patterns is time consuming if at all possible. We propose an alternative method which allows for subsurface fracture pattern prediction without abundant sampling.

The proposed method is twofold. First the fracture pattern length, spacing and clustering distribution are predicted using a geomechanical model. This numerical model uses rock properties and geological boundary conditions as input data. Secondly, we examine the micro-fractures in the rock from which we can establish orientation and openness of the fractures (Laubach, 1997; Laubach et al., 2000; Laubach, submitted). The combination of these two methods provides a means for estimating flow in subsurface fracture systems without extensive sampling. The present discussion will focus on the geomechanical modeling parameters. Specifically, we will investigate the subcritical index value, a rock property, which exerts control on fracture pattern development (Olson 1993; Renshaw and Pollard, 1994; Renshaw, 1996; Olson, 1997). This study will investigate systematic variations of the subcritical index with several other rock properties using a material science model developed for metals and ceramics as a guide.

Subcritical fracture model

The geomechanical model used to predict subsurface fracture patterns is based on subcritical fracture growth. In the case of critical fracture growth, a fracture will propagate at a rupture velocity near the shear wave velocity of the material whenever the stress intensity (K_I) at the fracture tip exceeds the fracture toughness of the material (K_{Ic}). However, fractures can develop and propagate at much lower velocities under long term loading conditions, even though the stress intensity is less than the fracture toughness (e.g. Atkinson, 1984; Segall, 1984). This condition, in which a fracture propagates at stress intensity values below the fracture toughness but above a threshold stress intensity factor (K_I^*), is called subcritical fracture growth.

Multiple competing mechanisms can cause subcritical fracture growth. Of these, stress corrosion crack growth is the most well-known (Atkinson and Meredith, 1989a). In this process, strained atomic bonds are further weakened by the presence of water or another chemical reactive agent (Atkinson and Meredith, 1989a). This weakening of the bonds permits fracture propagation at stress intensity factors below the critical fracture toughness. Significant progress has been made in the development of subcritical fracture growth theory, explaining many previously confusing observations (Atkinson and Meredith, 1989b).

Fracture propagation velocity is correlated to stress intensity through the following empirical relation:

$$v = A \left(\frac{K_I}{K_{Ic}} \right)^n \dots\dots\dots (1)$$

- v = Fracture propagation velocity
- K_I = Mode I stress intensity factor
- K_{Ic} = Fracture toughness
- A = Critical fracture propagation velocity (constant)
- n = Subcritical fracture index (constant)

The critical fracture propagation velocity (rupture velocity), A , and the subcritical fracture index, n , can be measured in the laboratory. Subcritical index values have been determined for glass, single crystal, polycrystalline ceramics and rocks (e.g. Atkinson, 1984). It has been shown that subcritical index values vary with rock type (Atkinson and Meredith, 1989b). Likewise, it has been shown that subcritical fracture index exerts control on fracture attributes such as length, spacing (Olson 1993; Renshaw and Pollard, 1994) and connectivity (Renshaw, 1996; Olson, 1997). This is illustrated by the output of the geomechanical model (Fig. 1). Increasing the subcritical index from $n=5$ to $n=80$, but keeping all other conditions equal, increases fracture clustering and spacing (Fig. 1). Fracture length increases from $n=5$ to $n=20$, but decreases with further increase in subcritical index value (Fig. 1).

The subcritical index is a material/rock property, and we expect characteristic fracture patterns to develop under identical loading histories within one rock type. From experimental data based on single crystals and polycrystalline ceramics we know that the following 6 factors influence subcritical fracture growth (Atkinson and Meredith, 1989b): 1) strain energy release rate, 2) temperature, 3) chemical environment, 4) pressure, 5) rock microstructure and 6) residual internal strains. These influencing factors are based on results obtained from metals, ceramics and glass. However, sedimentary rock is inherently different from these materials. Rocks have porosity, grain size

distributions, cement volume and composition, and thus a wide range in microstructure. Therefore, the first step in our investigation of the systematics of subcritical index variations is an assessment of how microstructure influences subcritical index values. A second step is the investigation of the chemical environment. Subcritical growth is a chemical process that depends on the fluid type present (Atkinson and Meredith, 1981). Within petroleum reservoirs fluid saturation and fluid distribution is variable, which may change the subcritical index value and, in turn, may alter the ultimate fracture pattern.

In the following sections we will discuss a theory proposed for metals and ceramics. Although this theory has not been developed for sedimentary rock, we will use it to guide our assessment of systematic variations within sedimentary rock samples. Whether or not our results fall within the expected analytical trend(s) will provide insight into the validity of the material science theory to sedimentary rock.

Microstructure

The energy required to create a fracture is proportional to the fracture surface area and its specific surface energy (Lawn and Wilshaw, 1975). Within granular material three processes have been observed to take place that increase the energy necessary for fracture propagation: 1) fracture wandering: due to intergranular fracturing the crack-path is not straight and therefore longer than a comparable planar feature (Wu et al., 1978; Gesing and Bradt, 1983); 2) microcracking: within the cracktip stress field, numerous micro cracks develop (Gesing and Bradt, 1983; Han and Suresh, 1989); and 3) fracture branching: fractures have been observed to form two or more separate branches (Wu et al., 1978). Fracture branching is associated with fast or critical fracture growth (Lawn and Wilshaw, 1975) and is not addressed in this discussion.

Whether a fracture grows intergranular (fracture propagates along the grain boundaries through the material present between the grains) or transgranular (fracture propagates through the grain) in polycrystalline materials depends on flaw/grain size ratio (Rice et al., 1980; Mussler et al., 1982). For intergranular fracture growth the grains remain intact, whereas for transgranular fracture growth the grains are fractured. Thus in intergranular fracture growth the grains remain intact, whereas in transgranular fracture growth the grains are fractured. As the ratio of flaw/grains size increases, the proportion of intergranular fracture with respect to transgranular fracture increases (Rice et al., 1980; Mussler et al., 1982). Scanning electron microscope secondary electron images reveal that most of the fracture propagation occurs intergranular in sedimentary rock (Olson et al., 2001). We assume intergranular growth provides a lower resistance path than transgranular fracturing and will be the dominant fracture process. Accordingly, we postulate that cement present between the detrital grains plays an important role in subcritical fracture growth within sedimentary rock.

The theory as postulated by Gesing and Bradt (1983) assumes that flaws ahead of the fracture tip are linked as grain boundaries lose cohesion. The crack extension force that has to be applied to the main crack in order to extend a flaw, a , can be calculated from the stress field analysis around the crack tip. The main fracture is assumed to only propagate if the apparent extension force provides sufficient energy to propagate all micro-flaws in the crack-tip stress field. Thus the macro-fracture will only propagate when the local stress intensity factor at all the micro-flaws exceeds the stress intensity necessary for the micro-flaws to propagate. This condition is satisfied when the apparent crack extension force equals the average extension force for all micro-flaw sizes. The flaws, which link to form the main crack, are always one grain facet, d , away from the crack tip since the crack is assumed to propagate along the grain boundaries. These assumptions and the assumption the crack extends, on average, with subcritical fracture velocity until the local fracture toughness is exceeded, lead to the following equation (Gesing and Bradt, 1983):

$$n = c \times \frac{a}{d} \times \frac{G}{G_0} \dots\dots\dots (2)$$

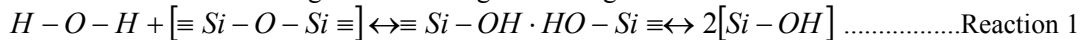
where a is flaw length, d is facet or grain size, G is the applied crack extension force, G_0 is critical crack extension force (a material property) and c is a constant.

Equation 2 provides for preliminary predictions of subcritical index within sedimentary materials (Fig. 2). We expect the subcritical index of a material to decrease when the grain size of the material increases without changing the microstructure or the chemical environment of the material.

This is illustrated in figure 2 by a decrease in slope on a log-log plot of normalized stress intensity vs. subcritical fracture velocity. Likewise, a decrease in surface energy, which we postulate corresponds to a change in cement type from quartz cement (surface energy = 1.34 J m⁻², Atkinson and Avdis, 1980) to calcite cement (surface energy = 0.27 J. m⁻², Atkinson and Avdis, 1980) is expected to increase the subcritical index value (Fig. 2).

Reactive environment: water saturation

As noted, the reactive environment at the crack-tip influences subcritical fracture growth. Reactive agents such as water can excite the bonds, and these excited bonds are easier to break than non-excited bonds (Atkinson and Meredith, 1989b). For example Scholz (1972) and Martin (1972) proposed that silica bonds undergo the following weakening in a water rich environment:



where the reaction speed depends on the availability and accessibility of water. This bond excitation is not restricted to silica. Similar results have been found in other materials, but the reaction taking place is not as well characterized as Reaction 1 (Atkinson and Meredith, 1989b).

The accessibility of water to the silica bonds is another important factor for subcritical fracture growth, so understanding the distribution of water within pores is important. Minerals have a natural wettability, which is the tendency for one fluid to spread on or adhere to a solid surface in the presence of other immiscible fluids. Almost all reservoir minerals are strongly water-wet (Gant and Anderson, 1988). However, exposure to different pore fluids can alter this state to preferentially oil-wet. When sandstone is preferentially water-wet, any water present will adhere to the mineral surface, thereby making the rock more susceptible to bond excitation. In oil-wet rock, accessibility of water to the bonds is reduced, thus bond excitation is diminished. As Holder et al. (2001) noted, we expect a relationship between wettability and subcritical index; oil-wet rock should have a higher subcritical index than water-wet rock.

Experimental measurements

Our next step is to experimentally determine to what extent sedimentary rocks follow the theories derived for metals and ceramics. A constant displacement double torsion testing procedure was used to determine subcritical index values (Evans, 1972; Williams and Evans, 1973). This testing procedure is widely used for subcritical fracture growth measurements, because the stress intensity is independent of fracture length. This feature simplifies data reduction and provides for measurements on opaque samples. Modifications in the testing procedures proposed by Holder et al. (2001) were used, in order to minimize testing complication due to the compliant and heterogeneous nature of sedimentary rocks.

The test samples were selected from the Travis Peak Formation. The sandstones in this sand rich, Lower Cretaceous, fluvial-deltaic deposit have a wide range of grain size, quartz and carbonate cement (Dutton et al., 1988). After testing, thin sections of the samples were made and inspected with a petrographic microscope to collect data on grain size, cement, porosity, and detrital grains. Suites of subcritical experiments were performed on the specimens (Table 1). In the following, we discuss the results in light of the theory from polycrystalline materials, starting with grain size and cement type and concluding with the chemical aspects.

Grain size

Values of subcritical index vary from rock type to rock type as well as within one rock type (Holder et al., 2001). In order to delineate variations with grain size only, we isolate specimens with similar mineral composition (Table 1). Within this subset, we find that subcritical index decreases when grain size increases (Fig. 3), conforming to the theory proposed by Gesing and Bradt (1983) and as seen in polycrystalline material (e.g. Navarette et al., 1976; Gesing and Bradt, 1983).

Unfortunately, smaller grain sizes within the Travis Peak have systematically higher clay content. Because clay is chemically charged and has a large surface area, we expect the subcritical index to vary significantly with clay content. Therefore, extension of samples to the smaller grain size regime is impeded. The correlation between subcritical index and clay content has not yet been investigated.

Carbonate content

According to the Gesing and Bradt (1983) correlation, we expect an increase in index value with decreasing quartz cement, increasing carbonate cement, decreasing grain size and increasing pore size for constant chemical environment (Fig. 2). However, we do not expect this correlation to hold if the rock contains a large percentage of carbonate cement. Large cement content will change the microstructure of the rock: porosity will decrease and pore size and shape will change. This change in microstructure will alter the energy balance and thus the subcritical index. Large carbonate cement percentages may alter the sample too much to be compared to samples containing small or no carbonate cement percentages.

The results show (Fig. 4) that for small (< 8 vol%) volume percentages of carbonate, variations in subcritical index follows the Gesing and Bradt (1983) trend. The subcritical index increases as carbonate content increases. However, for large values of carbonate volume percentage (> 8 vol%) we see that the trend reverses (Fig. 4), which we attribute to a change in microstructure of the rock.

The model we have used only takes into account the amount of carbonate cement present in the rock and assumes the detrital grains of the samples to be identical. However, some specimens contain variable amounts of clays and feldspars in addition to variations in their detrital quartz grains. These clay and feldspar variations will change the overall trend and obscure systematic changes within the trend. Also grain sizes vary among samples with different carbonate cement percentages, and some of the variation shown in Figure 4 may be related to these grain size variations.

Artificial cement

In order to investigate the effects of cement on subcritical index, artificial cement was introduced into some of the rock samples. This artificial cement mimics secondary carbonate cement, but is more controllable than natural cement variations. Two cements were used: salol (Salicylic Acid, $C_6H_4(OH)CO_2H$) which melts at temperatures above 40 °C and is solid for temperatures below this threshold, and sodium silicate (Na_4O_4Si), a water soluble compound. The low-viscosity molten salol penetrates the pores of the sample and reduces porosity, whereas water-soluble sodium silicate is deposited by evaporation. Salol has a hydroxyl group which could influence subcritical fracture growth as described in reaction 1, but sodium silicate does not. Samples bathed in salol showed a marked reduction in subcritical index from 53 ± 11 to 14 ± 6 , and samples soaked in sodium silicate yielded a value of 25 ± 3 . The larger reduction with salol cement is consistent with the added chemical effect from the hydroxyl ion.

An additional suite of tests was carried out using a single test specimen. By re-using the same specimen, sample-sample variations in microstructure are avoided. Four tests were carried out on the sample, which was prepared using standard methods. The sample was tested twice under dry conditions and then was soaked in salol. After treatment with salol, the sample was tested again. As before, the subcritical index decreased (from 56 ± 3 to 14 ± 6). A clear increase in rock strength as well as a reduction in subcritical index is observed in the velocity-stress intensity plot (Fig. 5).

We conclude that artificial cementation with either salol or sodium silicate decreases the subcritical index value. This decrease is consistent with the response of natural samples to large carbonate cement content (Fig. 4). The amount of artificial cement added in these tests is not controlled. Samples are submerged in the cement, taken out and then left to solidify. We expect to have filled most of the pore space with the artificial cement, and we postulate that this corresponds to large amounts of secondary carbonate cement within a natural sample. We see that after treatment with both cements the subcritical index decreases. A possible cause for this decrease in subcritical index is a decrease in porosity, which would correspond to decreasing pore/flaw size. Returning to the theory for polycrystalline materials we see that a smaller flaw size corresponds to a smaller subcritical index value. Further testing is required to fully understand and quantify this trend.

Water saturation

Another factor controlling subcritical index is the chemical environment, especially water content. In order to characterize this effect samples were tested both under dry (ambient air) conditions and submerged in water. Water is a reactive fluid as described in Reaction 1, thus we expect a decrease in subcritical index as samples are submerged (Atkinson and Meredith, 1989b).

Accordingly, the value of dry (ambient air) subcritical index value minus wet subcritical index value ($n_{\text{dry}} - n_{\text{wet}} = \Delta$) should be positive. However, as Figure 6 shows, these specimens do not always follow this trend. The plot of Δ vs. grain size (Fig. 6) shows that grain size plays an important role in this correlation. A part of this dependence can be attributed to the surface area of a sample. When samples are tested in ambient air, a small quantity of water is available to weaken the atomic bonds. If the surface area of the sample is large (e.g. small grain size samples), insufficient water is present to weaken all the bonds. On the other hand, when submerging these small grain size samples, sufficient water is present to weaken the bonds, and a pronounced change (large positive Δ) in subcritical index is expected. Likewise for large grain sizes we expect enough water to be present while testing in ambient air to weaken the bonds. Thus when submerged in water the correlation will be less pronounced. This however does not explain the negative values for Δ obtained.

For specimens from two depths, samples were soaked in toluene and then soaked in oil (Table 1). These samples were tested in air, and both showed an increase in subcritical index beyond the one standard deviation range. Oil droplets decrease the accessibility of water to the silica bonds, thus allowing less of the bonds to be excited, and an increase in the subcritical index is expected. It should be noted that samples of depth 9837 ft contain 12.5 vol% carbonate cement. We conclude that despite this change in rock constituents the correlation with oil content still holds.

From these tests it is apparent that microstructure can impact the effects of chemical environment on subcritical index values. Subcritical index generally increases with oil content. Subcritical index decreases with water content (Atkinson and Meredith, 1989b), but grain size alters the dependence of subcritical index on water content (Fig. 6). Further testing is required to quantify whether microstructure or chemical environment is dominant in subcritical index measurements on sedimentary rock.

Discussion: Controls on subcritical index

The subcritical index depends on a number of parameters, and trend analysis in rock is difficult because variations in one parameter can overprint another. Sample selection is such that sample attributes are only known after testing. It is virtually impossible to keep all variables but one constant for natural samples. However, some trends can be identified.

For the same chemical environment, we expect a higher index value in fine-grained materials than in coarse-grained materials. This observation, combined with the geomechanical model simulation of fracture pattern attributes (Fig. 1), enables us to predict that fracture families in coarser grained material will be shorter and more closely spaced than fracture families in fine grained materials. Many sedimentary environments show a gradation in grain size, and we expect that the fracture spacing, length and connectivity will not remain constant within such a stratigraphic hierarchy.

Rocks consist of many different minerals, each with their specific surface activity. Because chemical environment influences subcritical index differently for various minerals, rocks with dissimilar grain composition cannot be directly compared. A sample consisting of carbonate grains and quartz cement will behave differently than a sample consisting of quartz grains and carbonate cement. However, we expect that the deviations from the virgin curve will trend similarly (Fig. 2). A virgin curve is a curve that represents rock samples that consist of only one mineral type.

We have assumed that cementation occurs as overgrowths, and that the surface area created by the overgrowth correlates with grain size. Quartz cement is more likely to be deposited as overgrowths on detrital quartz grains (Pettijohn, 1975). Carbonate cement in quartz-rich sandstones typically does not occur as overgrowths but may show a variety of microstructural shapes because the mineralogy of the cement is different from the mineralogy of the detrital grains (Pettijohn, 1975). Due to these textural differences, microstructure within carbonate-cemented sandstones is highly variable. Subcritical index trends with varying volumes of carbonate cement are thus more difficult to predict

Micro-fractures as proxies for macro-fractures

Subsurface flow behavior not only depends on fracture length, spacing and clustering, but also on the degree of fracture filling. The overall subsurface flow pattern depends on whether fractures are open or closed to flow, and estimates of fracture filling must accompany prediction of fracture

patterns in order to fully characterize the flow pattern. For this purpose micro-fractures and diagenetic observations can be used as proxies for macro-fractures (Laubach et al., 2000; Laubach, submitted). Micro-fractures have previously been shown to be good predictors of fracture strike in the Travis Peak Formation (Laubach, 1997).

The degree to which large fractures are sealed by late cements can be inferred from cement patterns because cements that are contemporaneous with fracturing events do not completely fill macro-fractures. For a given burial history and time of fracturing there is a threshold below which fractures are completely filled, and above which fractures are partly to completely open (Laubach et al., 2000; Lander et al., 2002). Hence, late (or postkinematic) cement precipitation after the fracturing event is the main cause of fracture closure for large fractures (Laubach, submitted), and fracture openness can be predicted by estimating the amount of cement precipitated after the fractures were formed (= postkinematic cement; Laubach, submitted) using observations of those cements present in the rock mass (not the fractures). If large amounts of the pore space are filled, macro-fracture openness has degraded considerably and the fracture will not be open. Likewise, if small amounts of pore space are filled with postkinematic cement, macro-fractures should be open.

By dividing the postkinematic cement volume by the post fracture pore volume we obtain a degradation index (Dg) (Laubach et al., 2000) that predicts fracture openness (Fig. 7). If values are larger than 50% we expect macro-fractures to be closed, whereas for values below 50% we expect macro-fractures to be at least partly open. As part of a larger study, we measured degradation at several depths in the same wells where we collected subcritical crack index data. Overall, degradation in the Travis Peak is highly variable, but in this area the samples mostly have degradation values less than 50% (Fig. 7). Four depths (depth of 154 ft, 410 ft, 1825 ft and 1838 ft below the top of the Travis Peak Formation) show degradation values in excess of 50% (Fig. 7). Only fractures present in these four depths are predicted to be closed to flow. In the area where we collected subcritical crack index samples, Travis Peak fractures should be open to fluid flow, and the dominant control on flow patterns should be fracture distributions such as those predicted by the geomechanical model.

Conclusions

Grain size, cement, and porosity dominate the subcritical index value, given the same chemical environment. Subcritical index decreases with increase in grain size as proposed by the theory for polycrystalline materials. For small carbonate percentages the subcritical index increases with increase in carbonate cement content. However for large carbonate percentage the trend is reversed and subcritical index decreases with carbonate content. We attribute this decrease to a decrease in flaw size that reduces the subcritical index (Gesing and Bradt, 1983). This hypothesis is substantiated by the observation that subcritical index decreases with introduction of large volumes of artificial cement. Furthermore, samples with small grain sizes show a pronounced decrease in subcritical index with water content, whereas large grain size samples do not.

We conclude that the Travis Peak Formation has a subcritical index value of 50 to 60. If geological boundary conditions such as strain values are estimated accurately, this information allows for prediction of a general subsurface fracture pattern within the Travis Peak as depicted in Figure 1. Cement in the fracture system will modify these trace patterns, reducing apertures (and thus trace lengths) and in some cases entirely closing fractures, as is locally observed in the Travis Peak Formation (Laubach, 1989). The most damaging cements are postkinematic phases that tend to close large fractures. The presence of these cements can be quantified even where fractures have not been sampled (Laubach, submitted). Thus prediction of fracture flow in the Travis Peak Formation as well as other formations can be constrained by using mechanical modeling to derive a characteristic fracture pattern, and then modifying the pattern with independent evidence about fracture openness. This approach provides a quantitative basis for prediction of subsurface fracture-assisted fluid flow.

References

- Atkinson, B.K., and V. Avdis, 1980, Technical note, fracture mechanics parameters of some rock-forming minerals determined using an indentation technique: *International Journal of Rock Mechanics, Mining Science & Geomechanics Abstracts*, v. 17, p. 383-386.

- Atkinson, B.K., 1984, Subcritical crack growth in geological materials: *Journal of Geophysical Research*, v. 89, no. B6, p. 4077-4114.
- Atkinson, B.K., and P.G. Meredith, 1981, Stress corrosion cracking of quartz: a note on the influence of chemical environment: *Tectonophysics*, v. 77, p. T1-T11.
- Atkinson, B.K., and P.G. Meredith, 1989a, The theory of subcritical crack growth with applications to minerals and rocks: *Fracture mechanics of rock*, B. K. Atkinson (editor), Academic press geology series, London, p. 111-166.
- Atkinson, B.K., and P.G. Meredith, 1989b, Experimental Fracture mechanics data for rocks and minerals: *Fracture mechanics of rock*, B. K. Atkinson (editor), Academic press geology series, London, p. 477-526.
- Dutton, S.P., and L.S. Land, 1988, Cementation and burial history of a low-permeability quartzarenite, Lower Cretaceous Travis Peak Formation, East Texas: *Geological Society of America Bulletin*, v. 100, no. 8., p. 1271-1282.
- Evans, A.G., 1972, A method for evaluating the time-dependent failure characteristics of brittle materials and its application to polycrystalline alumina: *Journal of Material Science*, v. 7., p. 1137-1146.
- Gant, P.L., and W.G. Anderson, 1988, Core cleaning for restoration of native wettability: *SPE Formation Evaluation*, v. 3, no. 1, p. 131-138.
- Gesing, A.J., and R.C. Bradt, 1983, A microcrack model for the effect of grain size on slow crack growth in polycrystalline Al_2O_3 : *Fracture mechanics of Ceramics*, v. 5, R.C. Bradt, A.G. Evans, D.P.H. Hasselman, and F.F. Lange (editors), Plenum Press, New York, p. 569-590.
- Han, L.X., and S. Suresh, 1989, High-temperature failure of an alumina-silicon carbide composite under cyclic loads: mechanisms of fatigue crack-tip damage: *Journal of the American Ceramic Society*, v. 72, no. 7, p. 1233-1238.
- Holder, J., J.E. Olson, and Z. Philip, 2001, Experimental determination of subcritical crack growth parameters in sedimentary rock: *Geophysical Research Letters*, v. 28, no. 4, p. 599-602.
- Lander, R.H., J.F.W. Gale, S.E. Laubach, and L.M. Bonnell, 2002, Interaction between quartz cementation and fracturing in sandstone (abs.): *AAPG Annual Convention Program*, v. 11, p. A98-A99.
- La Pointe, P.R., and J.A. Hudson, 1985, Characterization and interpretation of rock mass joint patterns: *Geological Society of America Special Paper 199*, 37 p.
- Laubach, S.E., submitted, Practical approaches to predicting open and sealed fractures: *AAPG Bulletin*.
- Laubach, S.E., 1997, A method to detect natural fracture strike in sandstones: *AAPG Bulletin*, v. 81, no. 4, April, p. 604-623.
- Laubach, S.E., 1989, Fracture analysis of the Travis Peak Formation, western flank of the Sabine Arch, East Texas: *The University of Texas at Austin Bureau of Economic Geology Report of Investigations No. 185*, 55 p.
- Laubach, S.E., R. Marrett, and J. Olson, 2000, New directions in fracture characterization: *The Leading Edge*, v. 19, no. 7, July, p. 704-711.
- Lawn, B.R., and T.R. Wilshaw, 1975, *Fracture of brittle solids*, Cambridge University Press, Cambridge, 204 p.
- Marrett, R., 1997, Permeability, porosity, and shear-wave anisotropy from scaling of open fracture populations: *Fractured reservoirs; characterization and modeling*, E. Thomas (editor), p. 217-226.
- Martin, R.J., III, 1972, Time-dependent crack growth in quartz and its applications to the creep of rocks: *Journal of Geophysical Research*, v. 77, no.8, p. 1406-1419.
- Mussler, B., M.V. Swain, and N. Claussen, 1982, Dependence of fracture toughness of alumina on grain size, and test technique: *Journal of The American Ceramic Society*, v. 65, no. 11, p. 566-572.
- Navarette-Guijosa, A., W.P. Minnear, and R.C. Bradt, 1976, Effect of grain size on subcritical crack growth in alumina: Presented at the Am. Ceram. Soc. Annual Meeting, Cincinnati, Ohio, 1-6 May.
- Olson, J.E., 1993, Joint pattern development: effects of subcritical crack growth and mechanical crack interaction: *Journal of Geophysical Research*, v. 98-B7, p. 12251-12265.

- Olson, J.E., 1997, Natural fracture pattern characterization using a mechanically-based model constrained by geologic data – moving closer to a predictive tool: 36th U.S. Rock Mechanics Symposium.
- Olson, J.E., Y. Qiu, J. Holder, and P. Rijken, 2001, Constraining the spatial distribution of fracture networks in naturally fractured reservoirs using fracture mechanics and core measurements: SPE Annual Technical Conference and Exhibition: New Orleans, LA.
- Panek, L.A., 1985, Estimating fracture trace length from censored measurements on multiple scanlines: Proceedings of the international Symposium on Fundamentals of Rock Joints/ Björkliden/15-20 September, p. 13-23.
- Pettijohn, F.J., 1975, Sedimentary rocks: Third Edition, Harper & Row, Publishers, New York, 628 p.
- Renshaw, C.E., 1996, Influence of subcritical fracture growth on the connectivity of fracture networks: Water Resources Research, v. 32, no. 6., p. 1519-1530.
- Renshaw, C.E., and D.D. Pollard, 1994, Numerical simulation of fracture set formation: a fracture mechanics model consistent with experimental observations: Journal of Geophysical Research, v. 99-B5, p. 9359-9372.
- Rice, R.W., S.W. Freiman, and J.J. Mecholsky Jr., 1980, The dependence of strength-controlling fracture energy on the flaw-size to grain-size ratio: Journal of The American Ceramic Society, v. 63. no. 3-4, p. 129-136.
- Rives, T., M. Razack, J.-P. Petit, and K.D. Rawnsley, 1992, Joint spacing: analogue and numerical simulations: Journal of structural Geology, v. 14, no. 8/9, p. 925-937.
- Scholz, C.H., 1972, Static fatigue of quartz: Journal of Geophysical Research, v. 77, no. 11, p. 2104-2114.
- Segall, P., 1984, Rate-dependent extensional deformation resulting from crack growth in rock: Journal of Geophysical research, v. 89, no. B6, June 10, p. 4185-4195.
- Snow, D.T., 1970, The frequency and apertures of fractures in rock: International Journal of Rock Mechanics and Mining Science, v. 7, p. 23-40.
- Williams, D.P., and A.G. Evans, 1973, A simple method for studying slow crack growth: Journal of Testing and Evaluation, v. 1, p. 264-270.
- Wu, C. Cm., S.W. Freiman, R.W. Rice, and J.J. Mecholsky, 1978, Microstructural aspects of crack propagation in ceramics: Journal of Materials Science, v. 13, p. 2659-2670.

Table 1: Test results of the Travis Peak Formation

Well [*]	Depth	Detrital quartz grains	Quartz Cement	Carbonate Cement	Grain size	Subcritical index		
						Dry	Wet	Oil
	(ft)	(%)	(%)	(%)	(mm)			
1	5962	59	20	10	0.105	50±12	--	--
1 ^{**}	6206	60.5	16.5	2.5	0.097	65±4	66±5	--
1	6270	72	10.25	14.5	0.102	61±14	54±16	--
1	6295	52	19	18	0.097	51±12	--	--
1 ^{**}	7457	76.25	14.25	0	0.150	56±16	56±9	--
1 ^{**}	7506	72.75	18.75	0	0.155	58±15	70±8	--
2 ^{**}	5952	68.5	12	1.5	0.208	61±8	70±7	--
2 ^{**}	6244	68.25	13.75	0.75	0.129	54±7	52	--
3	6633	67	10.5	11.5	0.108	81±17	--	--
4	7737	70.3	17.3	1	0.058	42±7	63±9	--
5 ^{**}	10141	74.75	11.75	3.25	0.094	77±19	54±16	--
6 ^{**}	9817	73.7	17.3	0	0.186	53±11	60±15	--
6	9837	73.5	9.5	12.5	0.222	69±8	--	82±4
6 ^{**}	9880	74.75	18	0	0.262	52±10	--	70±1

^{*} Wells: 1) Holditch Howell #5, 2) Mobil Cargill #14, 3) Marshall Werner Sawmill #5, 4) Arkla #1 J.O. Pate, 5) Ashland #1 SFOT, and 6) Holditch SFE #2.

^{**} Samples used for grain size correlation.

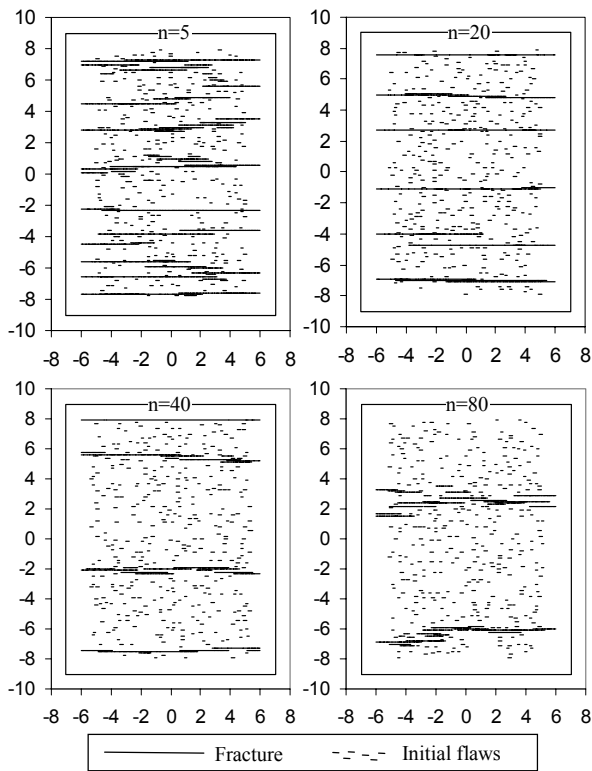


Figure 1: Fracture trace maps for numerical subcritical crack propagation simulations for different subcritical crack indices, using 400 initial flaws. Each case used an identical crack-perpendicular extensional strain rate. Note increasing fracture density with decreasing n , and fracture clustering for $n=40$ and $n=80$. From Olson et al. (2001).

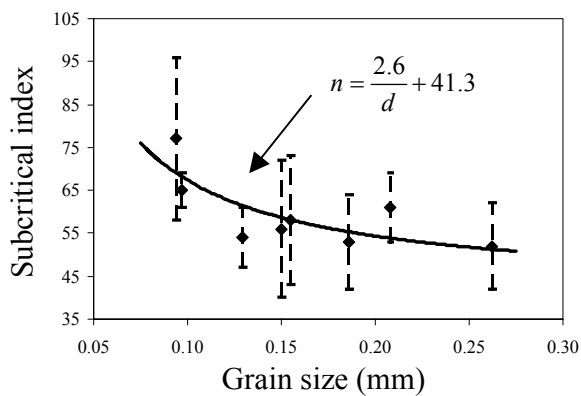


Figure 3: Grain size (mm) vs. subcritical index plot. The curve fit shows that the results follow the predictions based on polycrystalline materials, where subcritical index is inversely proportional to grain size (d).

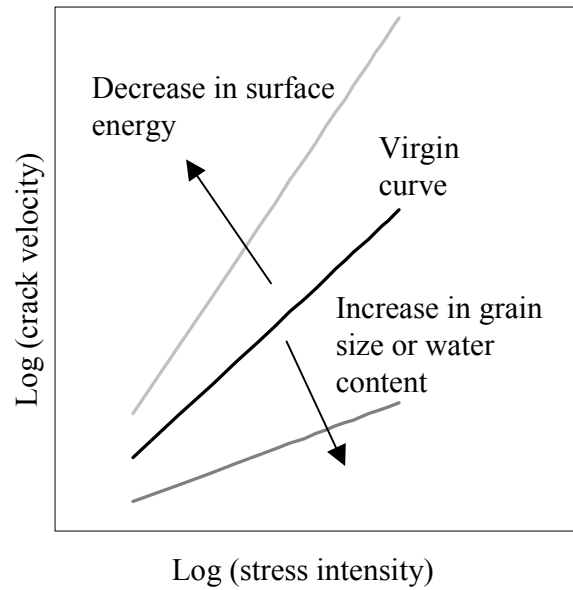


Figure 2: Log of stress intensity vs. log of fracture velocity. The slope of this line ($n =$ subcritical index value) is hypothesized to decrease with increase in grain size and water content and increase with a decrease in surface energy.

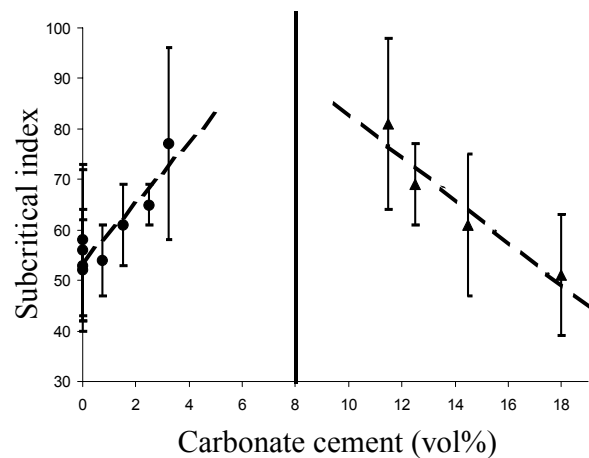


Figure 4: Variation in subcritical index with carbonate cement (vol%). For carbonate values below 8 vol% samples follow the predictions as specified for polycrystalline materials (Gesing and Bradt, 1983). For values larger than 8 vol%, samples behave in the opposite sense.

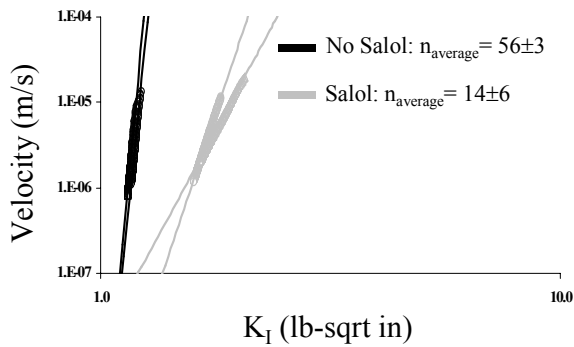


Figure 5: Subcritical fracture velocity vs. stress intensity. Four tests were carried out on one sample from a depth of 9817 ft. First the sample was tested in air after a standard preparation procedure (black curves). After these tests were completed the sample was soaked in Salol and dried. The sample was tested again (light grey curves) and a marked reduction in subcritical index was observed. The thin black and grey lines are trend lines fitted through the data. The thicker part on the curve corresponds to the data collected.

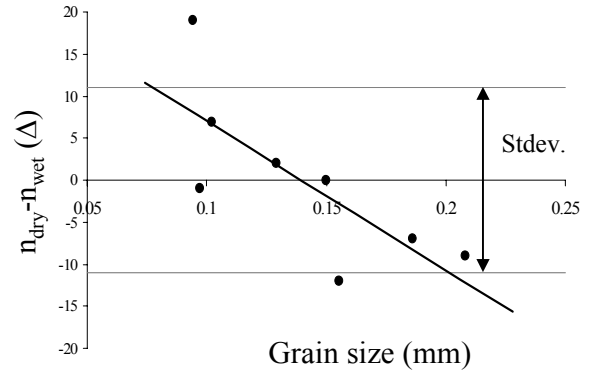


Figure 6: Difference between dry subcritical index value and submerged subcritical index value (Δ) vs. grain size. According to the literature this value should be positive since subcritical index decreases with increase in water content. However, we find this not to be true for large grain size values.

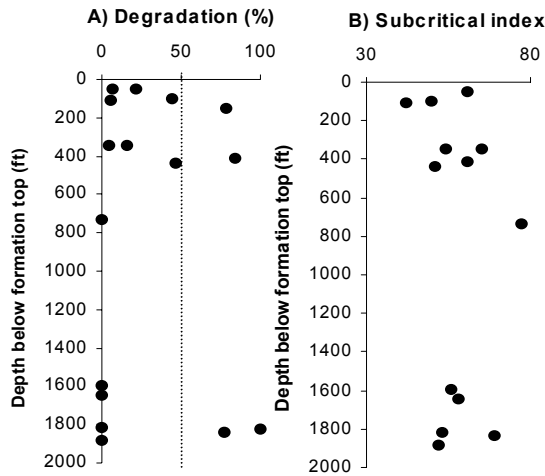


Figure 7: A) Degradation vs. depth below formation top. Large degradation values correspond to sealed micro-fractures indicating that macro-fractures will be largely non conductive. Values below 50% indicate mostly open fractures (Degradation analysis by Stephen Laubach). B) Subcritical index vs. depth below formation top. Combination of the two methods allows for subsurface fracture pattern prediction.

Reactive Transport Modeling in Fractures and Two-phase Flow

by

Myeong Hwan Noh, B.S.; M.S.

DISSERTATION

Presented to the Faculty of the Graduate School of
The University of Texas at Austin
in Partial Fulfillment
of the Requirements
for the Degree of

DOCTOR OF PHILOSOPHY

THE UNIVERSITY OF TEXAS AT AUSTIN

December 2003

UMI Number: 3122776



UMI Microform 3122776

Copyright 2004 by ProQuest Information and Learning Company.

All rights reserved. This microform edition is protected against
unauthorized copying under Title 17, United States Code.

ProQuest Information and Learning Company
300 North Zeeb Road
PO Box 1346
Ann Arbor, MI 48106-1346

Reactive Transport Modeling in Fractures and Two-phase Flow

Publication No. _____

Myeong Hwan Noh, Ph.D.
The University of Texas at Austin, 2003

Supervisor: Larry W. Lake

This study presents a mathematical model to simulate hydrodynamics and fluid-mineral reactions in a fracture within permeable media. Fluid convection, diffusion and precipitation / dissolution (PD) reactions inside a finite space are solved as a simplified representation of natural fracture mineralization. The problem involves mass transfer within the fluid accompanied by chemical reaction at the fracture surface. Mass-conservation equations for components in the fluid are solved, and these are coupled with chemical reaction at the fracture surface. The intent of this model is to show the time evolution of fracture aperture shrinkage patterns caused by the calcite cementation. We present the aperture width distribution along the fracture. In this study, we consider the precipitate as porous media and allow porosity and permeability in the cement. Therefore, the calcite cementation completely fills eventually.

As a second subject, the reactive transport model of CO_2 sequestration in aquifers is studied. Geologic formations are considered as a target for the seques-

tration of CO_2 from stationary sources such as power plants or large industrial facilities. Deep saline aquifers have a large potential storage capacity for CO_2 and they are ubiquitous in sedimentary formations. CO_2 can be sequestered in geologic formations by three principal mechanisms: hydrodynamic trapping, solubility trapping and mineral trapping. Mineral trapping is the most stable way of CO_2 sequestration in aquifers. Storage capacities of CO_2 for each trapping mechanism are presented using GEM, a commercial program from Computer Modeling Group Ltd. We also present the analytical solutions for the miscible displacement and compare them with the numerical results. Developing methods for increasing the mineral trapping creates stable repositories of carbon dioxide and that decreases mobile hazards such as leakage of CO_2 to the surface.

Table of Contents

Acknowledgments	v
Abstract	vi
List of Tables	xi
List of Figures	xii
Chapter 1. Introduction	1
Chapter 2. Literature review	4
2.1 Characterization of fractured reservoirs	4
2.2 Flow modeling in fractured reservoirs	6
2.3 Diagenesis of sedimentary rocks	11
2.3.1 Quartz cementation of sandstone	11
2.3.2 Carbonate diagenesis	13
2.3.3 Issues of supply and delivery of $CaCO_3$ for cementation . . .	15
2.3.4 Cementation of carbonate	16
2.4 Influence of saturation states and flow velocity on the amount of calcite precipitated in a fracture	19
Chapter 3. Convection, diffusion and surface reaction in a fracture	29
3.1 The kinetics of precipitation and dissolution	29
3.1.1 Basic considerations	29
3.1.2 The role of nucleation at the solid-solution interface	32
3.1.3 Calcite precipitation kinetics	35
3.1.4 The effect of pressure on the solubility of minerals	36
3.2 Development of mathematical model	39
3.3 Numerical scheme	45

3.4	Simulation results for a parallel plate model	47
3.4.1	Concentration profiles by dimensionless groups	47
3.4.2	Aperture width profiles	52
3.4.3	Analytical considerations	60
3.5	Summary and conclusions	65
Chapter 4. Modeling of carbonate cementation in non-homogeneous fractures		67
4.1	Introduction	67
4.2	Generation of fractures with rough surfaces	68
4.3	Mathematical model for fluid flow in fracture	78
4.3.1	Formulation of changing aperture width by shock formation approach	78
4.3.2	Mass balance of a component in fractures	82
4.3.3	Mass balance on the fluid	84
4.3.4	Dimensionless approach	86
4.3.5	Discretization of equations	88
4.4	Results for fracture filling with rough surfaces	90
4.4.1	Parallel plate model	90
4.4.2	Analytical approach	92
4.4.3	Characteristics of dimensionless numbers	95
4.4.3.1	Damköhler number and capacity factor	95
4.4.3.2	Specific surface area	96
4.4.4	Simple rough surface	98
4.4.5	Different inlet concentrations for each component	100
4.4.6	Simulation with rough surfaces	102
4.5	Summary and conclusions	115
Chapter 5. Reactive transport model for CO_2 disposal in aquifers		118
5.1	Introduction	118
5.2	Mathematical model	121
5.2.1	Introduction	121
5.2.2	Gas solubility in an aqueous phase	122

5.2.3	Mineral precipitation/dissolution rates	124
5.3	Results and discussions for CO_2 sequestration model	125
5.3.1	Analytical considerations	125
5.3.1.1	Specific shock velocity when gas displaces water . .	125
5.3.1.2	Specific shock velocity when water displaces gas . .	131
5.3.2	Comparison of analytical solutions with simulation results . .	134
5.3.2.1	Model decription	134
5.3.2.2	Comparison of shock velocities for gas displacing water	138
5.3.2.3	Specific velocity of a concentration discontinuity for a base component	140
5.3.2.4	Comparison of shock velocities for water displacing gas	146
5.3.3	Capacity of CO_2 storage	147
5.4	Conclusions	162
	Bibliography	165
	Vita	181

**INCORPORATING SUBCRITICAL CRACK GROWTH
MECHANICS INTO NATURAL FRACTURE
CHARACTERIZATION FOR IMPROVED RESERVOIR
SIMULATION**

by

Zeno George Philip, B.Tech.; M.S.

Dissertation

Presented to the Faculty of the Graduate School of

The University of Texas at Austin

in Partial Fulfillment

of the Requirements

for the Degree of

Doctor of Philosophy

The University of Texas at Austin

December, 2003

**INCORPORATING SUBCRITICAL CRACK GROWTH
MECHANICS INTO NATURAL FRACTURE
CHARACTERIZATION FOR IMPROVED RESERVOIR
SIMULATION.**

Publication No. _____

Zeno George Philip, Ph.D.

The University of Texas at Austin, 2003

Supervisor: Jon E. Olson

In conventional reservoir simulation, grid block permeabilities must frequently be assigned values systematically larger than those observed in core measurements to obtain reasonable history matches. Although part of the discrepancy might be due to improper 3-D scaleup, part of it might be due to substantial flow through natural fractures unaccounted for in the simulation. Here, a method to obtain equivalent permeabilities from fracture networks generated by a geomechanical model, constrained by geologic deformation and mechanical properties of the reservoir rock, is presented.

A fracture mechanics based crack growth simulator, using laboratory measured subcritical indices and reservoir rock properties, rather than a purely

stochastic method, was used to generate fracture networks with realistic clustering, spacing and fracture length distributions. The effects of subcritical index and bed-thickness on fracture attributes such as mean and total lengths were observed.

These fracture networks were represented in a finite-difference simulator explicitly by using enhanced grid cell permeabilities and implicitly by using non-neighbor connections. Coupled fracture-matrix fluid flow simulations of the fracture networks, under uniform pressure boundary conditions, were performed to obtain equivalent permeabilities. Permeability enhancements by factors of between 2 and 10 were observed.

The results also indicate that even though the permeability of individual fractures is highly sensitive to the fracture aperture, the computed equivalent permeabilities of a weakly-connected fractured region are not. They are more sensitive to the total and mean fracture lengths, as well as the nature of the fracture pattern, which include connectivity and clustering attributes. Superposing diagenetic effects (mineralization) on a fracture network can also reduce overall equivalent permeabilities.

Equivalent permeability estimates made on the fracture networks under uniform flow rate boundary conditions generate lower values than those obtained with uniform pressure boundaries. Comparison of the equivalent permeabilities and flow behavior for fractured networks embedded in a larger homogeneous unfractured matrix indicate that uniform flow rate boundaries yield more reliable estimates of the equivalent permeability than uniform pressure boundaries.

Table of Contents

List of Tables.....	xii
List of Figures	xiv
1. Introduction.....	1
1.1 Objective	1
1.2 Fractured Reservoirs Worldwide	2
1.3 A Review of the Modeling of Fractured Reservoirs	8
1.3.1 Discrete Network Models.....	8
1.3.2 Continuum Models.....	12
2. Problem Statement	26
3. Generating Representative Fracture Networks	29
3.1. Stochastic Fracture Network Modeling.....	29
3.2 Linear Elastic Fracture mechanics.	32
3.2.1 Subcritical Crack Growth.....	35
3.3 Experimental Determination of subcritical crack index:.....	41
3.4 Geomechanical Simulation	47
4. Finite Difference Flow Simulation.....	67
4.1 Explicit Fracture Representation.....	67
4.2 Non-neighbor Connections	68
4.3 Model Verification	72
4.3.1 Single-Fracture Analytical Solution.....	73
4.3.2 Chirlin Solution	74
4.3.3 Effect of x and y grid discretization for NNC representation	76
4.3.4 Effect of y-direction grid discretization for explicit fracture representation	77
4.3.5 Effect of larger matrix permeability.....	78

5. Flow Modeling of Simulated Fracture Networks.....	85
5.1 Equivalent Permeability of a Simulation Grid.....	85
5.2 Results and Discussion of the Flow Simulation using Explicit Fracture Representation.....	86
5.2.1: Dependence of equivalent permeability ratio on the total strain.....	87
5.2.2: Dependence of equivalent permeability ratio on the total length.....	89
5.2.3: Dependence of equivalent permeability ratio on the mean length.....	90
5.2.4: Dependence of equivalent permeability ratio on the mean aperture.....	91
5.2.5: Comparison of equivalent permeabilities obtained in this study with those obtained elsewhere, using stochastically generated fractures	92
5.3 Flow Simulation on SWCF fracture network using NNC.....	94
5.4 Other Factors Affecting Equivalent Permeability	95
5.4.1 Synkinematic Cement	95
5.4.2 Postkinematic Cement.....	98
5.5 Effect of Well Boundary Conditions.....	99
5.6 Summary	101
6. Analysis of Boundary Conditions	115
6.1 Introduction	115
6.2 Uniform Pressure versus Uniform Flow rate Boundary condition	117
6.3 numerical flow simulation studies.....	122
6.3.1: Stand-alone Fractured Region.....	125
6.3.1.1: Uniform Pressure Boundary Condition.....	125
6.3.1.2 Uniform Flow Rate Boundary Condition.....	127
6.3.2: Fractured Region Embedded in a Non-fractured homogeneous region	129

6.3.3: Comparison of Stand-Alone Fracture Networks under Different Boundary Conditions with the Embedded Fracture Networks	131
7. Conclusions	153
Appendix A: Comparison of Explicit Fracture Representation and NNC simulations	156
Appendix B: Comparison of Cardwell-Parsons Limits with Equivalent Permeabilities obtained from Flow Simulations	158
References	163
Vita	175

8. Appendix - FRAC Technology Transfer Meeting

The Fracture Research and Application Consortium is an industrial sponsors group that funds much of our research related to fractured reservoirs and provides much of the cost-sharing for the DOE contract. This group consists of 10 to 12 member companies (membership varies from year to year). The summer 2003 meeting consisted of a 1.5 day hands-on workshop in Jackson, WY for applying microcrack analysis, scaling analysis, and ECLIPSE simulation of discrete fracture patterns for permeability estimation. This was followed by a 2 day field trip to central Wyoming, looking at the interaction of fractures and folds. Finally, the research review meeting lasted for 2 days in Jackson, WY. The agenda from the 2003 research meeting follows.

Fracture Research & Application Consortium

Summer 2003 Research Meeting

Snake River Lodge
Jackson Hole, Wyoming
July 21 and 22, 2003

Dear FRAC Member:

On behalf of Randy Marrett, Jon Olson, and the **Fracture Research & Application Consortium** team, welcome to the 2003 Summer Research Meeting.

The theme of this meeting is the issue of fracture intensity—how to define, measure, and predict. Our presentations will examine progress in obtaining site-specific information about fracture intensity, new ways of thinking about fracture patterning that link statistical and mechanics concepts, and plans for research to use core data to better our understanding of fracture intensity at the seismic scale.

We will also look at progress in linking geomechanical and diagenetic models, and the potential of this approach to better predict the attributes of fractures that are central to their control on fluid flow. This research aims to improve our understanding of how fracture patterns develop. We have recently learned that the U.S. Department of Energy will support our research on these basic science issues, key leverage for your support of our efforts on this topic.

As described in the introductory slides, the project has achieved several milestones in the past year. Among those to be discussed at this meeting, we:

- Successfully measured average fracture spacing using scaling methods in typical Rocky Mountain tight gas sandstone;
- Took the first steps in automating collection of data to make scaling measurements a common component of fracture evaluation;
- Formulated a theory of fracture spatial distribution that links scaling and fracture mechanics;
- Tested use of geomechanically derived fracture patterns in fluid flow simulation;
- Greatly added to our store of measurements of the key rock property, the subcritical crack index;
- Measured opening histories of fractures, among other observations of linkages amongst structural and diagenetic features;
- Showed that models of cement precipitation during fracture opening are feasible.

These results highlight the project goals of new fundamental understanding of fractures linked directly to practical applications. They also demonstrate that exploring the linkages amongst quantitative fracture measurements at all scales, mechanics, and diagenesis continues to be a productive area of inquiry for both fundamental and practical advances.

We will not have time to cover all of the science conducted by FRAC since our last meeting, but the project website continues to grow and evolve. We will examine some exciting new developments for making case study results readily available online. Last Thursday and Friday we also debuted a 1.5 day applications course that we hope will be useful to Member companies.

As always, central to the Research Meeting is your input on the path ahead. We look forward to the planned discussions, particularly those scheduled on Tuesday on the outcrop and afterwards. On the following pages you will find our synopsis of the FRAC research plan, slide copy for all presentations, and copies of the applications workshop notes and exercises.

Steve Laubach

Fracture Research & Application Consortium

Summer 2003 Research Meeting

Delegates

ChevronTexaco

Wayne Narr
Eric Flodin

Shell International Exploration & Production

Dan Worrall
Mashiur Khan
Orlando Ortega
John Tabor
Scott Wilkins

Devon Energy

Mike Cameron

Petrobras

Francisco Fontes
Renato Matos

PDVSA

Celia Bejarano

Saudi Aramco

Mark Prudden

Williams Exploration & Production

Steve Cumella

Schlumberger

Dick Plumb

Marathon

Jeff Chen

Ecopetrol

Alberto Ortiz

Instituto Mexicano Del Petróleo

Manual Grajales
Gustavo Murillo
Luis Velasquillo

PEMEX

David Zamora

Tom Brown, Inc.

Terri Olson
Bill Hobbs
Ray Johnson
Fred LeGrand
Bob Brooks
Ted Enterline
Glenn Bixler
Greg Anderson
Hal Harper
Dave Thomas
John Southwell
David Entzminger
Huabo Liu

Repsol YPF

Rene Manceda
Ricardo Viñes
German Botessi
Fernanda Raggio
Juan Homovc
Pedro Kress
Joy Smith
Virginia Martinez
Rodrigo Limachi
Gaston Orioabala
Alejandro Franco
Philippe Molina

iReservoir

Hai Zui Meng
James R. Gilman

Fracture Research and Application Consortium

Agenda, Monday July 21

Research Meeting 8.00am – 5.45 pm

Snake River Lodge
Jackson Hole, Wyoming

7.30am Welcome. Coffee and pastries.

8.00am – 12.00pm Morning presentations.

- Site-specific fracture intensity
- Automation of image collection
- Horizontal core review
- Quantifying spatial scaling
- Fractal and harmonic arrangement of fractures
- Discussion

12:00 – 1.00pm Buffet in hotel

1.00 – 3.15pm

- Fracture pattern generation and flow modeling
- Subcritical crack index. New test results and insight
- Fracture opening histories measured
- Structural diagenesis modeling
- Discussion

3.15 – 3:30pm Break and posters

- Introduction to new model initiatives
- Hybrid geomechanical stochastic reservoir-scale fracture pattern prediction
- Introduction to seismic fracture calibration initiative
- Multi-component synthetic seismogram modeling of layered fractured media
- Seismic fracture intensity measurement and calibration

5.45pm Close

Fracture Research and Application Consortium

Agenda, Tuesday July 22

Research Meeting

7.30am – 5.00 pm

Rendezvous Peak Area and Snake River Lodge
Jackson Hole, Wyoming

7.30am Welcome. Coffee and pastries.

8.00am – 8.15pm Introduction to field trip

Fracture patterns in dolomite
Fracture length distributions and patterning

9:00 Depart Tram Dock for field trip

9.30 – 1.30pm

Field trip to view fracture dolomite.
Lunch on outcrop (We will provide sandwiches, drinks)

3.15 – 3:30pm Presentations and discussion

Status of Ellenburger fractured dolomite/karst study

Introduction to new model initiatives

Trap scale fracture patterns
Fracture porosity evolution

Other new initiatives – Pilot studies

Hybrid geomechanical stochastic reservoir-scale fracture pattern prediction
Introduction to seismic fracture calibration initiative
Multi-component synthetic seismogram modeling of layered fractured media
Seismic fracture intensity measurement and calibration

5.00pm Close